NASA CR - 134731

LOW VOLTAGE 30-cm ION THRUSTER DEVELOPMENT

FINAL REPORT

OCTOBER 1974

BY

ION PHYSICS DEPARTMENT STAFF

HUGHES RESEARCH LABORATORIES

A DIVISION OF HUGHES AIRCRAFT COMPANY

3011 MALIBU CANYON ROAD
MALIBU, CALIFORNIA 90265

PREPARED FOR

NATIONAL AERONAUTICS AND SPACE ADMINISTRATION
NASA LEWIS RESEARCH CENTER

CONTRACT NAS 3 - 16528

JAMES S. SOVEY, PROGRAM MANAGER

1. Report No.	2. Government Accession No.	3. Recipient's Catalog No.
NASA CR-134731		

4. Title and Subtitle	5. Report Date
LOW VOLTAGE 30-cm ION THRUSTER DEVELOPMENT	November 1974
	6. Performing Organization Code

7. Author(s)	8. Performing Organization Report No.
H.J. King, et al.	
	10. Work Unit No.

9. Performing Organization Name and Address	11. Contract or Grant No.
Hughes Research Laboratories 3011 Malibu Canyon Road Malibu, California 90265	NAS 3-16528 and NAS 3-18334
	13. Type of Report and Period Covered
12. Sponsoring Agency Name and Address National Aeronautics and Space Administration Lewis Research Center 21000 Brookpark Road Cleveland, Ohio 44135	Contractor Report - Final 16 May 1972 - 30 Sept. 1974
	14. Sponsoring Agency Code

15. Supplementary Notes

Project Manager; James S. Sovey, NASA-Lewis Research Center, Cleveland, Ohio

16. Abstract

The basic goal of the work described in this report was to advance the development status of the 30-cm Electron Bombardment Ion Thruster from a laboratory model to a flight-type engineering model (EM) thruster. This advancement included the more conventional aspects of mechanical design and testing for launch loads, weight reduction, fabrication process development, reliability and quality assurance, and interface definition, as well as a relatively significant improvement in thruster total efficiency. The achievement of this goal was demonstrated by the successful completion of a series of performance and structural integrity (vibration) tests.

In the course of the program essentially every part and feature of the original 30-cm Thruster (from NAS 3-14140) was critically evaluated. These evaluations, in conjunction with work at NASA LeRC, led to new or improved designs for the ion optical system, discharge chamber, cathode isolator vaporizer assembly, main isolator vaporizer assembly, neutralizer assembly, packaging for thermal control, electrical terminations and structure. The most significant improvement, for both performance and reliability, was the use of "compensated dished grids." Optimization of the discharge chamber configuration and the use of a "magnetic baffle" also substantially increased thruster efficiency. The application of titanium to certain structural components produced a significant weight reduction.

The performance of the EM thruster developed during this program includes an efficiency of 71.5%, specific impulse of 3000 s, thrust of 2.63 kW. These performance values, including corrections for ion beam divergence and double ions, represent an improvement of about 10% from previous work.

17. Key Words (Suggested by Author(s))	18. Distribution Statement
Electric Propulsion Ion Propulsion 30 cm Ion Thruster Power Conditioning Automatic Controller Mercury Propellant	UNCLASSIFIED - Unlimited

19. Security Classif. (of this report)	20. Security Classif. (of this page)	21. No. of Pages	22. Price*
Unclassified	Unclassified	241	$3.00

* For sale by the National Technical Information Service, Springfield, Virginia 22151

Page intentionally left blank

Page intentionally left blank

FOREWORD

The work described herein was performed in the Hughes Research Laboratories Ion Device Physics Department of the Hughes Aircraft Company in Malibu, California. This department is managed by Mr. J.H. Molitor. The work was performed under Contracts NAS 3-16528 and NAS 3-18334, monitored by Mr. J.S. Sovey of NASA Lewis Research Center. Major technical contributors to this effort were:

H.J. King	Project Manager for NAS 3-16528 and Ion Optics Design
R.L. Poeschel	Assistant Project Manager for NAS 3-16528, Thruster Optimization
D.E. Schnelker	Project Manager for NAS 3-18334, Mechanical Design and Fabrication
B.G. Herron	Control System Design and Optimization
C.R. Collett	Thruster Evaluation and Life Testing
T.D. Masek	Final Report

TABLE OF CONTENTS

LIST OF ILLUSTRATIONS

LIST OF TABLES

SUMMARY

The basic goal of the work described in this report was to advance the development status of the 30-cm Electron Bombardment Ion Thruster from a laboratory model to a flight-type engineering model (EM) thruster. This advancement included the more conventional aspects of mechanical design and testing for launch loads, weight reduction, fabrication process development, reliability and quality assurance, and interface definition, as well as a relatively significant improvement in thruster total efficiency. The achievement of this goal was demonstrated by the successful completion of a series of performance and structural integrity (vibration) tests.

In the course of the program essentially every part and feature of the original 30-cm thruster (from NAS 3-14140) was critically evaluated. These evaluations, in conjunction with work at NASA Lewis Research Center (LeRC), led to new or improved designs for the ion optical system, discharge chamber, cathode isolator vaporizer assembly, main isolator vaporizer assembly, neutralizer assembly, packaging for thermal control, electrical terminations and structure. The most significant improvement, for both performance and reliability, was the use of "compensated dished grids". Optimization of the discharge chamber configuration and the use of a "magnetic baffle" also substantially increased thruster efficiency. The application of titanium to certain structural components produced a significant weight reduction.

The nominal performance characteristics of the EM thruster developed during this program are the following:

Performance Parameter	Full Power	73% Power	43% Power
Total Efficiency, %	71.5 ± 1.0	69.5 ± 1.0	61.6 ± 1.0
Specific Impulse, s	3000 ± 10	2900 ± 10	2560 ± 10
Thrust, N	0.128 ± 0.002	0.094 ± 0.001	0.056 ± 0.001
Input power, kW	2.63	1.92	1.14

These performance values include corrections for ion beam divergence and Hg^{++} which had not been included in most previous thruster performance ratings. The significant magnitude of these corrections became more fully appreciated during this program. The total efficiency of about 71.5% represents an improvement of 8 to 10% over the results of contract NAS 3-14140.

The contract under which this work was performed was one of three concurrent programs sponsored by NASA LeRC related to the 30-cm thruster development at Hughes Research Laboratories (HRL). The related contracts were directed toward endurance testing (NAS 3-15523) and thruster advanced technology (NAS 3-16949). In the process of performing these interrelated activities, substantial technology, design, fabrication and testing experience was exchanged. Thus, the product of this work (i.e., the EM thruster) incorporates contributions from all three contracts. This report is intended to be (1) a complete description of the "Low Voltage Thruster" contract-related work, and (2) a summary of critical supplemental contributions from the other two contracts.

I. INTRODUCTION

Mercury ion thrusters, as a fundamental part of an electric propulsion system, have been recognized as an efficient means of primary propulsion for future space vehicles. The growing recognition of ion propulsion advantages and capabilities is demonstrated by NASA support for Solar Electric Propulsion (SEP) Technology Development, space vehicle preliminary design studies, and low thrust mission design studies.

The present program was initiated in May 1972 with the basic goal of advancing the development status of the 30-cm thruster. The advancement program included structural and mechanical design to meet expected launch loads, weight reduction, fabrication process development, reliability and quality assurance, complete documentation, interface definition, and a significant thruster efficiency increase. The starting point for this work was the thruster developed under Contract NAS 3-14140.[1] As the contract progressed, requirements and recommendations from NASA activities resulted in additional design and testing tasks, as well as the agreement that the final product of this contract would be an EM thruster. In-depth design reviews were conducted with the LeRC program manager to discuss and plan the implementation of as many "user" requirements as possible.

In parallel with this contract work, personnel at LeRC maintained an active 30-cm thruster test program to develop design concepts, evaluate various components, evaluate HRL proposed designs, provide recommendations, and generally minimize the risk in the EM thruster development. The work performed under this contract was directed and coordinated so as to make maximum use of LeRC results. This mutual exchange of ideas and data significantly enhanced the EM development program.

In addition to the work covered by this contract (NAS 3-16528), two other related programs, sponsored by NASA LeRC, were performed concurrently by HRL. The two programs were directed toward

endurance testing (NAS 3-15523)[2] and thruster advanced technology (NAS 3-16949).[3] The EM design contains significant contributions from these programs by sharing the solutions to mutual problems. The general interrelationship of the three programs and the major results of each is illustrated in Fig. 1. Specific portions of the EM design contributed by the related programs will be summarized in appropriate sections of this report with references provided to the original detailed discussion.

The content of this report will be divided into subject categories in order to trace the technical development of each component or assembly. However, a strict chronological or task history will not be followed due to the rather complex relationships between this work, LeRC activities, and the two concurrent programs. The following summary should provide an adequate historical background to put the remainder of the report in perspective.

The first six months of the program were devoted to ion optical system development, component optimization, discharge chamber improvement, performance mapping, and mechanical design. The work resulted in the construction, electrical performance mapping, and vibration testing of a "600-Series" (stainless steel construction and dished grids) thruster. A design review during the eighth month was held to present these results to LeRC, Marshall Space Flight Center (MSFC) and Jet Propulsion Laboratories (JPL). During this review the need was expressed for a mechanical interface compatible with a two point gimbal support concept. The space vehicle system weight penalty associated with adapting from the 600-series thruster design to the JPL and MSFC gimbal mount would be unacceptable.

A program revision was issued to modify the thruster design to accommodate a gimbal mount interface. This design modification also provided an opportunity to incorporate improvements in the discharge chamber configuration resulting from activities at LeRC and HRL, and to include component technology improvements resulting from HRL life test experience with a 400-series thruster. The structural

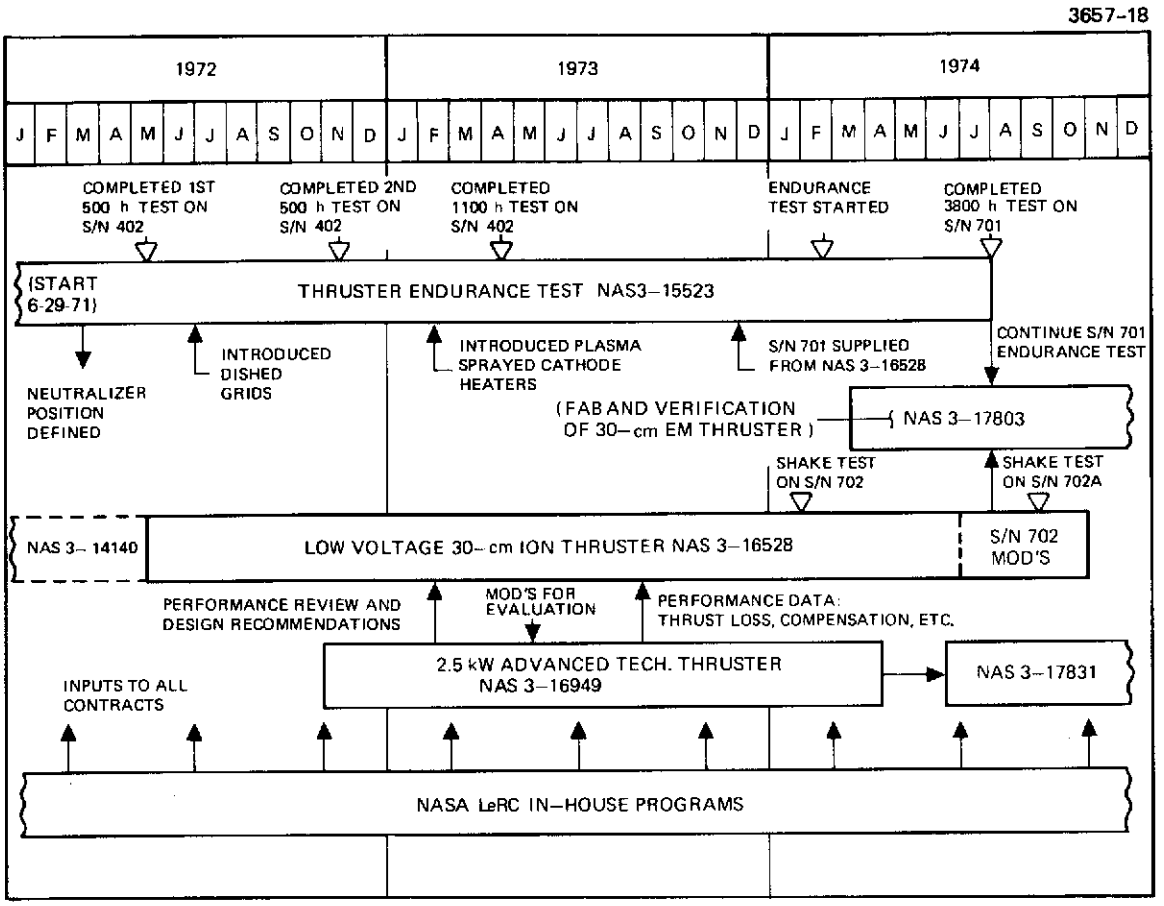

Fig. 1. General relationship between concurrent contracts from 1972 to 1974.

redesign, to meet the gimbal interface requirements, added significant weight. To minimize this impact, the material used in many of the thruster members was changed to titanium. In addition, the cathode vaporizer and isolator were separated from the cathode and mounted in a cooler location on the back plate. This was done to reduce the heat flux from the cathode to the vaporizer. A design review was held in the twelfth month to obtain approval for the 700-series thruster fabrication with titanium and incorporation of compensated dished grids.

The first 700-series thruster (S/N 701) was placed in test during the sixteenth month. The major delay in completing the thruster was due to delays in fabrication of titanium parts. At this point in the program, the 700-series thrusters were designated as EM's. After about two months of performance, beam divergence, and Hg^{++} mapping, thruster S/N 701 was delivered to LeRC for use in the endurance test program (NAS 3-15523).*

The second EM thruster (S/N 702) was assembled and performance checked during the nineteenth month of the contract, in preparation for vibration testing. Propellant line fractures and failures in the neutralizer assembly were discovered during 9 g sine and random vibration tests. Additional damage to the backplate support beams, and to components supported by the backplate, occurred during 19 g sine tests. Suggested modifications of the thruster backplate support beams were approved by LeRC and the repair of thruster 702 began during the twenty fourth month. This design modification also provided the opportunity to improve the wiring and feedline interfaces.

Following the repair, the thruster designation was changed to S/N 702-A. (The new design resulting from the modifications and repair was designated as the 800-series thruster.) Thruster S/N 702-A was performance tested, shake tested, and re-performance tested to evaluate the suitability of the modifications. Although some damage was incurred during the shake test, the failures were of a correctable

*As of Oct. 30, 1974 thruster 701 had completed 6000 hours of testing.

nature, and the second performance test showed that the operating characteristics were unchanged. The 800-series thruster design is illustrated in Figs. 2 and 3, showing thruster 702-A.

M10535

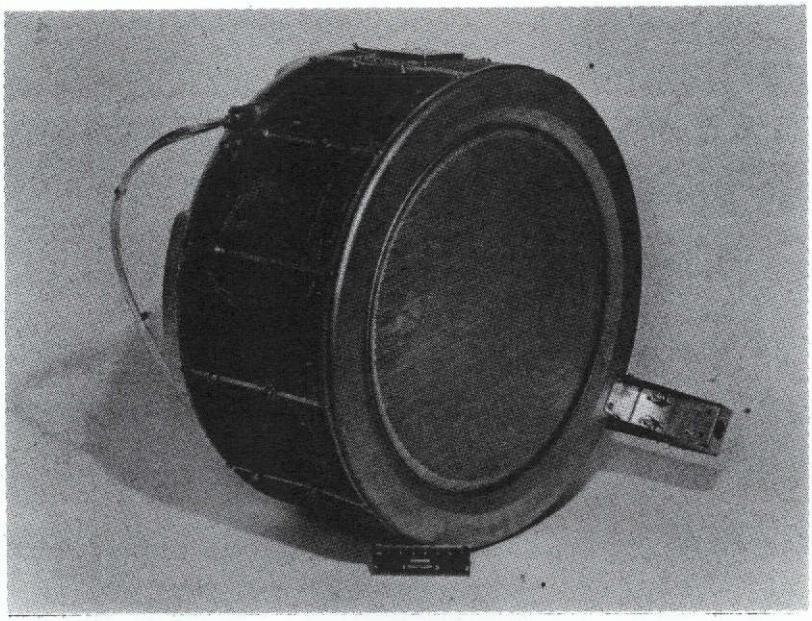

Front view

M10537

Rear view

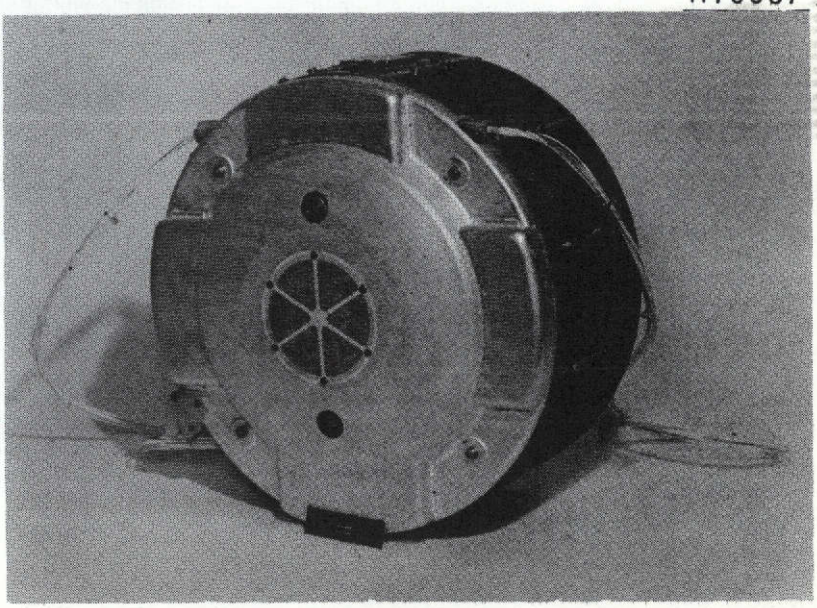

Fig. 2. Photographs of thruster S/N 702-A (800 series design).

M10536

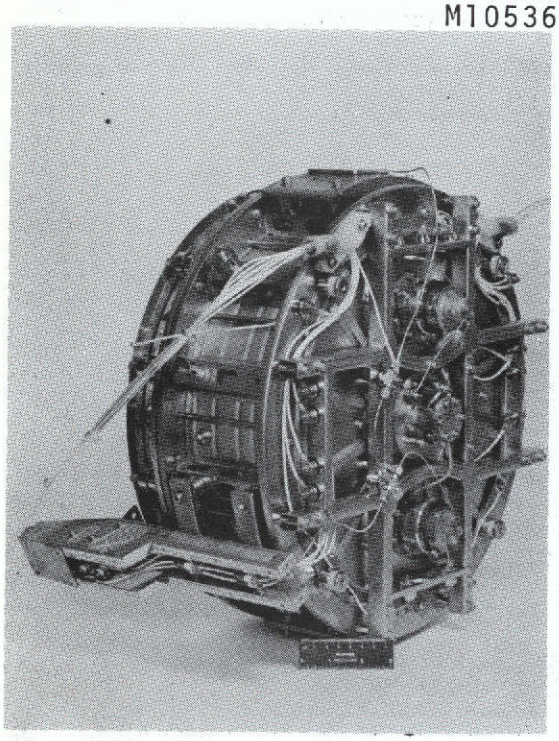

M10543

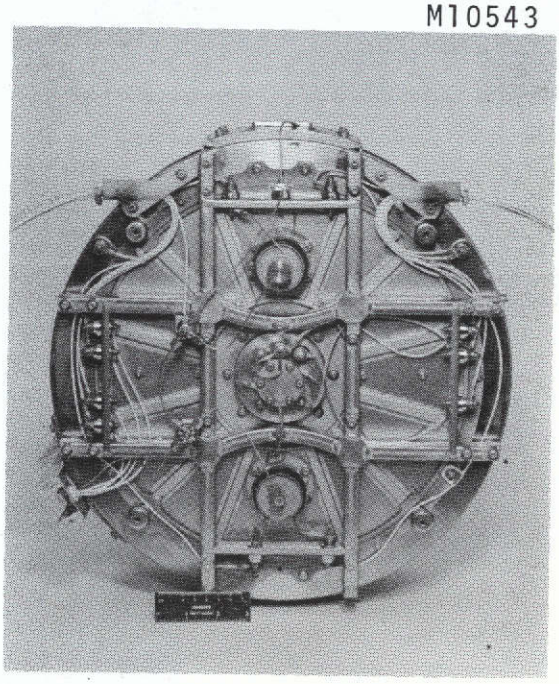

Fig. 3. Photographs of thruster S/N 702-A with ground screen and rear cover removed.

II. THRUSTER DEVELOPMENT

The 30-cm thruster development progress, during the period of May 1972 through Sept. 1974, is described in this section. The work discussed includes the design and fabrication of many thruster components, and assemblies such as the ion optical system, cathodes, isolator-vaporizer, neutralizer, discharge chamber, and thruster mechanical designs. Thruster control and power processing work performed under the contract will also be discussed in this section. The time phasing of this work is shown by Fig. 4.

Component and assembly tests are discussed to indicate the basis for design improvements. However, thruster overall testing, including performance and dynamics, is presented in Section III. Engineering model thruster characteristics are summarized in Section IV.

A. Ion Optical System

The ion optical system has been found to be the most critical thruster assembly in terms of requirements on thruster stability, efficiency, and lifetime. To adequately meet these thruster requirements, the optics must have the following characteristics:

- Design life in excess of 10,000
- Structural stability and mechanical reproducibility
- High ion extraction efficiency
- Low beam divergence
- Light weight

The ion optical (or ion extraction) system is basically a pair of thin (~1/2 mm) molybdenum plates perforated with 10^4 small (~2 mm diameter) matching apertures. These plates must be positioned parallel to each other, with ~1/2 mm interelectrode spacing. The upstream or screen electrode defines the plasma boundary in the discharge chamber,

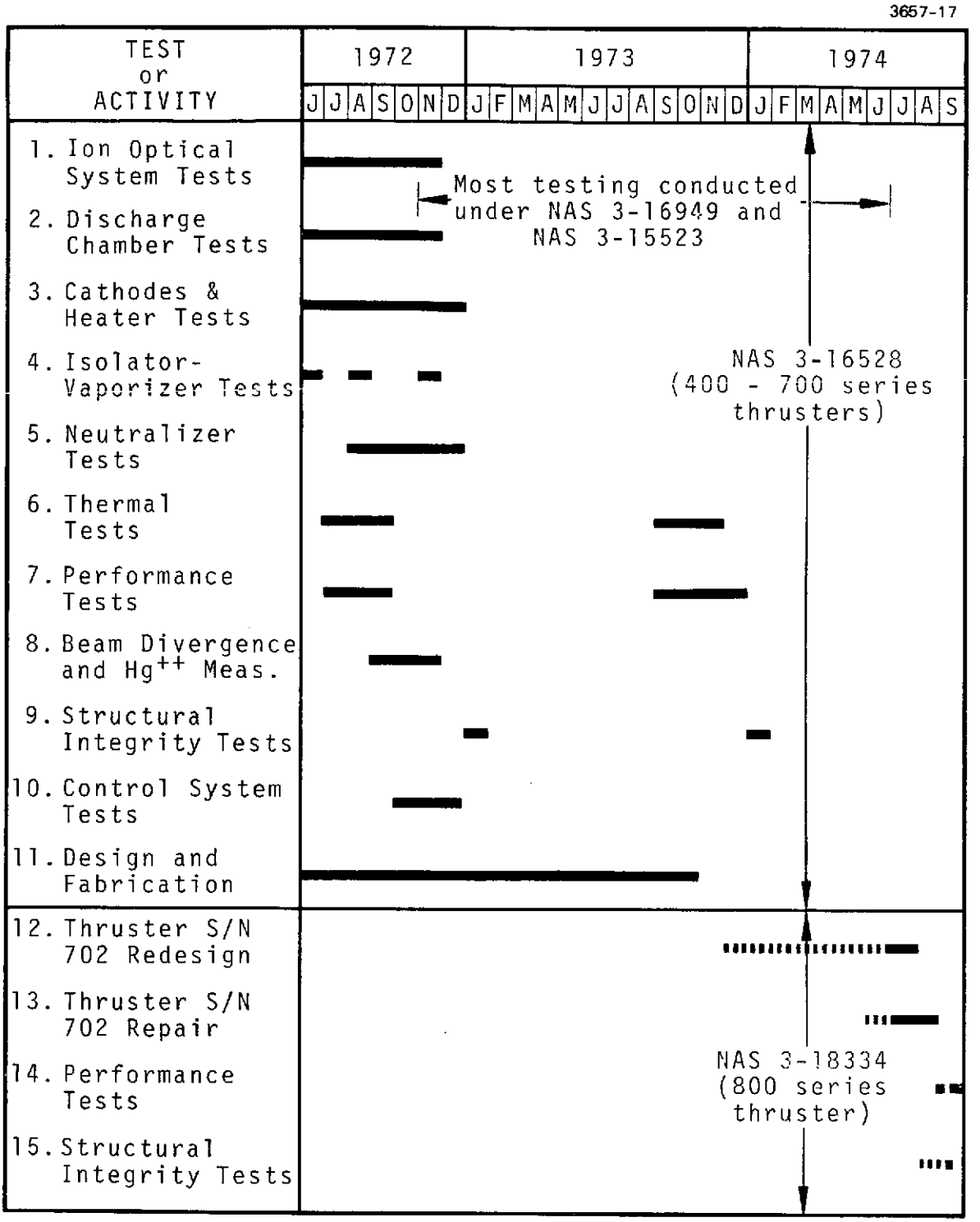

Fig. 4. Time phasing of work performed on contract.

while the electric field produced between the electrodes accelerates and focuses a beam of positive ions from the plasma through each pair of screen-accelerator apertures.

Past experience had indicated that this basic design concept was a functional means of extracting ions from the plasma. However, for the 30-cm thruster it was found that such a simple concept made it difficult, if not impossible, to reliably maintain the close interelectrode spacing with flat electrodes. Various methods for maintaining grid spacing have been attempted in previous programs. At the outset of this contract the decision to utilize curved or "dished" electrodes was made, based on test results obtained at LeRC.[4] A dished grid optical assembly is shown in Fig. 5. The dish depth (2.1 cm) and general hydroforming technique were defined by the LeRC program manager. Although considerable experimental effort was required to perfect and standardize the fabrication procedures, the basic dished structure immediately provided sufficient structural rigidity to permit reproducible performance of a particular electrode set. Thus, the repeatability and ruggedness characteristics allowed a parametric study to be performed to evaluate the effect of design variables. The performance parameters of eight of the electrode sets tested during this program are shown in Table 1.

1. Selection Of Ion Optical System Dimensions

The specific goal of these tests was to compare thruster performance as a function of the following parameters:

- Interelectrode spacing
- Accelerator thickness
- Aperture size
- Number of apertures
- Aperture shape (i.e., round versus hexagonal)
- Fractional open area
- Depth of "dish"

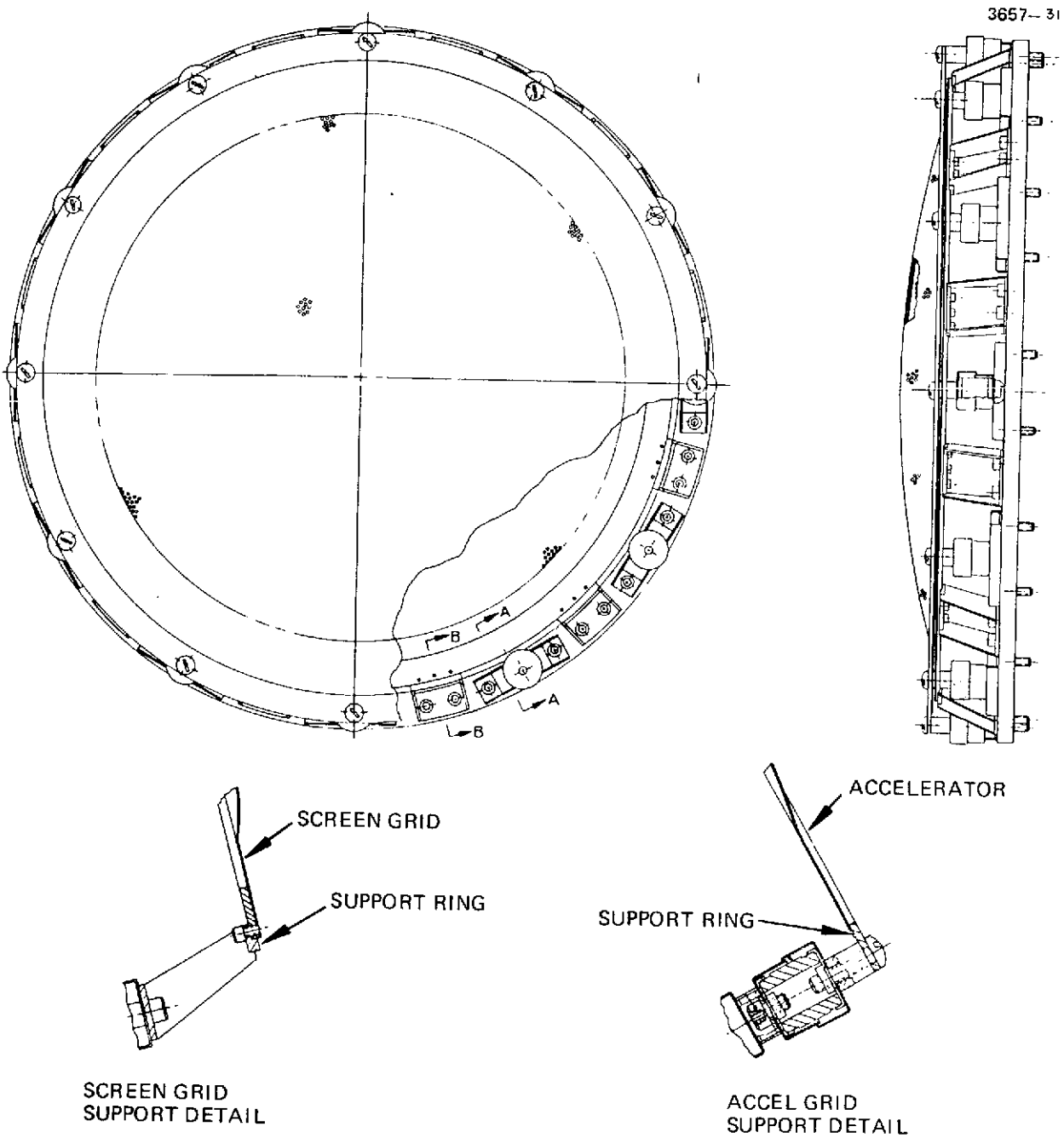

Fig. 5. 700-series thruster dished grid ion optical system assembly.

TABLE 1

Grid Set Dimensions and Minimum Operating Voltages

Grid Set, S/N	Dimensions, cm Dia/c-c/t Screen/ Accelerator	Spacing, cm	R, Net to Total Voltage	Minimum Total Voltage, V		
				1.0 A	1.5 A	2.0 A
601	0.216/0.254/0.038 0.191/0.254/0.038	0.071	Varied	1200	1420	1580
608	0.216/0.254/0.038 0.173/0.254/0.076	0.071	Varied	1260	1480	1580
609	0.241/0.279/0.038 0.193/0.279/0.076	0.076	0.500 0.625	1520 1540	1800 1800	2120 2140
609	0.241/0.279/0.038 0.193/0.279/0.076	0.063	0.500 0.625	1380 1280	1380 1420	1570 1580
611	0.241/0.279/0.038 0.241/0.279/0.038	0.089	0.500 0.625	1440 1400	1760 1760	1940 1880
614	0.279/0.317/0.051 0.224/0.317/0.076	0.063	0.500 0.625	1340 1380	1600 1560	1780 1760
623	0.208/0.234/0.038 0.179/0.234/0.076 (Hex)	0.065	0.500 0.625	1640 1480	1780 1660	1820 1780
626	0.208/0.234/0.038 0.179/0.234/0.076 (1 cm Dish, Hex)	0.102 (0.051 at edge)	0.625	1.080	1300	1470
634	0.241/0.279/0.038 0.193/0.279/0.076 (0.03 cm Forming Spacing)	0.056	0.500 0.625	1500 1580	1850 1820	1980 1900
642[a]	0.091/0.221/0.051/0.5 0.152/0.221/0.038	0.063	0.73	-	1200	-
644[a]	0.191/0.221/0.05/0.5 0.152/0.221/0.038	0.051	0.73	-	1120	-

[a]Sets 642 and 644 are "compensated" 0.5%.

T1447

In the course of these tests, it was also possible to compare:

- Forming procedures
- Stress relieving procedures
- Spot welded versus brazed screen support ring attachment (see Fig. 5)
- Number of support rings

The comparison was made on the basis of measuring:

- The system perveance at 1.0, 1.5, 2.0 A at various "R" ratios
- The discharge chamber performance (i.e., eV/ion versus η_m) at the above currents
- The beam profile with each system at various beam currents and R ratios
- The performance of the neutralizer with each ion optical system.

The voltages shown in Table I were derived from perveance curves where accelerator current is plotted as a function of the total accelerating voltage. The minimum voltage was consistently determined by the intersection of a 30° line tangent to the curves and the horizontal line indicating minimum accelerator current. This was done for two R ratios (net to total voltage) as shown. The grid spacing measurement represents nominal values in the center region of the grid.

Beam profiles for a number of the grid sets are shown in Fig. 6. These profiles were taken with the multiple-probe array, plotting the points through the thruster centerline. The thrust factors and the calculated beam currents, as determined from the data and a computer program, are also shown on the figure. (The computer program used to reduce data and compute thrust losses is discussed in Section III.) Accelerator current, as a function of R ratio for various grid sets with constant total voltage, is shown in Fig. 7. As R decreases, the accelerator current rises sharply. The onset of "electron backstreaming" occurs for values of R greater than about 0.8.

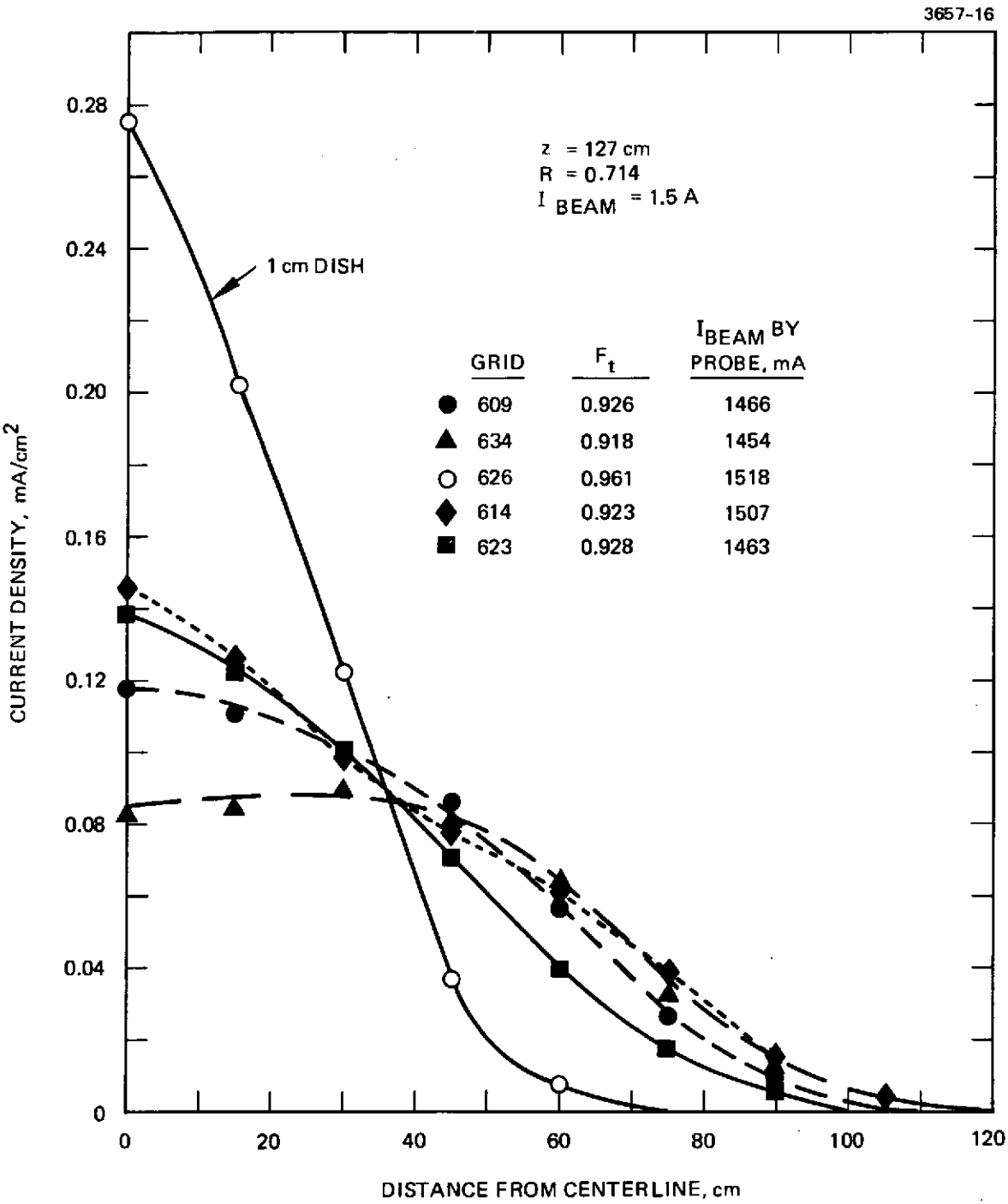

Fig. 6. Beam current density as a function of radial position for five grid sets.

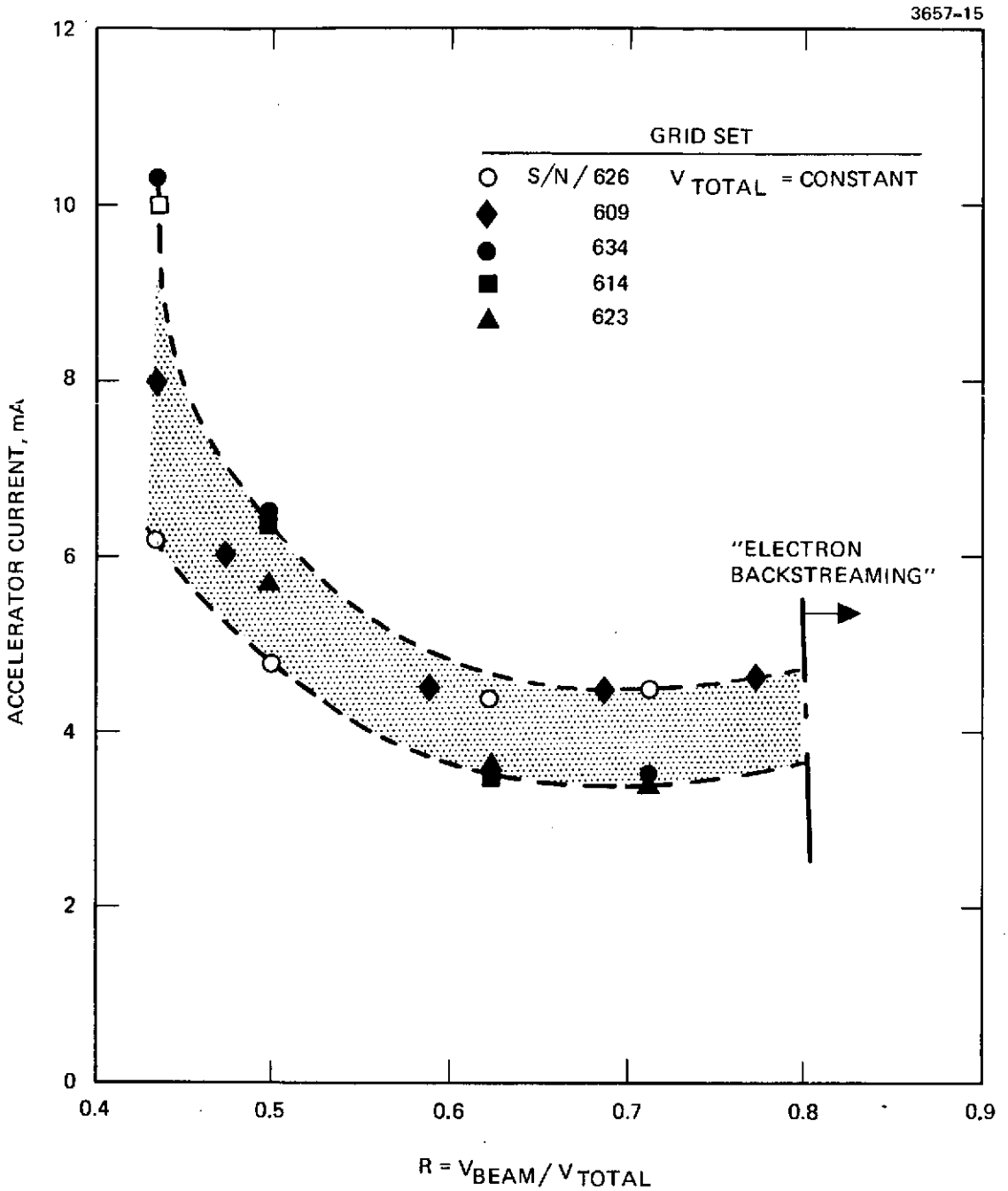

Fig. 7. Accelerator current as a function of R ratio.

In an effort to determine design criteria for ion optical systems, the data from all grid sets utilizing circular apertures were plotted in the manner shown in Fig. 8. This plot shows the current per aperture as a function of total accelerating voltage. The average perveance per hole appears to be approximately constant, dependent only on grid spacing. The data are somewhat scattered due to the variation in cold grid spacing for a given optics set, as well as the variation in grid spacing under various operating conditions.

Some general conclusions were made concerning the ion optical systems tested:

- The total voltage requirements as expected are highly dependent on grid spacing (e.g., reducing spacing from 0.08 cm to 0.055 cm on grid set 609 reduced the voltage required at 2.0 A beam current from 2.1 kV to 1.6 kV).

- At a given spacing, the thicker (0.076 cm versus 0.038 cm) accelerator grid tends to raise the total voltage.

- The average perveance per aperture is approximately a constant for a given spacing.

- Degradation of discharge chamber efficiencies occurred with the use of hexagonal aperture grid nets. However, this degradation is believed to have resulted from increased accelerator grid open area.

- Grid set S/N 609 with spacing less than 0.065 cm was found to be the most favorable of those tested in terms of perveance and discharge chamber performance. Perveance characteristics of grid set 609 are shown in Fig. 8.

In parallel with the HRL ion optical system studies, personnel at LeRC were evaluating and advancing these designs.[5] An alternate to the design of grid set 609 was recommended by the LeRC program manager. The significant dimensions of the alternate design (S/N 642 and S/N 644) are shown in Table 1. In addition, the technique of grid "compensation", to reduce thrust loss due to ion beam divergence,

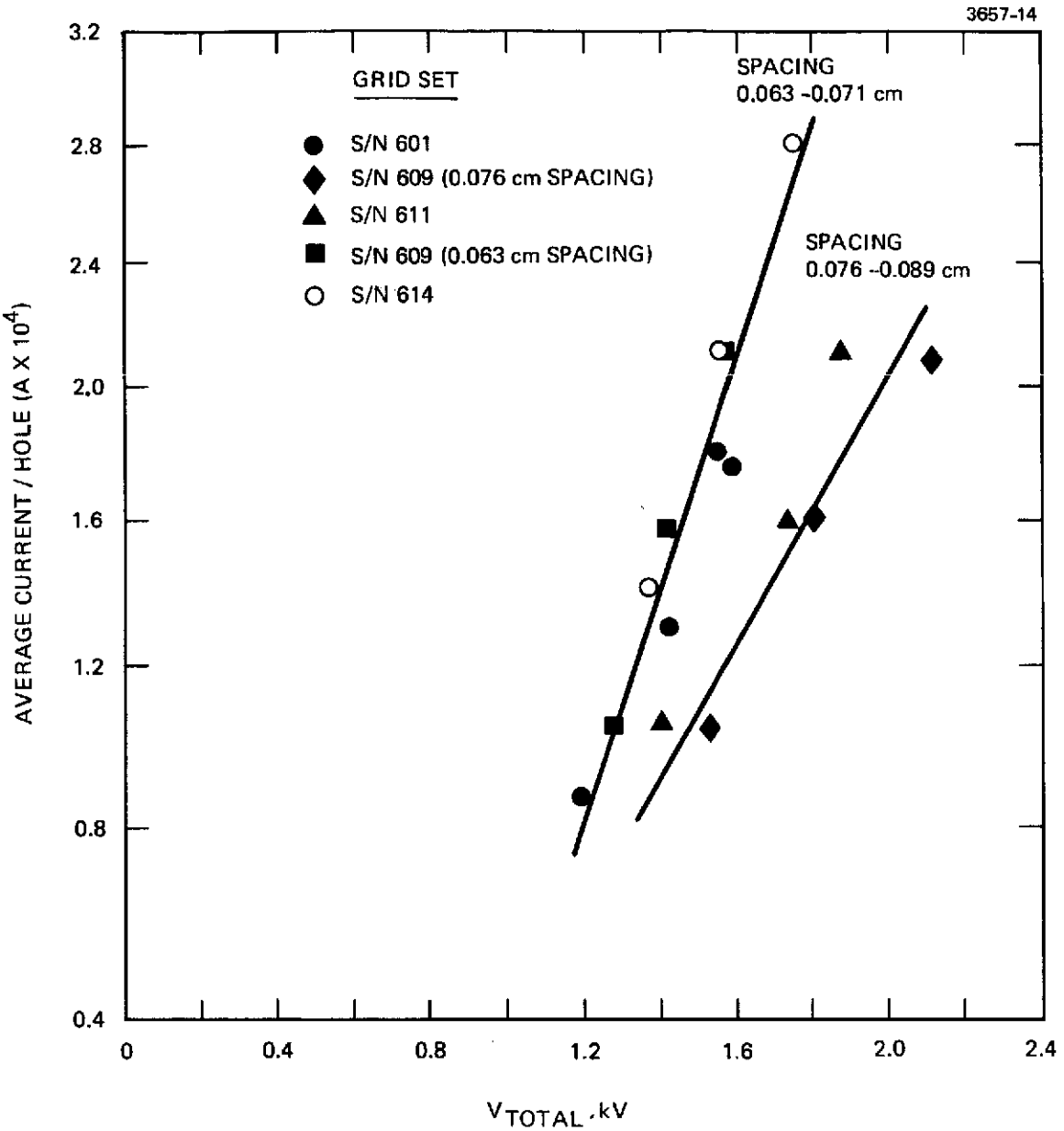

Fig. 8. Average beam current per grid aperture as a function of total voltage.

had been perfected by LeRC and by HRL under Contract NAS 3-16949. Thus, the ion optical system design adopted for the remainder of this contract and the EM thruster is that noted in Table 1, "compensated" as discussed in the following section.

2. Dished Grid Compensation

The techniques associated with dished grid compensation were developed concurrently under NAS 3-16949 and by personnel at LeRC.[4] A summary of that work is presented here to make the EM thruster development discussion more complete.

Ion thrusters with dished grids are subject to significant thrust losses due to the divergence of the ion beam.[6] This divergence is a consequence of the relative displacement in the centerlines of screen grid and accelerator apertures which results from both the geometry and fabrication technique for dished grids. Figure 9 shows the effective beamlet vectoring which results in beam divergence and associated thrust loss (see Fig. 10 for comparison of dished and flat grid beam current profiles). A change in the aperture center-to-center spacing pattern of one of the electrodes is necessary to effect a vectoring of the individual beamlets to provide paraxial trajectories. A change of less than 0.5% in the center-to-center aperture spacing will sufficiently converge the beam to eliminate such thrust losses. This change in spacing is termed "compensation".

Compensation of a dished grid set has been accomplished under this program by fabricating the screen grid with a slightly smaller center-to-center aperture spacing pattern than the accelerator. This reduction is accomplished photographically, and produces an offset as shown in Fig. 11. The offset is made so that each beamlet is deflected back parallel to the thruster axis to eliminate the divergence associated with dishing. Screen reduction is based on displacement of peripheral apertures to vector these beamlets by an angle ϕ_{max} given by

$$\phi_{max} \cong \sin^{-1} \frac{r_a}{R_a} \qquad (1)$$

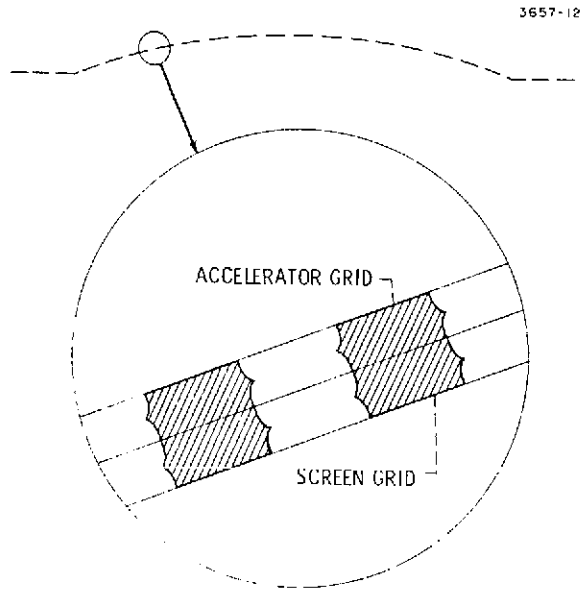

(a) AFTER HYDROFORMING AND STRESS RELIEVING.

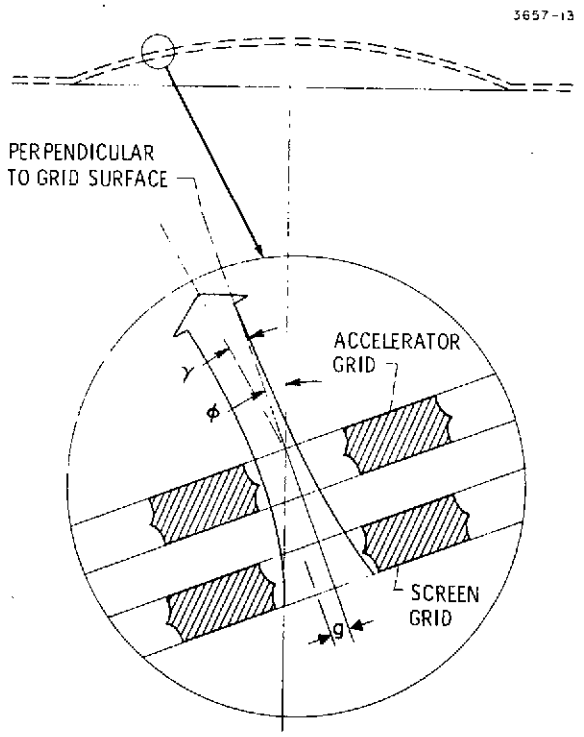

(b) AFTER SETTING GRID SPACING AND DURING OPERATION.

Fig. 9. Beamlet divergence due to aperture alignment.

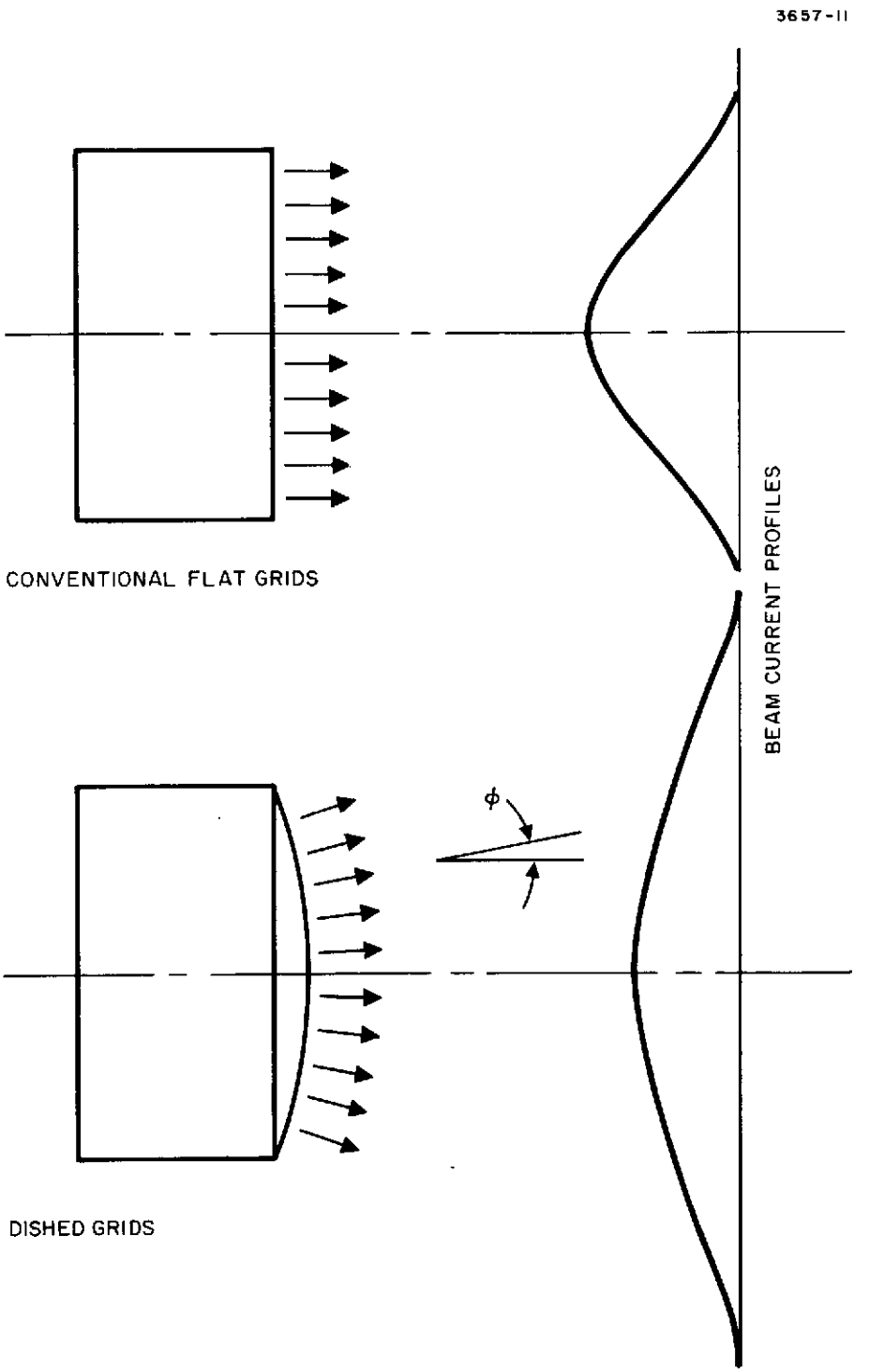

Fig. 10. Beam divergence due to spherically shaped, uncompensated grids.

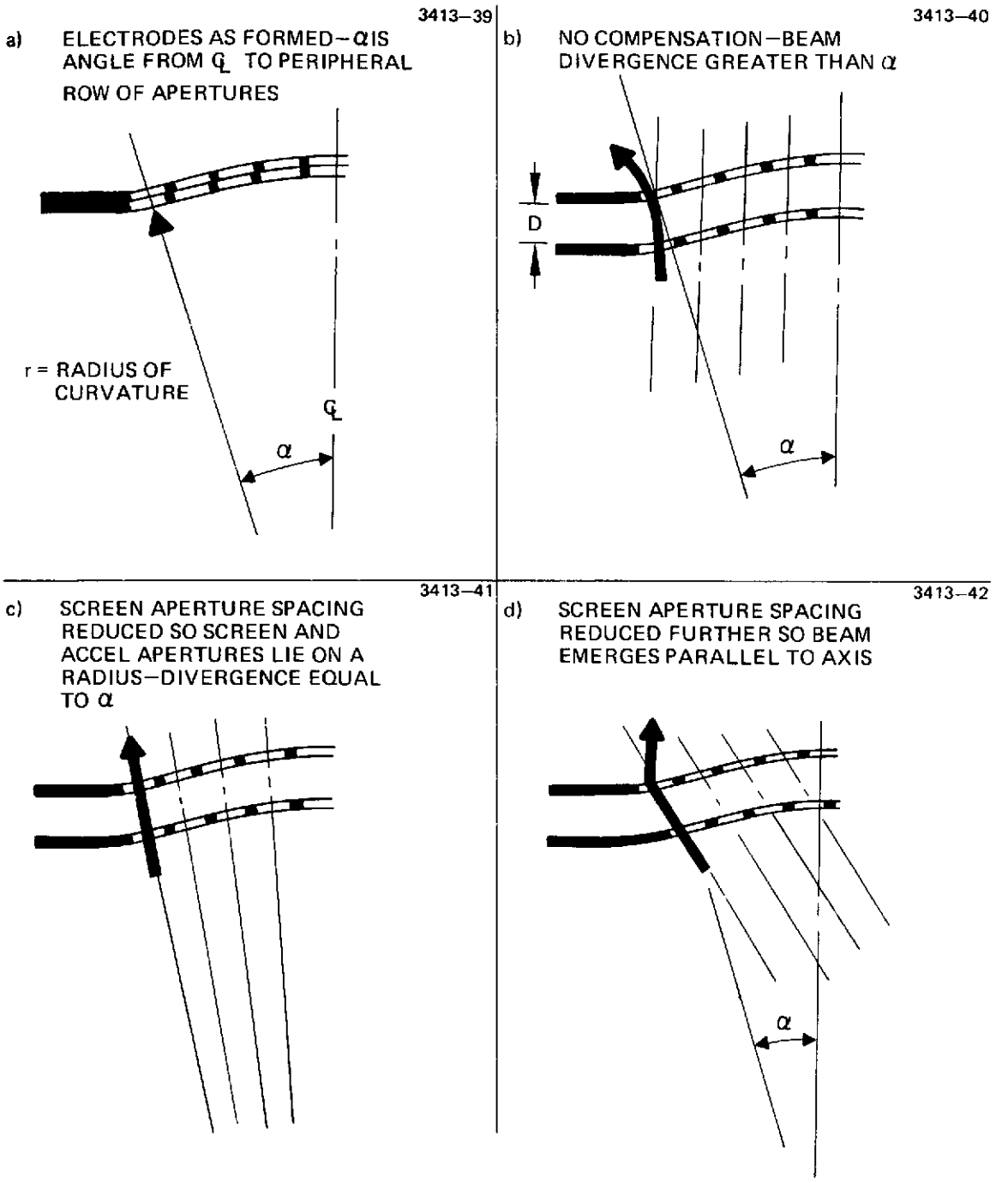

Fig. 11. Steps required to offset hole pattern to compensate for beam divergence.

where r_a is the radius of the accelerator aperture pattern and R_a is the radius of curvature of the accelerator grid. Figure 12 illustrates the percent of photographic reduction or compensation factor required for a selected aperture and grid spacing as a function of dish depth (radius of curvature). For the 2.1-cm dish depth, ϕ_{max} is approximately 17^o. The electrode aperture pattern adopted for the EM thruster produces direct interception at angles slightly greater than ϕ_{max}. A screen reduction of 0.43% compensates the trajectories for grid curvature. To allow for some misalignment in assembly procedures, a compensation of 0.4% has been specified.

3. Electrode Mechanical Stability

The interelectrode spacing is important since it strongly affects the perveance of the ion optical system, the voltage breakdown limits, and (to some degree) the direction and location of the thrust vector. For the dished grid approach the screen and accelerator are supported only at the edge and are thus free to move relative to each other when subjected to thermal or mechanical stresses.

The lower limit on dish depth is set by the requirement to avoid instabilities under vibration loading conditions. In the present program this limit was estimated experimentally by fabricating grids with dish depths as low as 1.3 cm. Such grids were believed to be marginal for withstanding the expected dynamic loads. A detailed analysis was not performed due to the time consuming nature of such a problem. However, a thermal analysis was performed to determine the optimum dish depth for a given compensation factor. It was found that under operating conditions the grids do not displace enough to require modification of the dish depth calculated for cold grids. In order to verify the mechanical stability of the electrode assembly under thermal stress the thruster components must be heated to their operating temperature in a vacuum environment both to insure that the correct temperature distribution is obtained, and to prevent damage to sensitive components. Thus, it was concluded that the grid spacing must be monitored while the thruster is operating.

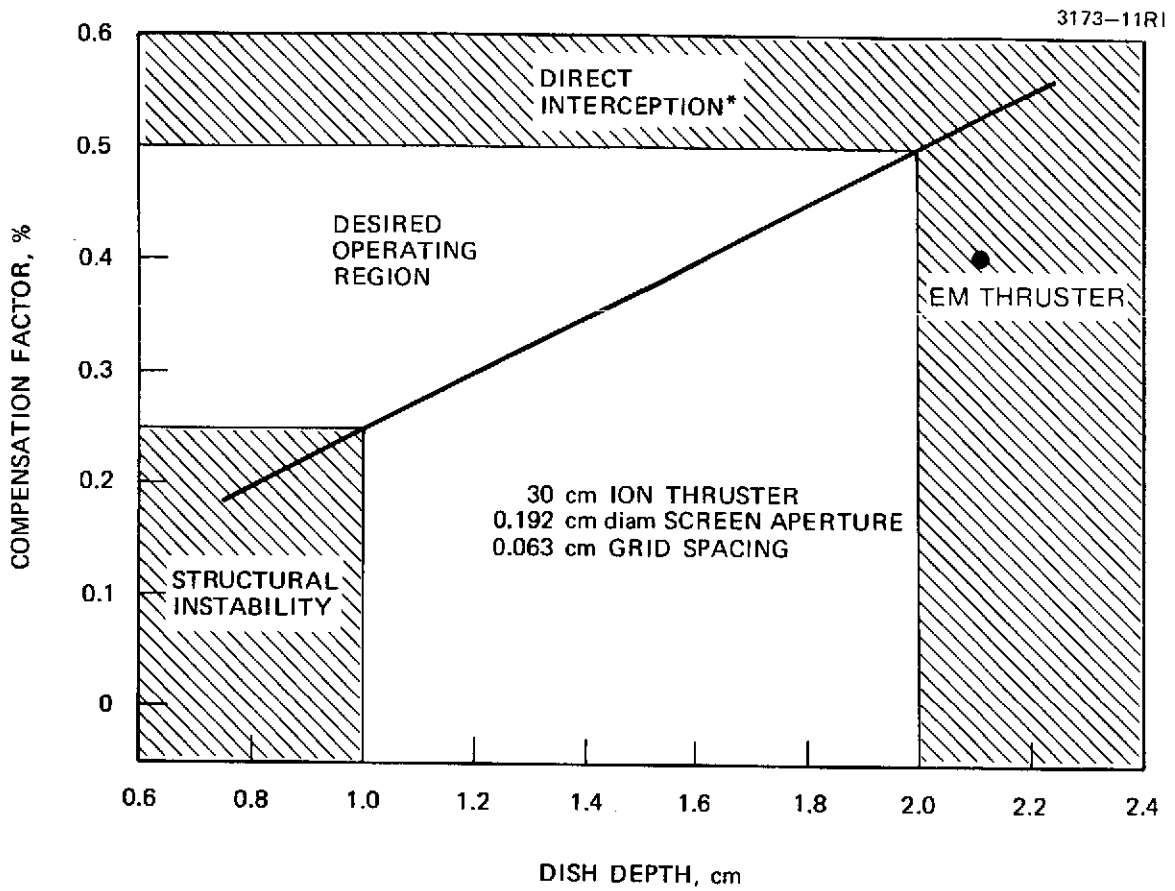

Fig. 12. Dished grid compensation as a function of dish depth.

A visual or optical observation is best suited to overcome the difficulties associated with the vacuum environment, the high voltages, and the high temperatures that accompany thruster operation. Laser interferometric techniques have the accuracy required for this application, but were rejected as unreasonably expensive to develop for this specialized situation. For these reasons, an alternate method of measuring grid spacing was investigated which involves the photographing of operating thruster ion optics in such a manner that the grid spacing can be determined from the photographs.

This technique appears to be advantageous for several reasons. No thruster modifications are necessary, testing is unaffected, little modification of the test facility is required, and the measurement can be made by one person.

When the grid set is photographed, a picture similar to that shown in Fig. 13(a) is obtained. This and all other photographs were taken through a 1400-mm Questar telescope with a Nikkon F camera and Polaroid film back using ASA 4000 type 107 Polaroid film at 1-s exposure.

From geometrical arguments illustrated in Figs. 13 and 14, it can be shown that the grid spacing d is given by

$$d = \frac{a + s}{2 \tan\theta} + \frac{g}{\tan\theta} - \frac{Xa}{A \sin\theta} - t_a - t_s \qquad (2)$$

where a and s are the accelerator and screen grid aperture diameters, t_a and t_s are the respective grid thicknesses, X and A are measured from the photograph, and θ is the angle to the grid surface normal at which the photograph is taken. The offset g can be determined from eq. 1.

This estimated offset and the measurements obtained from the photographs were used by a computer program to calculate the grid spacing. In practice X and A are measured, ϕ is known from marks placed on the accelerator grid, θ is computed, and g is calculated. If

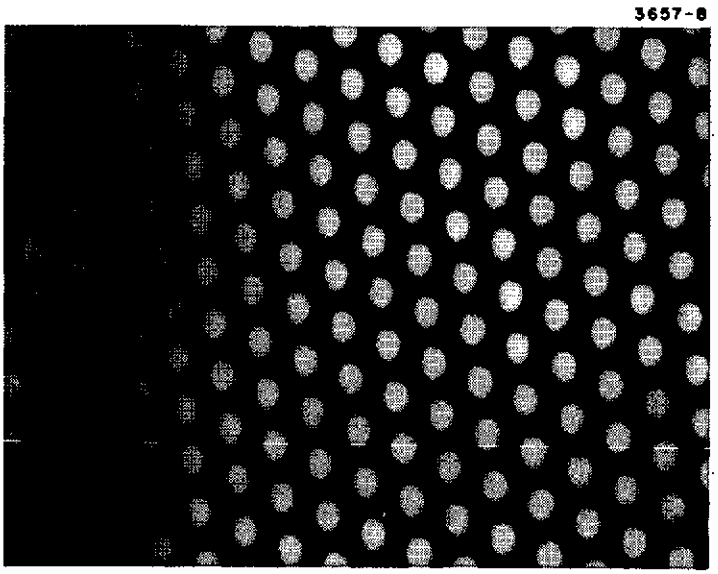

(a) Grids using Questar (1400 mm lens).

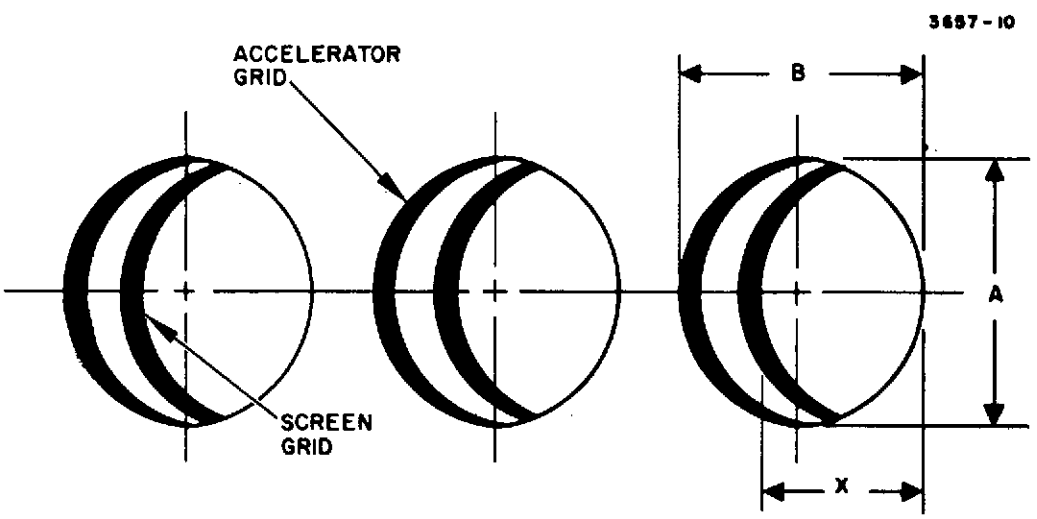

(b) Idealized photograph.

Fig. 13. Photographic definition of grid apertures.

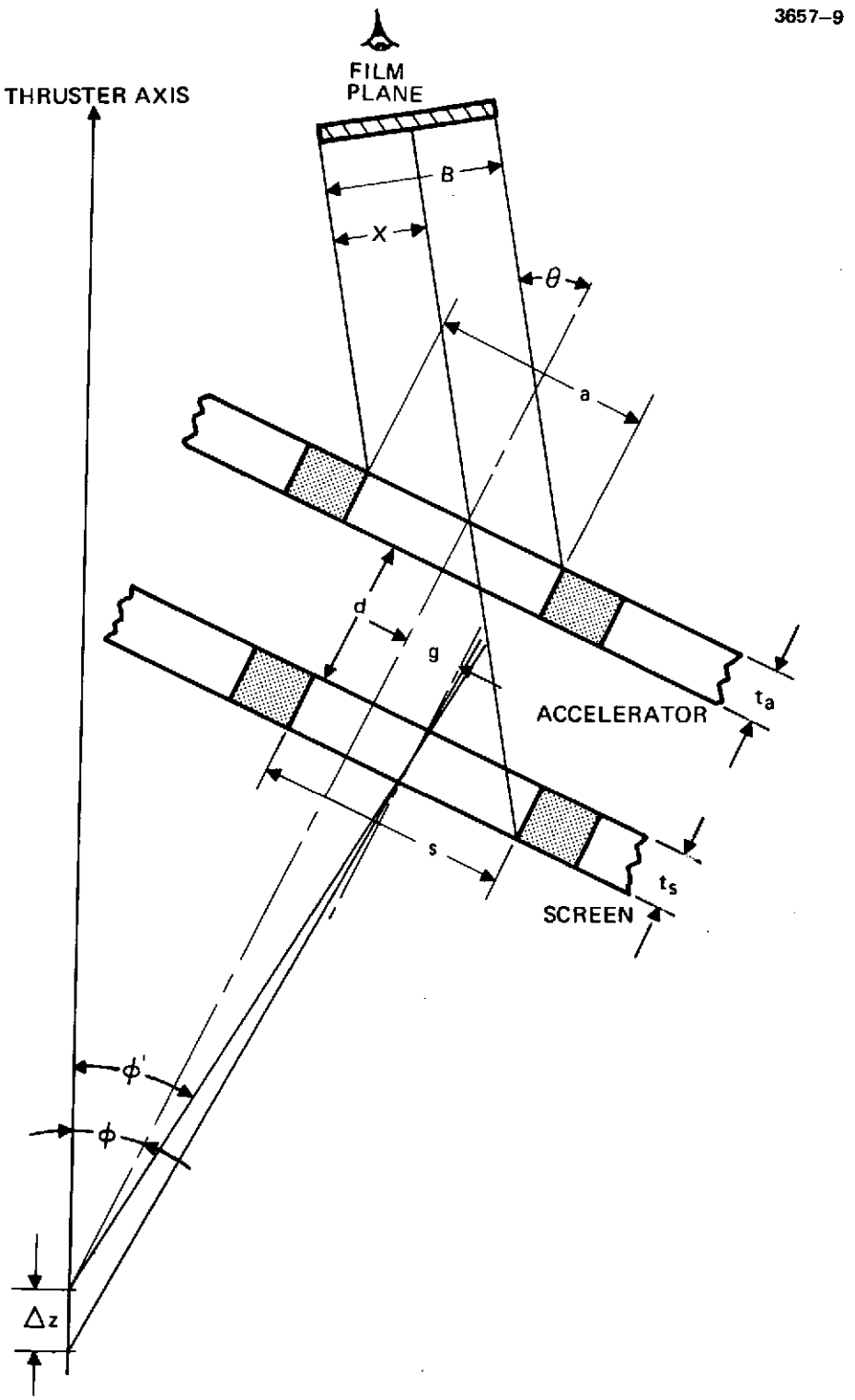

Fig. 14. Definition of dimensions for photographic determination of grid spacing.

the actual accelerator aperture diameter is divided into the measured diameter (A/a) a magnification factor for the photograph is obtained.

GRID is a computer program written in FORTRAN language and implemented on the GE-265 time sharing system. It is approximately 4500 characters in length and takes 15 s to perform this analysis. All physical characteristics of 35 sets of ion opitcs are cataloged in a disk file designated GRDATA which is accessed by GRID, through the 3 digit S/N number. Four subroutines (GRDSET, GTHERM, GSPACE, GAMMA) constitute much of the program and carry out the majority of thc computation.

During initial testing the resolution of the photographs proved to be inadequate for the desired degree of accuracy. The poor resolution was attributed to the poor optical characteristics of the Pyrex chamber port windows, inadequate interior lighting and excessive camera vibration.

To improve the data a high quality Water White Optical glass window was purchased. A high intensity quartz studio type flood light was installed in the chamber to provide greater illumination and shorter exposure times. Unnecessary pumps and equipment were turned off during the photographing and a more stable camera mount was implemented.

Results of measurements made on operating thrusters are shown in Tables 2 and 3. The radial variation in grid spacing for operation at 1.5 A of beam current and a screen voltage of 1.3 kV is shown in Table 2. These data were obtained with grid set S/N 609. The variation in centerline grid spacing as a function of thruster power level is shown in Table 3 for grid set S/N 611. It is believed that these measurements are correct to within 10% of the true spacing.

4. Selected Ion Optical System

As a result of the tests performed under Contract NAS 3-16528, NAS 3-16949 and NAS 3-15523, and concurrent work at NASA LeRC, an ion optical system design was selected for the 800-series EM thruster. The pertinent dimensions are identical with grid sets 642 and 644 in Table 1, except that 0.4% compensation was selected

TABLE 2

Grid Spacing Determined Optically – Radial Variations

	Distance from Center, cm			
Spacing, cm	0.0	5.4	8.9	13.3
Measured Cold Spacing	0.081	0.071	0.074	0.089
Measured Operating Spacing	0.061	0.066	0.074	0.086

T1448

TABLE 3

Grid Spacing Determined Optically – Variations with Beam Current

	Beam Current, A		
Parameter	1.0	1.5	2.0
I, A	5.5	8.3	11.0
V_d, V	38.0	40.0	40.0
V_b, V	1000.0	1000.0	1000.0
Interelectrode Grid Spacing[a] (cm)	0.075	0.074	0.065
Grid Spacing[b] (cm)	0.077	0.074	0.071

[a]Grid spacing calculated by "GRID" from photographs.

[b]Grid spacing calculated by "GRID" from assumed model.

Note: Grid spacing measurements were made at center of optics along thruster axis. Spacing in this region was measured to be 0.079 cm before operation.

T1449

for 800-series thrusters. Typically, a screen-to-accelerator spacing of about 0.066 cm (0.061 cm minimum to 0.071 cm maximum)is recommended. A dish depth of 2.1 cm is used on both grids. The selected grid mounting design, using a titanium support ring is discussed in the next section. Testing of thruster S/N 702-A (i.e., the 800-series prototype) used the titanium support ring.

a. Perveance – Typical perveance characteristics of the selected ion optical system design are shown in Fig. 15. The "minimum voltage", determined as discussed previously, for the 700/800-series grid design is in the range of 1100 to 1200 V for a beam of 2.0 A. The minimum voltage varies slightly among grids sets due to slight differences in material properties, assembly tolerances, and uncertainties in thruster operating parameters.

A comparison of perveance measurement methods is illustrated in Fig. 15. The normal method maintains constant discharge current and allows the beam current to vary with total voltage. The alternate method maintains constant beam current by adjusting of the discharge current. The constant beam current method probably provides a more accurate evaluation of the ion optical system capability.

b. Results of Dishing and Compensation – As noted previously, "dishing" was provided to obtain the grid stability required to survive launch vibration. "Compensation" was then necessary to direct ion beamlets, originating on the curved surface, in an axial direction. The 0.4% compensation selected for the 800-series thruster provides beamlet redirection without causing direct ion impingement on the accelerator. However, the individual beamlets have an inherent divergence due to ion thermal motion. All but this small divergence is corrected by compensation. The thrust loss correction factor required (see Section IIIA) for the 700/800-series design is about 0.99%. This value is equivalent to an average beam divergence angle of about 8°.

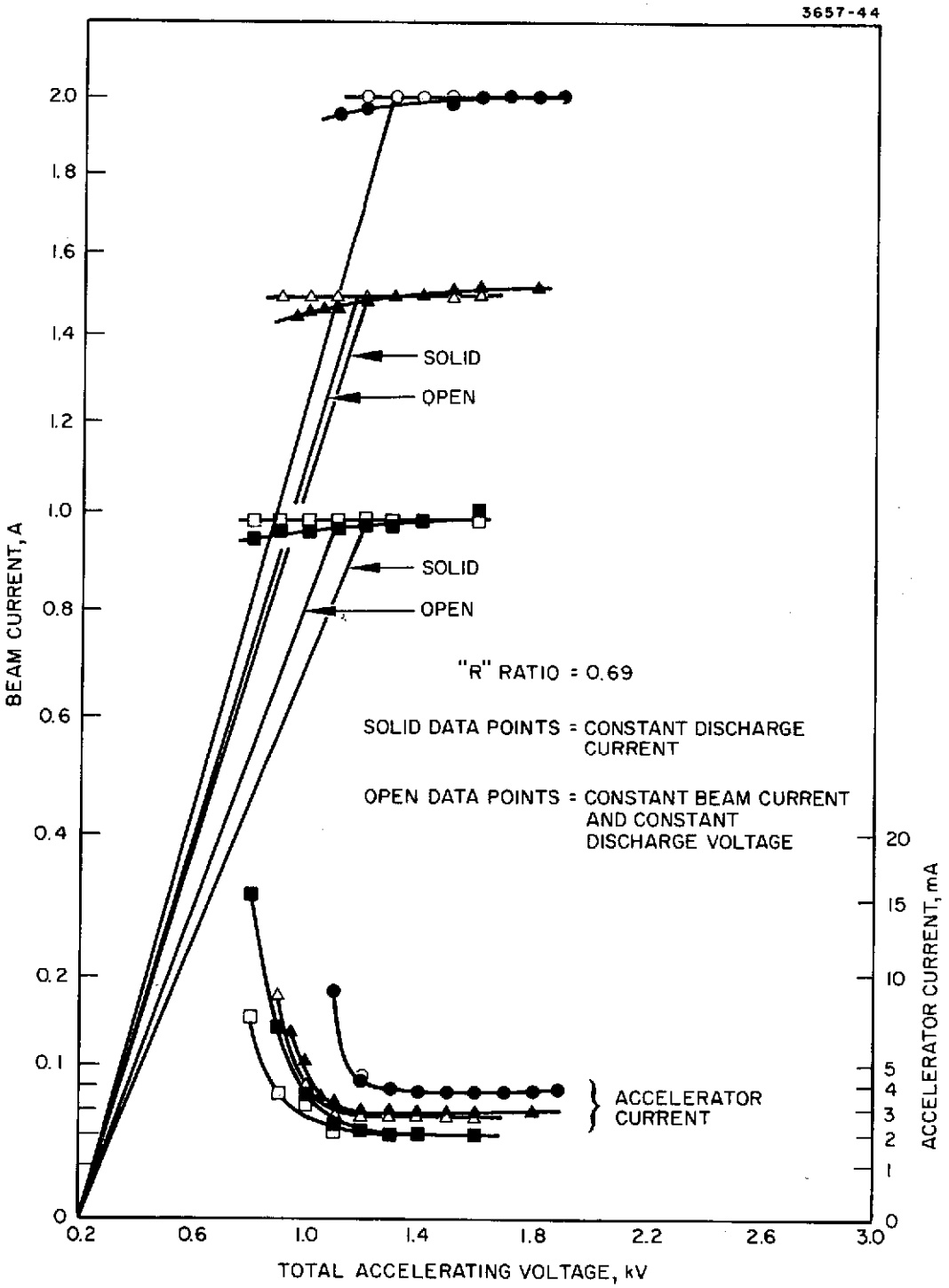

Fig. 15. Perveance characteristics for 700/800-series thruster ion optical system.

5. Ion Optical System Mechanical Design

The ion optical system is a complicated assembly which requires precise mechanical alignment and stability to assure proper electrical performance and long operating lifetime. It consists of two thin molybdenum plates (0.050-cm and 0.038-cm thick), 35 cm in diameter and spaced 0.05-cm apart. The screen grid is perforated with $\sim 10^4$ apertures of about 0.19-cm diameter through which the ion beam and thermal radiation from the discharge chamber pass. During operation, the heat load (which is greater at the center than the periphery), coupled with the relatively poor thermal conduction of the perforated structure, causes the center of each grid to rise from 50°C to 100°C above the temperature of the edge. Thermal stresses, therefore, naturally cause a dishing, or "oil canning" effect.

Several support structures including interelectrode supports were evaluated in an attempt to produce a stable configuration with flat electrodes; in all cases these were unreliable. The final solution has been to hydroform the electrodes into a dished configuration (see Fig. 5). While the fabrication and assembly of this subsystem is still very critical, it is now possible to reliably and reproducibly fabricate ion extraction systems of this design. The final alignment and spacing procedure has been empirically established so that the relative positions of the screen and accelerator electrodes are correct at operating temperature.

a. Grid Fabrication Procedure – The screen and accel electrodes are fabricated from low carbon arc cast molybdenum sheets. The blank sheets are first imprinted on both sides with photoresist by Buckbee Mears Corporation. The printed blanks are returned to HRL to be formed in the special fixture and large hydraulic press shown in Fig. 16. The accelerator and screen electrodes are dished by simultaneous hydrostatic forming at a clamping force of 9800 psi around the grid periphery. The press is instrumented with pressure gauges, heater controls, thermocouples, and a digital readout which measures the depth of the formed dish while the process takes place.

M8550

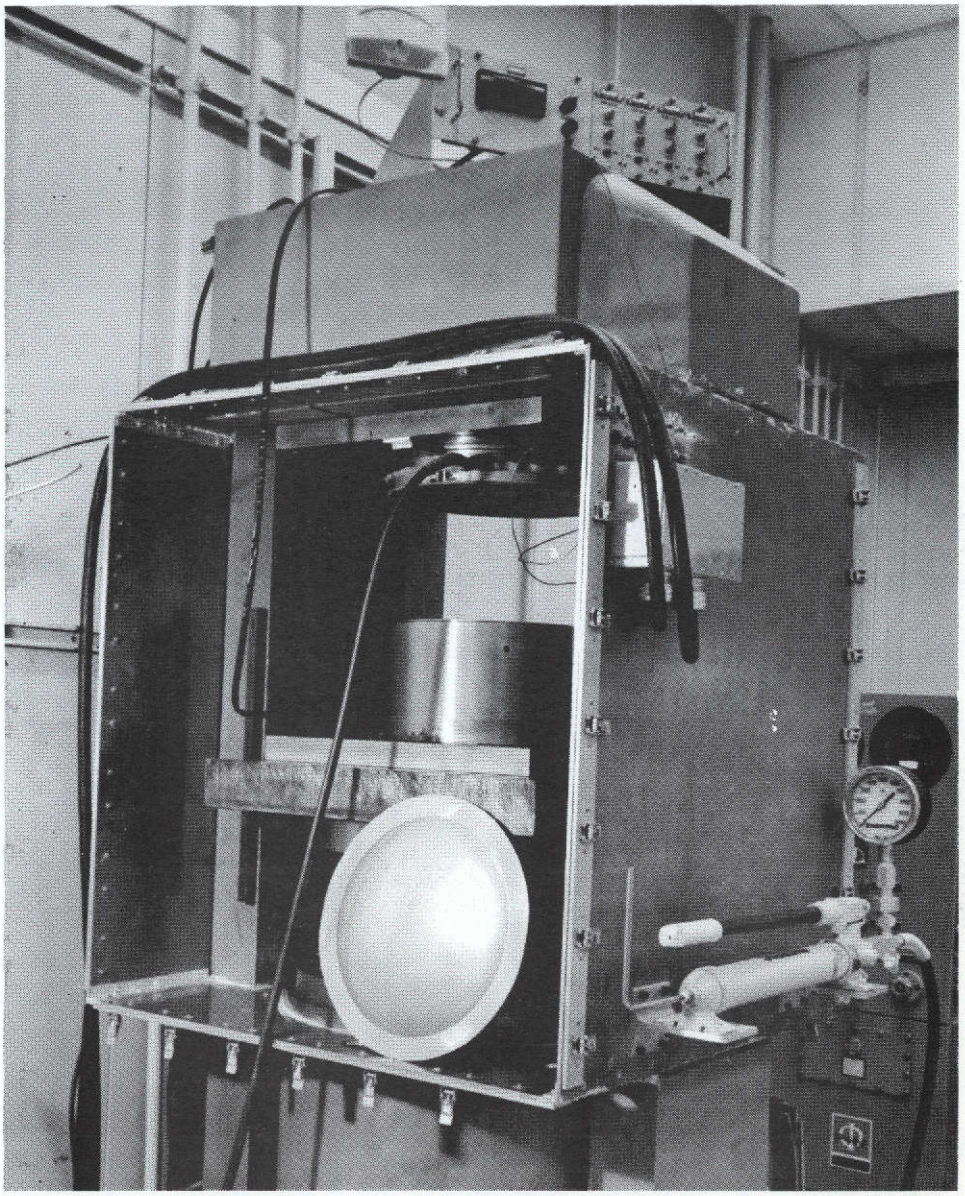

Fig. 16. 30-cm dished grid hydroforming press and fixing.

The grids are formed by pumping hydraulic oil from a separate system into the top of the forming fixture until the desired free form shape is achieved.

Since molybdenum is known to be more readily formed at temperatures above the ductile-brittle transformation temperature of ~100°C, heaters are provided to warm the forming fixture and grids in the vicinity of the forming process. After the grids are formed, they are returned to the vendor for final etching of the hole pattern.

The grids are then stress relieved in the fixture shown in Fig. 17. The grid set is carefully centered in the fixture and clamped by twelve 1.27-cm bolts at the outer edge. The unclamped center plug is weighted with a 34 kg molybdenum mass, and the entire assembly is loaded in a large vacuum furnace and the fixture is fired in vacuum at 1000°C for three hours.

After stress relieving, the grids are set up in the assembly fixture, shown in Fig. 18, which aligns the hole pattern with respect to the grid stiffening rings. Four 0.292-cm diameter holes are drilled in each grid for subsequent alignment on the mounting structure and the stiffening rings are lightly spotwelded in position with precut 0.005-cm thick Silcoro brazing material in place. The grid assemblies are then loaded into a special brazing fixture and the unit is fired in a hydrogen atmosphere at 850°C for one hour. This completes the fabrication of the electrode assemblies.

b. Main Support Ring, 400 to 700 Series Thruster – The ion optical system main support ring fabrication technique is critical in order to achieve a flat, structurally sound, lightweight base on which the grids are mounted. In the 400 to 700 series optical system the ring is fabricated by welding two thin hydroformed rings together with a cross section, as shown in Fig. 19. The ring assembly is provided with threaded inserts to which the screen and accelerator mounting brackets are attached. Stress relieving between heavy flat ground plates at 1000°C and final machining of the top and bottom surfaces provides a flat mounting plane.

M10026

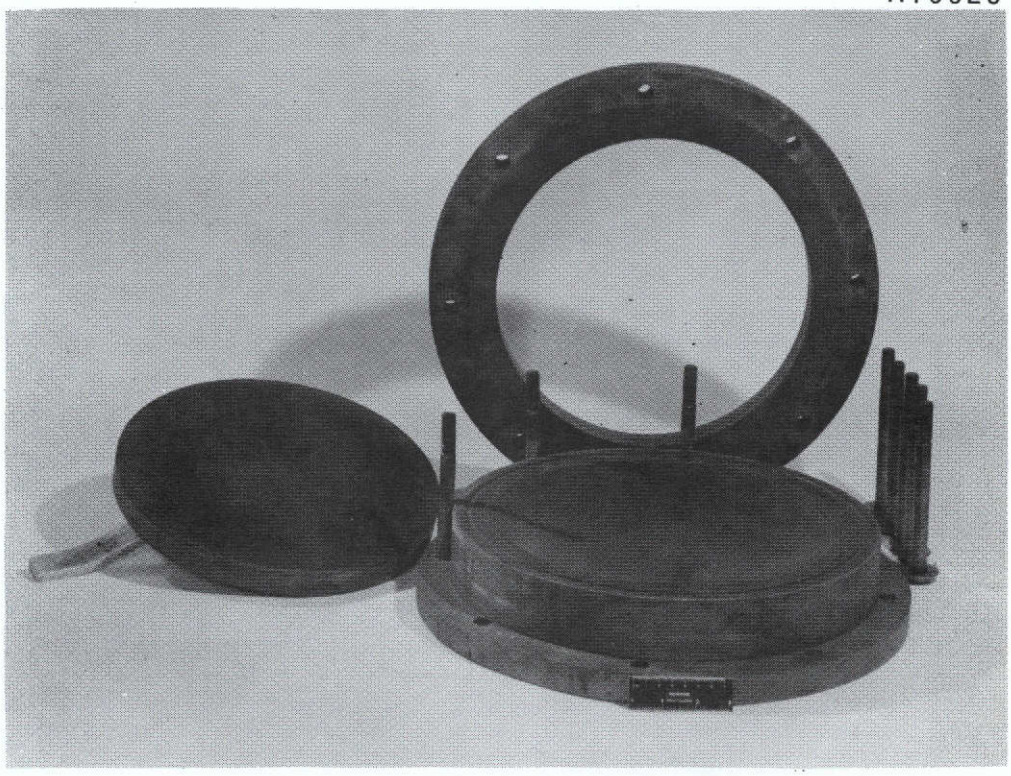

Fig. 17. Dished grid stress relieving fixture.

M10028

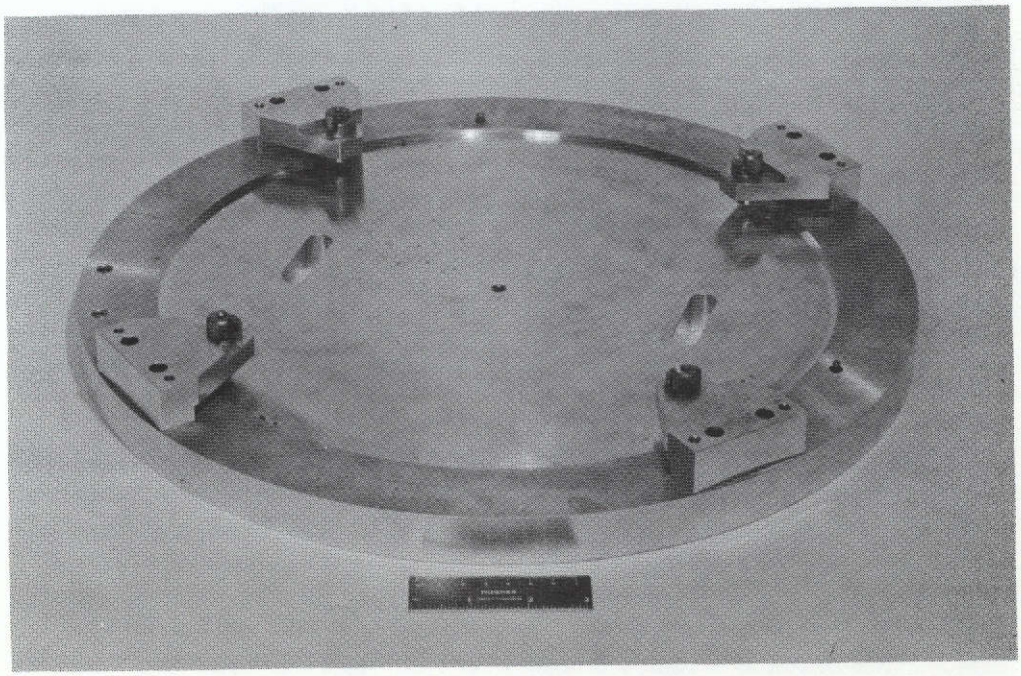

Fig. 18. Dished grid alignment fixture.

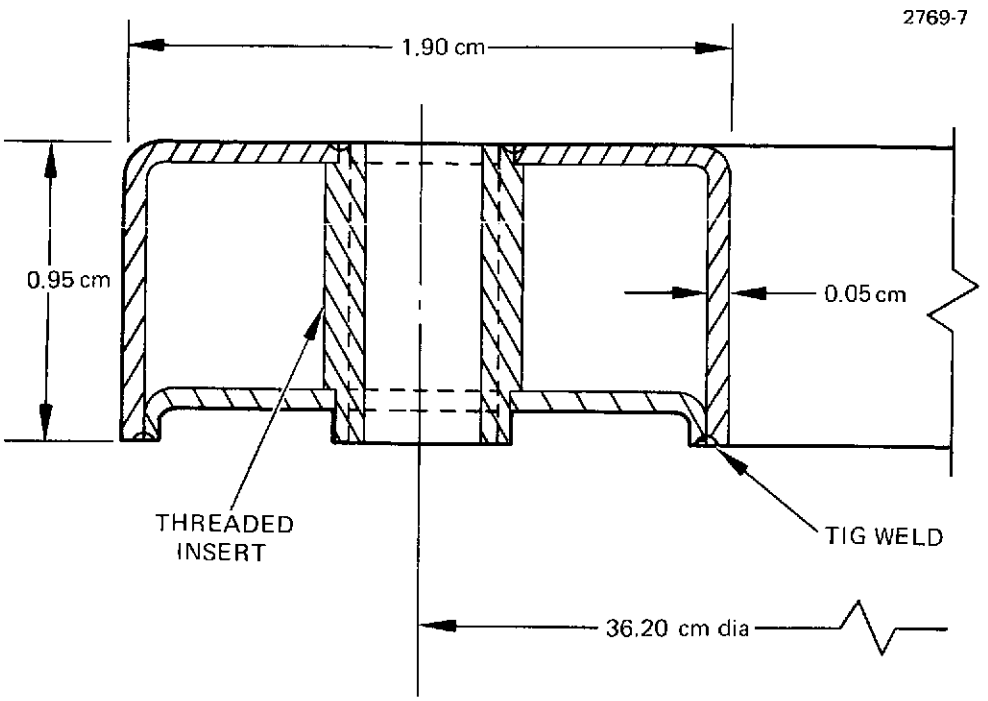

Fig. 19. Cross section of electrode support ring for 300-700 series thruster.

c. Main Support Ring, 800-Series Thruster — Although the 300 to 700 series optics support ring provided relatively good structural characteristics, an improved design was developed for the 800-series thruster. The new design illustrated in Figs. 20 and 21, reduces the complexity of assembly, improves grid flatness, and provides more rigid structural properties.

The support ring is fabricated from commercially pure titanium plate. After rough machining of the ring, the 12 gussets are welded into position. Final machining, with the rigidity added by the gussets, allows accurate parallelism between the screen and accelerator mounting surfaces, as well as precision flatness to be maintained. The solid cylindrical web design eliminates the screen grid mounting brackets and provides a "sealed" discharge chamber.

The titanium support ring design uses 0-80 screws to mount the screen grid directly to the machined flange. The accel grid is mounted to a molybdenum grid support ring in a similar manner. The grid support ring is then attached to the titanium ring through 12 shielded insulators. This technique eliminates the time consuming brazing, heat treating, and aperture alignment processes used in the previous design.

The assembly shown in Fig. 21 was developed as part of a Hughes funded program. Shake testing of this optics assembly was conducted under Contract NAS 3-18334 to verify its suitability for the 800-series thruster. This first assembly was also used in the vibration test of Thruster S/N 702-A (Section III).

d. Accel Insulator Fabrication — The accel insulators are ground from prefired Wesgo AL300 high purity alumina and the ends are metallized by conventional techniques at the Electron Dynamics Division of Hughes Aircraft Company, Torrance, California. The end caps are then brazed with OFHC pure copper in a hydrogen atmosphere. The insulator assembly is then ground flat on each end, ultrasonically cleaned, and grit blasted with high purity alumina (Al_2O_3) prior to final assembly. The grit blasting unit used for this operation was purchased

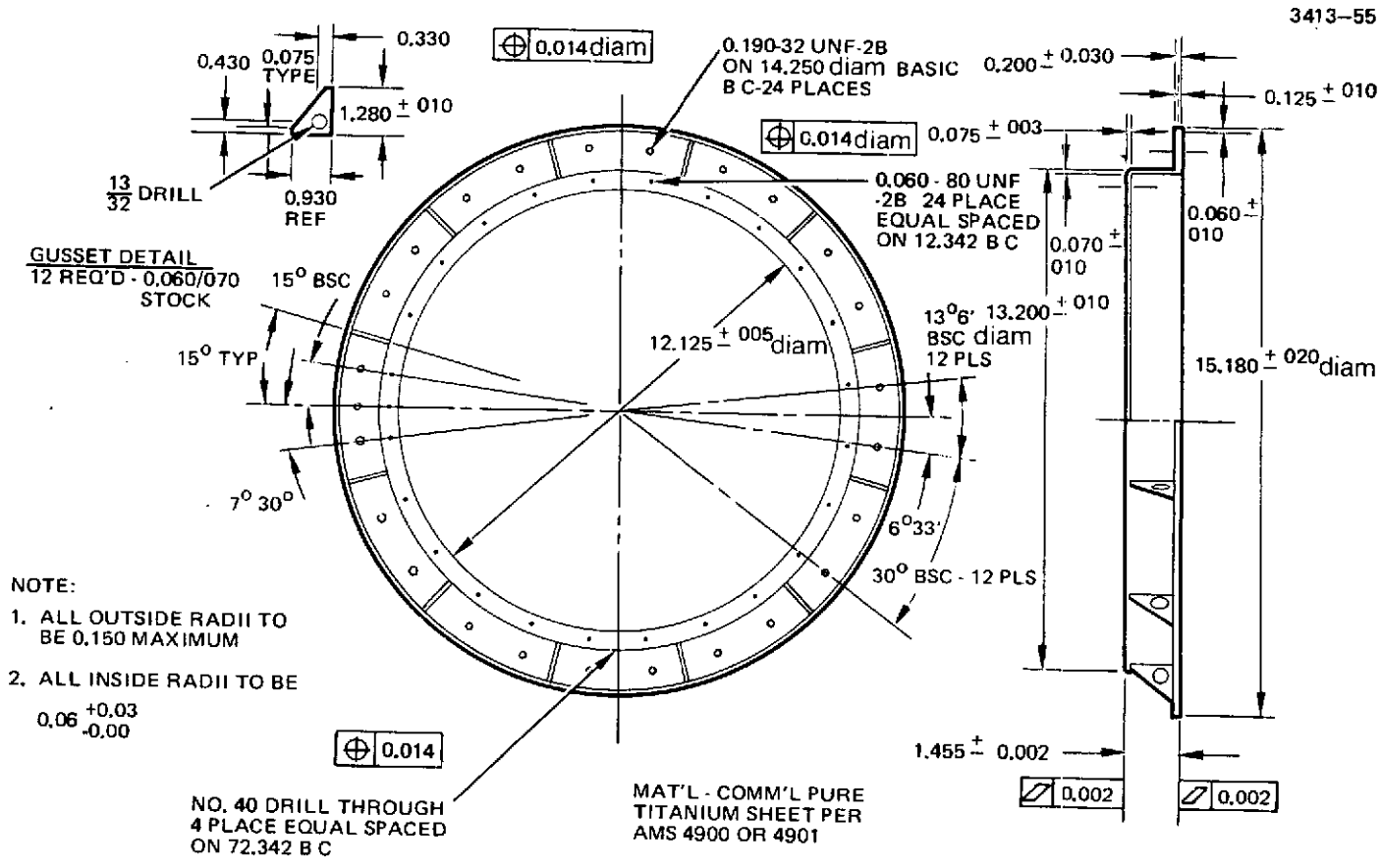

Fig. 20. Electrode support ring design for 800 series thruster.

M10403

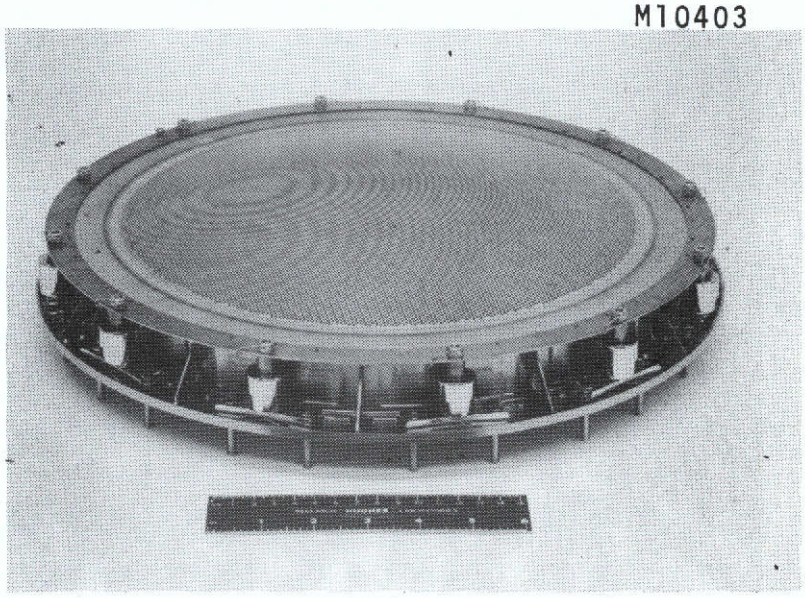

(a) Downstream view

M10404

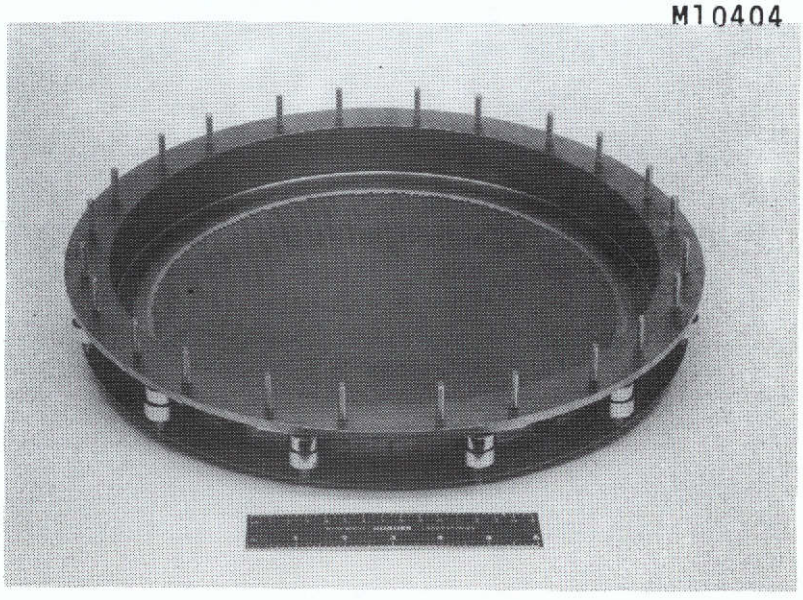

(b) Upstream view

Fig. 21. Ion optical system assembly using titanium support ring.

especially for this operation and is also used for final cleaning of the high voltage isolators of the MIV and CIV assemblies.

e. Ion Optical System Final Assembly – In the final assembly of the ion optical system it is critical to assure that the grids are attached to the mounting structure in a stress-free condition. Such a condition is necessary so that thermal stresses placed on the assembly during normal operation will not cause shorting or unpredictable performance. Accurate grid alignment and spacing is essential to long-term stability and lifetime. The grid mounting planes are carefully checked for flatness and uniform height at each mounting point prior to attaching the screen and accelerator assemblies. These surfaces are required to be flat within 0.005 cm for successful grid performance. Numerous measurements are taken at each assembly step and recorded in the assembly log book. Finally, grid spacing is measured at several points across the surface and recorded on a data sheet as shown in Fig. 22.

f. Bench Checkout Procedure – A thermal simulator was constructed to examine the structural integrity of the grids during bench testing. This simple device consists of a series of flat circular electrical heaters arranged concentrically, similar to those of an electric stove element. These were placed inside an insulated cylinder large enough to hold the electrode system. By independently controlling the power to each ring a wide range of thermal conditions can be simulated. Test temperatures are measured either with attached thermocouples, contact thermocouples, or estimated from precalibration of the thermal simulator. Electrical properties are typically monitored during the test with an electronic "megger" (1000 V dc) which reads to 1000 MΩ yet does not damage the grids under short circuit conditions.

B. Cathodes

Early in the program, a significant amount of work was performed to evaluate cathode designs and to identify the role of oxide

30 cm OPTICS ASSEMBLY RECORD
SCREEN ACCELERATOR SPACING CHART

DATE: _____
TECH: _____

MOUNTING RING ASSEMBLY S/N _____
ACCELERATOR ELECTRODES S/N _____
NOTES: _____
_____
_____

SCREEN ELECTRODES S/N _____
NOTES: _____
_____
_____

TYPE _____
DRAWING NO. _____
APERTURE dia _____
SPACING CTR/CTR _____
THICKNESS _____

DRAWING NO. _____
APERTURE dia _____
SPACING CTR/CTR _____
THICKNESS _____

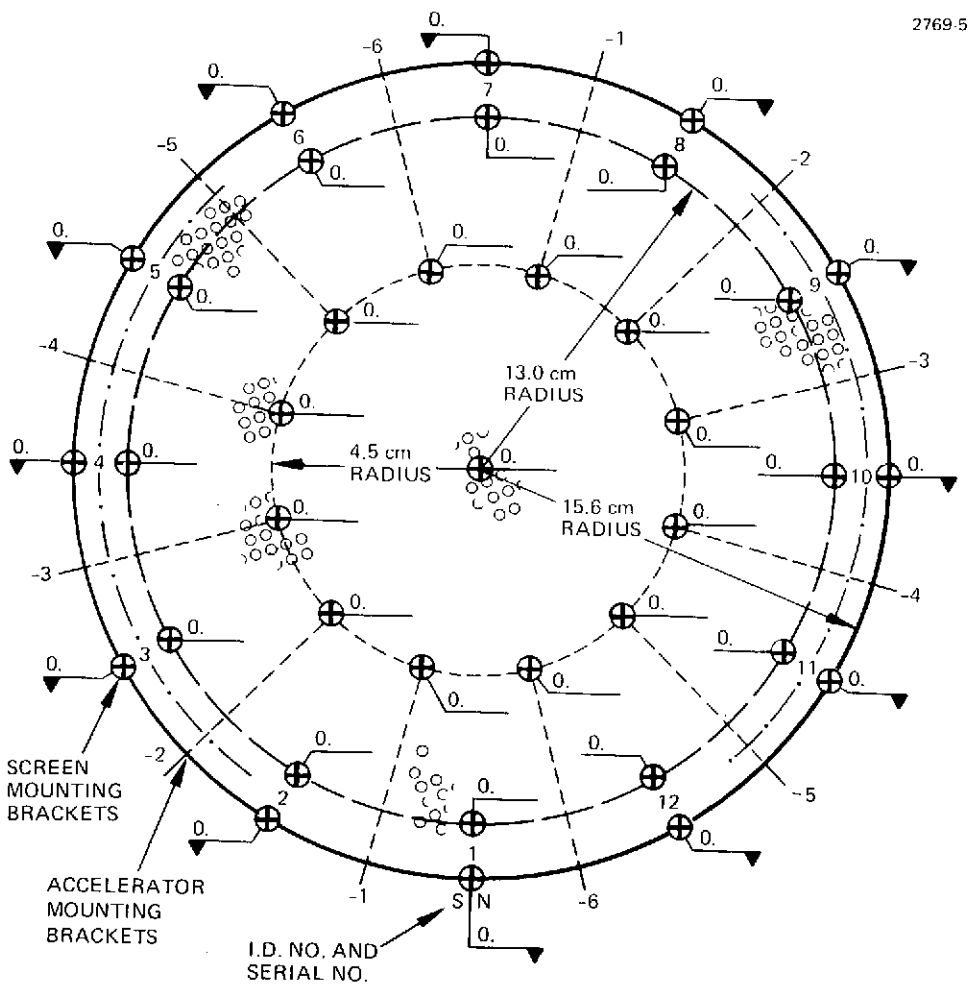

Fig. 22. Grid spacing data sheet.

coatings in thruster cathode operation.[7] This work provided insight into cathode operation, insert design, and heater design. A relatively detailed description of several parametric cathode studies is presented in Appendix A.

Based on the work discussed in Appendix A, and work performed concurrently at NASA LeRC,[8,9] a cathode design for the EM thruster was selected. The thermal criteria used for cathode designs are: (1) tip temperature of 1100°C maximum, (2) insert temperature of 850°C maximum and 600°C minimum, (3) main cathode input power of 75 W up to ignition and, (4) neutralizer cathode input power of 50 W up to ignition.

A thermal analysis of the cathode showed that the heat loss is predominantly by radiation from the incandescent tip, with conduction down the tube playing a minor role. Therefore, it is possible to control the operating temperature range by adjusting the radiating area of the tip. The thermal profile of the main cathode final design is illustrated in Fig. 23 for startup and operating conditions. The axial position of the insert is chosen so as not to exceed the maximum insert temperature criterion. The heat shields are necessary to improve the heater efficiency in the startup mode.

The hollow cathode assembly, shown in Fig. 24, employs a plasma or flame sprayed heater configuration (the latest EM thruster components are flame sprayed). The first step in the fabrication is to apply a 0.013-cm thick tungsten coating to the heater area of the cathode tube. A 0.025-cm thick Al_2O_3 coating is then sprayed over the tungsten. Two 0.013 cm by 0.075 cm Mo/Re straps are electron beam welded to the tube and the heater coil is attached by electron beam welding (EBW) to the straps and heater lead as shown in Fig. 24. The heater lead and clamp is then OFHC copper brazed to the tube and the final coating of alumina is sprayed to a thickness of about 0.025 cm. The final assembly steps depend on whether the cathode is to be used as a main cathode or as a neutralizer cathode.

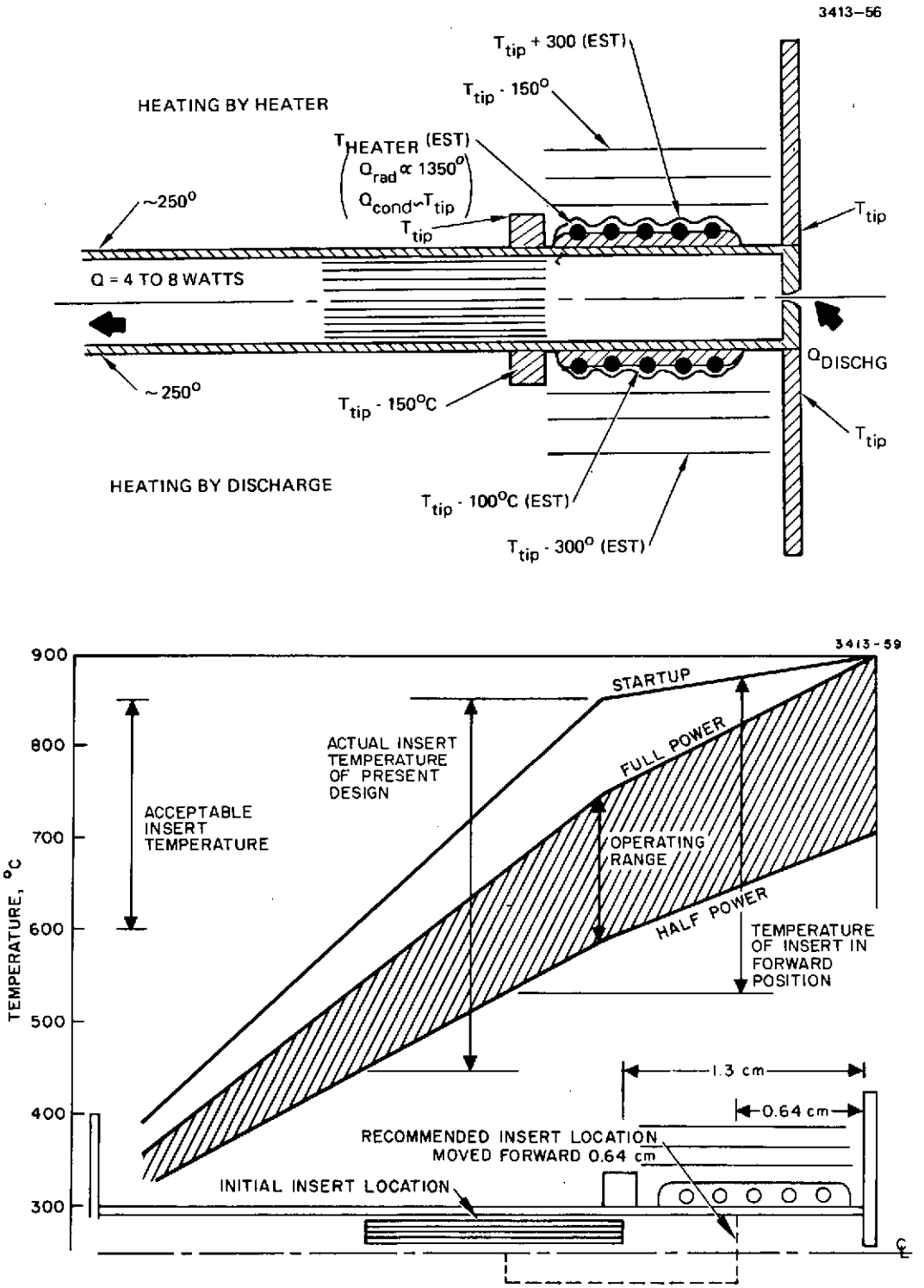

Fig. 23. Cathode thermal model and predicted temperature profiles.

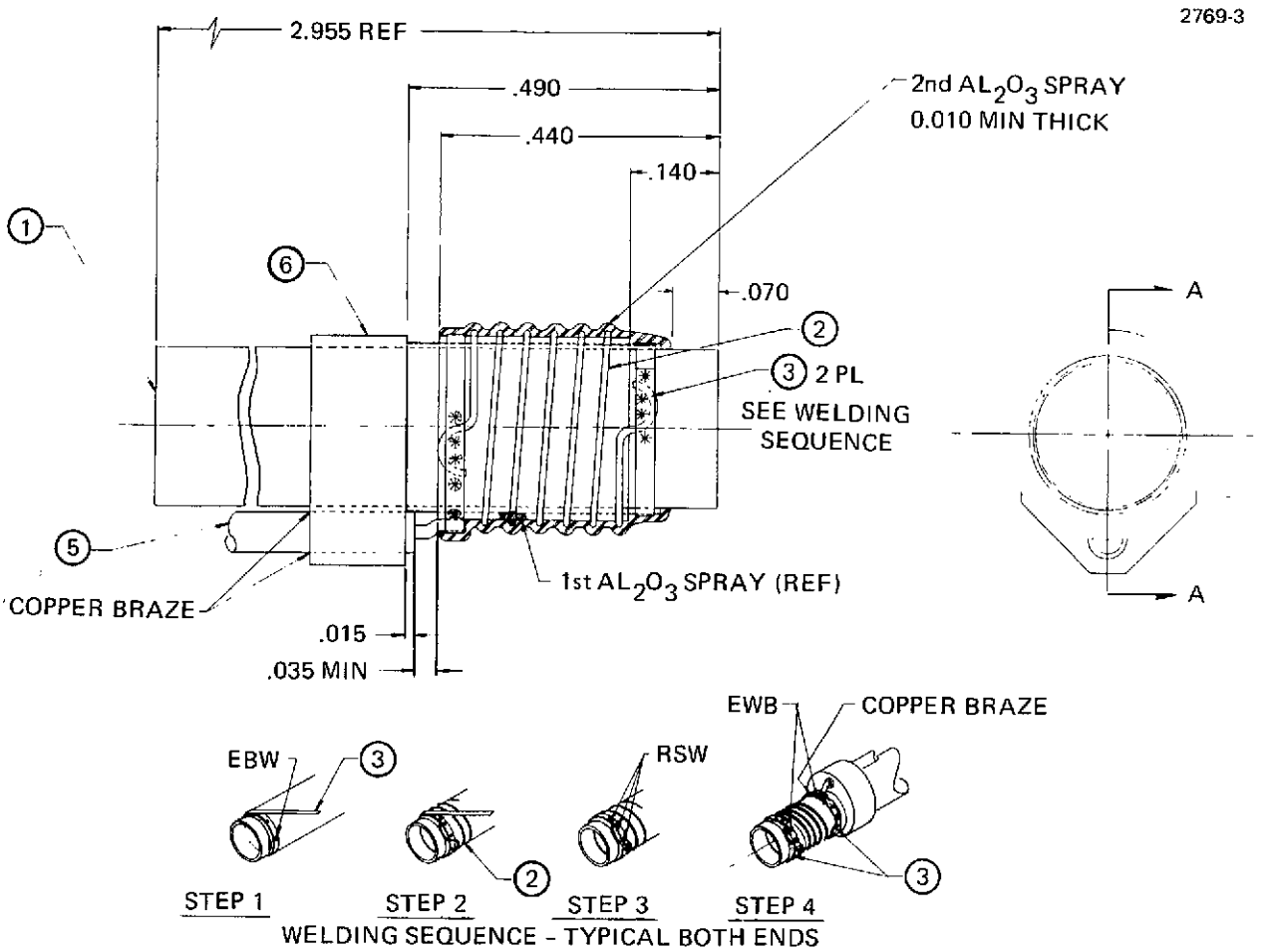

Fig. 24. Basic cathode with sprayed heater.

For main cathodes, an orifice disk, as shown in Fig. 25, and a radiating flange are EBW in place. The tube is cut to length and electron beam welded into the cathode mounting flange. The heater terminal is brazed to the lead by rf brazing in a belljar. Finally, the heat shields and insert are installed to complete the assembly as shown in Fig. 25.

The neutralizer cathode requires only 50 W for ignition and does not utilize a tip radiator or heat shielding. Thus, after installing the heater elements in the basic cathode assembly, a neutralizer cathode is made by electron beam welding the orifice disk into place and brazing on the heater terminal. The cathode orifice disk is 0.15-cm thick with a straight 0.038-cm diameter hole. Additional details of the neutralizer assembly are presented in Section II-C-3.

C. Isolator-Vaporizer Assemblies

Isolators are used in each of the three propellant feed lines (main, cathode, and neutralizer) to provide electrical isolation between thruster voltages and the grounded propellant system. The isolator, placed downstream of the vaporizer in each line, must withstand the voltage difference (1100 V for main and cathode isolators: 100 V for the neutralizer) as well as conduct mercury vapor. Since the isolator and vaporizer designs are closely associated, the combined isolator-vaporizer assemblies for the three applications are discussed in this section.

The designs developed under contract NAS 3-14140 were used as the baseline for this contract. Long term tests at NASA LeRC and at Hughes indicated that the electrical capabilities of the cathode and main isolators (CIV and MIV respectively) were deteriorating after a few hundred hours of operation. After extensive testing and analysis at LeRC and corroborative tests at Hughes, the isolator design was modified, and a carefully controlled fabrication procedure was established. These corrections apparently have been successful in producing a long life isolator assembly design. The following sections discuss this work in detail and present the designs used in the

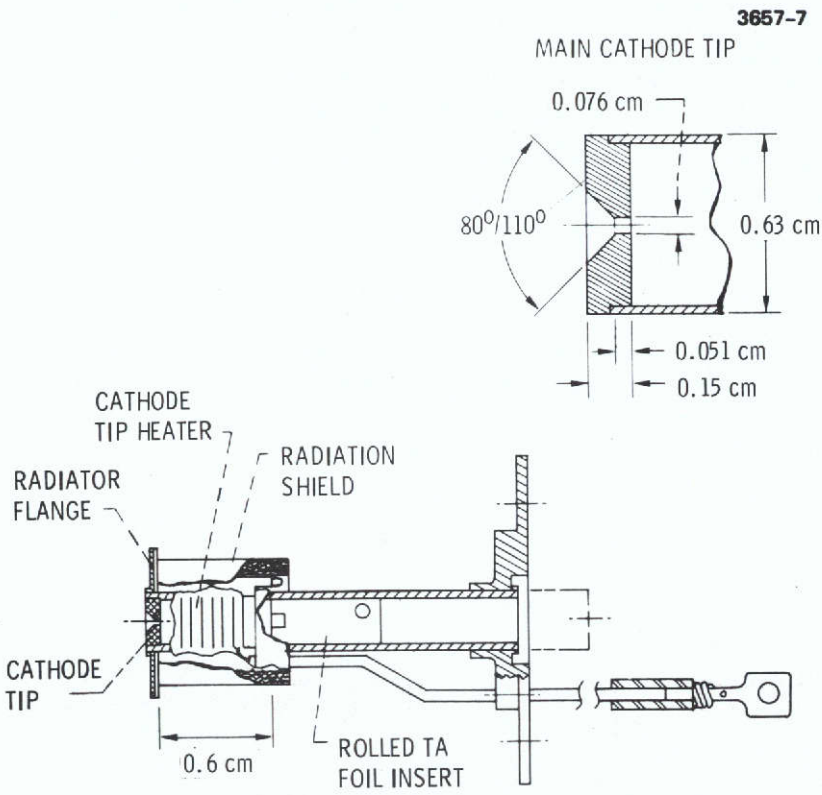

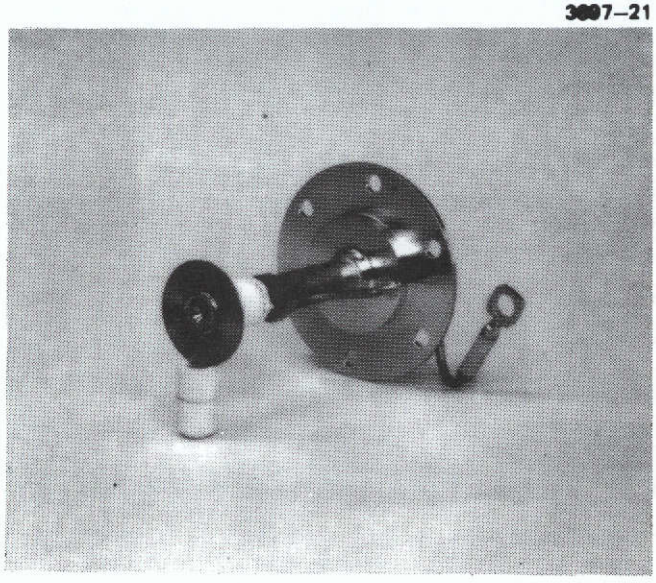

Fig. 25. Main cathode assembly.

engineering model thruster. Vaporizer flowrate versus temperature data are presented in Section III.

1. Isolator Breakdown Tests

At the outset of the contract, a CIV assembly of the type shown in Fig. 26[1] was placed in test to determine the breakdown potential as a function of mercury flow rate, and as a function of operating time. The CIV (serial number 409) was operated with the vaporizer at ground potential and the cathode at positive potential. The leakage current was measured with a 100 μA meter. To monitor temperatures, thermocouples were placed on the cathode tip, the cathode end of the isolator section, the vaporizer end of the isolator section, and the vaporizer.

After the mercury flow and the component temperature was stabilized, the potential of the cathode was gradually increased while the leakage current was monitored. Typically, the leakage was less than 0.5μA (the minimum detectable level on the meter) to the point where the breakdown is initiated. For example at 2090 V potential the current was less than 0.5 μA and at 2100 V the leakage current was 40 μA. The breakdown voltage was taken to be the highest voltage at which the leakage was less than 0.5 μA.

The CIV was operated continuously for 104 h. The observed breakdown potentials as a function of mercury flow are shown in Fig. 27. There was no evidence of any change in either the electrical characteristics or the vacuum integrity of the CIV after this period of operation.

2. Isolator Leakage and Design Recommendations

Although the breakdown tests indicated the ability of the basic design to prevent breakdown, additional tests were required to demonstrate long life without degradation. Tests then being conducted at NASA LeRC[10] and under the concurrent Hughes contracts, indicated that degradation was indeed occurring after a few hundred hours. Such degradation was exhibited by a continuous increase in leakage current.

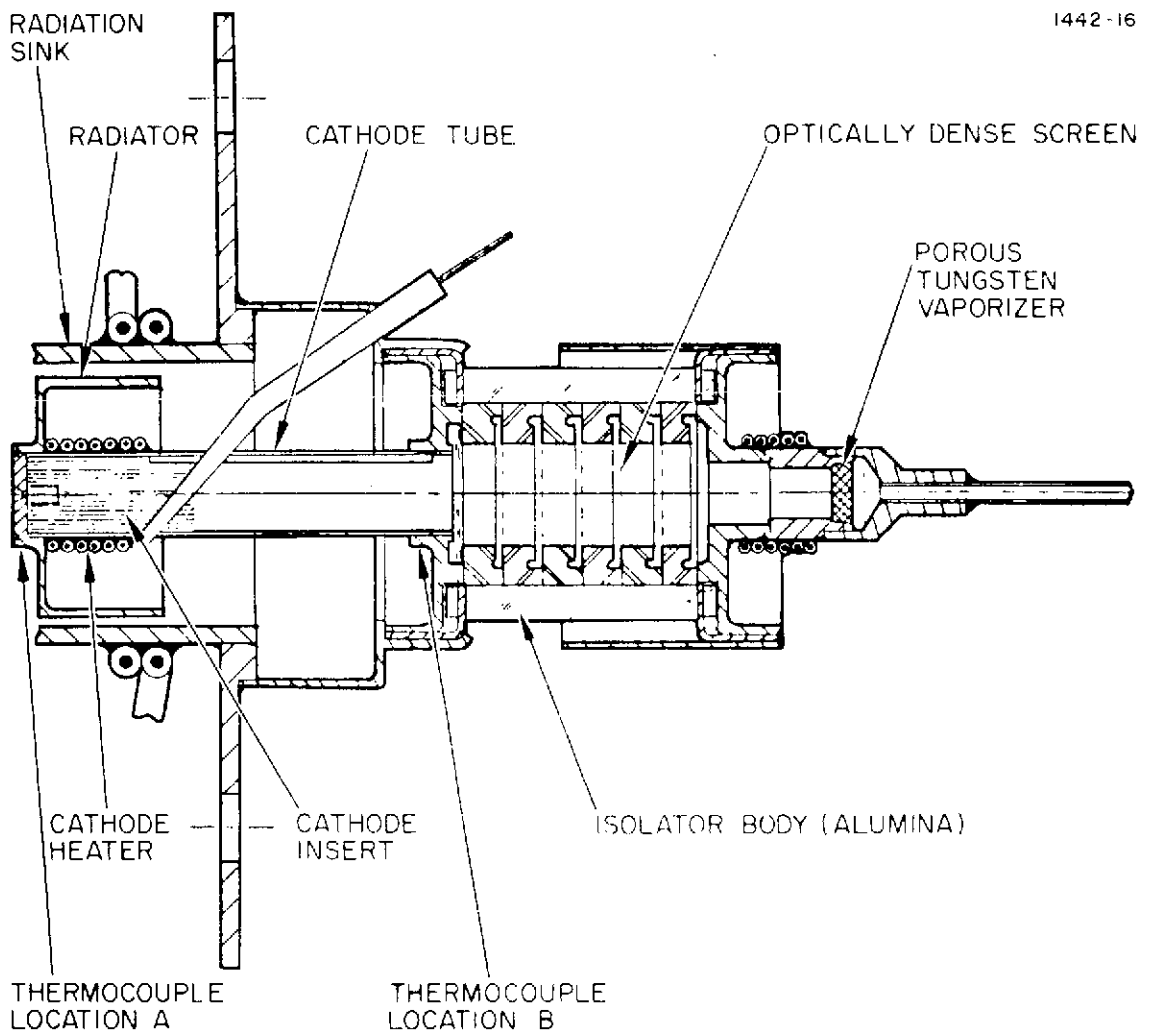

Fig. 26. 300 and 400-series thruster cathode-isolator-vaporizer (CIV) assembly.

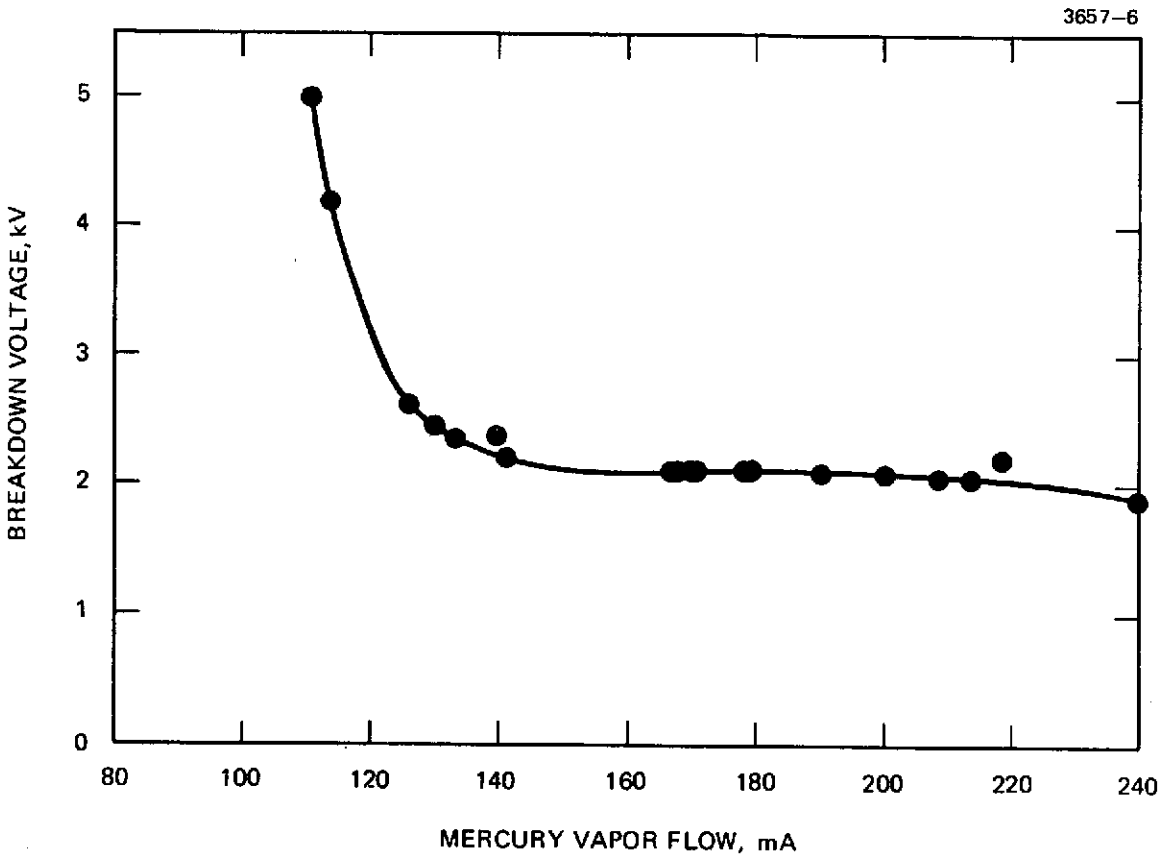

Fig. 27. Isolator breakdown voltage as a function of mercury flowrate.

A comprehensive investigation was initiated at NASA LeRC to determine the degradation mechanism and to recommend solutions. The conclusions of this study bear heavily upon the final isolator-vaporizer design/fabrication and are presented here for reference. The conclusions were:

a. Isolator external leakage is caused by the deposition of metal and/or metal oxides on the ceramic surface. This was indicated by:

- Semiconductive nature of the surface
- Onset of leakage conforming to the theoretical characteristics of such a coating
- Oxidation of various isolator components leading to failures
- Lack of dependence upon facility conditions
- Onset of leakage being extremely temperature dependent

b. Isolator design and fabrication features should include:

- Overlapping stainless shields, as shown in Fig. 28, crimped in place
- Al-300 Alumina
- Kovar end caps
- Tig welding where possible
- Nickel plating over all braze surfaces
- No spot welding on the isolator or in assembly area
- avoidance of any source of oxidation
- Avoidance of the use of silver in any form
- Clean raw alumina material by grinding surfaces

- Bead blast alumina surfaces with high purity Al-300 powder for final cleanup; protect all metal surfaces during this process.

3. Main Isolator Vaporizer (MIV) Assembly

The previous discussion characterized the basic isolator portion of the MIV assembly shown in Fig. 28. The vaporizer is a porous tungsten disc electron beam welded (EBW) into a tantalum housing, which in turn is attached to the upstream end of the isolator. A coaxial heater is brazed with Nicrobraz 135 to the vaporizer assembly. The isolator heater is also brazed to the downstream flange with Nicrobraz 135, and this unit is tungsten inert gas (TIG) welded to one end of the alumina isolator assembly. Heater specifications for the MIV are shown in Table 4.

The isolator is fabricated at an outside vendor by OFHC copper brazing Kovar flanges to the WESGO AL 300 alumina insulator tube. After joining the isolator and the flange, the isolator is loaded with the alumina rings and wire mesh separating screens, and the vaporizer subassembly is TIG welded in place. The stainless steel mounting flange is then TIG welded to the downstream flange and the completed assembly is nickel plated (0.0005 cm maximum thickness). Finally, the outer surface of the alumina insulator is grit blasted with the special cleaning unit and the nickel plated sputter shields are attached.

The thermal constraints for the MIV assembly are:

a. Isolator temperatures

- $200^{\circ}C$ minimum to prevent mercury condensation
- Minimum temperature rise during operation to ensure long lifetime ($T_{max} \sim 350^{\circ}C$)

b. Vaporizer temperature

- Controllable in the range 280 to $340^{\circ}C$ to adjust mercury flowrate.

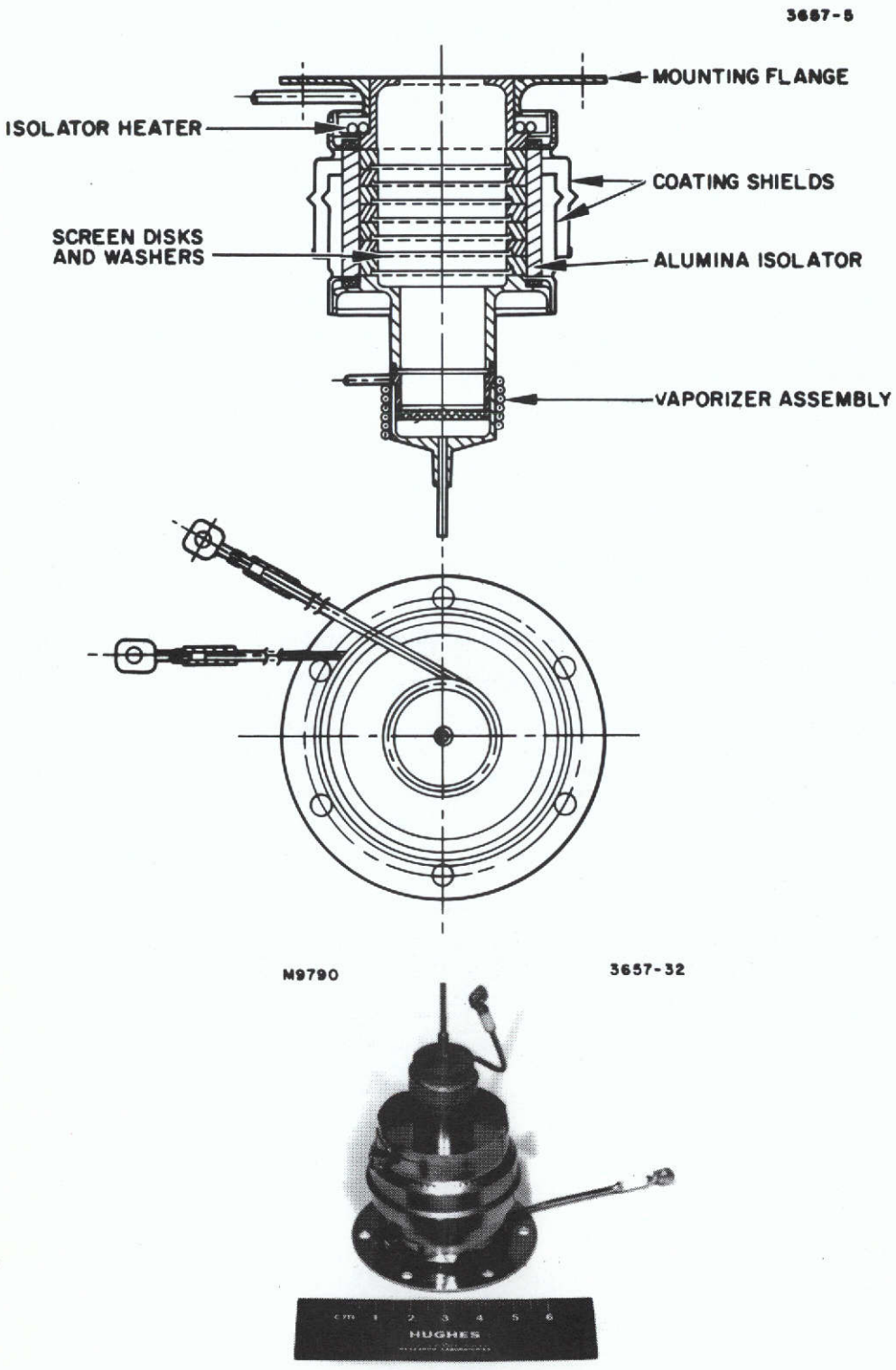

Fig. 28. 700-series thruster main isolator vaporizer (MIV) assembly.

TABLE 4

MIV Heater Specifications

	Main Isolator	Main Vaporizer
Part Number	B1025330	B1024917
Conductor Material	Nichrome V	Nichrome V
Conductor Diameter, cm	0.025	0.025
Sheath Material	Inconel	Inconel
Sheath Diameter, cm	0.100	0.100
Insulation Material	MgO	MgO
Number of Turns (approximately)	2	6
Resistance (Ω)	4.65± 0.23@25° C	6.50± 0.32 @25° C

T408

4. Cathode Isolator Vaporizer (CIV) Assembly

In the designs developed under NAS 3-14140 the cathode isolator was mechanically, and therefore thermally, integrated with the cathode itself on the thruster centerline. At full power operation even the modest amount of power (~8 W) conducted along the cathode tube would heat the cathode isolator to >400°C. At this temperature several isolator failures were observed. As a result of work on NAS 3-16949, the operating temperature was lowered by moving the cathode isolator to a location on the thruster backplate diametrically opposite the main isolator. At this location the cathode isolator operating temperature is approximately the same as the main isolator. Mercury from the isolator is carried to the cathode through a small tube which is initially heated by the isolator heater. The tube temperature is maintained by thermal conduction from the discharge chamber when the thruster is in operation.

The isolator-vaporizer design is shown in Fig. 29. This unit is fabricated and assembled in a manner similar to that described for the MIV, except that an additional feed tube and flange are added to direct the mercury flow to the cathode tube. The 0.240-cm diameter by 0.05-cm wall mild steel tube is brazed to the isolator flange and stainless steel feed tube flange. This subassembly is shown after brazing in the special fixture in Fig. 30. A portion of the isolator heater is also brazed to the feed tube to preheat the tube during startup conditions. Heater specifications for the CIV are shown in Table 5.

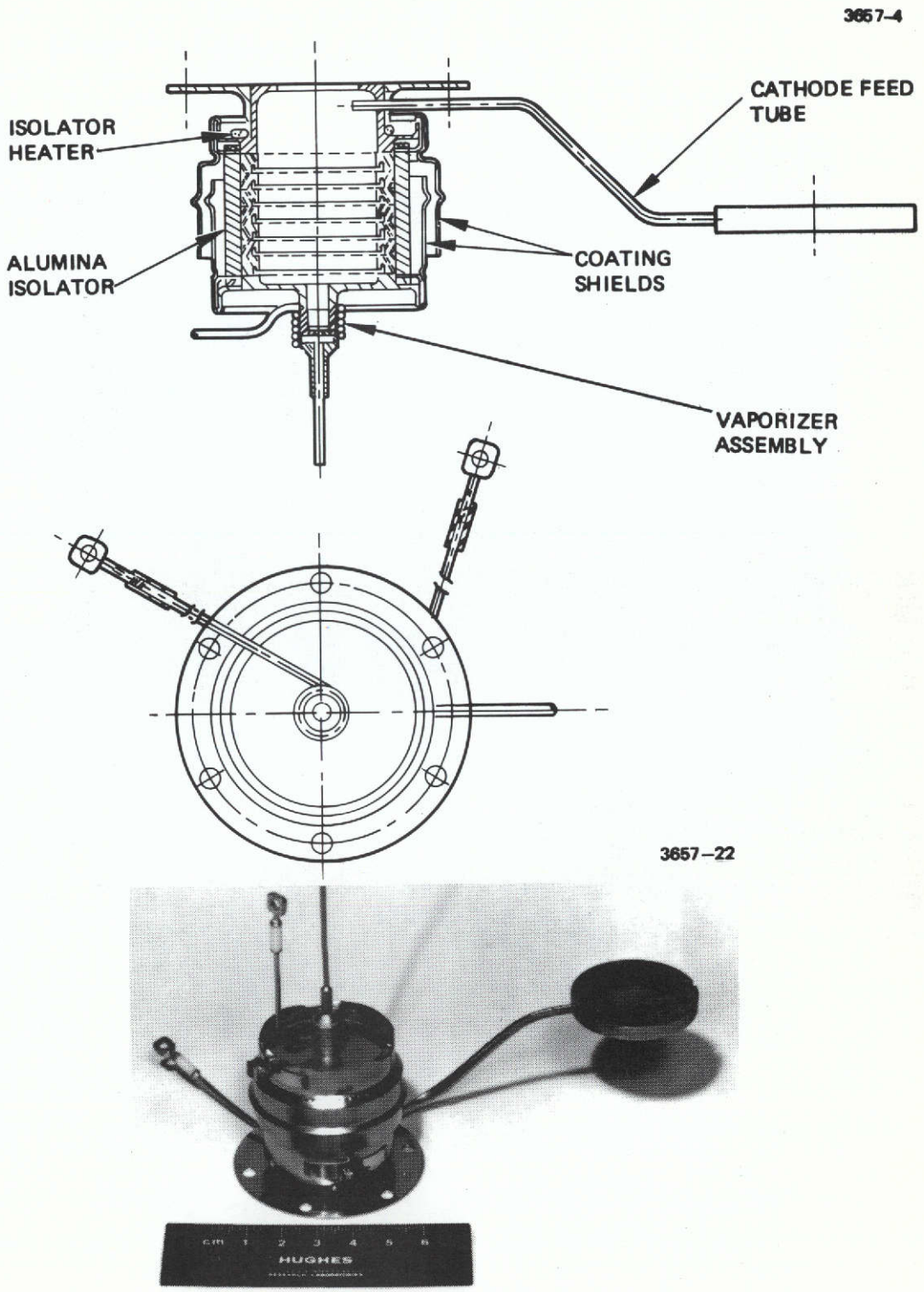

Fig. 29. 700-series thruster cathode isolator and vaporizer assembly.

M10030

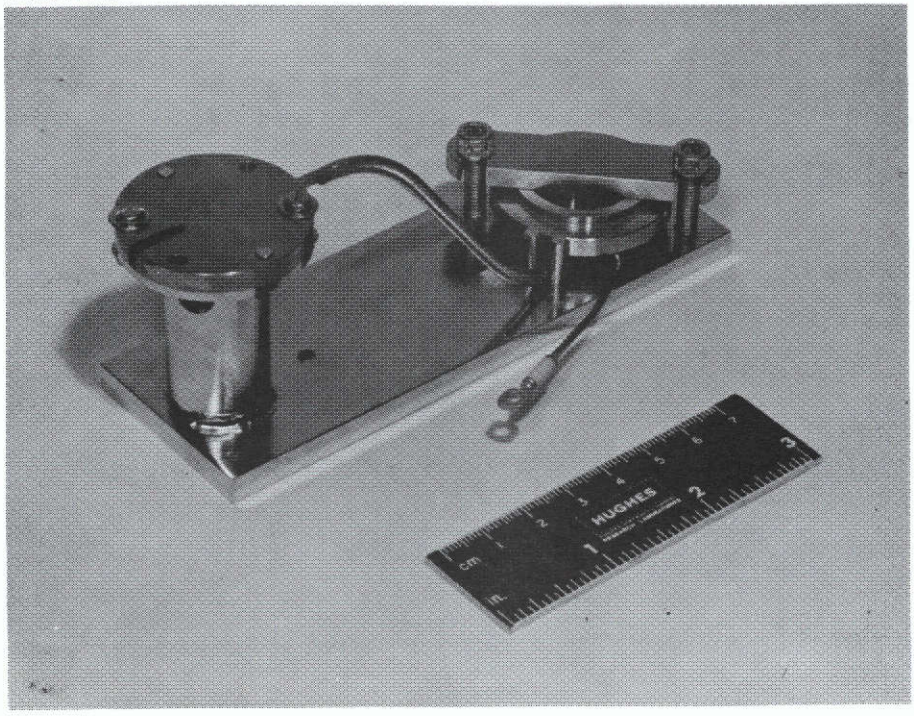

Fig. 30. CIV feed tube and cathode flange brazing fixture.

TABLE 5

CIV Heater Specifications

	Cathode Tip	Vaporizer
Part Number	B1025262	B1025330
Conductor Material	Tungsten/26% Rhenium	Nichrome V
Conductor Diameter , cm	0.025	0.025
Sheath Material		Inconel
Sheath Diameter, cm	0.040[a]	0.100
Insulation Material	Al_2O_3[a]	MgO
Number of Turns (approx.)	8	2
Resistance, Ω	1.15 ± 0.05 at 25°C	2.86 ± 0.14 at 25°C

[a]Flame Sprayed

T348R

The isolator-vaporizer subassembly is then joined to the cathode assembly (Fig. 25) by means of a 0.01-cm thick annealed tantalum seal. The cathode, isolator, and vaporizer are installed in a baffle subassembly. This total CIV assembly is shown in Fig. 31.

5. Neutralizer Isolator Vaporizer (NIV) Assembly

The neutralizer tube subassembly, excluding keeper, brackets, and mounting hardware, is shown in Fig. 32. The isolator section is first assembled by OFHC copper brazing the tantalum shield and vaporizer housing to the ends of an Al-300 alumina tube. Screen baffles, as used in the CIV and MIV, are not required due to the low voltage level. The vaporizer plug and feed tube are EBW in place and the vaporizer heater is brazed to the housing. Heater specifications for the NIV are shown in Table 6.

The basic hollow cathode design and fabrication technique is identical to the main cathode assembly and no differentation is made in the assembly procedure until the orifice is welded in place. The two tube supports are copper brazed to the cathode tube; the cathode insert and baffle are installed, and the tube and isolator sections are EBW together to complete the tube assembly.

The keeper, insulators, shields, and mounting brackets are mated with the tube subassembly to complete the entire NIV assembly, as shown in Fig. 33. The operating characteristics of the neutralizer assembly and the keeper design selection are discussed in Section III in conjunction with thruster testing.

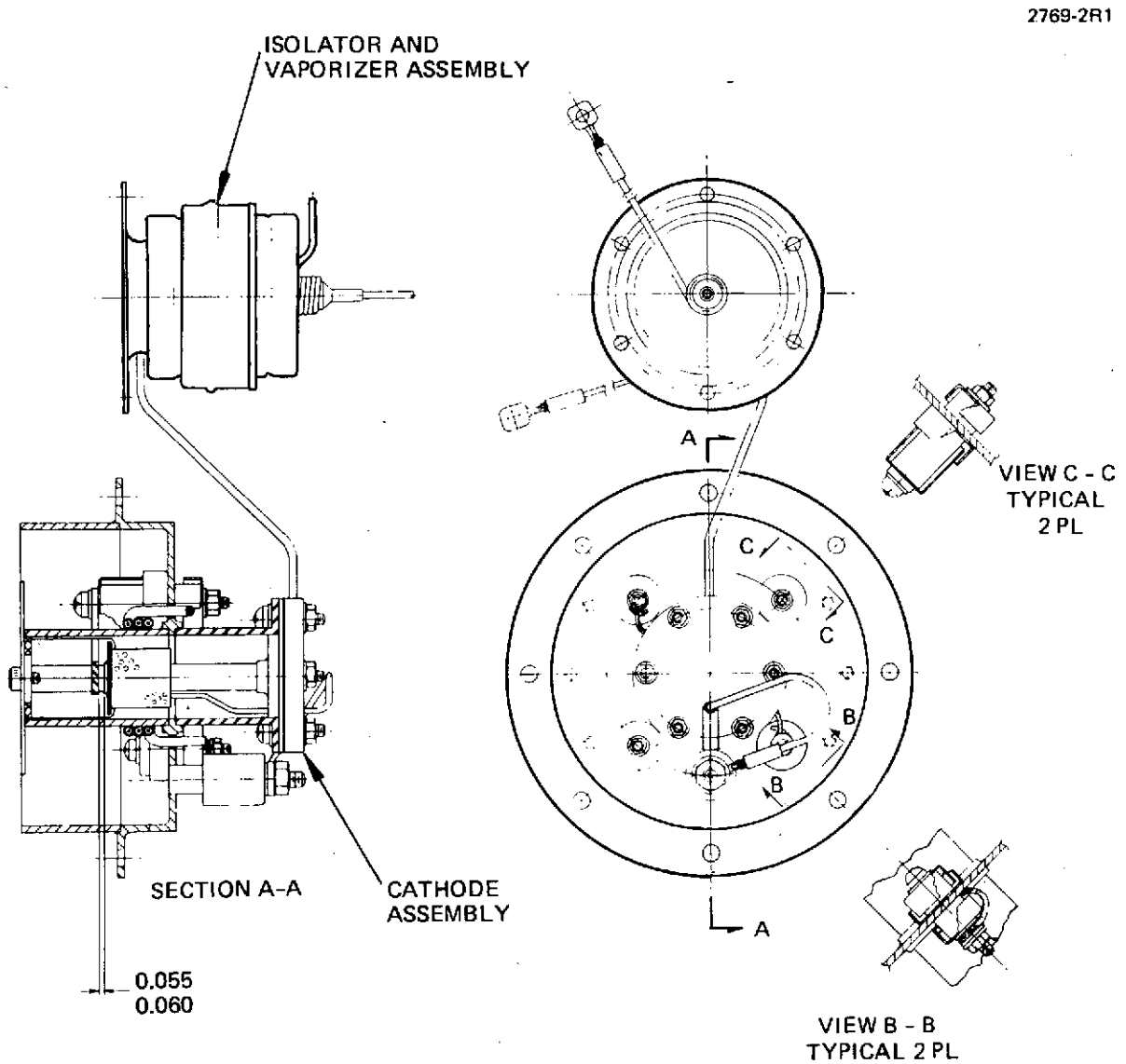

Fig. 31. Drawing of CIV assembly, including cathode pole and magnetic baffle.

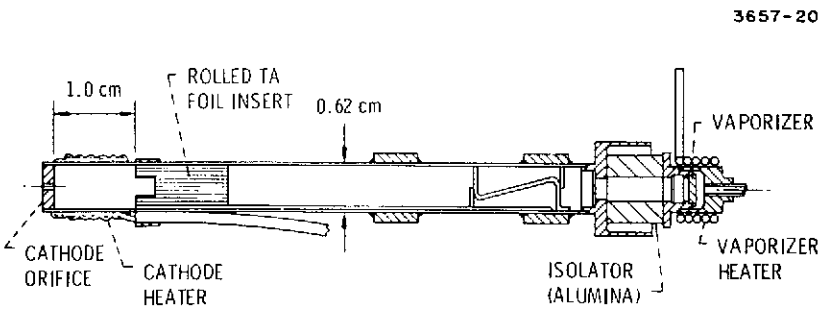

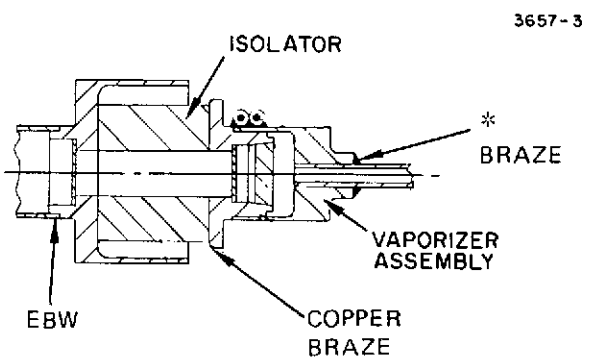

*Changed to nicrobraze for 800-series thruster

Fig. 32. Drawing of neutralizer tube assembly.

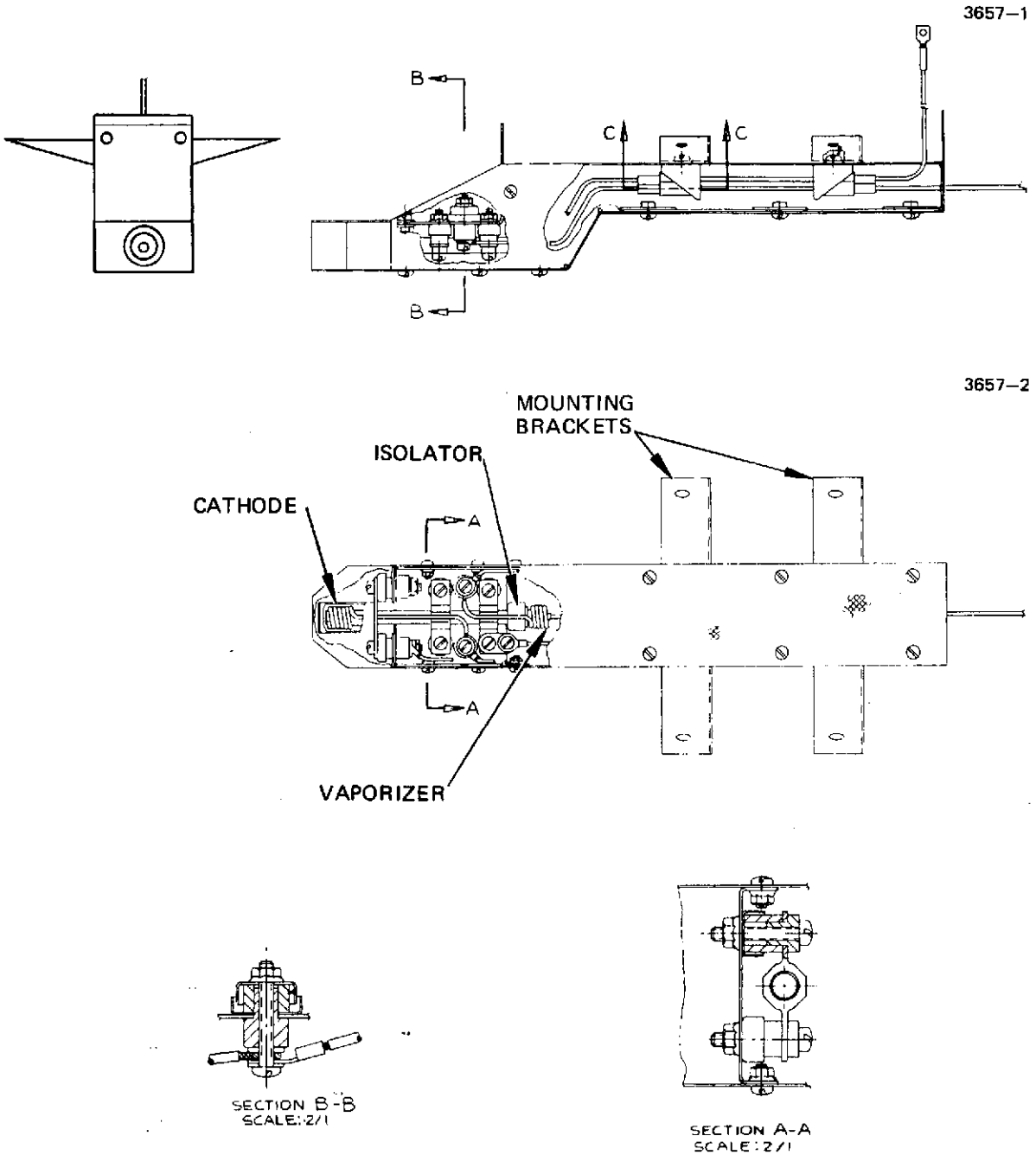

Fig. 33. Neutralizer assembly, including keeper configuration.

TABLE 6

Neutralizer Heater Specifications

	Cathode Tip	Vaporizer
Part Number	D1026367C	B1024543
Conductor Material	Tungsten/26% Rhenium	Nichrome V
Conductor Diameter, cm	0.025	0.025
Sheath Material		Inconel
Sheath Diameter, cm	0.040[a]	0.100
Insulation Material	Al_2O_3[a]	MgO
Number of Turns (approximately)	8	5
Resistance, Ω	1.15 ±0.05 at 25°C	2.86±0.14 at 25°C

[a]Flame sprayed.

T412R

D. Discharge Chamber Assembly

The prime function of the discharge chamber assembly of an electron bombardment ion thruster is to ionize the neutral propellant gas. The design of the discharge chamber is based on the crossed-field or Penning discharge principle, whereby an electrical discharge is maintained at relatively low internal pressure by restricting the flow of electrons from cathode to anode with an appropriate magnetic field. Components of the discharge chamber assembly include the thruster shell which contains the neutral propellant gas, a propellant distributor, permanent or electromagnets and iron pole pieces for providing the electron containing magnetic field, an electron emitter, and an electron collector or anode.

Advancement of the discharge chamber design under this program was based on the configuration developed under the preceding Low Voltage Ion Thruster Program (NAS 3-14140)[1] which is shown in Fig. 34. This discharge chamber assembly consisted of a thin walled, stainless steel, sheet metal shell strengthened by ribs and support struts; a toroidal propellant distributor which dispenses the propellant through optically dense, low transmission screened openings; permanent magnets and soft iron polepieces; a variable magnetic baffle controlled, hollow cathode electron emitter; and a stainless steel sheet metal anode. Although the ion optical system assembly has the primary function of extracting and accelerating ions to form a well colliminated beam, it should also be considered an essential component in the operation of the discharge chamber. During the early phases of this program, modifications and improvements of the ion optical system assembly governed the performance characteristics of the discharge chamber assembly more than any other factor.

The discharge chamber assembly which evolved as the engineering model thruster design under this program incorporates a number of changes which were dictated primarily by structural requirements. These changes are described in detail in a following section and include the substitution of titanium for almost all of the stainless steel elements,

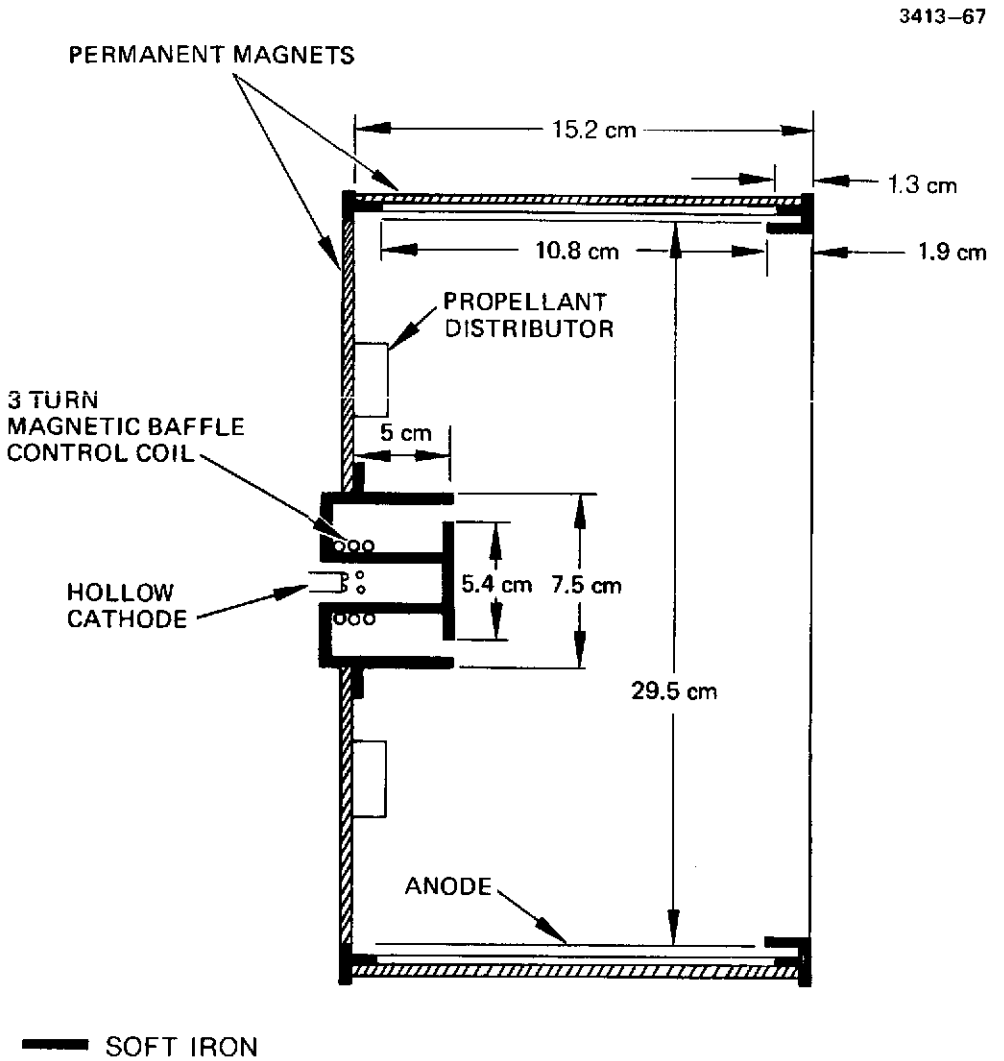

Fig. 34. Schematic of 30-cm divergent magnetic field thruster (NAS 3-14140).

dished grid ion optical system electrodes, and construction of the discharge chamber shell so that it is now the structural support element for the entire thruster assembly. This last structural requirement was recognized at a design review midway through this program (see Figs. 2 and 3) based on spacecraft interface requirements. As a consequence, design modifications which had been developed under other programs and offered significant performance improvements (NAS 3-16949 and NASA LeRC internal programs) were incorporated into the redesign of the engineering model thruster under this program. These modifications provide increased discharge efficiency and their development and evaluation is discussed in detail elsewhere.[3] This section describes the parameter variations prior to structural redesign as well as the properties of the final configuration.

1. Discharge Chamber/Ion Optical System Interactions

In the process of selecting the optimum ion optical system specifications, a number of grid designs were evaluated with the thruster discharge configuration shown in Fig. 34. Specifications and operational characteristics for some of these grid designs are summarized in Table 7. Past experience has indicated that discharge efficiency is improved (eV/ion decreased or propellant utilization increased) by increasing the transmission or geometric open area of the screen grid electrode. Increase of screen grid open area was carried to the practical extreme by use of hexagonal aperture shape (grid set SN 623, 626) but the discharge efficiency was found to decrease rather than increase as anticipated. It is now known that the reason for this behavior is the relatively large open area of the accel electrodes used, which allows neutral atoms to escape from the discharge chamber more readily. As shown in Table 8, the grid system design finally adopted and another design tested in the companion program activities[3] display improved performances, primarily due to a reduction in accelerator grid open area. Since these data were obtained with thrusters of the more advanced engineering model design, the comparison must be made on the basis of grid SN 638 which is

TABLE 7

Grid System Specifications and Performance Parameters

SN	Screen Grid			Accel Grid			C-C Aperture Spacing, cm	Minimum Total Voltage, V	Beam Current, A	Discharge Loss eV/ion	Discharge Propellant Utilization, %	Cathode Propellant Flow, mA	Mag Baffle A-T	Comments
	Thickness, cm	Aperture Diameter, cm	Open Area, %	Thickness, cm	Aperture Diameter, cm	Open Area, %								
601	0.038	0.216	66	0.038	0.191	51	0.254	1450 1400 1150	2 1.5 1.0	220 220 220	93.6 90.9 83.5	150 102 95	40.5 30.4 20.3	5.24 cm diam baffle 38 V discharge voltage
609	0.038	0.241	68	0.076	0.193	43.5	0.279	1600 1500 1300	2.0 1.5 1.0	220 220 220	95.6 91.6 87.4	136 139 148	28.9 21.7 14.5	5.72 cm diam baffle 38 V discharge voltage
611	0.038	0.241	68	0.038	0.241	68	0.279	1900 1400	2.0 1.0	220 220	91.6 82.9	123 119	27.5 13.8	5.72 cm diam baffle 40 V discharge voltage
614	0.051	0.279	70	0.076	0.224	45	0.317	1800 1400	2.0 1.0	220 220	93 83.4	157 148	27.5 13.8	38 V discharge voltage
623	0.038	0.208	79.5	0.076	0.178	57.9	0.234	1800 1500	2.0 1.0	220 220	93.5 81.6	136 146	27.5 13.8	38 V discharge voltage Hexagonal shaped apertures
626	0.038	0.208	79.5	0.076	0.178	57.9	0.234	1450 1300	2.0 1.0	220 220	88.5 79.3	158 146	27.5 13.8	38 V discharge voltage Hexagonal apertures 1 cm dish depth
634	0.038	0.241	68	0.076	0.193	43	0.279	1950 1700	2.0 1.0	220 220	94.3 86.4	166 148	27.5 13.8	38 V discharge voltage

T-1455

TABLE 8

Improved Grid System Specifications and Performance Parameters

SN	Screen Grid			Accel Grid			C-C Aperture Spacing cm	Beam Current, A	Discharge Loss eV/ion	Discharge Voltage, V	Cathode Propellant Flow, mA	Discharge Propellant Utilization, %	Mag Baffle A-T	Thruster, SN	Comments
	Thickness, cm	Aperture Diameter, cm	Open Area, %	Thickness, cm	Aperture Diameter, cm	Open Area, %									
638	0.038	0.241	67.7	0.076	0.193	43.5	0.279	2.0	200	37	67	91.5	44	403A	5.1 cm diam baffle
644	0.038	0.191	67.6	0.051	0.152	43.3	0.221	2.0 1.5	185 185	37 37	100 94	95.6 90.9	45 34	301A	5.1 cm diam baffle
NASA 35	0.038	0.203	75.2	0.038	0.122	27.2	0.234	2.0 1.5	185 185	37 37	84 88	93 95	21 26	301B	Hexagonal shaped apertures 5.4 cm diam baffle

T-1456

identical to SN 609 except for screen grid hole pattern reduction. Grid set SN 644 is representative of the design chosen for the engineering model thruster and NASA 35 carries the high screen open area, low accel open area concept very nearly to the limit.

Variations in the ion optical system parameters, like those shown in Tables 7 and 8, affect the operation of the discharge chamber as well as the efficiency. This is observed primarily with respect to the ability of the magnetic baffle or combination of physical baffle size and magnetic baffle control current to adjust cathode propellant flow rate for operation in the 80 to 150 mA (equivalent) range. At flow rates near the high end of this range, efficiency deteriorates. At the low end of the range, the discharge mode tends to shift from a mode characterized by low voltage and high current to one characterized by higher voltage and low current. Specific behavior of this type is also affected by power supply characteristics and control circuitry which provides proportional control of the cathode vaporizer heater. In general, it has been possible to obtain optimum performance for any given grid design by minor changes in the baffle diameter or magnetic baffle.

2. Discharge Chamber Magnetic Configurations

The magnetic field strength and optical distribution throughout the discharge chamber determines the discharge volume in which the ionization processes predominate. Electron bombardment or Kaufman ion thrusters have predominantly employed permanent magnets and soft iron pole pieces in divergent magnetic configurations, like the one shown in Fig. 34 to provide the required magnetic field. The plasma is formed in this configuration in a cone shaped region defined by the acceleration system screen as the base and the cathode orifice at the apex. Maximum plasma density is obtained on the thruster axis, slightly downstream of the cathode pole tip and baffle. The extracted ion beam has a radial current density distribution that is typically parabolic.

The final engineering model discharge chamber magnetic configuration was based on results obtained at NASA LeRC. Magnet specifications to meet structural symmetry requirements were generated under the 2.5 kW Advanced Technology Ion Thruster Program (NAS 3-16949). Figure 35 shows the thruster configuration and pole piece dimensions and Table 9 compares the magnetic field distributions obtained in resultant thruster fabrications. A comparison of the magnetic circuits for thrusters S/N 301A and S/N 701 is shown in Fig. 36. The magnetic field radial and axial components for the selected design are shown in Fig. 37. These plots were obtained with thruster S/N 702-A.

As illustrated in Table 10, thruster S/N 701 displayed performance characteristics closely matching those of the laboratory prototype (S/N 301-A). Subsequent operation of thruster S/N 701 prior to endurance testing required an increase in the baffle diameter to obtain discharge stability with lower magnetic baffle ampere-turn requirements dictated by power supply limitations. Installation of a 5.4 cm diameter baffle provided satisfactory operation with 36 ampere-turns baffle coil excitation (8 A with 4.5 turns).

E. Thruster Mechanical Design

The thruster mechanical design has been substantially changed during the performance of this program. Using the 300-series thruster shown in Fig. 38 which was developed under Contract NAS 3-14140 as a baseline,[1] the primary mechanical changes included:

- Dished grids to replace flat grids with center supports
- Improved ion optical system mounting structure
- Structural additions to allow two point gimbal mounting of the thruster
- Stiffening across the back plate to prevent "oil canning"
- Relocation of the CIV in a cooler position

3413-19

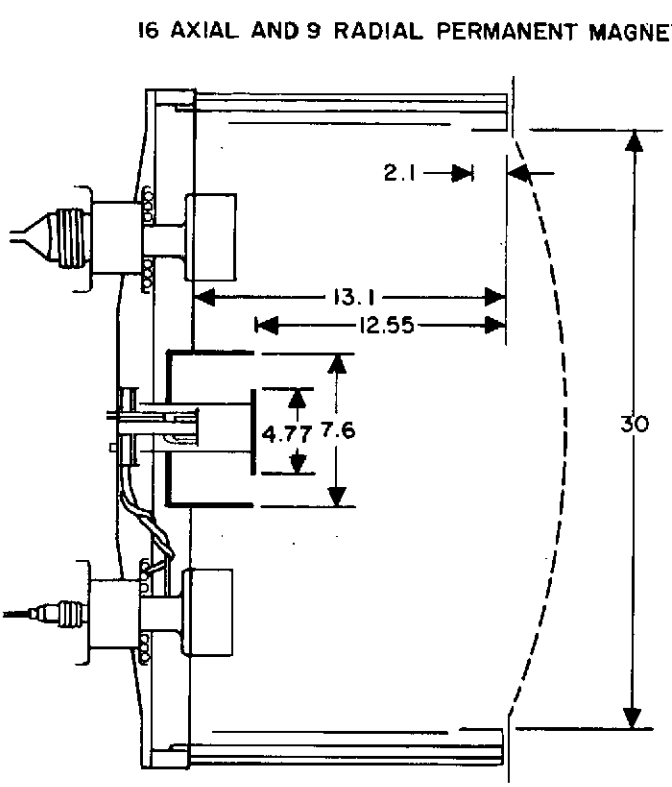

ALL DIMENSIONS ARE GIVEN IN cm

(a) DISCHARGE CHAMBER CONFIGURATION (SN 301-A)

3413-20

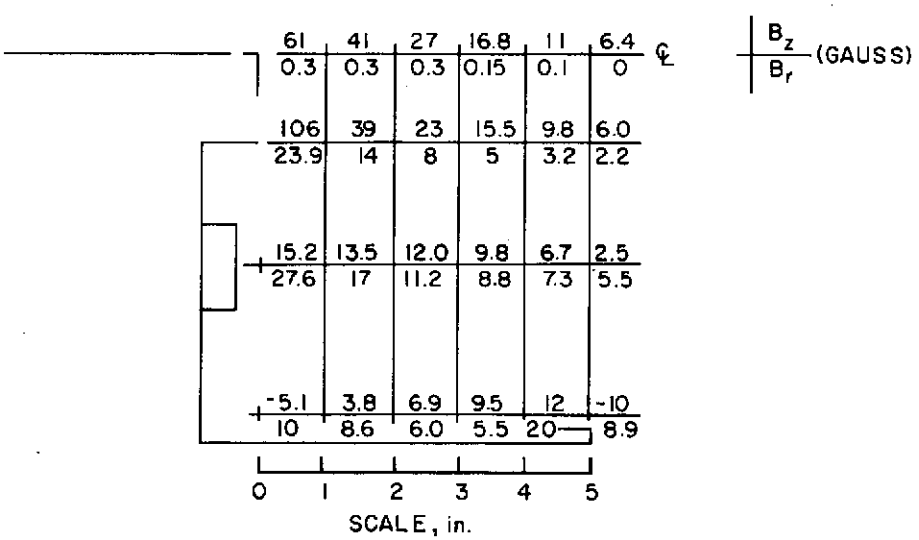

(b) MAGNETIC FIELD STRENGTH DISTRIBUTION

Fig. 35. Laboratory prototype EM thruster discharge chamber specifications.

TABLE 9

Comparison of EM Design Thruster Magnetic Field Distributions

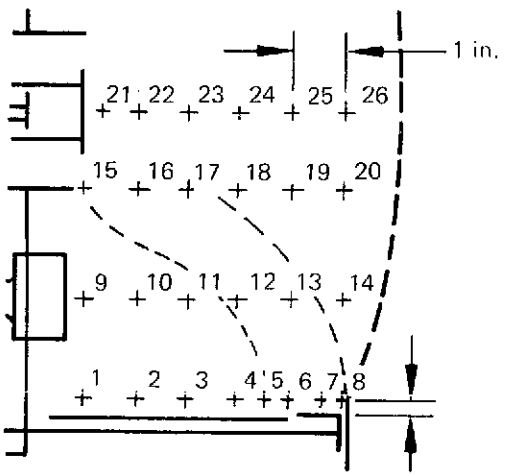

MEASUREMENT GRID

	Axial Magnetic Field Values, Gauss				Radial Magnetic Field Values, Gauss			
Thruster SN	301-A	301-B	701	702	301-A	301-B	701	702
Measurement Grid Location								
1	-4.4	-2.9	-2.3	-3.4	12.0	16.4	14.8	12.3
2	1.8	2.6	2.9	2.9	9.5	11.0	10.2	9.7
3	5.3	5.7	6.0	6.3	7.0	7.9	7.8	7.3
4	8.1	8.3	8.5	9.1	6.0	7.2	7.1	6.4
5	10.7	9.7	10.3	10.9	7.5	8.9	10.2	7.8
6	14.8	9.7	11.9	12	17.5	15.7	16.8	15.7
7	3.1	2.0	2.6	3.2	18.0	13.8	15.7	14.3
8	-9.2	-5.1	-6	-5.3	7.0	7.8	9.2	8
9	12.5	16.1	14.4	16.9	31.0	29.1	28.9	30
10	13	14.3	13.7	14.9	18.6	18.1	17.8	18.3
11	11.6	12.2	11.8	12.9	12.5	12.1	11.9	11.8
12	10	9.7	9.6	10.5	9.0	9.6	8.9	8.8
13	6.8	6.8	6.9	7.4	7.0	8.1	7.6	7.2
14	3.6	3.3	3.4	4.0	5.5	6.0	5.8	5.6
15	112	104	110	90	29.5	27.8	28.1	20.0
16	42	38.4	38.5	39	15.0	13.4	13.4	13.9
17	26	23.5	24.4	25.1	8.9	8.3	8.4	8.2
18	16.6	15.3	15.6	16.5	5.3	5.9	5.3	5.0
19	10.5	10.2	10.5	11.1	3.5	4.5	3.8	4.0
20	6.7	6.6	6.7	7.1	2.5	3.2	2.9	2.8
21	60	49.2	49.5	61.5				
22	45	39.5	41	42				
23	29	26.2	26.8	27.9				
24	19	16.8	16.9	18				
25	12	11.1	11.2	12				
26	8	7.1	7.1	7.65				

T1317

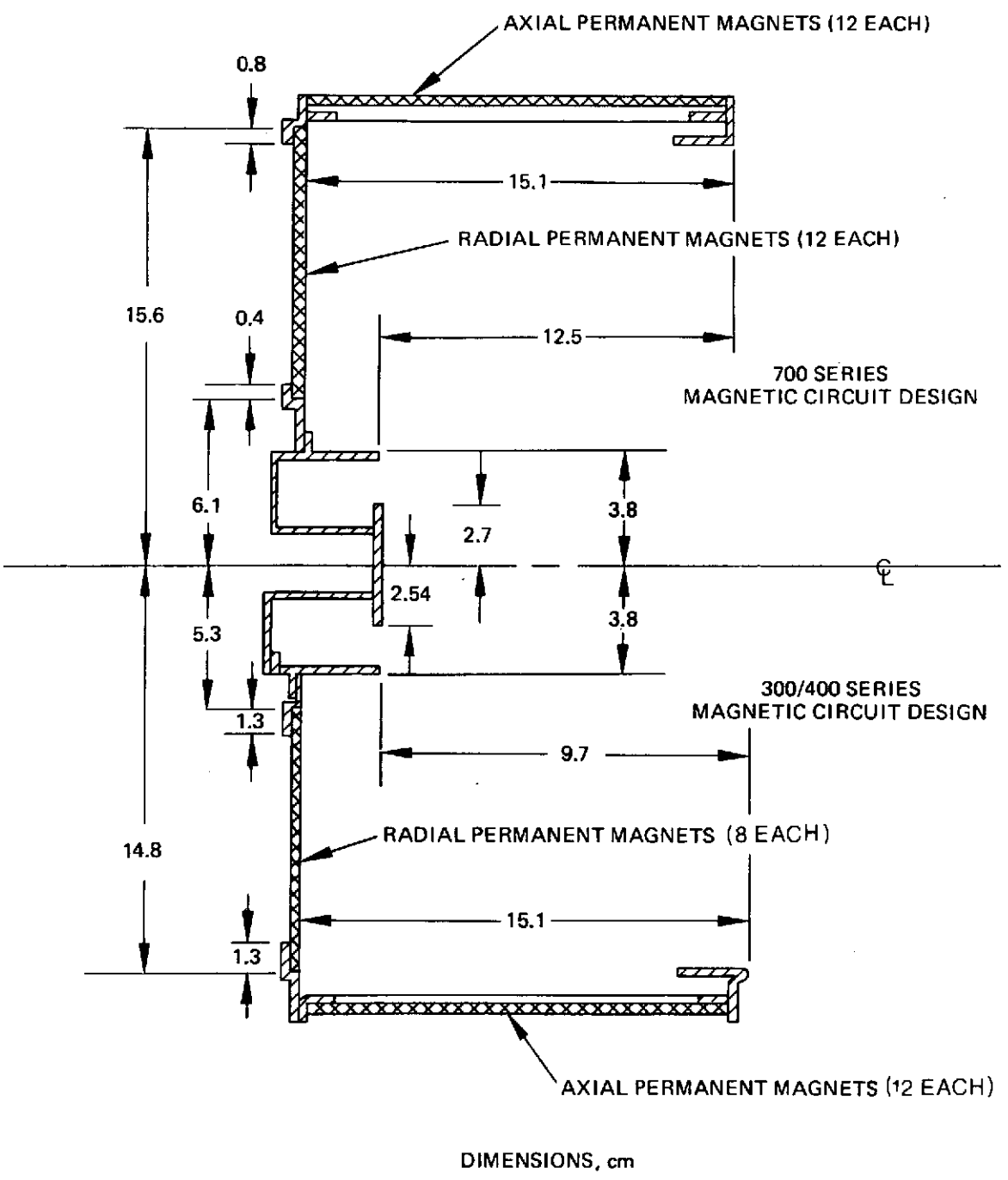

Fig. 36. Comparison of magnetic circuits of 400- and 700-series thruster designs.

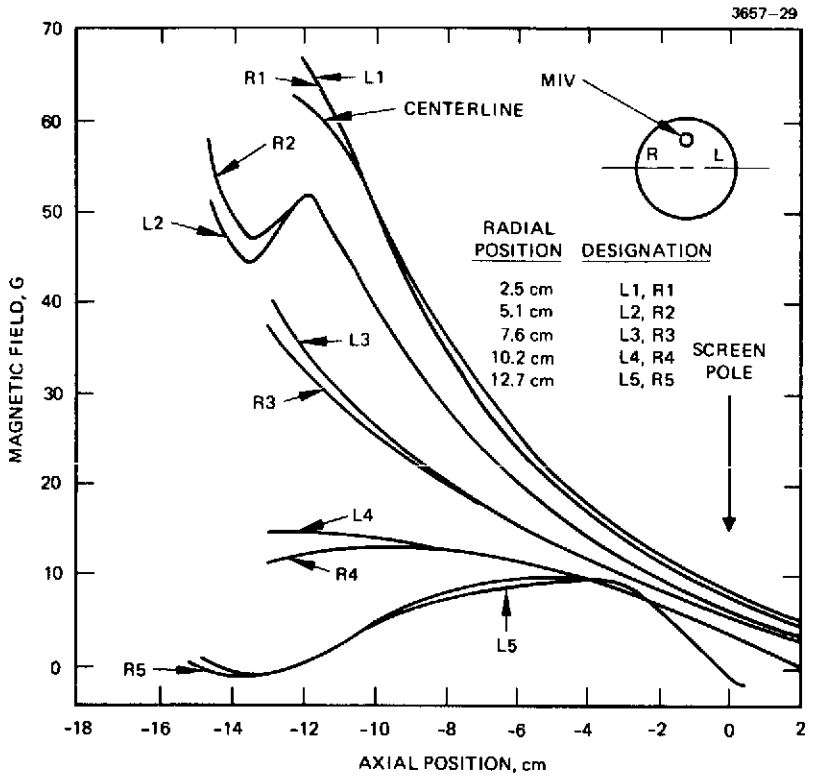

(a) Axial distribution

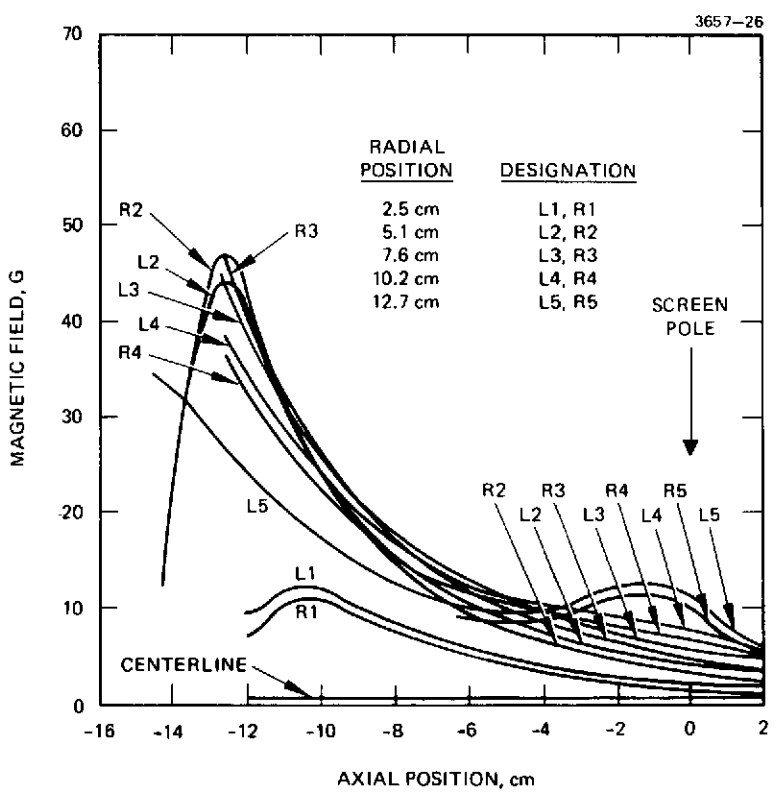

(b) Radial distribution

Fig. 37. Radial and axial magnetic field components for 700/800-series thruster designs.

TABLE 10

Comparison of Discharge Chamber Performance Obtained With Thrusters 301-A and 701

Thruster, SN	Grid System, SN	Beam Current, A	Discharge Voltage, V	Discharge Losses, eV/ion	Cathode Propellant Flow, mA (equiv)	Discharge Propellant Utilization, %	Baffle Coil, amp-turns
301-A	644	2.0	37	185	100	95.6	45
701	645	2.0	37	185	90	95.6	54
301-A	645	1.50	37	185	94	90.9	34
701	645	1.45	37	185	108	92.7	54
301-A	644	1.0	37	185	101	83.6	23
701	645	0.85	37	185	92	82.2	19

T1339

- Addition of terminals for all internal wiring
- Addition of a propellant manifold to connect all three vaporizers to a single feedline

The ion optical system was discussed previously in Section II. The other mechanical design changes will be discussed in this section.

1. 400-Series Design

The 400-series design thrusters were fabricated under Contract NAS 3-15523 for use in endurance testing and for delivery to NASA LeRC. Thrusters S/N 402 and 403 were utilized in this contract (NAS 3-16528) for ion optical system testing prior to construction of the 600- and 700-series thrusters. The 400- series design is similar to that shown in Fig. 38, with differences only in the CIV, MIV, and NIV design details.

Thruster S/N 402 was used in two 500-hour endurance tests with flat, center support type grids. Subsequently, dished grids were substituted and S/N 402A was tested for 1100 h. Additional details of the endurance test program and a summary of the disposition of the 400-series thrusters are contained in the contract reports on NAS 3-15523.

2. 500-Series Design

The 500-series designation was reserved to identify thrusters having vectorable ion optical systems. Early in this program vectorable flat grids were studied briefly. However, as discussed in Section II-A-4, the use of dished grids essentially precludes this vectoring concept. Thus, after the dished grids were adopted, the 500-series were superseded.

3. 600-Series Design

A primary objective of the contract was to verify the capability of the thruster to survive shake testing. The first thruster designed specifically to meet the shake requirements, shown in Fig. 39,

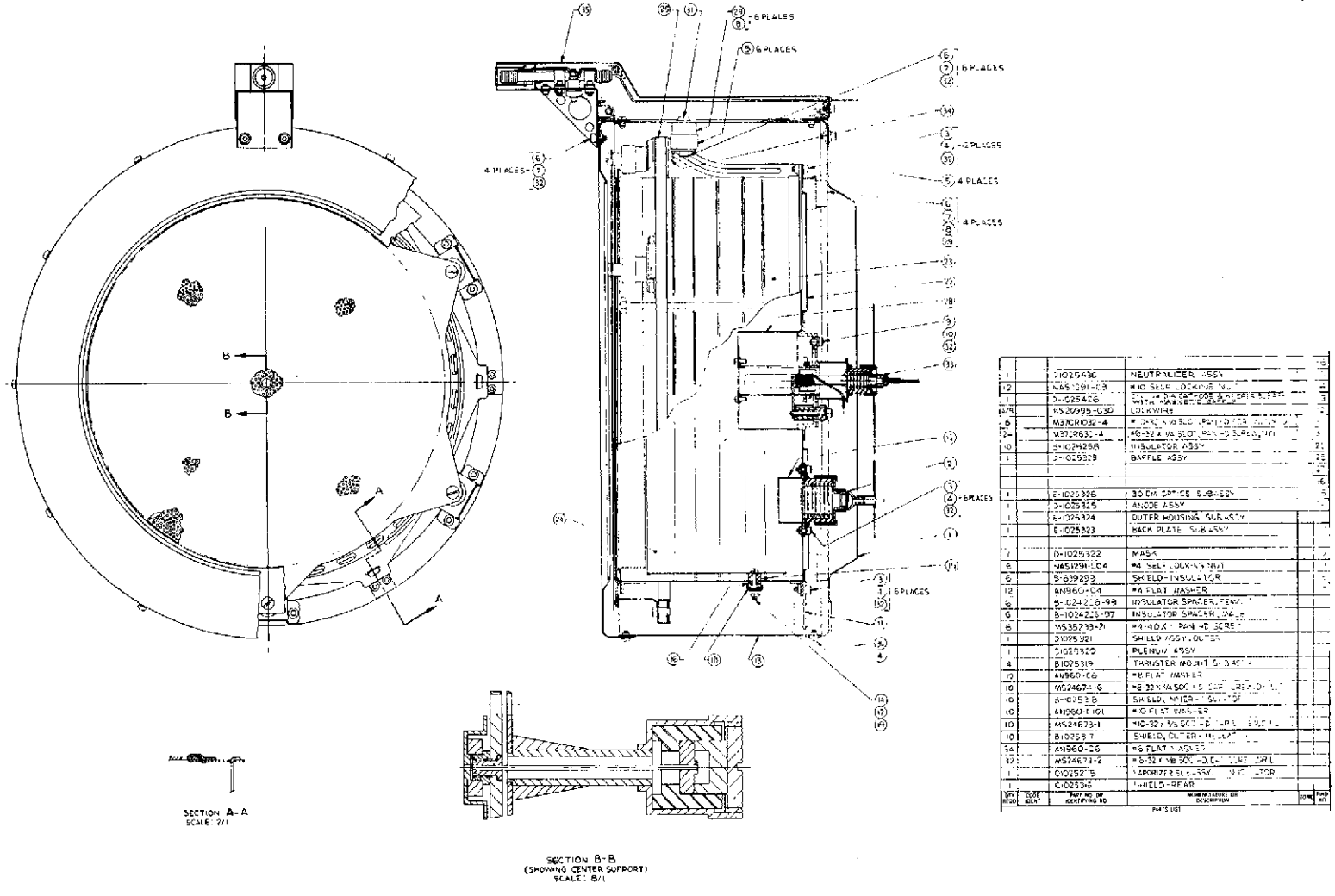

Fig. 38. 300/400-series thruster design (NAS 3-14140).

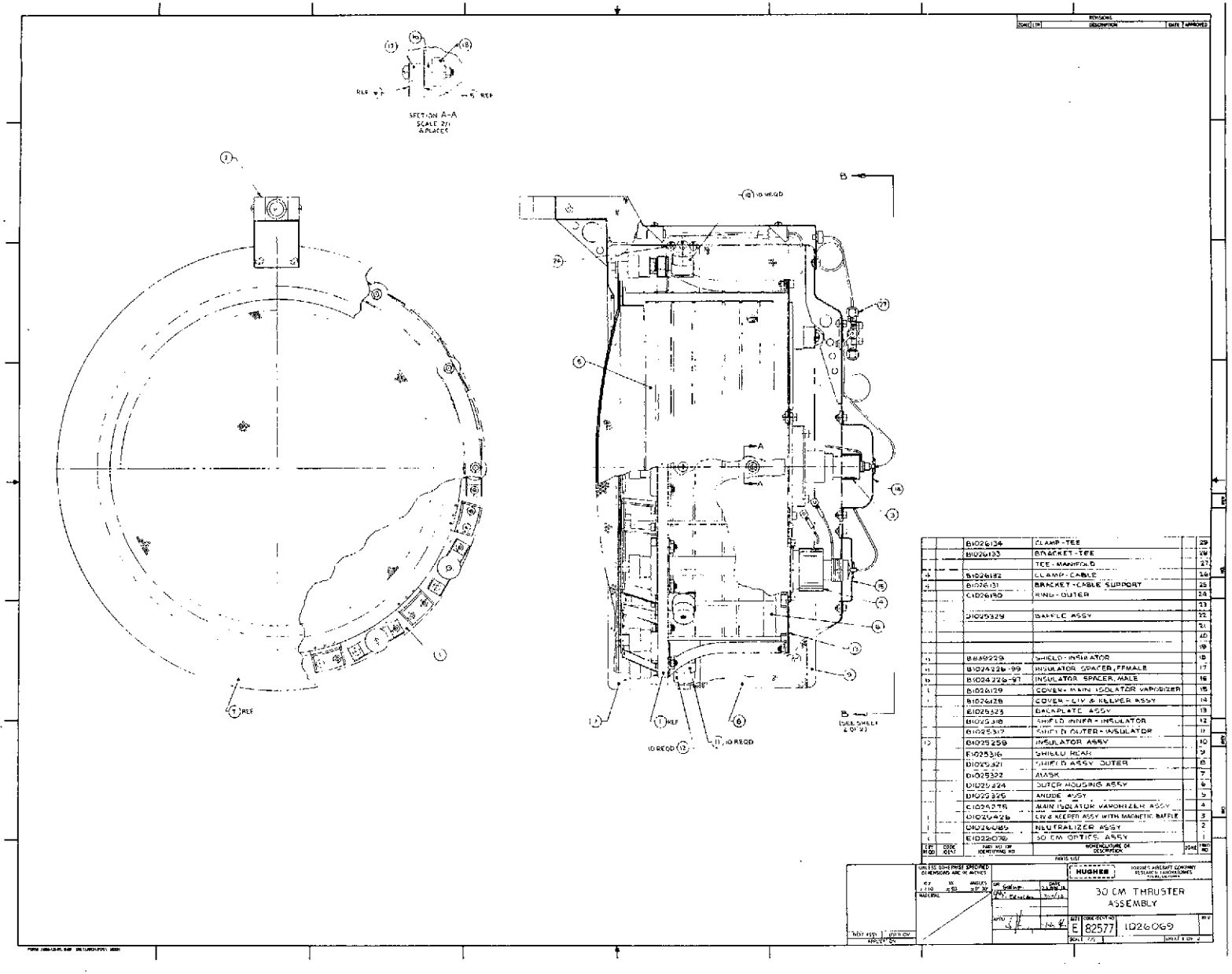

Fig. 39. 600-series thruster design.

was identified by the 600-series designation. The design changes made, relative to the 300/400-series, included:

- Use of dished grids
- Attachment of propellant lines at the vaporizers, to the ground screen
- A propellant manifold
- Twelve insulators for mounting the accelerator (instead of six).

A moderately successful shake test was performed on thruster S/N 601 as discussed in Section III. Although failures were experienced in this testing, valuable insight into the design strengths and weaknesses was obtained.

A detailed weight breakdown is presented in Table 11. Since the design goal was 7 kg, the 600-series thruster weight was unacceptable. The weight, shake test results, and an interest in mounting the thruster from two points on the girth to allow gimbaling, precipitated a major design revision.

4. 700-Series Design

As a result of design review recommendations by NASA LeRC and JPL, the thruster was redesigned and was designated as the Engineering Model (EM) thruster. Since this design is presently undergoing endurance testing, and since the 700-series thruster is quite similar to the final product of this program, a relatively detailed description of the design will be presented.

a. Structural Design – The design of the EM thruster provides a two-point thruster mounting configuration (180° apart) which is compatible with thruster system designs in which thrust vectoring is achieved by rotating the thruster about an axis normal to the thrust axis. The gimbal shafts are constrained in the axial direction on one side only, thereby imposing large transverse loads on the thruster assembly during launch. It is also desirable to provide mounting pads for the gimbal shafts which are accurately positioned

TABLE 11

Weight List for 600-, 700-, and 800-Series Thrusters

Item	Quantity	600-Series		700-Series		800-Series[a]	
		Material	Weight, g	Material	Weight, g	Material	Weight, g
Neutralizer Subassembly	1	[b]	300	[b]	255	[b]	346
CIV Subassembly	1	[b]	206	[b]	206	[b]	216
MIV Subassembly	1	[b]	151	[b]	165	[b]	170
Screen Stiffening Ring	1	Moly	330	Moly	184	[b]	–
Accel Stiffening Ring	1	Moly	366	Moly	220	Moly	215
Screen Electrode	1	Moly	173	Moly	175	Moly	146
Accel Electrode	1	Moly	500	Moly	380	Moly	322
Main Optics Support Ring	1	S. S.	360	S. S.	360	Ti	673
Screen Mounting Brackets	12	S. S.	240	S. S.	200	–	–
Accel Mounting Brackets	12	S. S.	113	S. S.	113	S. S.	113
Accel Insulators and Shields	12	Alumina and S. S.	236	Alumina and S. S.	236	Alumina and S. S.	236
Spacers	12	S. S.	48	Ti	8	–	–
Optics Fasteners	misc.	S. S.	197	S. S.	230	S. S.	188
Axial Magnet Retainer	12	S. S.	86	Ti	54	Ti	54
Axial Magnets	12	Alnico V	132	Alnico V	132	Alnico V	132
Radial Magnet Retainer	12	S. S.	10	Ti	22	Ti	22
Radial Magnet	12	Alnico V	170	Alnico V	270	Alnico V	270
Inner Magnet Retainer	1	Mild Steel	42	Mild Steel	42	Mild Steel	42
Outer Magnet Retainer	1	Mild Steel	184	Mild Steel	81	Mild Steel	81
Shield, Pole	1	Tantalum	22	Tantalum	22	–	–
Anode	1	S. S.	196	Ti	104	Ti	108
Outer Shell	1	S. S.	243	Ti	135	Ti	135
Pole	1	Mild Steel	159	Mild Steel	159	Mild Steel	165
Ring, Downstream	1	Mild Steel	235	Mild Steel	122	Mild Steel	122
Ring, Upstream	1	Mild Steel	173	Mild Steel	102	Mild Steel	102
Mask	1	S. S.	558	Ti	122	Ti	120
Rear Shield	1	S. S.	708	Al	252	Al	281
Outer Shield	1	S. S.	270	Al	211	Al	98
Plenum	1	S. S.	160	Ti	74	Ti	74
Insulation and Shields	20	[b]	183	[b]	365	[b]	365
Backplate	1	S. S.	354	Ti	192	Ti	184
Cover, Rear	1	S. S.	86	Al	13	Al	7
Anode Insulators and Shields	6	[b]	31	[b]	31	[b]	31
Cable Clamp	2	S. S.	22	Al	10	Nylon	58
Bracket-Tee	1	S. S.	18	Ti	10	–	–
Clamp-Tee	1	S. S.	7	Ti	5	–	–
Wire	1	Kapton and copper	152	Kapton and copper	185	Kapton and copper	265
Insulation	2	—	11		11		–
Frame Structure	1	S.S.	861	Ti	730	Ti	780
Baffle Assembly	1	–	168	–	250	Mild Steel	283
Rear Brace	2	–	–	Al	102	Ti	462
Gimbal Bracket	2	–	–	Ti	356	Ti	356
Fittings, Swagelok	1	S.S.	27	S.S.	27	S.S.	42
Connector, Electrical	2	–	101	–	–	–	–
Miscellaneous	misc.	–	360	–	360	–	497
Total, g			8959		7300		7758
Total, lb			19.73		16.08		17.09

[a]Based on thruster S/N 702-A.
[b]Combinations of Al_2O_3, tantalum, tungsten, stainless steel, inconel, MgO, and nickel.

T1521

and parallel so that a minimum of shimming and remachining is required to align the gimbal shafts with respect to each other and orthogonal to the thrust axis. Other important mechanical constraints are a 7 kg weight goal, flexibility in neutralizer and cable exit locations, and additional mounting pads in the event it is desired to mount the thruster from three or more points. In consideration of all these requirements, the design shown in Fig. 40 was conceived.

The basic structural element of this design is a cylindrical frame consisting of two annular rings supported by 12 box-type columns. The annular rings are channel-shaped sections located both at the backplate of the thruster and at the ion optics mounting interface. The rings are designed to carry loads in the transverse direction (in the plane of the ring), and have narrow flanges to resist twisting moments which may occur along the gimbal axis. The flanges also resist inplane twisting and bending forces which could be expected during vibration parallel to the thrust axis. The box-shaped columns strongly resist axial and bending forces.

Two beams are attached to the backplate of the thruster at the outer edges and to the cathode-isolator-vaporizer (CIV) mounting flange in the center. This serves to support the backplate with CIV, MIV (main isolator-vaporizer), propellant distributor, baffle assembly, and magnets during vibration parallel to the thrust axis. The gimbal mounting brackets are attached to the frame through six insulators. The bolt holes and two locating dowel holes are accurately positioned on each bracket with respect to the grid alignment holes by drilling in a precision fixture after final assembly has been completed. The pad dimensions and thruster envelope dimensions are shown in Fig. 41.

A computer static load and stress analysis was conducted in order to verify the adequacy of the design and aid in sizing of material thicknesses for the structural elements. The analysis was performed to design the structure as light as possible and with a minimum number of insulators and fasteners to assure that permanent deformation or failure of the structure does not occur during launch vibration with the goal of minimum weight penalty to the entire thruster system.

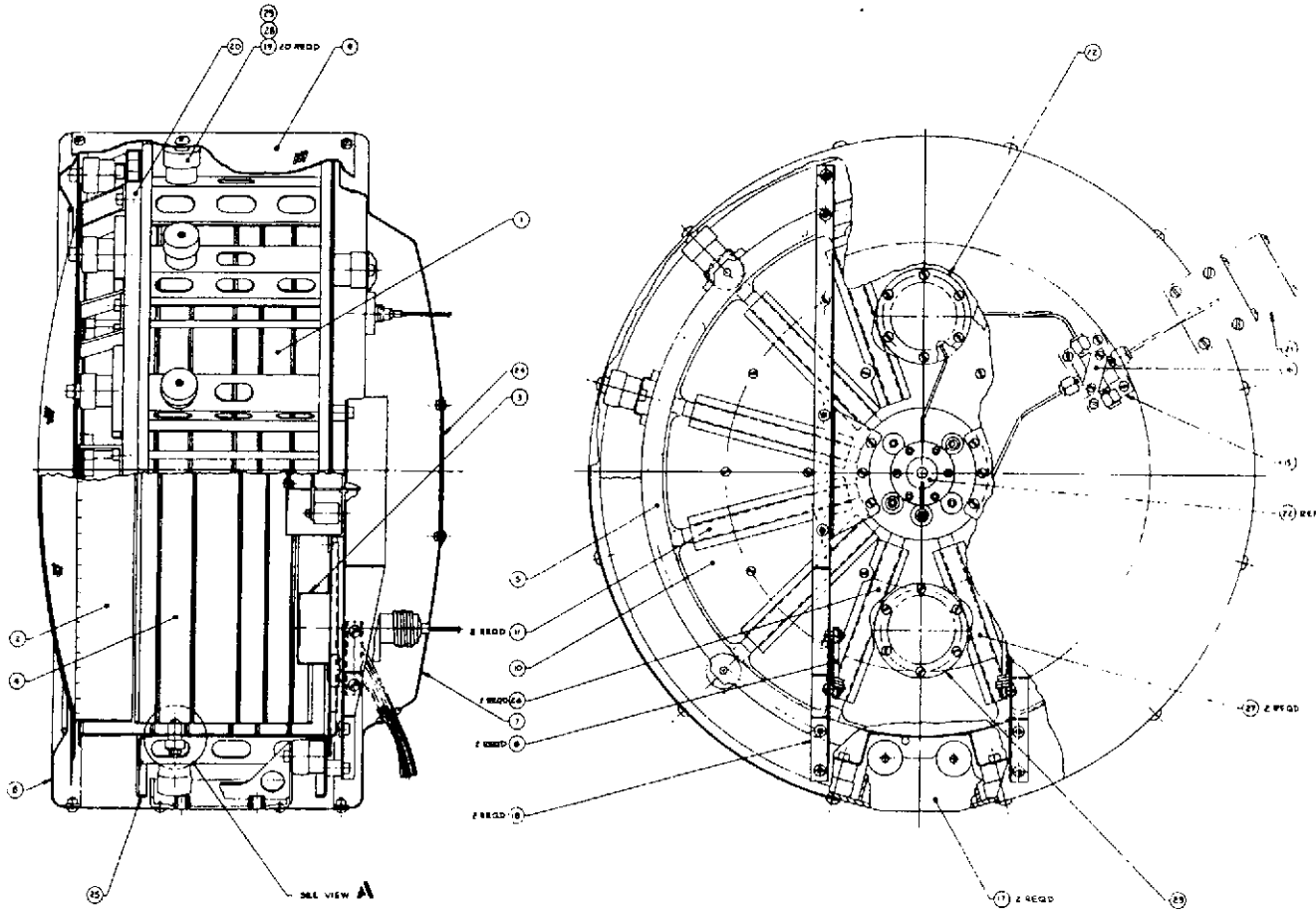

Fig. 40. 700-series thruster design.

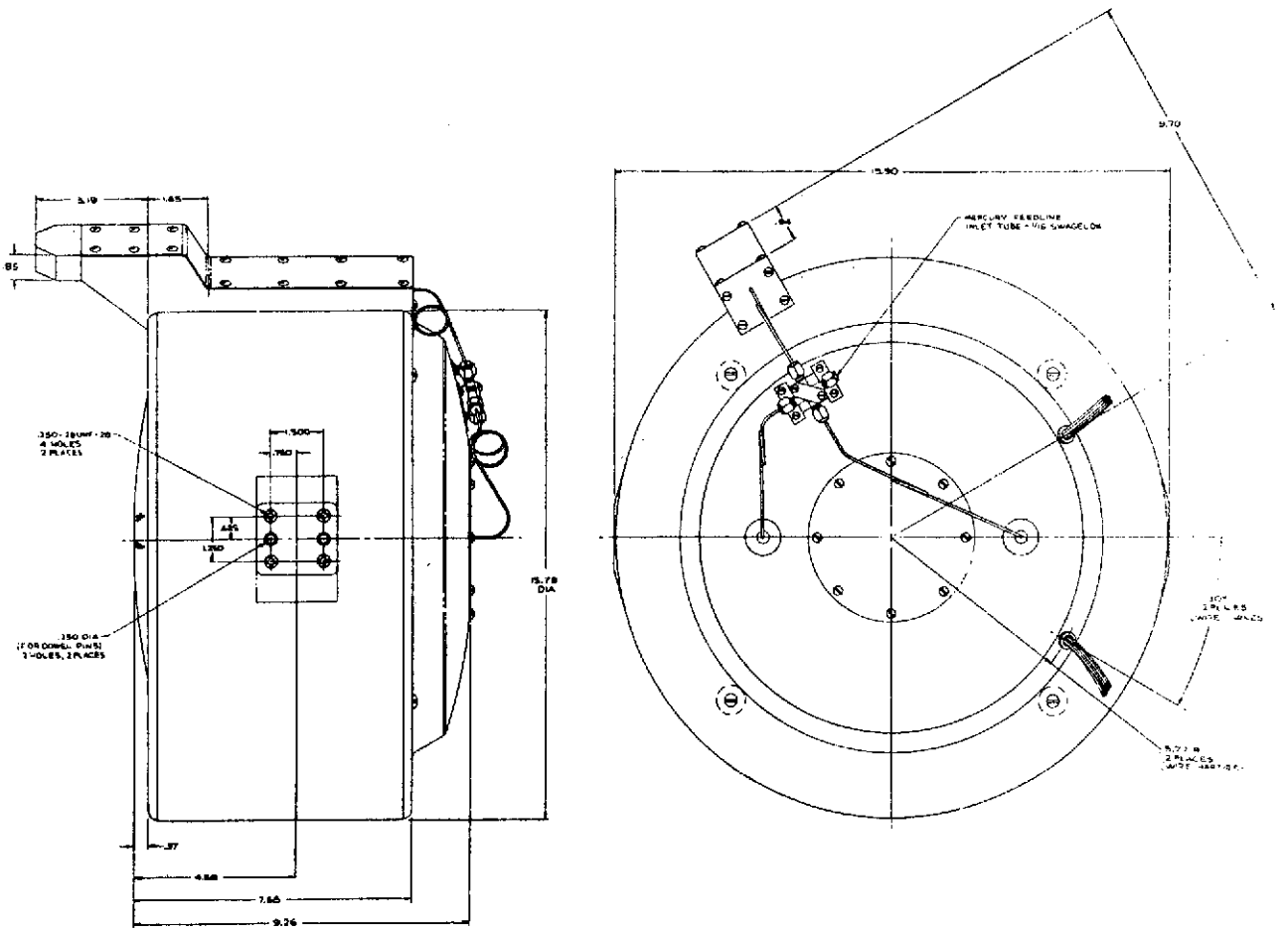

Fig. 41. 700-series thruster interface drawing.

To reduce the overall weight of the thruster assembly from the 9.0 kg of the prototype to the 7 kg goal, it was necessary to change materials of the discharge chamber and ground screen from stainless steel to titanium and aluminum. The entire discharge chamber, including anode, frame support assembly, propellant distributor, backplate, outer shell, and gimbal mounts is made of titanium and assembled by TIG and spotwelding methods. The ground screen, rear shield, and perforated outer shield are made of aluminum alloy (type 6061) and the downstream mask is titanium. A detailed weight breakdown of the EM thruster (S/N 701) is shown in Table 11. As shown, the weight of the 7.3 kg is within 5% of the original goal, including the capability for two point gimbaling.

b. Fabrication and Assembly – In the following discussion, the fabrication and assembly of the overall thruster is described. Note that details of the CIV, MIV, and NIV assemblies were discussed previously.

- Discharge Chamber and Ground Shield – This assembly is included in Fig. 40 with the other subassemblies attached. As described in the previous section, the basic structural element of this design is a cylindrical frame consisting of two annular rings supported by 12 box-type columns. The annular rings and vertical supports are fabricated by a vendor utilizing precision forming dies equipped with heaters necessary for successful forming of the titanium parts. These parts are assembled at HRL in a special assembly fixture as shown in Fig. 42. The parts are positioned in the fixture, clamped, and spotwelded prior to TIG welding in a large dry argon welding facility by the same vendor. The holes are then drilled while in the same fixture to assure precision hole location and repeatability.

The structure is removed from the fixture and the ion optics interface is ground to assure a flat mounting surface. The axial magnet retainers are then TIG welded to the frame. The outer housing is completed by spotwelding the outer shell, axial magnets, and magnetic rings in an argon atmosphere. The downstream pole is attached to the downstream magnetic ring by TIG welding at several places around the

M10027

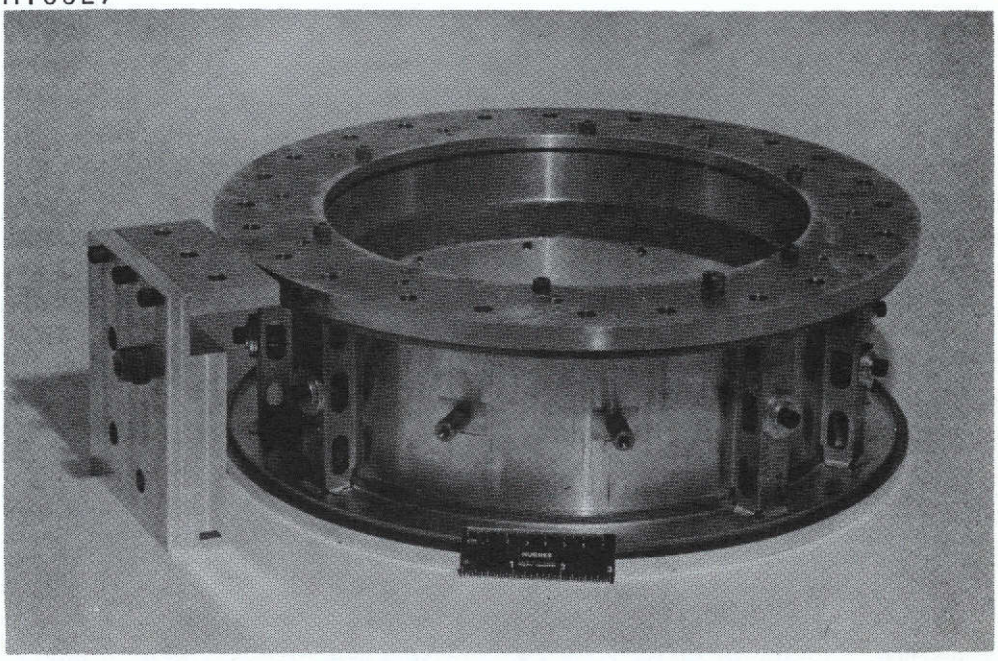

Fig. 42. Thruster shell structure welding and drilling fixtures.

periphery. The assembly at this point is shown in Fig. 43 and weighs 1290 g.

The 12 radial magnets are then attached to the backplate by 0.02-cm thick titanium magnet retainers by spotwelding. These magnet retainers are formed in the form die shown in Fig. 44.

- Thruster Final Assembly – Major subassemblies described are then assembled to form the complete thruster, as shown in Fig. 45. Two aluminum beams, seen in Fig. 46, are attached to the main cathode mount and the backplate of the thruster at the outer edges to provide a high conduction thermal path to the outer ring. Each gimbal mounting bracket is attached to the frame through six insulators. The bolt holes and two locating dowel holes are accurately positioned on each bracket with respect to the grid alignment holes by drilling in a precision fixture after final assembly has been completed. The pad dimensions and thruster envelope dimensions are shown in Fig. 41. The neutralizer and cable exit locations were specified for the EM thruster as shown.

c. Structural Verification – The details of the structural testing program on thruster S/N 702 are presented in Section III. The shake test at 18 g (sinusoidal) resulted in the failure of one of the rear plate support beams and portions of the neutralizer assembly. In order to correct the structural weaknesses observed, a separate repair contract was initiated (NAS 3-18334). However, in addition to the items changed solely for structural integrity, several additions and modifications were directed by the NASA program manager. The thruster design resulting from this activity was designated as the 800-series.*

*Thruster S/N 702 was modified to the 800-series design but was designated 702-A.

M9955

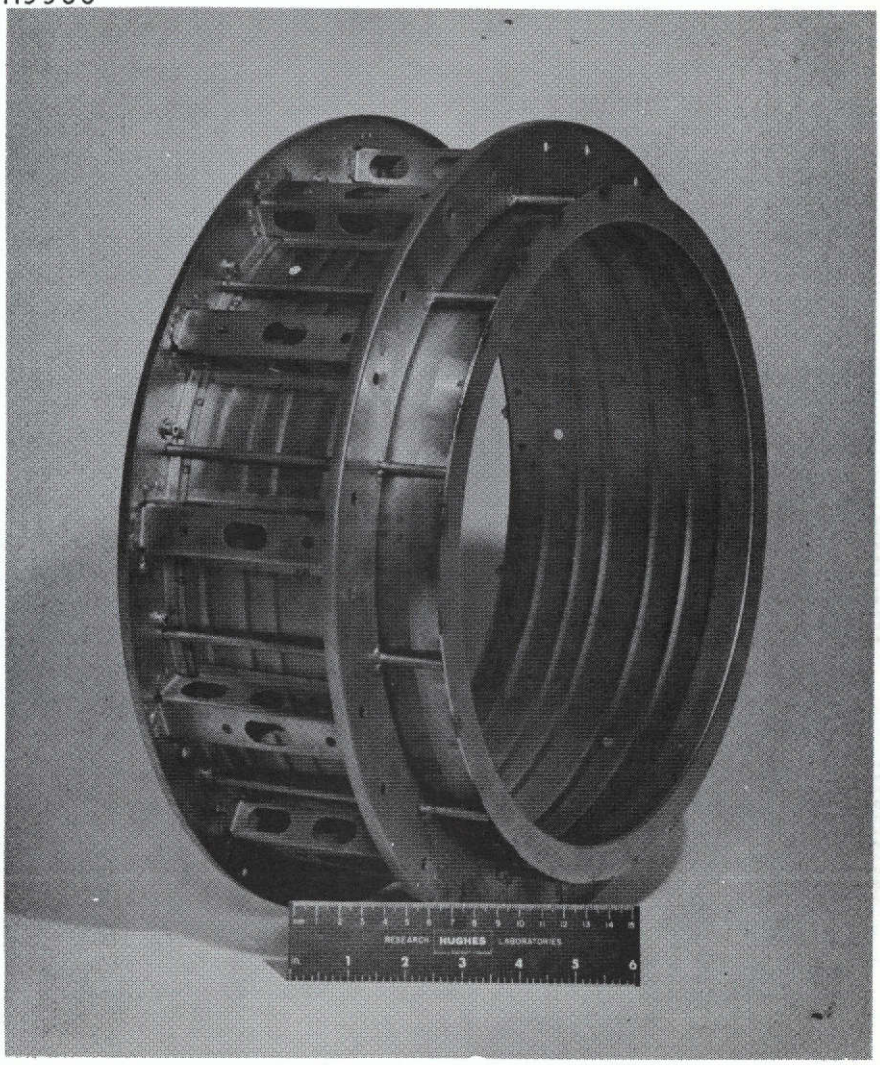

Fig. 43. 700- and 800-series thruster basic structure.

M10029

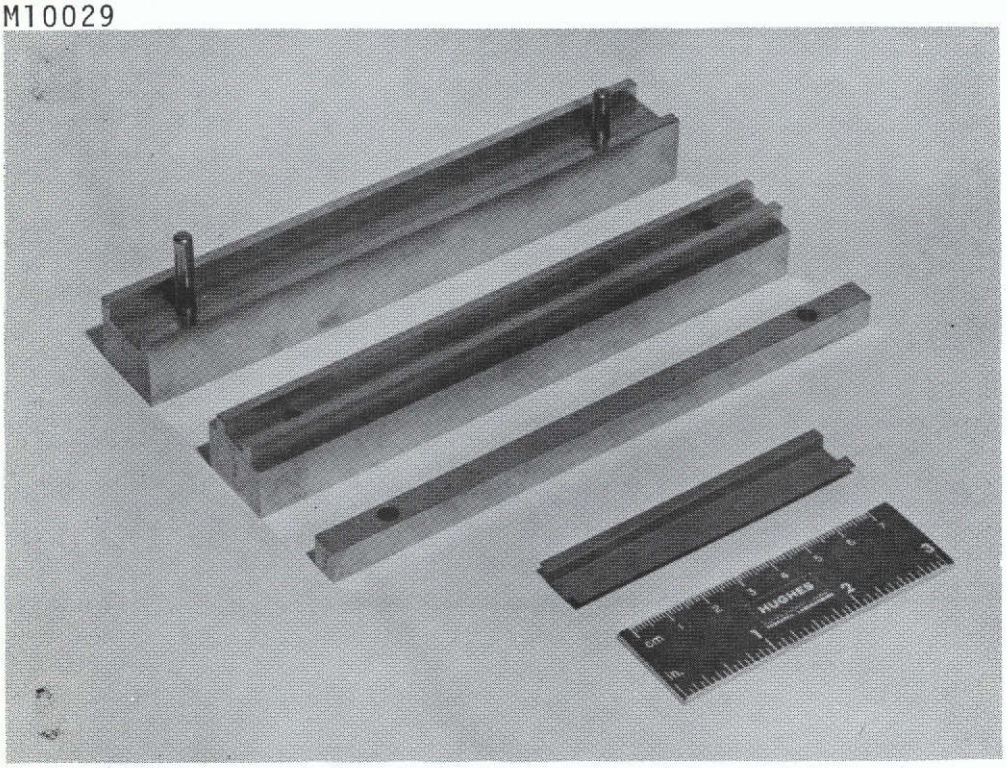

Fig. 44. Radial magnet retainer forming die.

M9963

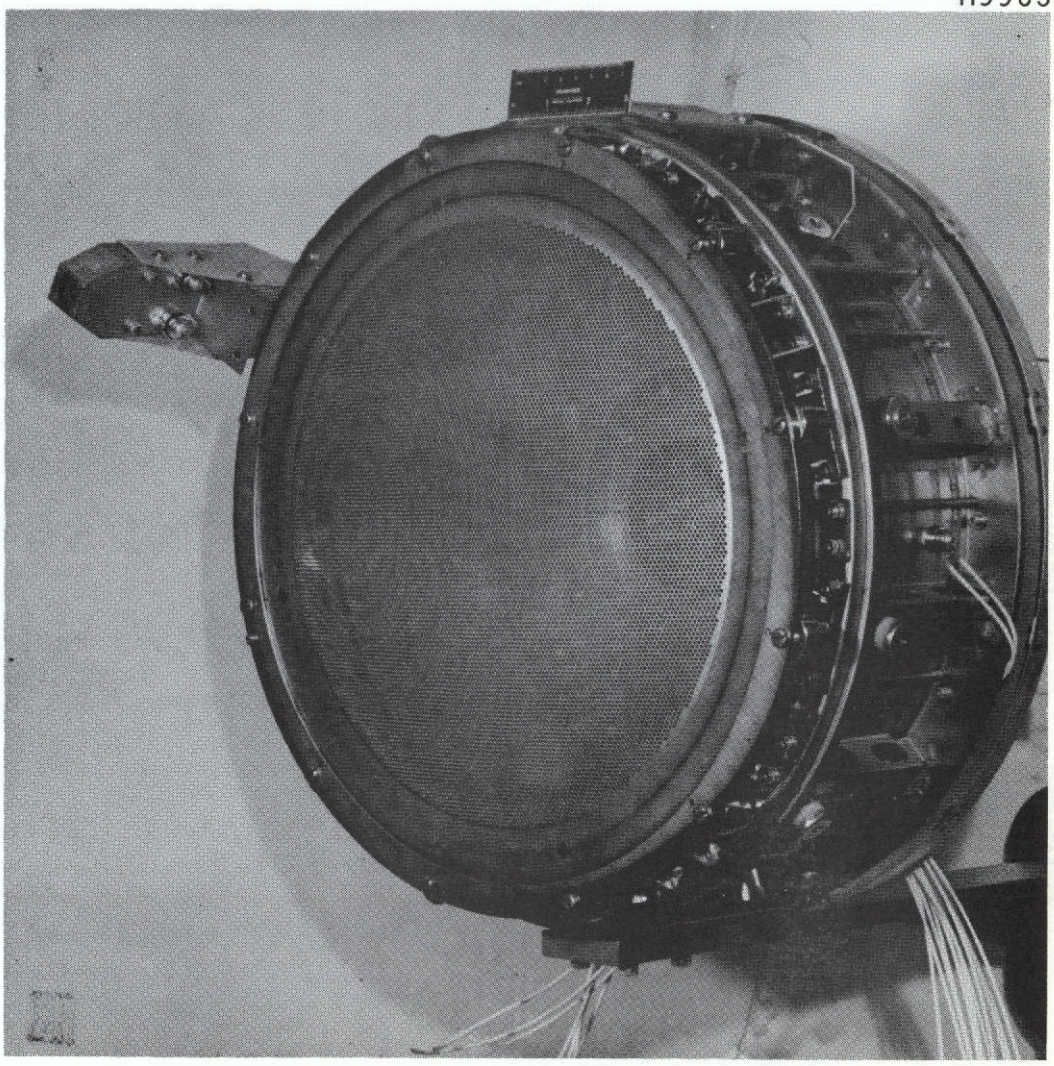

Fig. 45. Photograph of 700-series thruster without the ground screen, front view.

M9959

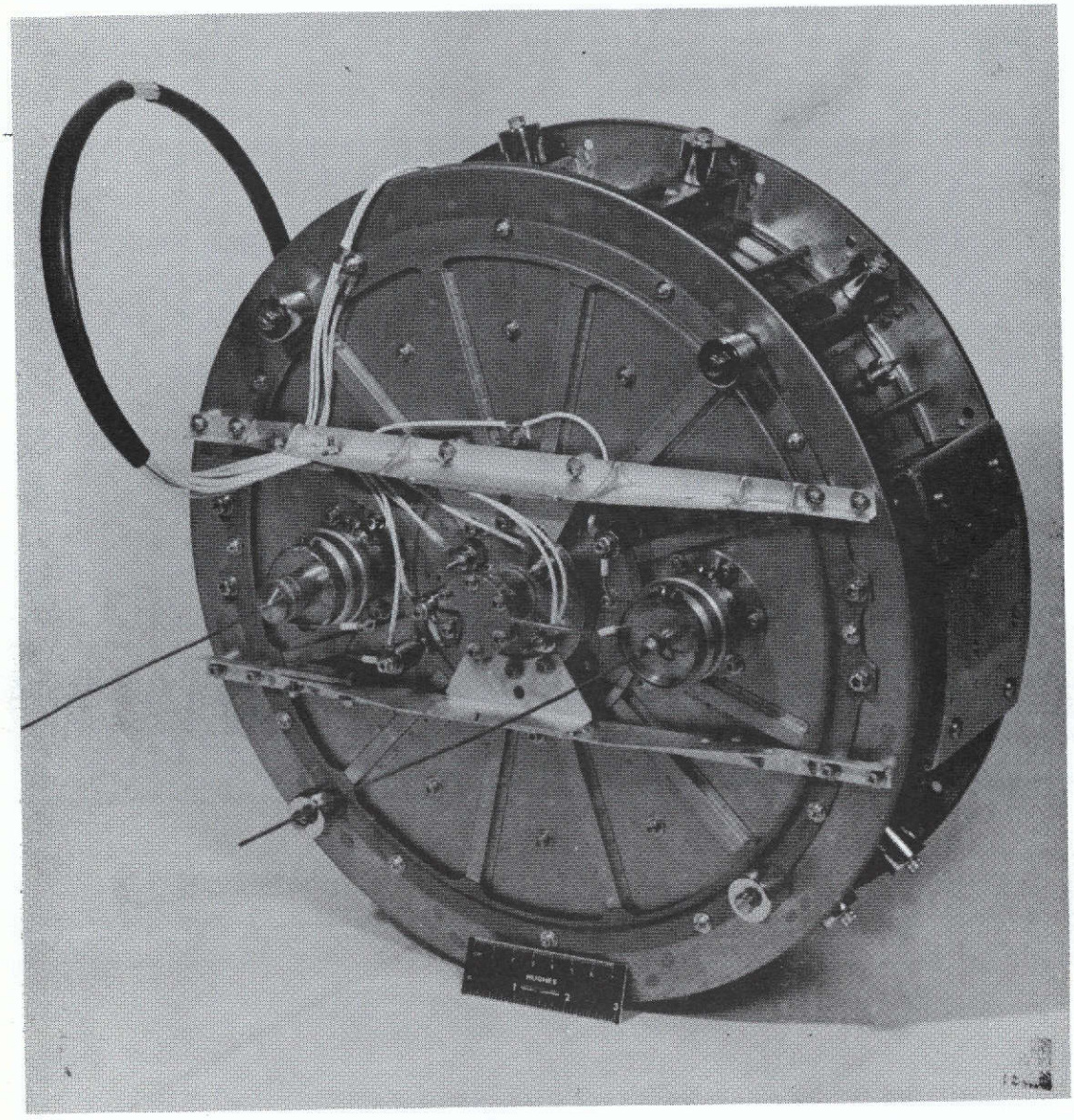

Fig. 46. Photograph 700-series thruster without ground screen, rear view.

5. 800-Series Design

The 800-series thruster design is illustrated in Figs. 47 and 48. The changes from the 700-series design include:

- Replacement of the aluminum rear beams with a titanium cross structure
- Addition of terminals under the ground screen for all wiring
- Location of a propellant manifold under the ground screen
- Relocation of the propellant inlet to the vaporizers (from on-axis to right angle)
- Addition of a wiring harness and support brackets
- Use of a chemically etched ground screen
- Use of the one piece ion optical system structure (Fig. 21)
- Modification of the neutralizer mounting structure.

The elements of the design modification center primarily around the thruster backplate structure except for minor modifications to the neutralizer assembly. Four hollow titanium beams (1.27 cm x 1.9 cm) serve to stiffen the backplate and support the cathode, isolator and plenum assemblies. Stainless steel feed lines exit the main and cathode vaporizer housings parallel to the backplate and manifold at two stations to ensure short feed line runs. Propellant manifolds are supported by double shadow shielded insulators. Provision for a temperature sensor is made on one surface of the exit manifold. This sensor is necessary to detect a frozen mercury feed system. The aluminum rear shield has four dip brazed caps at the periphery to allow sufficient separation to the rear braces. The rear shield is easily removed without disturbing the feed system or harness. The terminals, located in a relatively cool environment, provide ease of interfacing with power processing systems. The harness exits through a fiberglass impregnated nylon cable clamp.

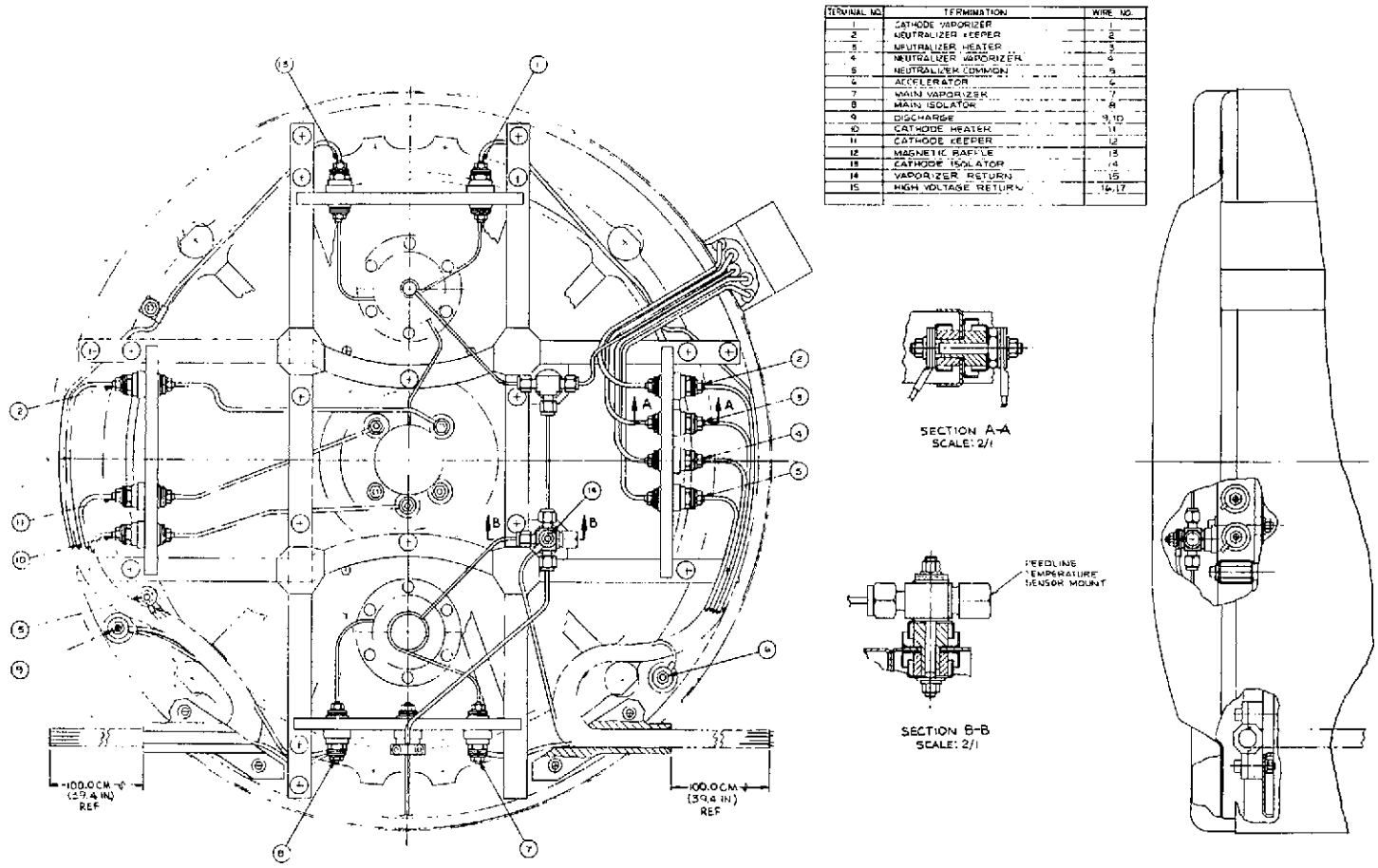

Fig. 47. 800-series thruster design, rear layout.

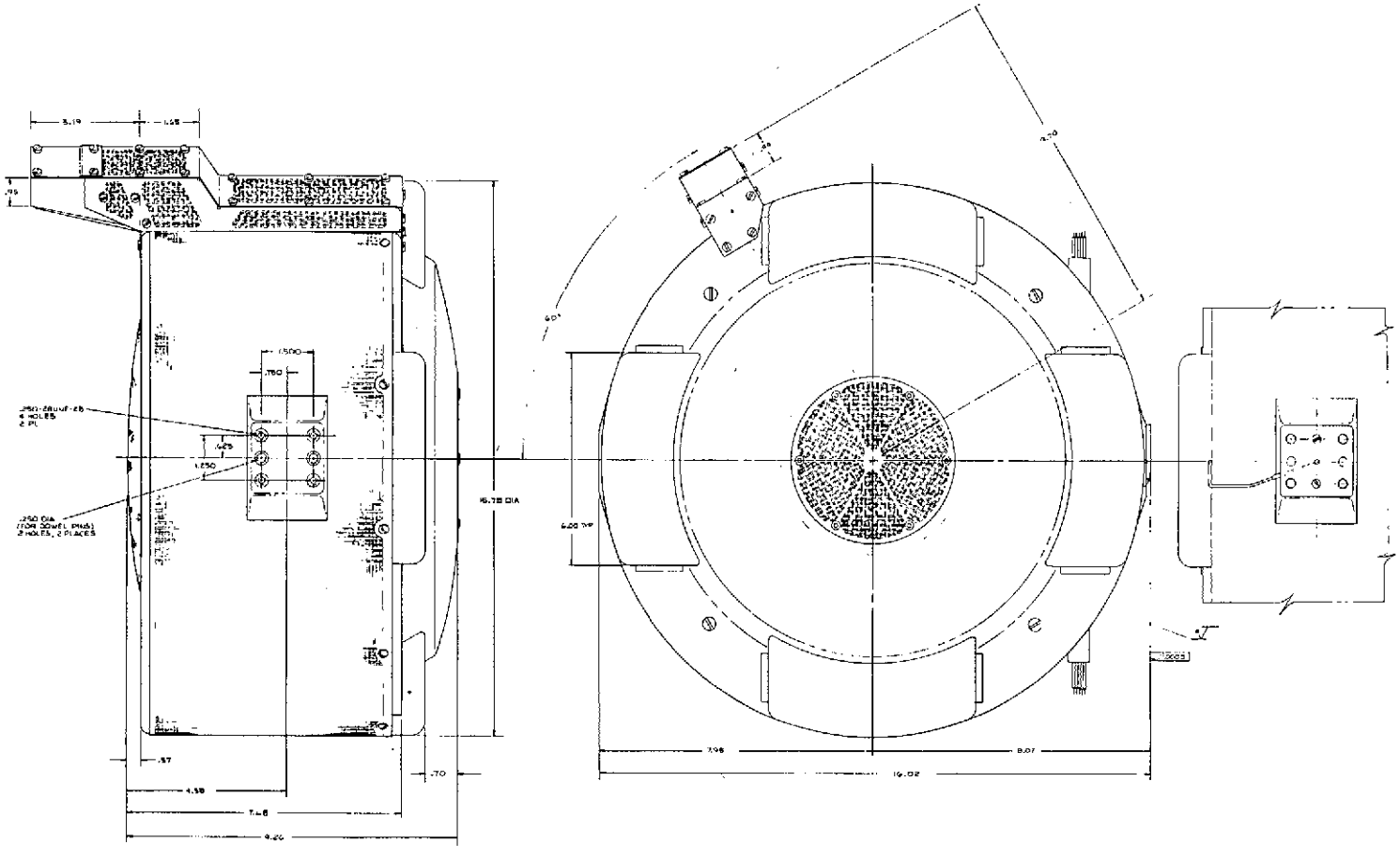

Fig. 48. 800-series thruster interface drawing.

The 700-series ion optics mount contained 12 screen grid mounting brackets which were attached to a tubular stainless-steel ring. This ring was then mounted to the titanium annular ring. Ion optics alignment was complicated by distortion of the stainless-steel ring and of the 12 mounting brackets. In the 800-series thruster this has been changed to a titanium mounting structure, which mounts directly to the annular ring. The screen grid (without a molybdenum stiffening ring) will mount directly to the titanium optics mount. Prior to incorporating the titanium optics assembly a successful vibration test was performed at vibration levels commensurate with the amplification factors derived from previous tests of S/N 702. Calibration on a thruster before and after vibration test indicates reproducible performance and good structural integrity. The optics assembly weight savings amounts to approximately 100 g.

In other respects, the 800-series thruster design and assembly is similar to the previously discussed 700 series. Photographs shown in Figs. 49 and 50 accurately represent the 800-series design, although the actual thruster shown is S/N 702-A. The structural integrity of the 800-series design was verified in shake tests described in Section III.

F. Thruster Control and Power Processing

Thruster operation and testing undertaken on the thruster development program used high frequency modularized transistor power processing circuitry which was especially configured to be similar in its electrical characteristic to flight systems.[11] Two such power processing systems were available. One unit is permanently located in the 9-ft-diameter vacuum chamber testing area. The implementation of the power and control circuitry in this system was previously reported (CR-120919).[1] The second unit available to the program was a new movable three bay test console, shown in Fig. 51, which contains a complete power conditioning subsystem, thruster controls and reasonably extensive instrumentation. Both systems were constructed using company funds and intended for use in support of thruster development programs.

M10542

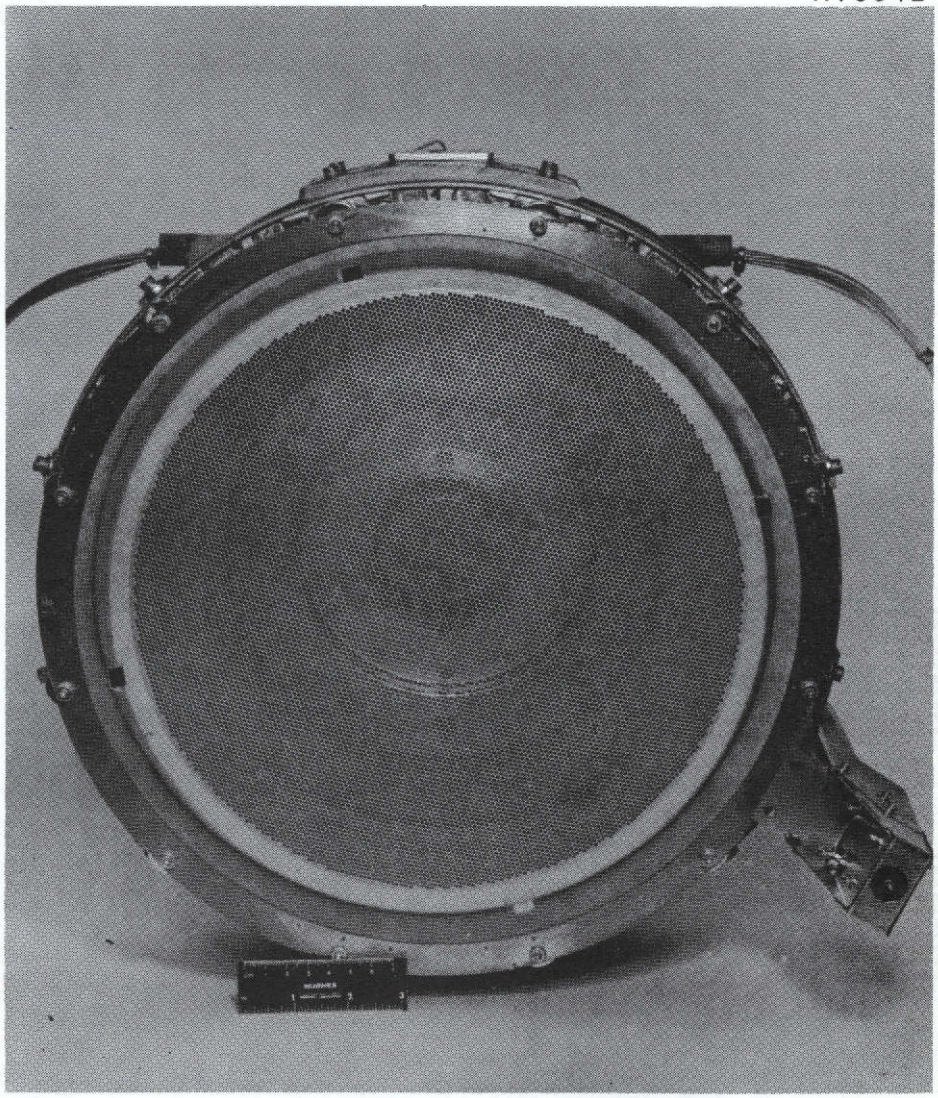

Fig. 49. Photograph of 800-series thruster without ground screen, front view.

M10543

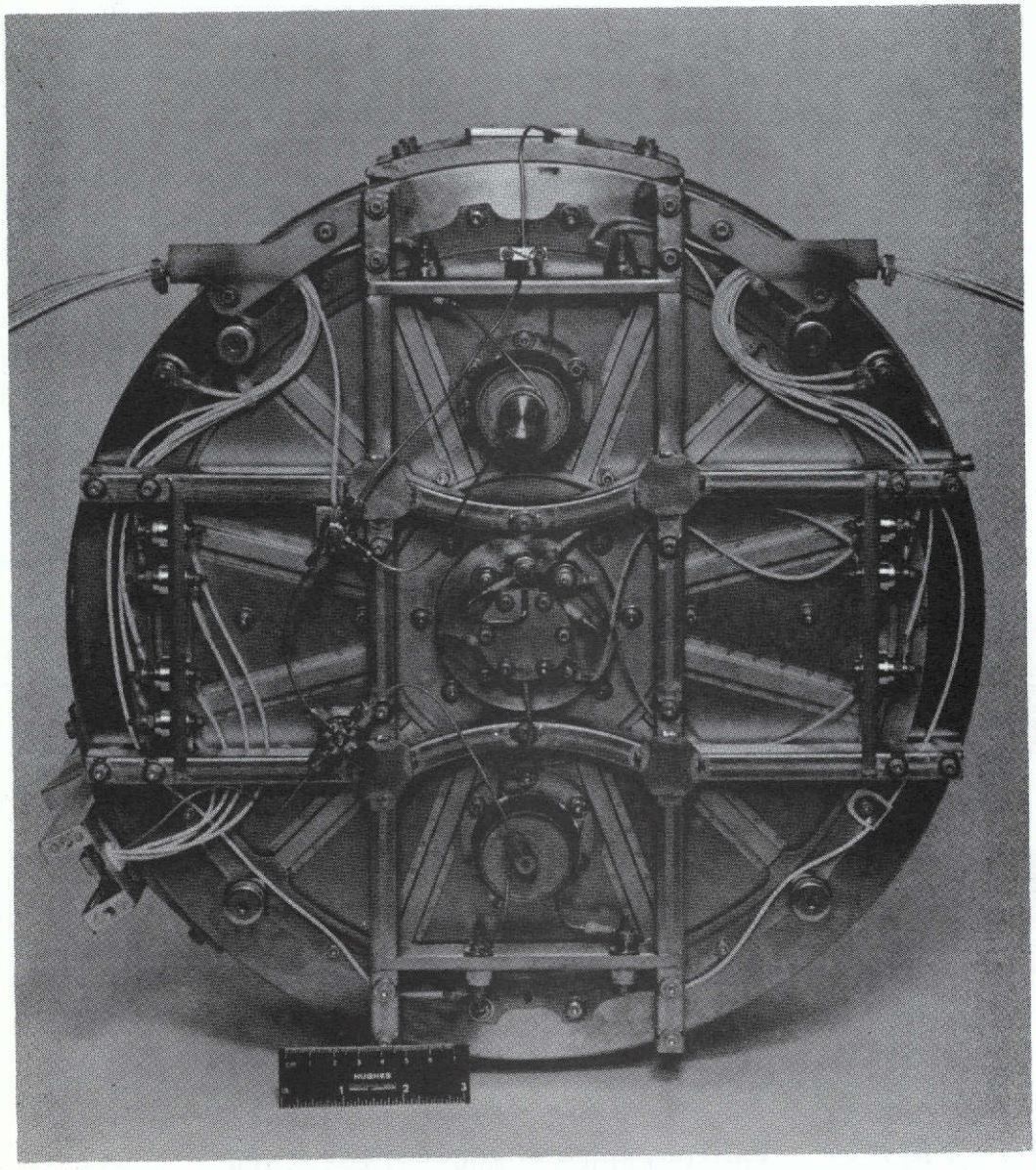

Fig. 50. Photograph of 800-series thruster without ground screen, rear view.

M9946 2722-7

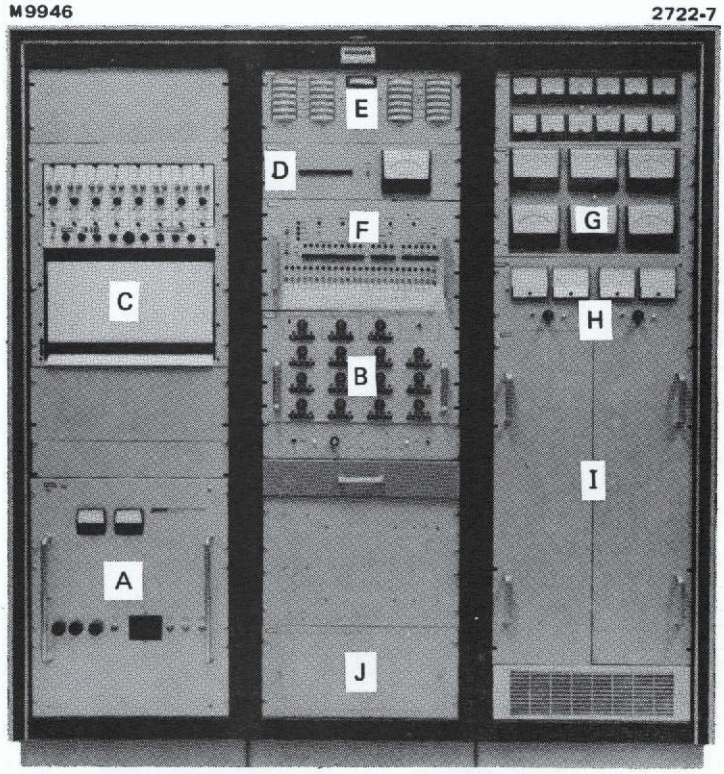

A. BUS POWER SUPPLY (+250 NOMINAL)
B. CONTROLLER
C. 8-CHANNEL STRIP CHART RECORDER
D. TRUE RMS DATA ACQUISITION AND METERING
E. TELEMETRY V&I METER PANEL
F. SEQUENCER
G. DIRECT READING OUTPUT V&I METER PANEL
H. AUXILARY ELECTRO-MAGNET POWER SUPPLIES
I. POWER PROCESSOR UNIT
J. PATCH PANEL AND SIGNAL CONDITIONING UNIT (COVER IN PLACE)

Fig. 51.
30-cm thruster three bay power processor test console.

The electronic-related task on the low voltage thruster program was the development of a sequencer to augment the existing power and control circuitry in the three bay test console to provide for programmed thruster startup and shutdown, and for automatic recovery from various anomalous thruster operating conditions. Originally the development phase for the sequencer was to include detailed circuit design, unit fabrication and integration/evaluation testing of the total system during thruster operation. Contracted effort on the sequencer, however, was terminated at the completion of design to allow greater emphasis to be placed on other program tasks. Soon after the design was completed, implementation of the sequence was initiated on company funds and successfully integrated into the console.

The details of the power processor test console functions and operations are discussed in Appendix B. Therefore, the discussion in this section will be limited to a brief summary of the sequencer functions and operational results.

The sequencer operates by choosing from among a selection of nine 24-bit digital commands contained in a read-only memory (ROM) and expanding the selected work into a 33-bit word suitable for presentation as the controller state word. The ROM also contains a tenth word position, or address, which allows an operator to enter a command word of his choosing by means of switches on the front panel. The ROM thus contains the startup and shutdown procedures as sets of digital command words. The assignment of these words as presently wired into the discrete components ROM is given in Table 12.

An example of sequencer operation during thruster startup is shown in Fig. 52. The startup can be performed automatically or with operator assistance. The time periods between some of the events illustrated in Fig. 52 are adjustable. That is, the time sequencing of heaters can be adjusted to match the characteristics of the thruster. The time required to start keepers or the discharge depends largely on the thruster. The reader is referred to Appendix B for a more complete discussion of the startup sequence.

TABLE 12

ROM Word Assignments 30-cm Thruster Sequencer

Address	Segment	Comments
0	Off	All supplies commanded off
1	Preheat	Activate vaporizers and heaters
2	Neutralizer Keeper	Ignite neutralizer keeper
3	Cathode Keeper	Ignite main cathode keeper
4	Discharge 1	Ignite discharge
5	Discharge 2	Hold until thermal equilibrium is established
6	Command Word	Transfer command word from front panel switches to sequencer outputs. This is the steady-state operating segments
7	High Voltages Off	This special command allows the thruster to be maintained in a hold mode with the high voltages off
8	Shutdown 1	First command of shutdown procedure
9	Shutdown 2	Final command of shutdown procedure. Return to 0 at completion

T1522

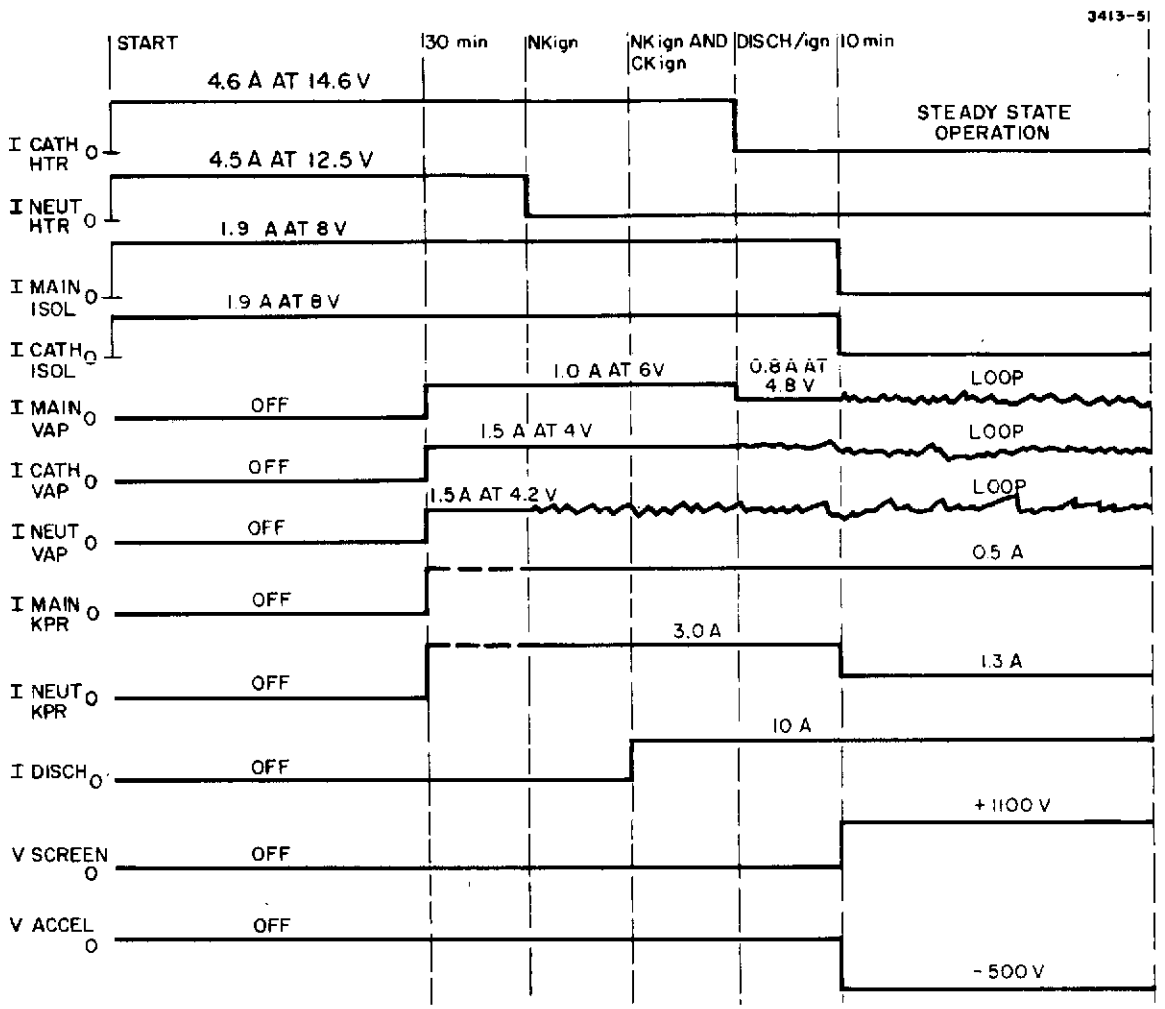

Fig. 52. Typical thruster startup sequence.

III. THRUSTER TESTING

A broad range of tests were performed during the conduct of this thruster development program. However, as noted previously, concurrent programs for endurance testing and advanced technology development substantially supplemented this work. The testing described in this section is intended to define the overall operational characteristics of the thruster. Component and subassembly tests, except for vaporizer calibration, were discussed in Section II. Vaporizer calibrations during both thruster tests and in bell jars are included here for comparison.

This section is divided into four topics: (1) Performance evaluation techniques, (2) performance corrections, (3) overall performance (total efficiency, specific impulse, and thrust) including corrections for double ions and beam divergence, and (4) structural integrity tests. Vaporizer calibrations and temperature measurements are included in Section III-B.

Thruster overall performance (efficiency, thrust, and specific impulse) must be estimated from measurements of electrical efficiency, propellant efficiency, ion beam divergence, and beam double ion content. The results presented in this report include work performed under Contract NAS 3-16949 to develop correction factors for double ions and beam divergence.

Structural integrity tests were performed for the 600-, 700- and 800-series* thruster designs. Although failures were encountered in the 600- and 700-series designs, only minor modifications to the 800-series are required to produce a dynamically qualified thruster design. The shake test results presented in this report are summarized from and referenced to the detailed test reports submitted to NASA as separate documents.

*Thruster 702-A was modified to the 800-series configuration for shake testing.

A. Performance Evaluation Techniques

The determination of thruster true performance requires accurate electrical measurements (using specific voltage reference points), flowrate measurements, correction for double ion content in the beam (introduces an error in computing ion mass flowrate), and correction for ion beam divergence (reduces axial ion velocity). The basic relationships defining thruster performance are as follows:

1. Thrust

$$T = \dot{m}\bar{v}$$

$$= \frac{I_b}{(\eta_1 + 2\eta_2)} \left(\frac{M}{e}\right) \bar{v} \tag{3}$$

$$= I_b V_b^{1/2} \left(\frac{2M}{e}\right)^{1/2} \left[\frac{(\eta_1 + \sqrt{2}\eta_2)}{(\eta_1 + 2\eta_2)}\right] F_t \tag{4}$$

$$= I_b V_b^{1/2} \left(\frac{2M}{e}\right)^{1/2} \gamma \tag{5}$$

where

$\dot{m}$ = Total propellant rate

$\bar{v}$ = Propellant average exhaust velocity

I_B = Beam current

M = Atomic mass

e = Electronic charge

g = Gravitational constant

η_1 = Mass fraction of Hg^+

η_2 = Mass fraction of Hg^{++}

$(\eta_1 + 2\eta_2)$ = Apparent mass utilization efficiency (measured in the lab)

$(\eta_1 + \sqrt{2}\eta_2)$ = Correction applied to ion velocity to account for ion contributions to $\bar{v}$

$$\left[\frac{(\eta_1 + \sqrt{2}\eta_2)}{(\eta_1 + 2\eta_2)}\right] = \alpha$$ = factor required to correct measured performance for Hg^{++}

$F_t = \cos\theta$ = "Thrust Loss" factor due to ion beam divergence

$\cos\theta$ = Average of the cosine of all beam trajectories

$\gamma = \alpha F_t$

2. True Specific Impulse

Specific impulse can be calculated directly from (5) using the definition

$$I_{sp} = \frac{T}{mg} = \frac{\bar{v}}{g} \tag{6}$$

or by multiplying the "electrical" specific impulse by the factor γ

$$I_{sp} = \left[\frac{(\eta_1 + 2\eta_2)}{g}\left(\frac{2eV_b}{M}\right)^{1/2}\right]\gamma \tag{7}$$

3. Total Efficiency

Thruster total efficiency results from the relationship between input power, thrust, and specific impulse. The derivation is presented here to clarify the source of certain terms appearing in the final result. The derivation starts with an energy balance for the ion beam.

$$\eta_e P = \frac{1}{2}\dot{m}_i v_i^2$$

$$= \frac{1}{2}\dot{m}(\eta_1 + 2\eta_2)\left[\frac{\bar{v}}{(\eta_1 + \sqrt{2\eta_2}\ F_t)}\right]^2$$

$$= V_b I_b$$

With the use of previously defined terms

$$P = \frac{T I_{sp} g}{2\eta_m \eta_e}$$

$$= \frac{T I_{sp} g}{2\eta_t} \qquad (8)$$

where

P = Thruster total input power

η_e = Electrical efficiency as measured

v_i = Ion velocity

$\dot{m}_i$ = Ion mass flowrate

$\eta_m = \left[\frac{(\eta_1 + \sqrt{2}\eta_2)^2}{(\eta_1 + 2\eta_2)}\right] F_t^2$ = True propellant utilization efficiency

$\eta_t = \eta_e (\eta_1 + 2\eta_2) \gamma^2$ = Thruster corrected total efficiency

The methods used to determine the α and F_t corrections are discussed in the next section. Thruster performance, with and without the corrections, is then discussed for the thruster configurations tested in Section III-C.

Primary electrical measurements and current flows are as shown in Fig. 53. This schematic is the standard setup for measurements taken during the present program. Other supplies, such as heaters and keepers, are clearly important in determining electrical

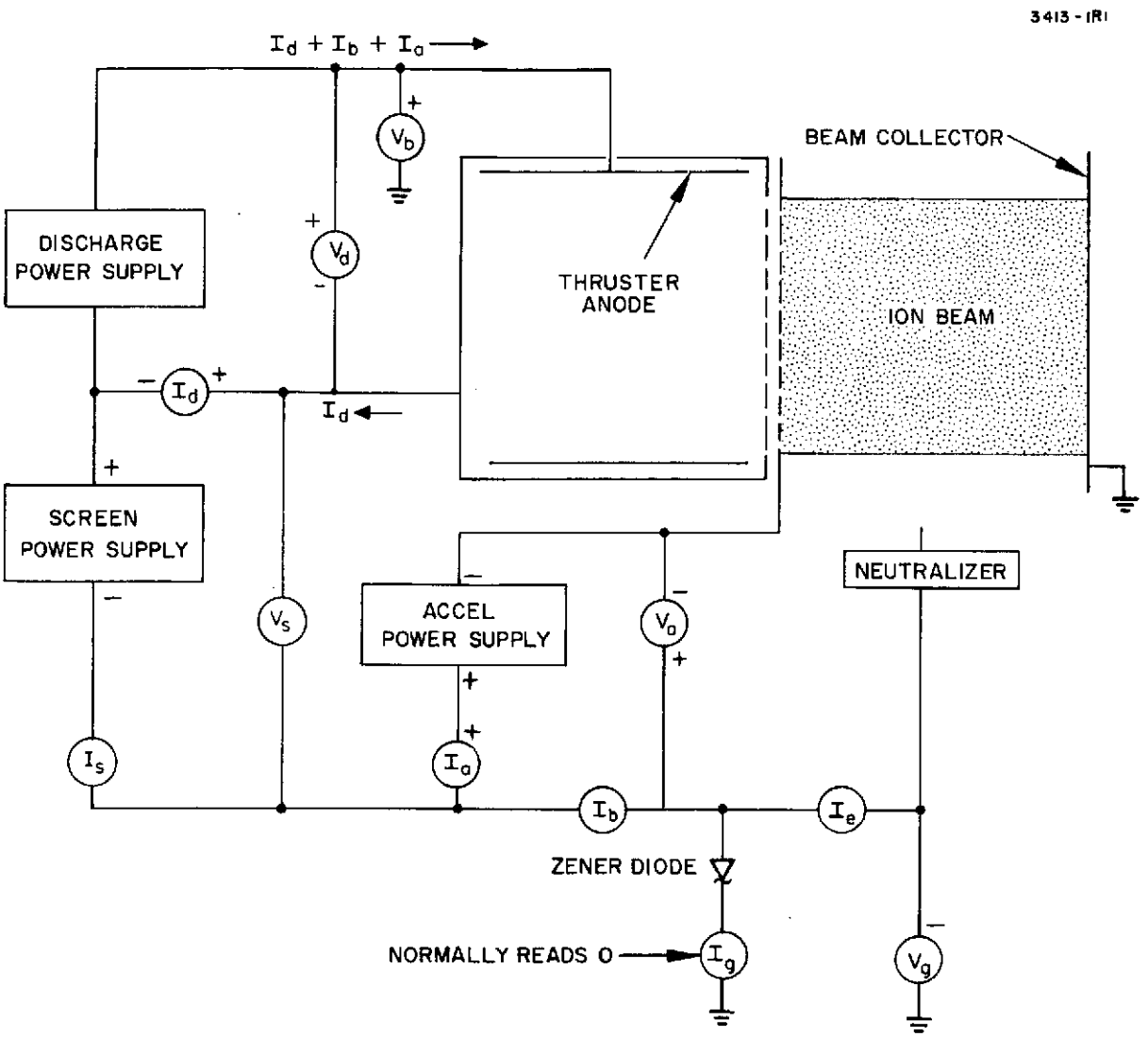

Fig. 53. Schematic of principal power supplies and meter locations used for performance measurements.

efficiency, but do not affect calculations of specific impulse or thrust. With the wiring connections shown in Fig. 53, the "Beam Voltage, V_b," appearing in earlier equations must take into account discharge voltage and beam-to-neutralizer coupling.

In the laboratory measurements, the ion beam is grounded to vacuum tank surfaces. The power processing is "floated" away from ground, to a voltage determined by neutralizer operating conditions but limited by the zener diode. In space operation, the beam potential (relative to spacecraft potential) will be determined by the voltage drop through the neutralizer "plasma bridge" (i.e., coupling voltage = V_c). The coupling voltage should be essentially equal to present laboratory measurements of V_g (Fig. 53).

The impact of discharge voltage on ion velocity results from the fact that ions "originate" at approximately anode potential. Thus, ions entering the beam at the screen grid have an initial energy of V_d. Taking both V_d and V_c (or V_g) into account, the net ion beam voltage is

$$V_b = V_s + V_d - V_c \tag{9}$$

where V_s is the screen power supply output voltage.

This clarification of voltage references and of current paths shown in Fig. 53 allows a definition of thruster electrical efficiency, η_e.

$$\eta_e = \frac{\text{power out}}{\text{power in}} \tag{10}$$

$$\text{Power out} = I_b V_b$$

$$\text{Power in} = (I_b + I_a) V_s + (I_d + I_b + I_a) V_d + I_a V_a + \text{other losses.}$$

Note that although the discharge power supply carriers ($I_b + I_d + I_a$), the experimental setup provides for measuring I_d alone. However, a direct measurement of I_b without I_a is not possible, so I_a must be subtracted from I_s to obtain I_b.

Two methods of monitoring mercury flow from propellant reservoirs have been used during this program. One method uses a standard laboratory glassware type calibrated pipette as a reservoir for each vaporizer. The reservoir level is read at regulat intervals, usually ten minutes, for a period of 1 to 2 hours. Data are plotted and a best fit straight line is fitted graphically to the points. Propellant flow is computed on the basis of 1.81 equivalent amperes per milliliter of mercury consumed per hour. A second method makes use of load cells as weighing devices for each mercury reservoir. Readout is obtained in digital form from the load cell electronics and can be calibrated directly (within a constant scale factor) using standard weights. Conversion to equivalent amperes is made on the basis of 0.1333 A per gram of mercury consumed per hour. These two methods of measuring mercury flow rate have been compared and found to agree within 1%.

In addition to these measurements for determining thruster performance, a significant amount of effort has been applied to documenting thruster dimensions, magnetic fields, and operating conditions for each discharge chamber configuration evaluated. This is an important aspect of developmental testing since design specifications will be necessary to convert the optimum configuration into more refined hardware. While it is impossible to assess, a priori, the impact of seemingly minor dimensional or configurational changes required to improve structure or reduce weight in a fully engineered thruster design, a complete record of preliminary experimental configurations facilitates the identification of possible differences responsible for changes in performance which may occur.

B. Performance Corrections

Measurement techniques for determining correction factors for double ion content and beam divergence were developed primarily under Contract NAS 3-16949[3, 12] The results of that work are summarized here since the corrections are fundamental to accurate performance estimates. The general nature of the corrections and their analytical relationship to true performance was discussed in the previous section.

A single ion beam probe is used to obtain the data necessary for determining double ion content and beam divergence. The probe unit is shown schematically in Fig. 54. It consists of a collimator, an ExB separator section, a drift tube, a separation aperture, and a collector. In order to focus on a sufficiently small area of the accelerator grid, a collimator with an acceptance half angle of 0.3° was chosen. Thus, at an axial distance of 38 cm the probe viewing area is $0.132\ cm^2$. The magnetic field is provided by a small 1400 G permanent magnet. The electric field plates are perpendicular and equal in length to the magnetic poles. The location of mass separator in relation to the thruster is shown in Fig. 55, where θ is the probe angle relative to the beam axis, and r is the probe radial position. Both the angular and radial positions of the probe are maintained with the use of stepper motors. A typical probe output trace is shown in Fig. 56, where the collector current is plotted as a function of voltage applied to the E-field deflection plates.

A data scan is taken by fixing the angle, θ , and measuring at a number of thruster radial positions, r, the single and double ion probe collector currents i^+ and i^{++}. These measurements are then repeated for a number of different angles. The data are collected on paper tape which furnishes a direct input into the computer. The experimental data obtained by this technique represents the angular current distribution, $i(\theta)$, measured in the vertical plane emanating from an area element at radius, r, on the vertical radius of the accelerator grid. Each set of $i_+(\theta)$ and $i_{++}(\theta)$ data points are integrated over θ to obtain the total $J_+(r)$ and $J_{++}(r)$ current densities at each

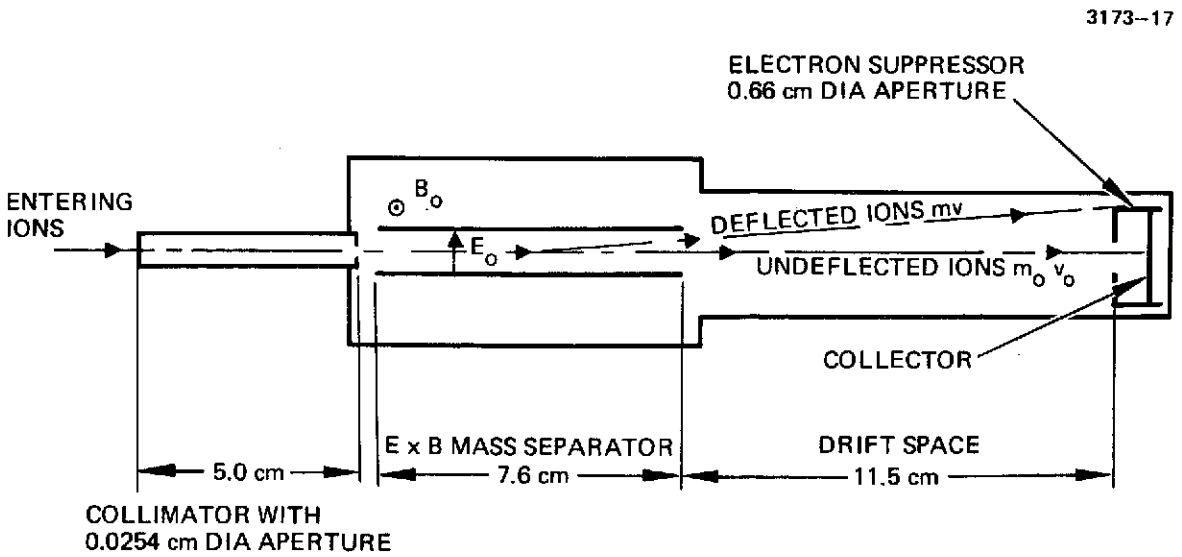

Fig. 54. ExB mass separator probe schematic.

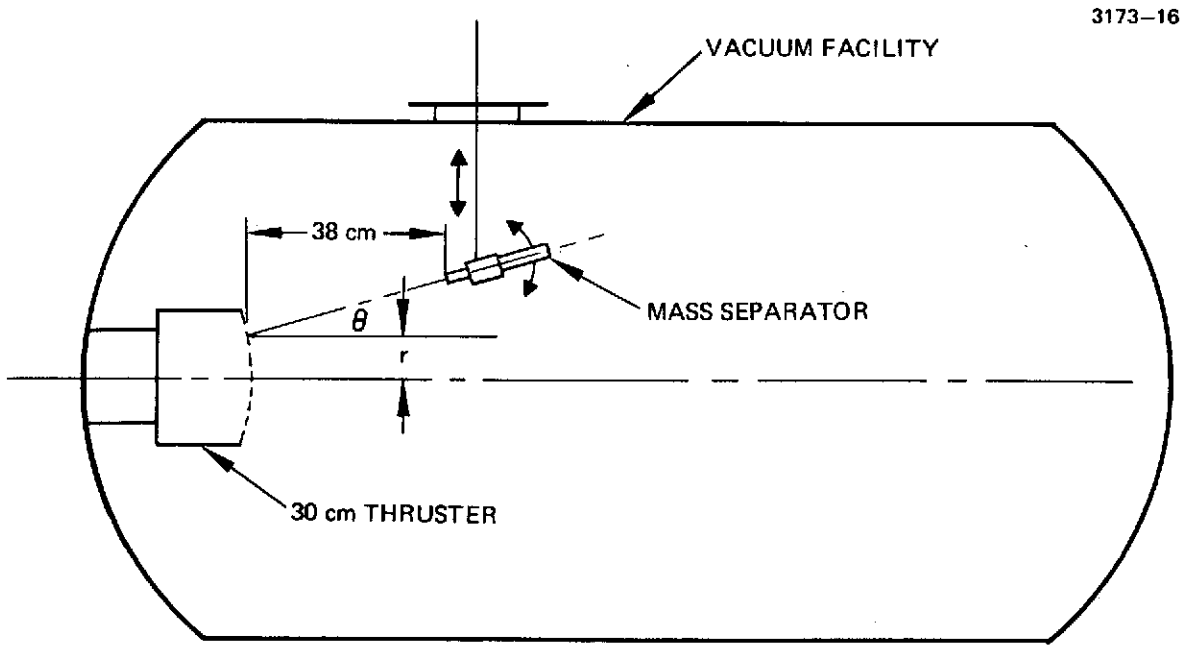

Fig. 55. Schematic of thruster and probe installation in vacuum chamber.

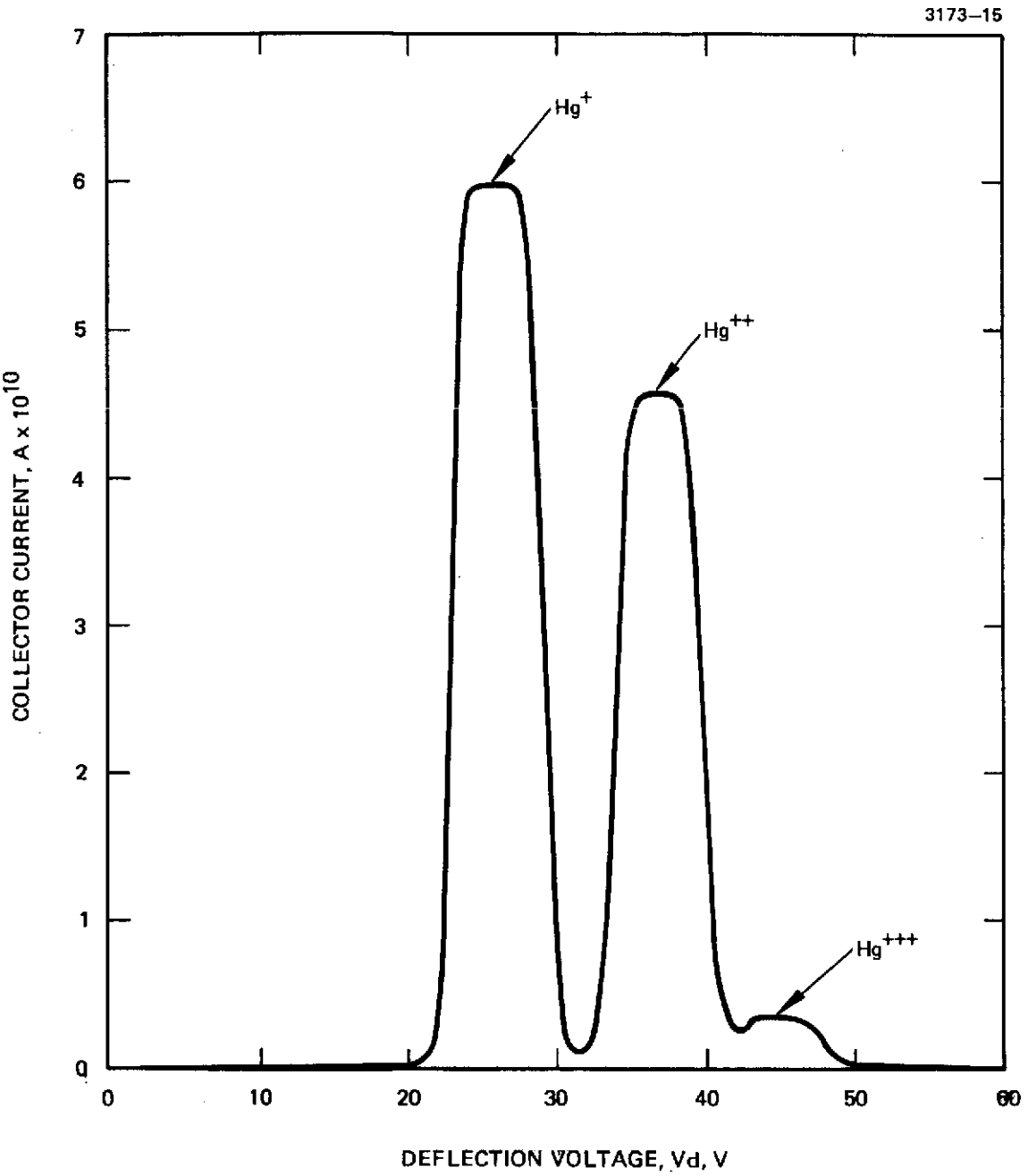

Fig. 56. Mass separator probe output trace; I_b = 2.0 A, V_d = 42 V.

radial position. By integrating the J_+ and J_{++} current densities over the accel grid, the total current fluxes I_+ and I_{++} are defined by

$$I_+ = \int_0^{R_{max}} J_+(r)\, 2\pi r\, d\, r, \tag{11}$$

$$I_{++} = \int_0^{R_{max}} J_{++}(r)\, 2\pi r\, d\, r, \tag{12}$$

where

$$J_{++}(r) = \int_{\theta_{min}}^{\theta_{max}} i_{++}\,(\theta,\ r)\, d\theta \tag{13}$$

and

$$J_+(r) = \int_{\theta_{min}}^{\theta_{max}} i_+\,(\theta,\ r)\, d\theta \tag{14}$$

Curves of these current distributions can be generated by the computer from thruster data as shown in Fig. 57.

The correction factor for double ions (α) can be defined in terms of the current fluxes or in terms of utilization efficiencies as discussed previously. The utilization values are related to current fluxes as follows.

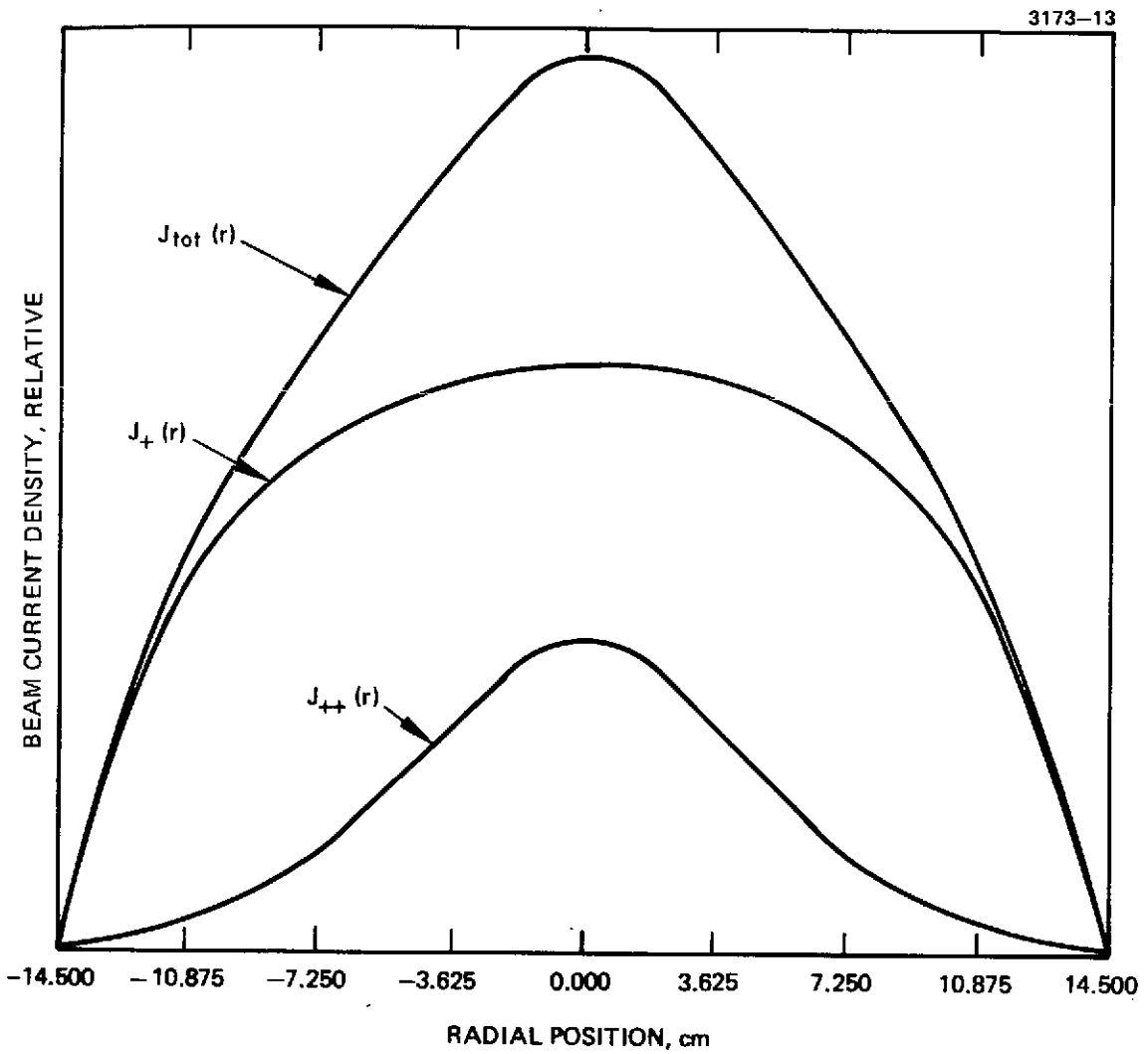

Fig. 57. Computer generated current density profiles for single and double ions.

$$\eta_1 = \frac{I_+}{\dot{m}} \cdot \frac{M}{e}$$

$$\eta_2 = \frac{I_{++}}{2\dot{m}} \cdot \frac{M}{e}$$

so using eq. (5)

$$\alpha = \left[\frac{(\eta_1 + \sqrt{2}\eta_2)}{(n_1 + 2\eta_2)} \right]$$

we find that

$$\alpha = \frac{I_+ + 0.707\, I_{++}}{I_+ + I_{++}} \tag{15}$$

Representative values of α are shown in Tables 13 and 14 for typical beam current and discharge conditions. All data in these tables were obtained with constant discharge losses of 185 eV/ion.[3]

Similarly, the beam divergence correction factor F_t is found by current weighting the elemental divergence factor obtained from the average cos θ at each radial position, and then integrating over the accelerator grid surface. Specifically,

$$F_t(r) = \int_{\theta_{min}}^{\theta_{max}} (i_+ + i_{++}) \cos\theta \, d\theta \Big/ \int_{\theta_{min}}^{\theta_{max}} (i_+ + i_{++})\, d\theta$$

TABLE 13

Correction Factors For Double Ions as a Function of Beam Current; V_d = 37 V, Discharge Losses = 185 eV/Ion

Thruster	Optics	I_B (A)	$\eta_1 + 2\eta_2$	$\frac{I^{++}}{I_{tot}}$	α
301-A	644	2.0	0.95	0.145	0.958
		1.5	0.91	0.115	0.967
		1.0	0.81	0.062	0.981
301-B	650	2.0	0.955	0.15	0.956
		1.5	0.90	0.116	0.906
301-B	656	2.0	0.91	0.139	0.959
		1.5	0.87	0.099	0.971
301-B	NASA 35	2.0	0.99	0.166	0.951
		1.5	0.96	0.127	0.963

T1341

TABLE 14

Correction Factors for Double Ions as a Function of Discharge Losses = 185 eV/Ion

I_b, A	V_d, V	$\eta_1 + 2\eta_2$	α
2.0	35	0.962	0.962
2.0	39	0.966	0.953
2.0	41	0.974	0.950
1.5	35	0.882	0.971
1.5	38	0.913	0.966
1.5	41	0.932	0.961
1.0	35	0.786	0.979
1.0	38	0.819	0.974
1.0	41	0.848	0.969

T1351

and

$$F_t = \frac{\int_0^{R_{max}} F_t(r)\, J_{tot}(r)\, 2\pi r\, dr}{\int_0^{R_{max}} J_{tot}(r)\, 2\pi r\, dr} \qquad (17)$$

Initial measurements and analysis of beam divergence for uncompensated grids indicated values of F_t of about 0.93. Since F_t^2 is used in total efficiency, such a large loss was significant. In order to reduce this loss, as discussed in Section II-A, grid hold compensation was introduced. The effect of compensation (0.5%) on beam profiles and F_t is shown in Fig. 58.[3] These data were obtained with a planar probe rather than the collimated probe illustrated in Fig. 54. Subsequent measurements with the collimated probe for grid sets 644, 650, 656, and 648 had F_t values of 0.994, 0.994, 0.939, and 0.985, respectively. These values were relatively insensitive to beam current or discharge conditions. Thus, grid compensation increased thruster total efficiency by about 10 percentage points (i.e., from about 0.62 to 0.72 total efficiency).

C. Thruster Operating Characteristics and Overall Performance

Thruster component and performance tests were conducted at several points in the program, as shown in Fig. 4. During the early phases, electrical performance was established as part of discharge chamber and ion optical system studies. The most important performance results obtained in that period were discussed in Section II. Other tests, such as neutralizer characterization, thermal mapping, and startup tests were also conducted throughout the first six months. Between late 1972 and mid 1974, a limited amount of testing was conducted under this contract. However, testing was resumed in mid

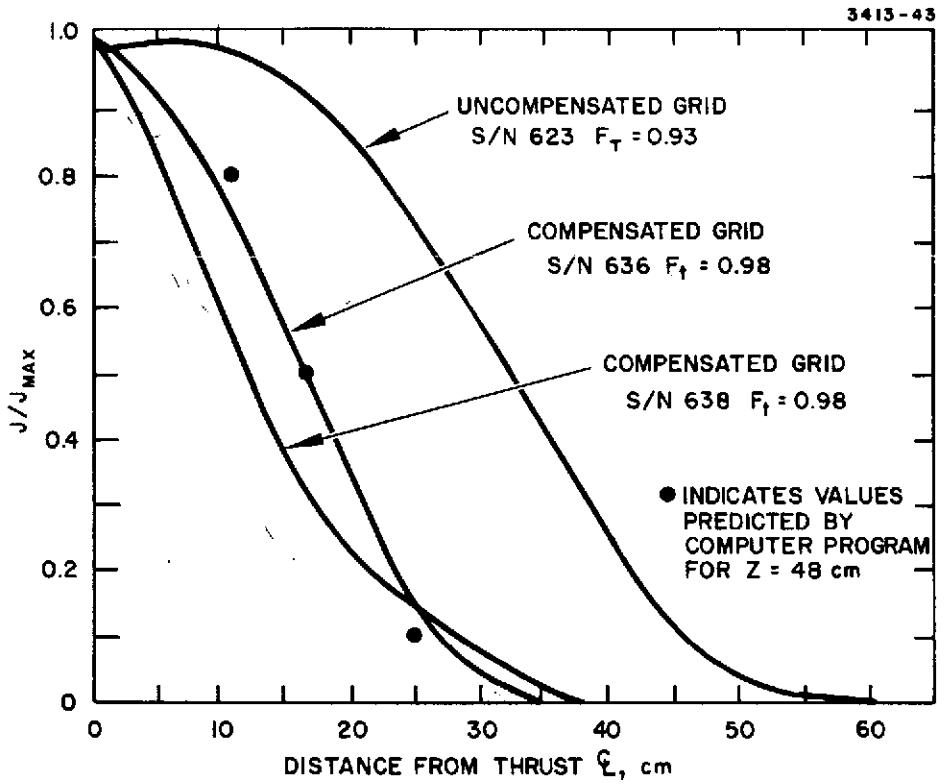

Fig. 58. Comparison of beam profiles of compensation and uncompensated grids.

1974 to evaluate the performance of thrusters S/N 702 and 702-A under NAS 3-18334. This testing included vaporizer calibration, neutralizer mapping, and general performance evaluation before and after shake testing.

The purpose of this section is to document significant overall test results and to describe the operating characteristics of the final thruster design produced in this program (800-Series).

1. Thruster Startup Characteristics

Tests were performed with thruster S/N 701 to determine startup power, temperature/time characteristics, and steady state equilibrium temperatures of critical components. Eighteen thermocouples were located at critical areas of the thruster during the startup tests and performance mapping. Areas such as the active areas of the electrodes and the cathode tips were not monitored because the presence of a thermocouple was expected to either perturb electrical performance or to require access holes in the thruster shell. Both consequences were considered undesirable. The thermocouple locations are shown in Fig. 59. The thermocouples were read on calibrated panel meters which were, of necessity, operated at high voltage in some cases. Thermocouple meter calibration and leakage currents probably limit the absolute accuracy of the temperature readings to $\pm 15^{\circ}C$.

For thruster startup, the cathode, neutralizer and isolator heaters are set to the values shown in Table 15. Startup temperature transients of the critical feed system components are shown in Fig. 60. Note that all points except the isolator flange at its attachment point to the thruster body reach the $200^{\circ}C$ point relatively quickly. This response prevents mercury condensation. Input power requirements as a function of time are shown in Fig. 61. The startup sequence described here is representative of the present design. Significantly shorter times would be difficult to achieve without additional heaters or a sacrifice of controllability.

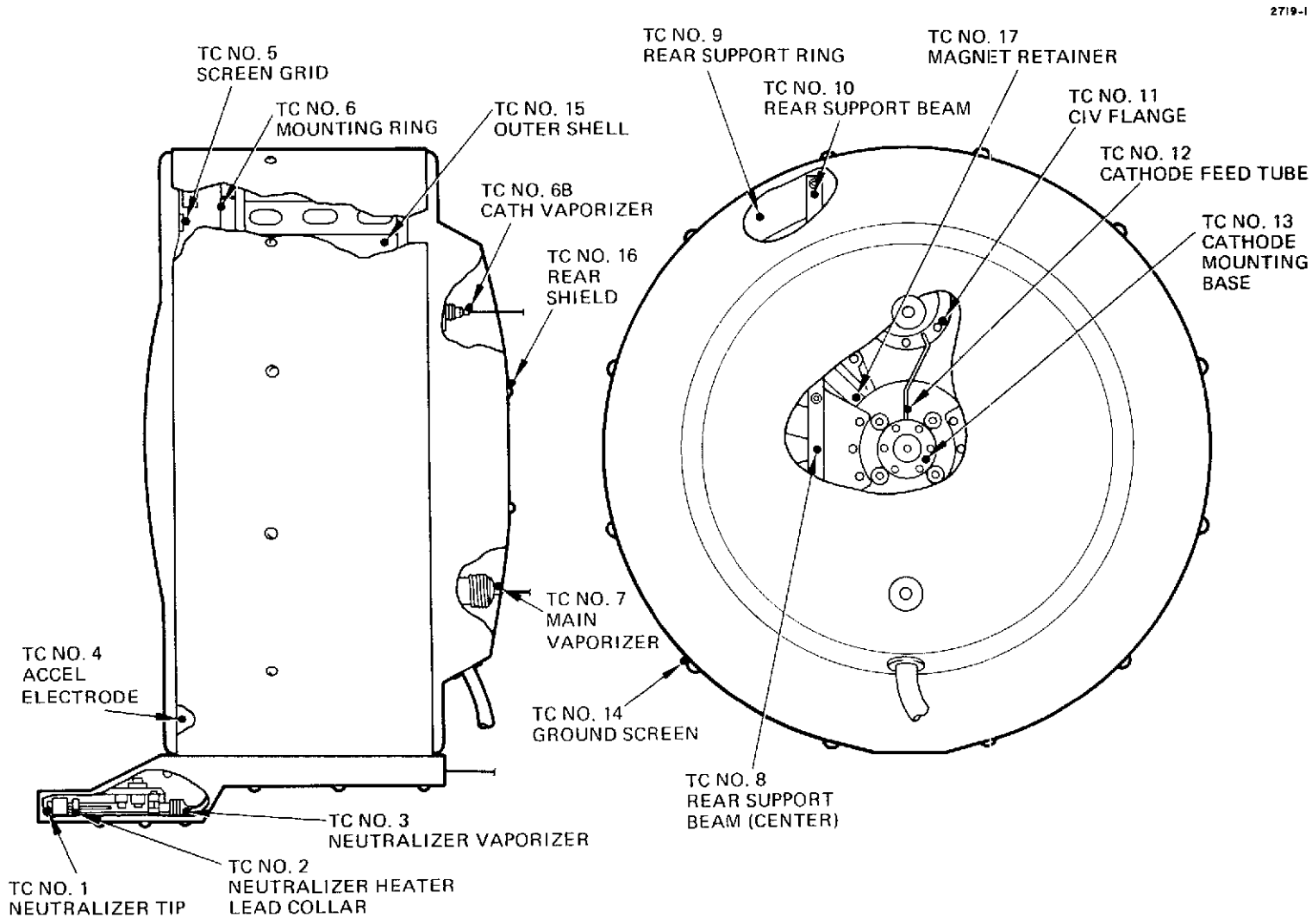

Fig. 59. Thermocouple locations for thruster temperature mapping.

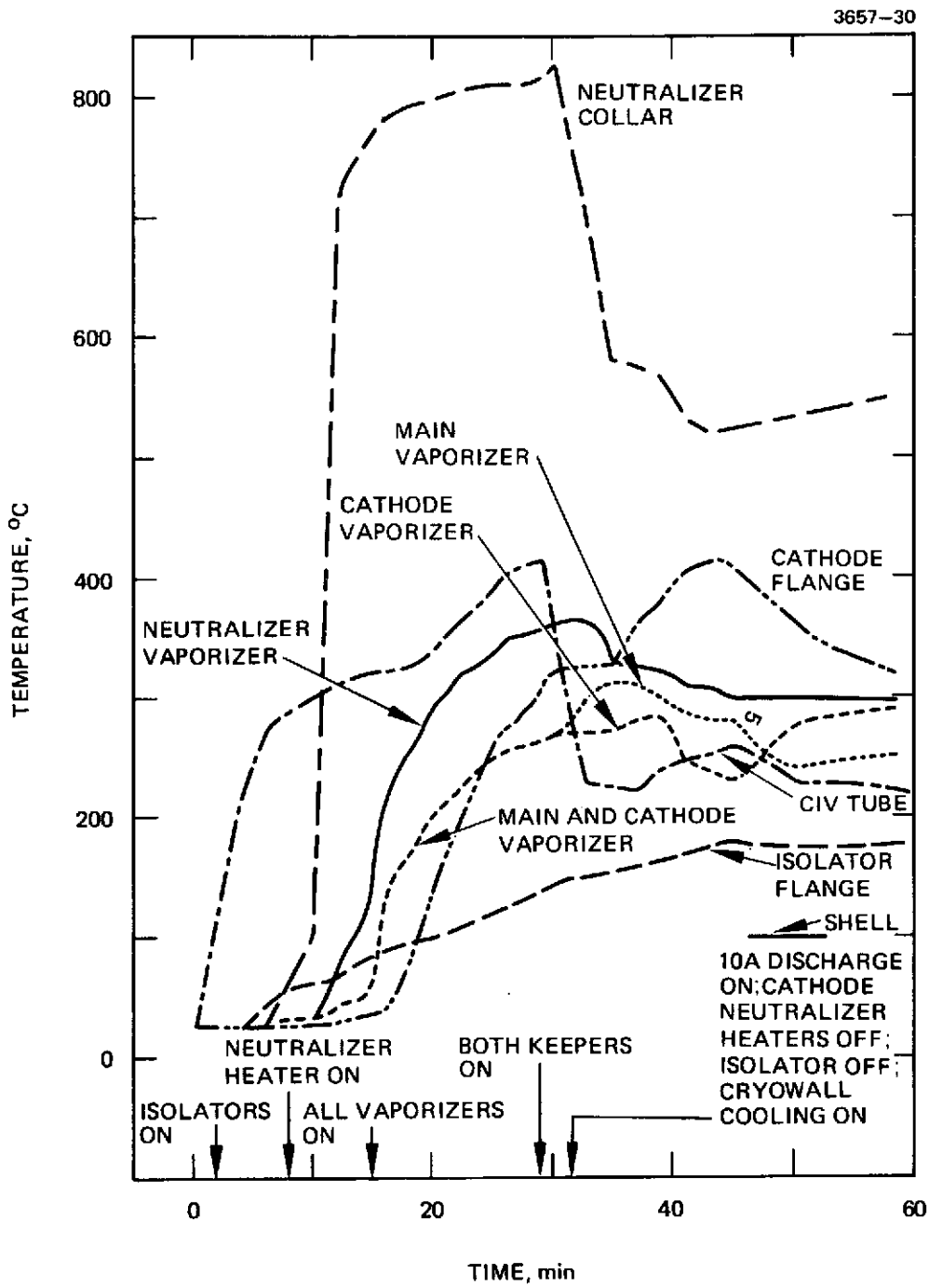

Fig. 60. Temperature history of thruster areas during startup.

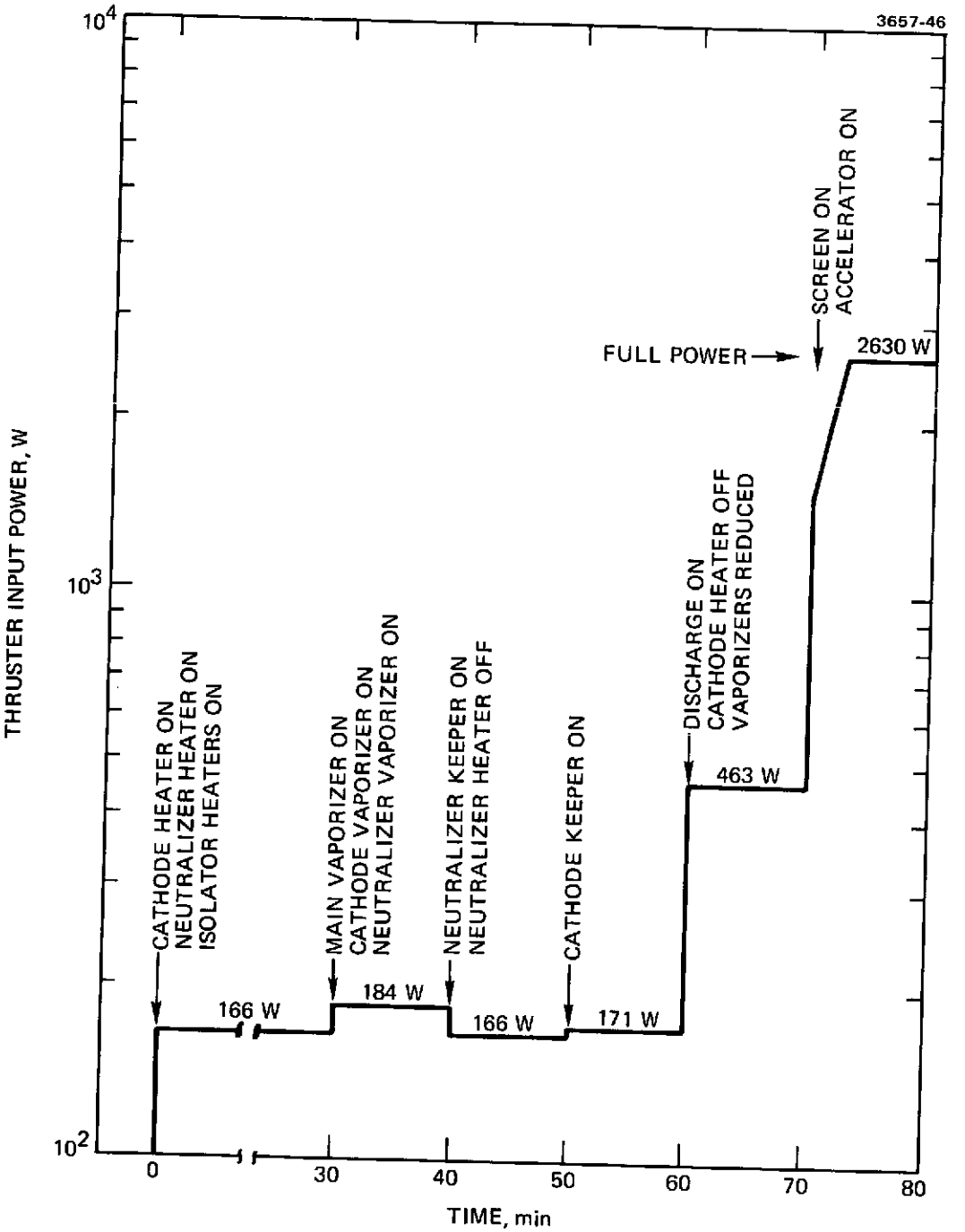

Fig. 61. Thruster input power requirements during startup.

TABLE 15

Typical Heater Parameters for Thruster Start-Up

Heater	Voltage, V	Current, A	Power, W
Cathode Heater	14.6	4.5	65.7
Neutralizer Heater	12.5	4.5	56.3
Main Isolator Heater	8.0	1.9	15.2
Cathode Isolator Heater	8.0	1.9	15.2
Main Vaporizer	6.0	1.0	6.0
Cathode Vaporizer	4.0	1.5	6.0
Neutralizer Vaporizer	4.2	1.5	6.3
Total	–	–	170.7

T1483

The equilibrium operating temperatures at the various locations are given in Table 16 for several beam currents. "Hot spots" which had occurred at the magnet retainer and the end of the isolator in the stainless steel prototype (600-series) design were not observed in the 700-series design. In addition, the edge of the screen and accelerator electrodes are as much as 40°C cooler than in the 600-series design and 70°C cooler than earlier measurements made with a flat grid system. The lower temperatures are attributed to improved discharge performance which resulted in lower power dissipation requirements.

2. Vaporizer Calibrations

Although the MIV, CIV, and NIV vaporizers were discussed in Section II, the flowrate versus temperature calibration results are presented here to provide a comparison between thruster and bell jar tests. Typical results for vaporizers fabricated for thruster S/N 702-A and the first 800-series thrusters are shown in Fig. 62. These data are considered accurate to about 2% since a

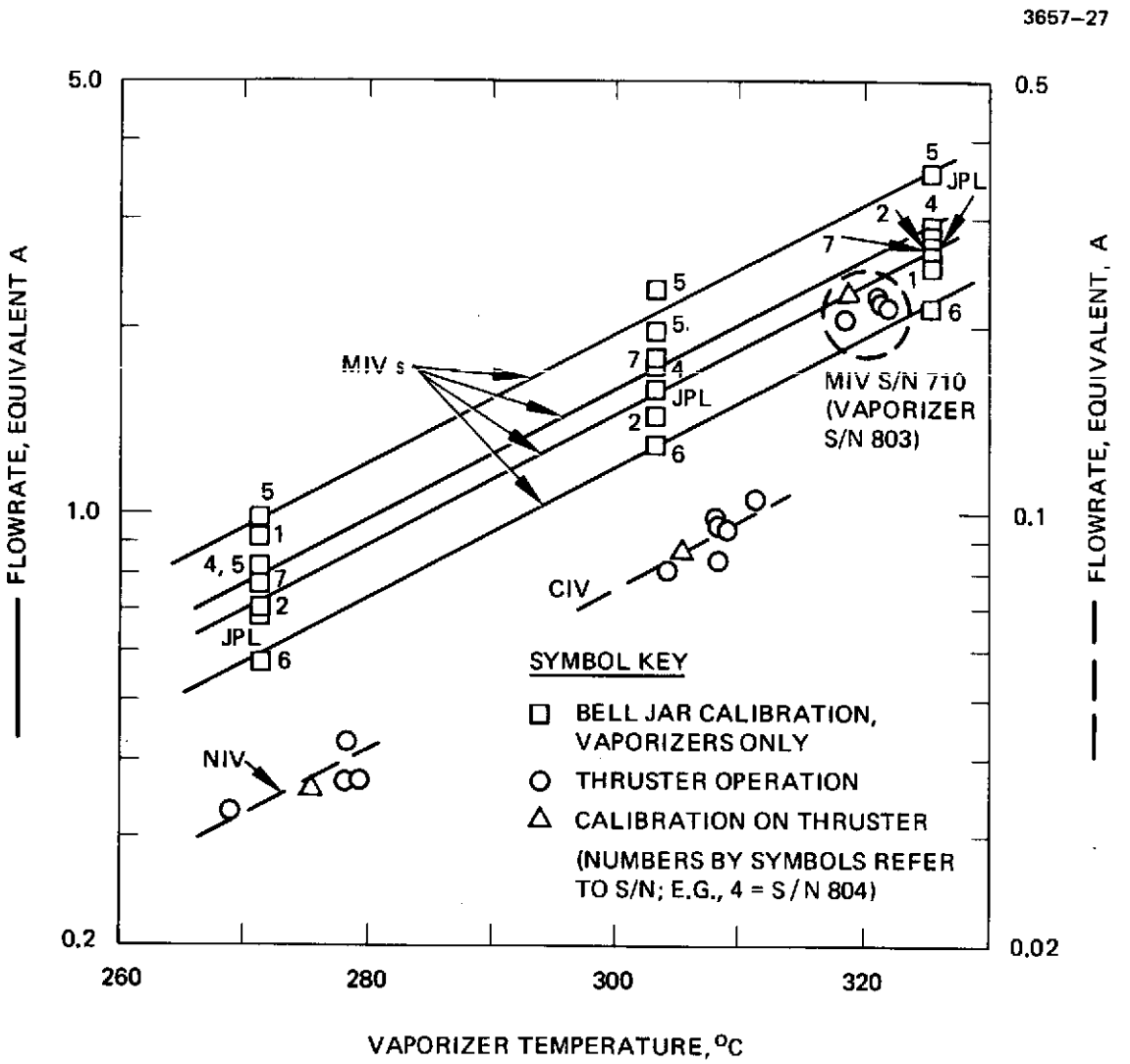

Fig. 62. Vaporizer flowrate calibration data for bell jar and thruster tests.

TABLE 16

Equilibrium Temperatures for Preliminary Operation of EM Thruster S/N 701 in a Cryopumped Test Facility

Beam Current	2 A	1.45 A	0.85 A
Temperature at Locations Shown in Fig.	°C	°C	°C
No. 1 neutralizer tip	900	-[a]	-
No. 2 nuetralizer heater lead collar	620	610	592
No. 3 neutralizer vaporizer	262	262	282
No. 4 accel electrode	150	120	85
No. 5 screen grid	215	205	165
No. 6A mounting ring	220	180	145
No. 6B cathode vaporizer	269	261	270
No. 7 main vaporizer	309	299	275
No. 8 rear support beam (center)	320	280	225
No. 9 rear support ring	180	160	130
No. 10 rear support beam (end)	240	210	170
No. 11 C-IV flange	260	240	210
No. 12 cathode feed tube	290	260	230
No. 13 cathode mounting base	410	360	300
No. 14 ground screen	160	140	120
No. 15 outer shell	220	190	155
No. 16 rear shield	170	145	125
No. 17 magnet retainer	280	245	205

[a]Thermocouple open circuited

T1484

compensated (for room temperature) bridge-type instrument was used for making all thruster thermocouple measurements. The same instrument was used to periodically check and correct the bell jar measurements.

For thruster full power conditions, the MIV and CIV deliver about 2.0 A and 0.09 A (equivalent) of flow respectively. As shown in Fig. 62, a temperature of 310 to 315°C is needed to obtain these flowrates. Therefore, these vaporizers are in range (290 to 320°C) considered acceptable for providing adequate closed loop control authority.

A comparison of thruster and bell jar results is summarized in Table 17. Thruster S/N 702-A was tested with thermocouples upstream and downstream of the vaporizer heater. The MIV, CIV, and NIV were also removed from the thruster and calibrated in a bell jar. The trends indicated were typical of results of several days of testing. Since the measurements are probably only accurate to about ±5°C, the temperature from the feedline cap to the isolator flange is essentially constant. However, it is interesting to note that for full power operation, heat is probably conducted to the isolator from the vaporizers (rather than from isolator to vaporizer). Finally, the results presented in Table 17 and Fig. 62 show that the bell jar calibrations, when performed with compensated or corrected instruments, provide a reasonable estimate of thruster flowrates.

3. Steady State Performance

Thruster steady state performance is defined by the specification of three of the four fundamental parameters (thrust, specific impulse, efficiency, and power). Laboratory tests directly determine power, mass flow rates, and uncorrected efficiency. Corrected efficiency, thrust, and specific impulse are calculated as discussed earlier in this section.

The original performance goals for 30-cm thruster development program are shown in Table 18 and Fig. 63. The original goal did not include corrections for double ions or beam divergence. As

TABLE 17
Vaporizer Temperature Variations Across CIV and MIV

Thermocouple Location	Temperature, °C[b]	
	Operating Thruster (S/N 702-A)	Thruster with Discharge Off[c]
1. Main Vaporizer		
a. Upstream[a]	318	315
b. Downstream[a]	316	316
2. Cathode Vaporizer		
a. Upstream[a]	309	307
b. Downstream[a]	303	302
3. Neutralizer		
(Downstream only)	271	274

[a]Upstream = Feedline inlet cap, on center for 800-series.
Downstream = Between vaporizer heater and isolator flange.

[b]Temperature needed to achieve flowrates of 2.0 A, 0.090 A and 0.035 A (equivalent) for the main, cathode, and neutralizer, respectively.

[c]With isolator heater on.

T1527

TABLE 18

Contract Goals for Thruster Efficiency at Several Power Levels

Parameters	Original Goal			Revised Goal[a]		
Beam Current, A	2.0	1.5	1.0	2.0	1.5	1.0
Beam Voltage, V	1000	1000	1000	1100	1100	1100
Beam Power, W	2000	1500	1000	2200	1650	1100
Discharge Power, W	440	330	220	440	330	220
Fixed Losses, W	70	70	70	70	70	70
Neutralizer Coupling, W	40	30	20	40	30	20
Total Input Power, W	2550	1930	1310	2750	2080	1410
Electrical Efficiency, %	78.5	77.5	77.0	80.0	79.3	78.0
Propellant Utilization:						
Discharge, %	93.2	91.7	88.2	93.2	91.7	88.2
Neutralizer, %[b]	97.6	97.0	95.8	97.6	97.0	95.8
Total Utilization, %	91.0	89.0	84.0	91.0	89.0	84.5
Overall Performance:						
Total Efficiency, %	71.0	69.0	65.0	73.0	70.6	65.9
Specific Impulse, S	2850	2800	2650	3018	2952	2802

[a]Including double ions and beam divergence; revised in September 1973.

[b]Utilization factor to correct for neutralizer flow.

T1485

electric propulsion space vehicle requirements became better defined during the period of this contract, the goals were adjusted slightly. However, as the magnitude of the corrections for double ions and beam divergence became known, the efficiency goal, shown in Fig. 63, was modified to include these corrections.

Performance data, representative of 700/800-series designs, are shown in Table 19. Key voltage and current measurements shown in the table were made in accordance with Fig. 53. Power supply outputs are presented in order to clarify power processor requirements. However, as discussed in Section III-A, the useful ion beam voltage and discharge current must be determined using eq. (9) as shown in Table 20. Thruster power efficiency is then computed from eq. (10). Neutralizer coupling power, or the power associated with floating the power processing in ground tests, is automatically included in computing ion beam power.

Although the total efficiency has far exceeded the original goals based only on metered data, the corrected efficiency is about 1.5 percentage points below the revised goal. Continuing investigations at NASA LeRC and at Hughes under Contract NAS 3-17831 presently show promise for exceeding the revised goal, particularly under throttled conditions.

D. Structural Integrity Tests

Three structural integrity vibration test programs were conducted during the course of this work to evaluate thruster structural design. The general features of these tests are summarized in Table 21. Details of the three thruster configurations tested were presented in Section II and a relatively complete description of the

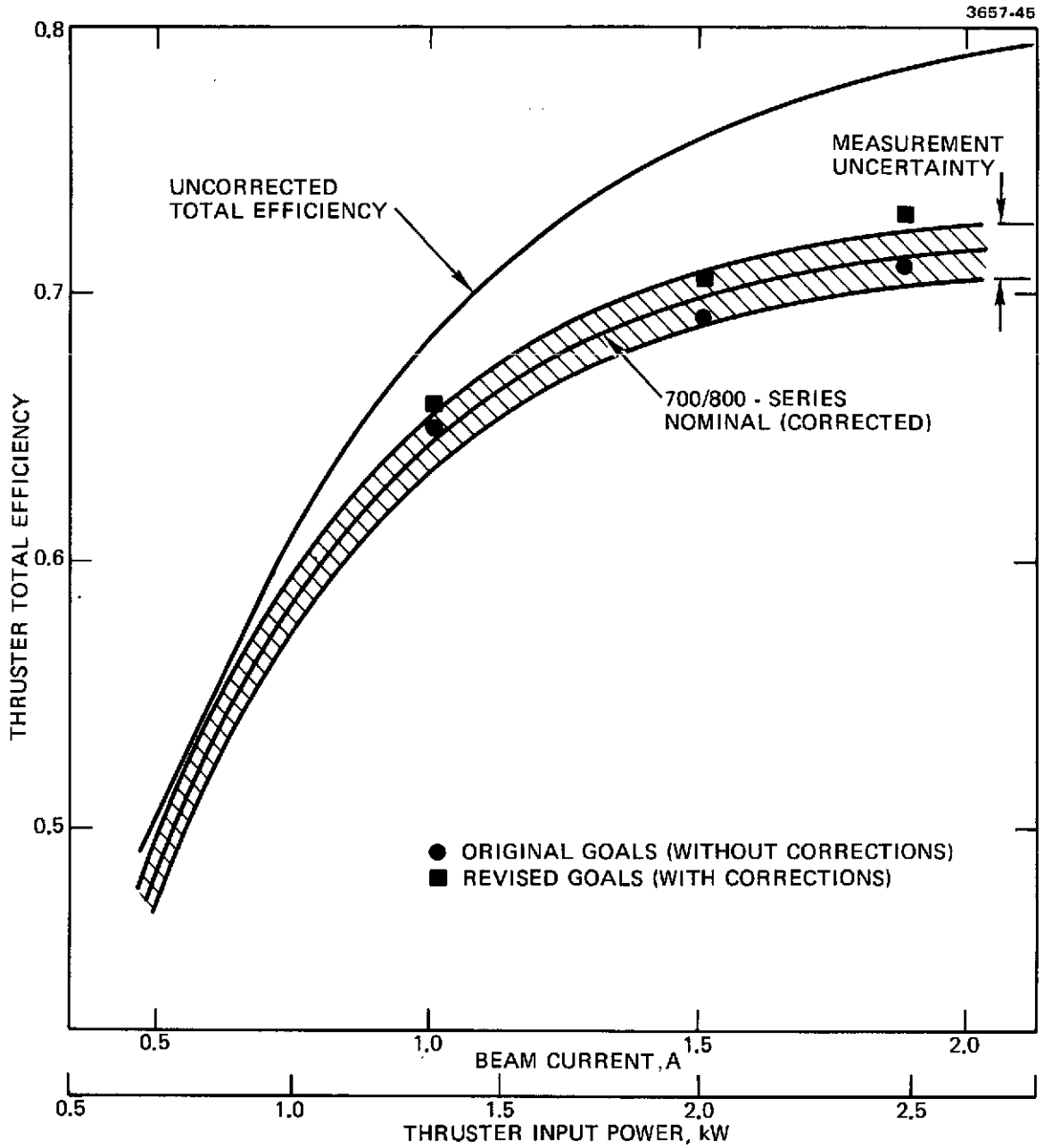

Fig. 63. Thruster efficiency as a function of power level; goals and final results.

TABLE 19

Typical Thruster Power Requirements as Seen by the Power Processor

Power Supply	Full Power			73% Power			43% Power			26% Power		
	Volts, V	Amp, I	Watts, P	Volts, V	Amp, I	Watts, P	Volts, V	Amp, I	Watts, P	Volts, V	Amp, I	Watts, P
Screen	1074	2.00	2148	1074	1.45	1557	1074	0.85	913	1074	0.50	537.0
Accelerator	500	0.0039	2	500	0.0025	1.3	500	0.002	1.0	500	0.001	0.5
Discharge	37	12.0	444	37.2	8.65	321.8	37.1	5.05	187.4	37.1	3.2	118.7
Cathode Heaters	0	0	0	0	0	0	0	0	0	0	0	0
Magnetic Baffle	0.4	3.5	1.4	0.4	3.5	1.4	0.4	3.5	1.4	0.4	3.5	1.4
Main Vaporizer	5.3	0.9	4.8	5.5	0.9	5.0	4.8	0.8	3.8	4.6	0.7	3.2
Cathode Vaporizer	2.9	0.9	2.6	3.2	1.0	3.2	3.3	1.1	3.6	3.4	1.1	3.7
Neutralizer Vaporizer	3.0	0.7	2.1	3.4	0.72	2.4	3.8	0.9	3.4	4.0	1.0	4.0
Isolator Heaters	0	0	0	0	0	0	0	0	0	0	0	0
Cathode Keeper	5.0	0.4	2.0	5.0	0.4	2.0	7.0	0.4	2.8	7.0	0.4	2.8
Neutralizer Keeper	14.0	1.3	18.2	13.4	1.3	17.4	13.3	1.3	17.3	15.7	1.3	20.4
Voltage to Ground	11	0	0	10.8	0	0	11.9	0	0	12.0	0	0
Total Power (watts)	2625			1912			1134			692		

T1487

TABLE 20

Thruster Performance Parameters for Typical Operating Conditions in Thrusters SN 701, 702, and 702-A

Power in Thruster Element	Full Power			73% Power			43% Power			26% Power		
	V, Volts	I, Amp	P, Watts	V, Volts	I, Amp	P, Watts	V, Volts	I, Amp	P, Watts	V, Volts	I, Amp	P, Watts
Beam	1100	2.00	2200	1100	1.45	1595	1100	0.85	935	1074	0.50	550
Accelerator	500	0.0039	2	500	0.0025	1.3	500	0.002	1.0	500	0.001	0.5
Discharge	37	10.0	370	37.2	7.20	267.8	37.1	4.20	158.8	37.1	2.7	100.2
Cathode Heaters	0	0	0	0	0	0	0	0	0	0	0	0
Magnetic Baffle[a]	0.4	3.5	1.4	0.4	3.5	1.4	0.4	3.5	1.4	0.4	3.5	1.4
Main Vaporizer	5.3	0.9	4.8	5.5	0.9	5.0	4.8	0.8	3.8	4.6	0.7	3.2
Cathode Vaporizer	2.9	0.9	2.6	3.2	1.0	3.2	3.3	1.1	3.6	3.4	1.1	3.7
Neutralizer Vaporizer	3.0	0.7	2.1	3.4	0.72	2.4	3.8	0.9	3.4	4.0	1.0	4.0
Isolator Heaters	0	0	0	0	0	0	0	0	0	0	0	0
Cathode Keeper	5.0	0.4	2.0	5.0	0.4	2.0	7.0	0.4	2.8	7.0	0.4	2.8
Neutralizer Keeper	14.0	1.3	18.2	13.4	1.3	17.4	13.3	1.3	17.3	15.7	1.3	20.4
Neutralizer Coupling	11	2.0	22.0	10.8	1.45	15.6	11.9	0.85	10.1	12.0	0.5	6.0
Total Power, watts	2625			1912			1134			692		
Propellant Flow	Amp, Equivalent			Amp, Equivalent			Amp, Equivalent					
Main Vaporizer	2.00			1.456			0.902			0.563		
Cathode Vaporizer	0.090			0.108			0.134			0.158		
Neutralizer Vaporizer	0.025			0.035			0.037			0.063		
Total, eq. mA	2.115			1.599			1.073			0.782		
Electrical Efficiency, %	83.8			83.5			82.5			79.5		
Propellant Efficiency, %	94.6			90.7			79.2			63.9		
Total Efficiency, % (Meter Value)	79.3			75.7			65.3			50.8		
Thrust Factors[b]												
Doubly Charged Ions, α	0.958			0.966			0.981			0.993		
Beam Divergence, F_{t_2}	0.995			0.994			0.992			0.990		
Efficiency Correction, γ^2	0.909			0.922			0.947			0.966		
Corrected Efficiency, %	72.0			69.8			61.8			49.1		
Corrected Propellant Utilization, %	86.0			83.6			75.0			61.7		
Effective Specific Impulse, sec	2990			2888			2556			2083		
Thrust, Newtons	0.128			0.094			0.056			0.033		

[a] Based on 10.5 turn coil as per tests under NAS 3-17831.

[b] Measured on engineering model thruster equivalent, S/N 301-B, under Contract NAS 3-17831.

T1523

TABLE 21

Structural Integrity Test Summary

Test No.	Thruster S/N	Test Dates	Contract No.	Testing Company	Test Location	Type of Tests
1	601	5 Jan, 1973	NAS 3-16528	AETL[a]	El Monte, California	1 g and 9 g sine - 3 axes 30 g shock - 3 axes 18 g sine - X axis
2	702	23 Jan, 1974	NAS 3-16528	AETL	El Monte, California	1 g and 9 g sine - 3 axes 19.8 g random - 3 axes 30 g shock - 3 axes 18 g sine - X axis
3	702-A	25 Sept, 1974	NAS 3-18334	AETL	Chatsworth, California	1 g and 11 g sine - 3 axes 19.8 g random - 3 axes 30 g shock - 3 axes

[a]Approved Engineering Test Laboratories, El Monte, California

T1486

vibration tests is provided in Appendix C. Thus, this section will be limited to a results summary and a brief description of modifications resulting from the tests.

Thruster S/N 601 survived the initial series of sinusoidal tests at 1 and 9 g acceleration levels, and 30 g shock tests. The vibration test fixture used for mounting the thruster was then found to exhibit low frequency harmonics that prevented meaningful random vibration tests. An 18 g level sine test was then performed in the x-axis only. This elevated level resulted in several failures as indicated in Table 22. More detailed information on the failures is presented in Appendix C. Although modifications were proposed to improve the 600-series structural design, new requirements on thruster mounting resulted in a design change (i.e., 700-series) rather than a modification of the 600-series.

TABLE 22

Results of Vibration Testing of Thruster S/N 601

Test	Experience and/or Failures
1. 9 g sine; x, y and z axes	1. No apparent damage
2. 30 g shock; x, y and z axes	2. No apparent damage
3. 18 g sine; x axis	3. (a) Two adjacent thruster support insulator brackets fractured (see Fig. 93).
	(b) Remaining four peripheral support insulators failed in shear.
	(c) Five rear ground shield support gussets failed.
	(d) "Oil canning" of the backplate was observed but did not result in any apparent damage.

T1524

Thruster S/N 702, mounted by using only the two gimbal pads, was subjected to the vibation tests indicated in Table 21. The failures experienced during these tests are summarized in Table 23. The primary failures were considered to be the neutralizer and the back-plate support beams. Modifications resulting from the shake test results, and from suggestions by the NASA Program Manager, were incorporated into a new thruster series.

Thruster S/N 702-A (i.e., the 800-series design prototype) was tested under the conditions shown in Table 21. The experiences of these tests are summarized in Table 24. In general, the failures experienced were not considered to be extremely serious. The ground screen had been substantially lightened from the previous design. However, since the ground screen does not contribute substantially to the overall structure, a redesign can be performed essentially independent of other components. The gimbal pad failure is attributed to fatigue resulting from vibration tests of thruster S/N 702 and 702-A. Since the insulators were not changed during the redesign of thruster 702, vibration loads had been applied for periods far exceeding those expected in a space vehicle application. The propellant feedline is believed to have failed as a result of motion of the gimbal pad. The MIV heater was found to have been damaged during thruster final assembly. With the exceptions noted above, thruster 702-A survived the structural integrity tests and was subsequently successfully operated at normal performance conditions.

TABLE 23

Results of Vibration Testing of Thruster S/N 702

Test	Experience and/or Failures
1(a). 9 g sine; x axis	1(a). No apparent failures.
1(b). 9 g sine; y axis	1(b). Neutralizer mounting bracket allowed neutralizer assembly to "flex." This motion caused the neutralizer housing to crack.
1(c). 9 g sine; z axis	1(c). MIV feedline fractured.
2(a). 19.8 g random; z axis	2(a). Neutralizer housing developed new cracks and neutralizer keeper shield failed.
2(b). 19.8 g random; y axis	2(b). No additional damage.
2(c). 19.8 g random; x axis	2(c). Propellant feedlines at the MIV and CIV assemblies fractured.
3. 30 g shock; x, y and z axis	3. No additional damage.
4. 18 g sine; x axis	4(a). Rear braces fractured near both attachment points. This fracture permitted the entire back-plate to "oil can" and resulted in damage to a number of other parts.
	4(b). The rear extension of the neutralizer cover was broken near the attachment points to the rear shield.
	4(c). Rear shield was fractured at the four mounting points at the rear of the thruster assembly.
	4(d). Two of the twenty-four attachment points of the outer shield/rear shield

TABLE 23

Results of Vibration Testing of Thruster S/N 702 (Continued)

Test	Experience and/or Failures
	were fractured due to excessive deflection at this interface. 4(e). The neutralizer feed tube was fractured at the point where it was clamped to the rear shield. 4(f). The main isolator heater was fractured at the mounting insulator. 4(g). Six of the twelve radial magnet retainers were broken loose from the backplate allowing two magnets to separate. 4(h). The 0.24 cm diameter feed line connecting the cathode and isolator sections of the CIV assembly was fractured and separated. 4(i). Two tabs on the outer magnet retainer were buckled. 4(j). The CIV and MIV vaporizer heater leads were fractured. 4(k). CIV cathode heater terminal cracked. 4(l). MIV and CIV isolator heater terminals fractured. 4(m). Both rear braces were fractured in several places. 4(n). The propellant distribution plenum was cracked at the corners and several screens were torn off the distribution posts.

T1525

TABLE 24

Results of Vibration Testing of Thruster S/N 702-A

Test	Experience and/or Failures
1(a). 11 g sine; x and y axes	1(a). No apparent damage
1(b). 11 g sine; z axis	1(b). Ground screen failed in two areas; ground screen replaced.
2(a). 19.8 g random; x axis	2(a). Ground screen failed in several areas as in item 1(b).
	2(b). Main vaporizer heater open circuit.
2(c). 19.8 g random; y axis	2(c). No additional damage.
2(d). 19.8 g random; z axis	2(d). Propellant feedline fractured near interface flange at gimbal pad.
3. 30 g shock; x, y and z axes	3. No additional damage was observed during testing. However, after removing the thruster from the test fixture, one gimbal pad was found to be loose. All six support insulators were broken.

T1526

IV. 800-SERIES THRUSTER CHARACTERISTICS SUMMARY

The purpose of this section is to provide a summary of major characteristics of the final thruster design produced under this program. The data included in this summary has been discussed in previous sections of this report.

A. Performance

Thruster performance values stated here include corrections for double ions and beam divergence, as defined in Section III-A. Total efficiency, specific impulse, and thrust are presented in Table 25 for three thruster power levels. The tolerance on the values in Table 25 is due to present measurement uncertainties.

TABLE 25

Performance Summary for 800-Series Thruster Design

Performance Parameter	Full Power	73% Power	43% Power
Total Efficiency, %	71.5 ± 1.0	69.5 ± 1.0	61.6 ± 1.0
Specific Impulse, s	3000 ± 10	2900 ± 10	2560 ± 10
Thrust, N	0.128 ± 0.002	0.094 ± 0.001	0.056 ± 0.001
Input power, kW	2.63	1.92	1.14

T1495

B. Power Requirements

1. Startup

During thruster startup from a cold condition, the time intervals and power levels required are shown in Fig. 64. The time intervals of the various power levels may be adjusted depending upon the initial temperature and thermal environment. The normal time required to reach full power is about 60 ± 10 min.

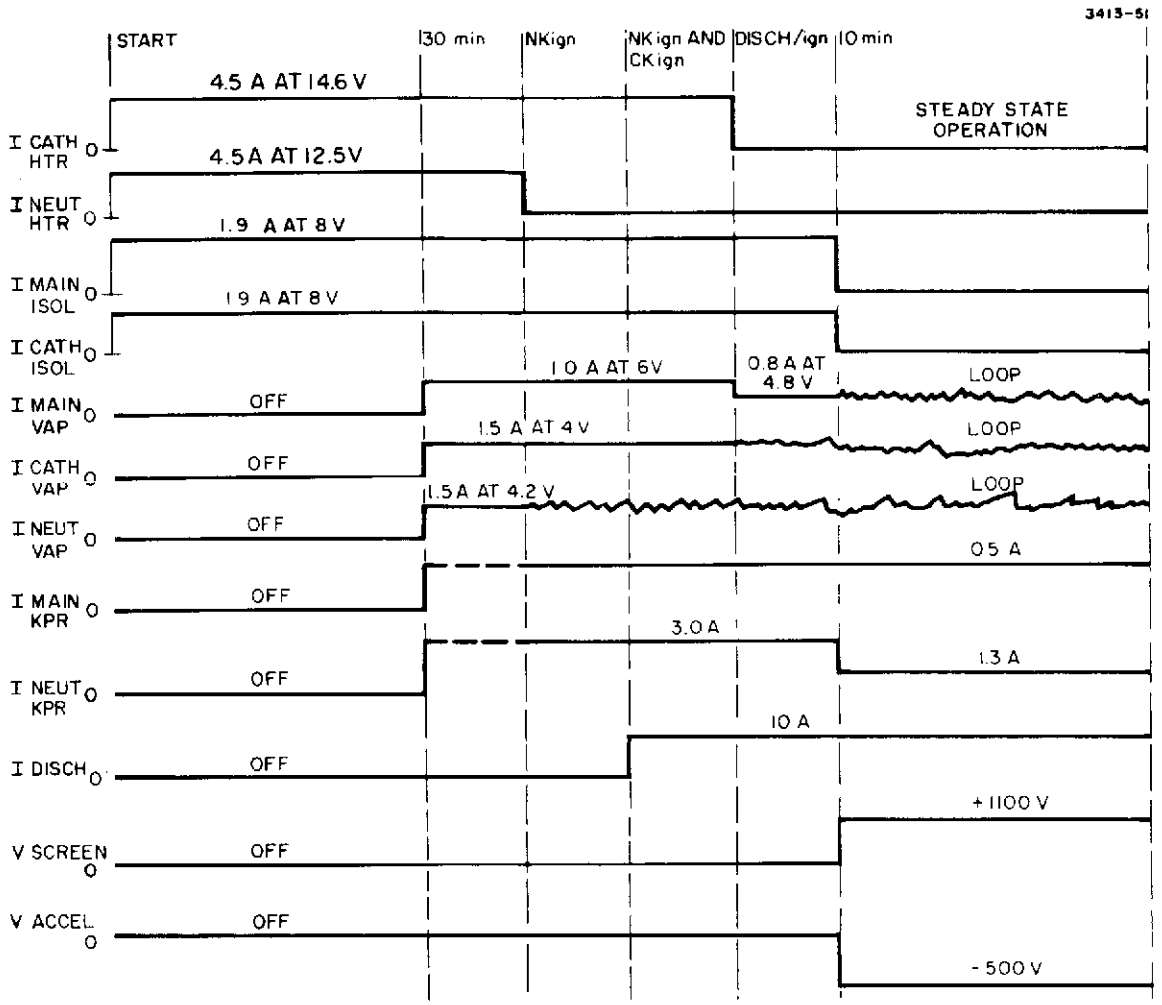

Fig. 64. Thruster startup sequence.

2. Normal Operation

At the end of the startup period, the thruster input power requirement is within about 1 to 2% of the long term operating point (for a given beam current). Small variations occur for one or two hours following startup due to thermal (dimensional) and feed system stabilization. The power requirements for thruster operation in the normal stabilized condition are shown in Table 26.

TABLE 26

Power Requirements During Normal Operation

Power Supply	Power, W		
	Full Power	73% Power	43% Power
1. Screen	2148.0	1557.0	913.0
2. Accelerator	2.0	1.3	1.0
3. Discharge	444.0	321.8	187.4
4. Cathode Heater	0	0	0
5. Magnetic Baffle	1.4	1.4	1.4
6. Main Isolator Heater[a]	0	0	0
7. Main Vaporizer	4.8	5.0	3.8
8. Cathode Isolator Heater[a]	0	0	0
9. Cathode Vaporizer	2.6	3.2	3.6
10. Neutralizer Cathode Heater	0	0	0
11. Neutralizer Vaporizer	2.1	2.4	3.4
12. Cathode Keeper	2.0	2.0	2.8
13. Neutralizer Keeper	18.2	17.4	17.3
Total	2625.1	1911.5	1133.7

[a]Heaters operated in parallel from a single power supply.

T1489

C. Electrical Interface

The electrical interface with the 800-series thruster is defined in Fig. 65. Separate wire bundles are provided for high voltage and low voltage connections. In addition, a vaporizer return, connected to the propellant manifold, is included to avoid using the feedline as a current conductor. A wire bundle length of 100 cm, external to the thruster, is provided.

D. Mechanical Interface

The mechanical or mounting interface for the 800-series design is illustrated in Fig. 66. This configuration provides two pads, spaced 16.02 in. and 180° apart, to allow for use with gimbals. Four 1/4-28 tapped holes are provided for mounting.

E. Propellant Interface

A single propellant line interface flange is provided on the gimbal mounting pad as shown in Fig. 66. The flange is secured to the gimbal pad with two flush mounted screws. The propellant line connection is made by attachment of a mating flange, or gimbal mount, to the feedline interface flange using the four mounting holes. A metal "V" seal, constrained in the mating flange, is crushed to provide propellant containment.

F. Thermal Properties

1. Startup

During the startup process, the various heaters raise the temperature of certain elements to allow keeper and discharge ignition, and beam current production. A typical temperature profile is illustrated in Fig. 67. This profile basically corresponds to the startup power profile shown in Fig. 64.

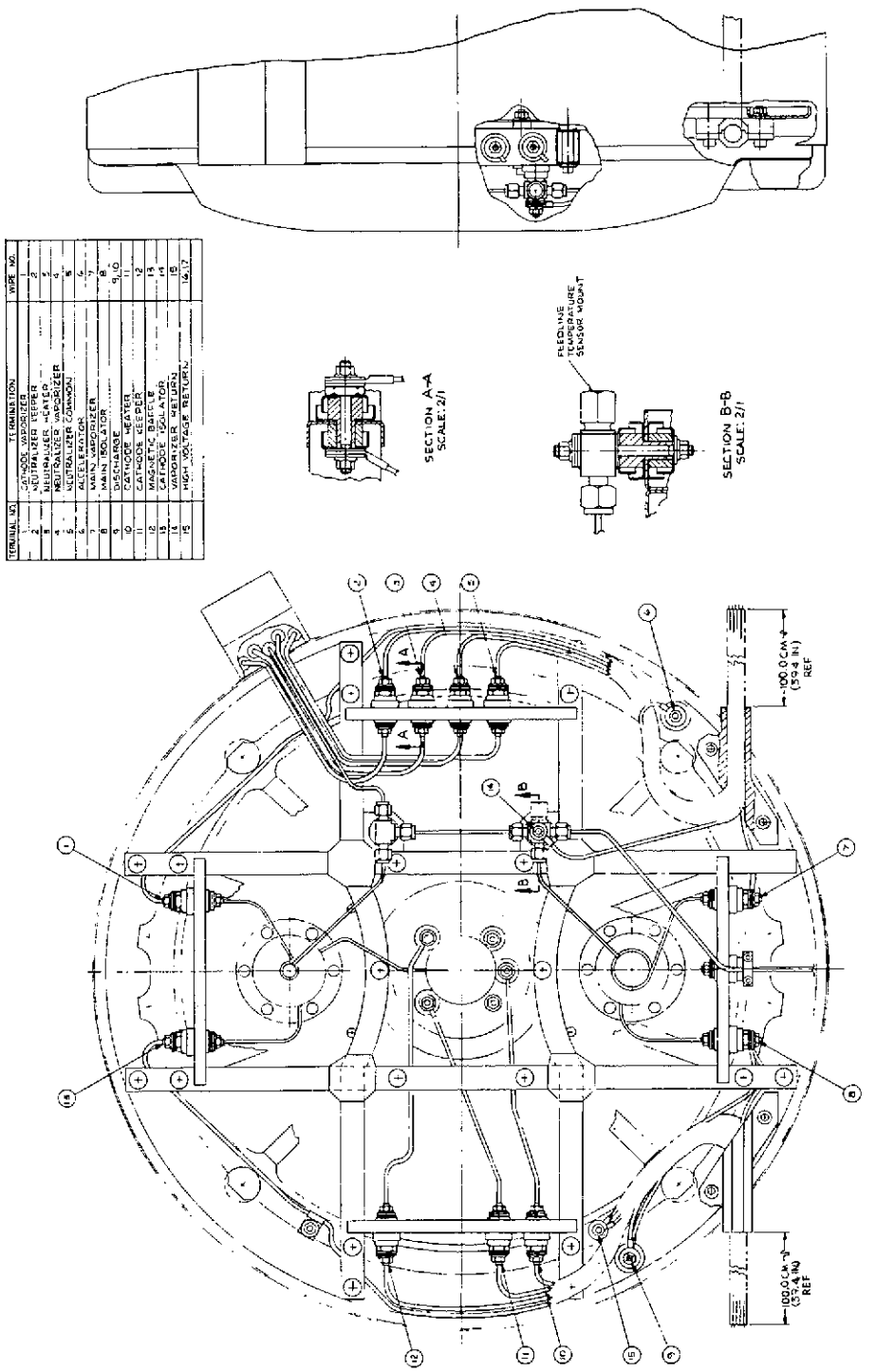

Fig. 65. Electrical interface definition.

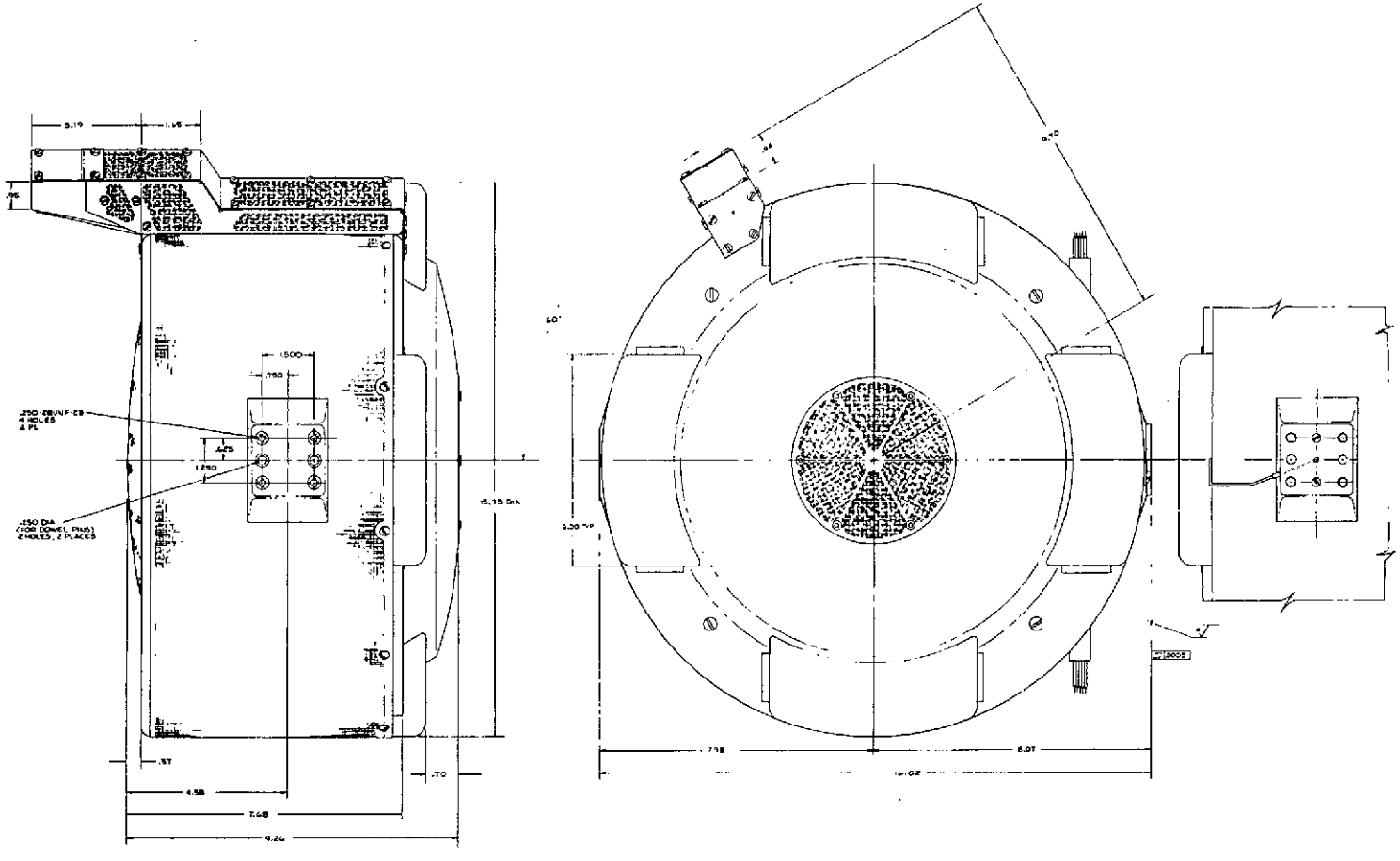

Fig. 66. Mechanical and propellant interface definition.

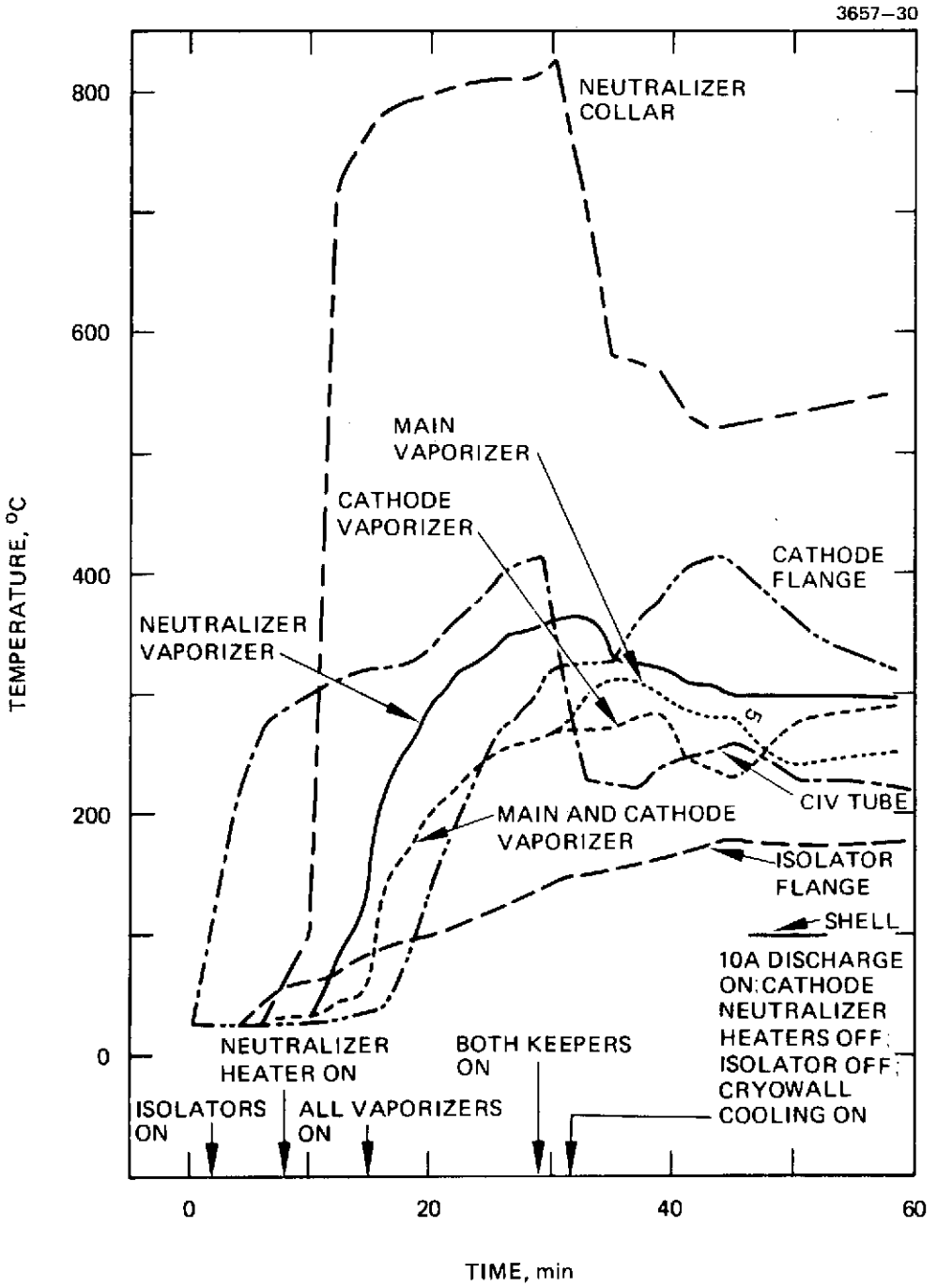

Fig. 67. Temperature of various components during thruster startup.

2. Normal Operation

A representative temperature distribution for steady state operation is shown in Table 27. Thermocouple locations are shown in Fig. 68. (Note that this temperature map was obtained with thruster 701. Slight differences can be expected with the 800-series thrusters.)

TABLE 27

Equilibrium Temperatures for Preliminary Operation of EM Thruster S/N 701 in a Cryopumped Test Facility

Beam Current	2 A	1.45 A	0.85 A
Temperature at Locations Shown in Fig.	°C	°C	°C
No. 1 neutralizer tip	900	-[a]	-
No. 2 nuetralizer heater lead collar	620	610	592
No. 3 neutralizer vaporizer	262	262	282
No. 4 accel electrode	150	120	85
No. 5 screen grid	215	205	165
No. 6A mounting ring	220	180	145
No. 6B cathode vaporizer	269	261	270
No. 7 main vaporizer	309	299	275
No. 8 rear support beam (center)	320	280	225
No. 9 rear support ring	180	160	130
No. 10 rear support beam (end)	240	210	170
No. 11 C-IV flange	260	240	210
No. 12 cathode feed tube	290	260	230
No. 13 cathode mounting base	410	360	300
No. 14 ground screen	160	140	120
No. 15 outer shell	220	190	155
No. 16 rear shield	170	145	125
No. 17 magnet retainer	280	245	205

[a]Thermocouple open circuited

T1484

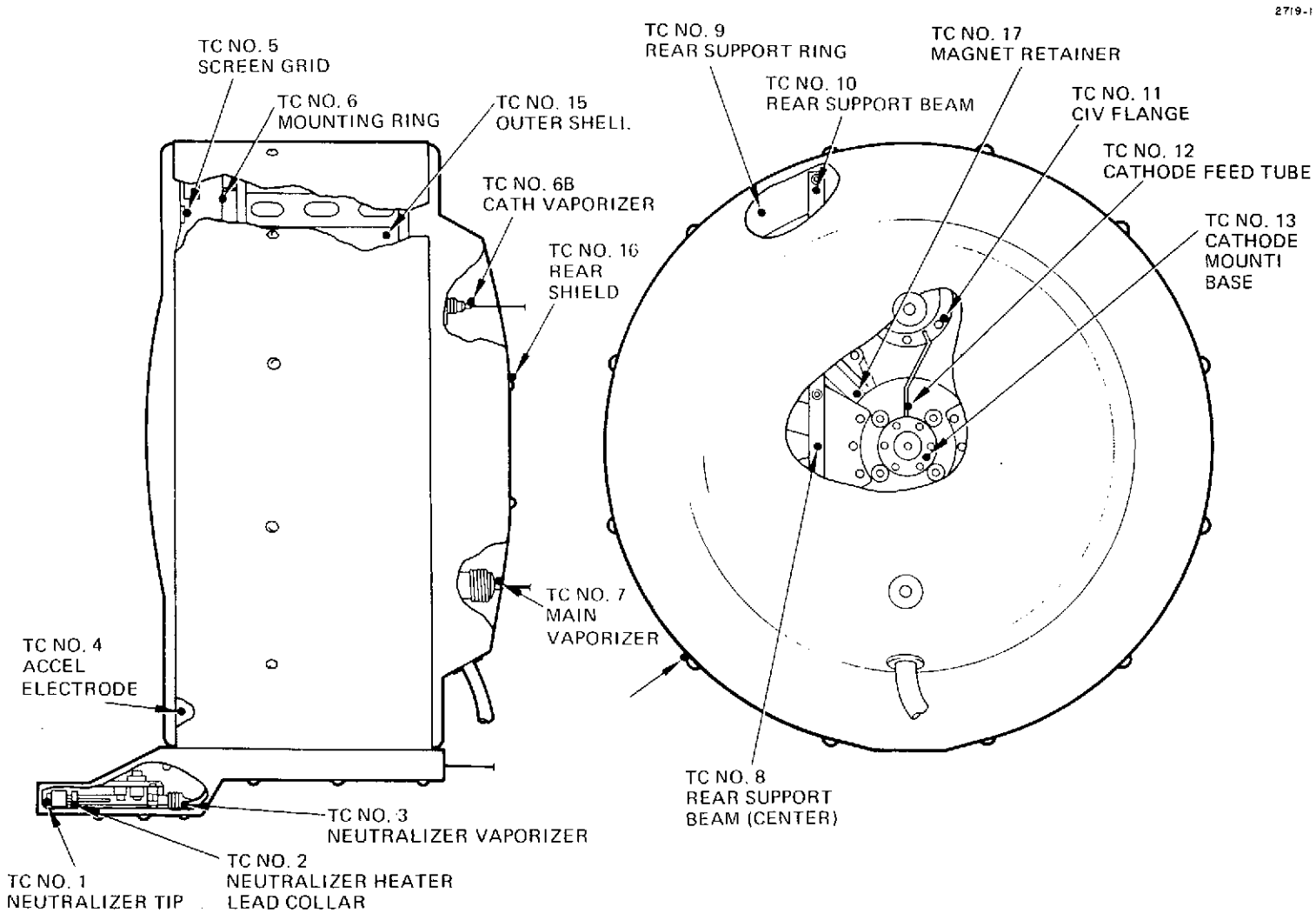

Fig. 68. Thermocouple locations on thruster.

3. Vaporizer Temperatures

Vaporizer temperature versus flowrate characteristics for MIV, CIV, and NIV are shown in Fig. 69. These data are representative of characteristics expected for thruster S/N 801 through 806. The NIV characteristic is expected to shift to a higher temperature operation by use of a more dense porous tungsten vaporizer disk.

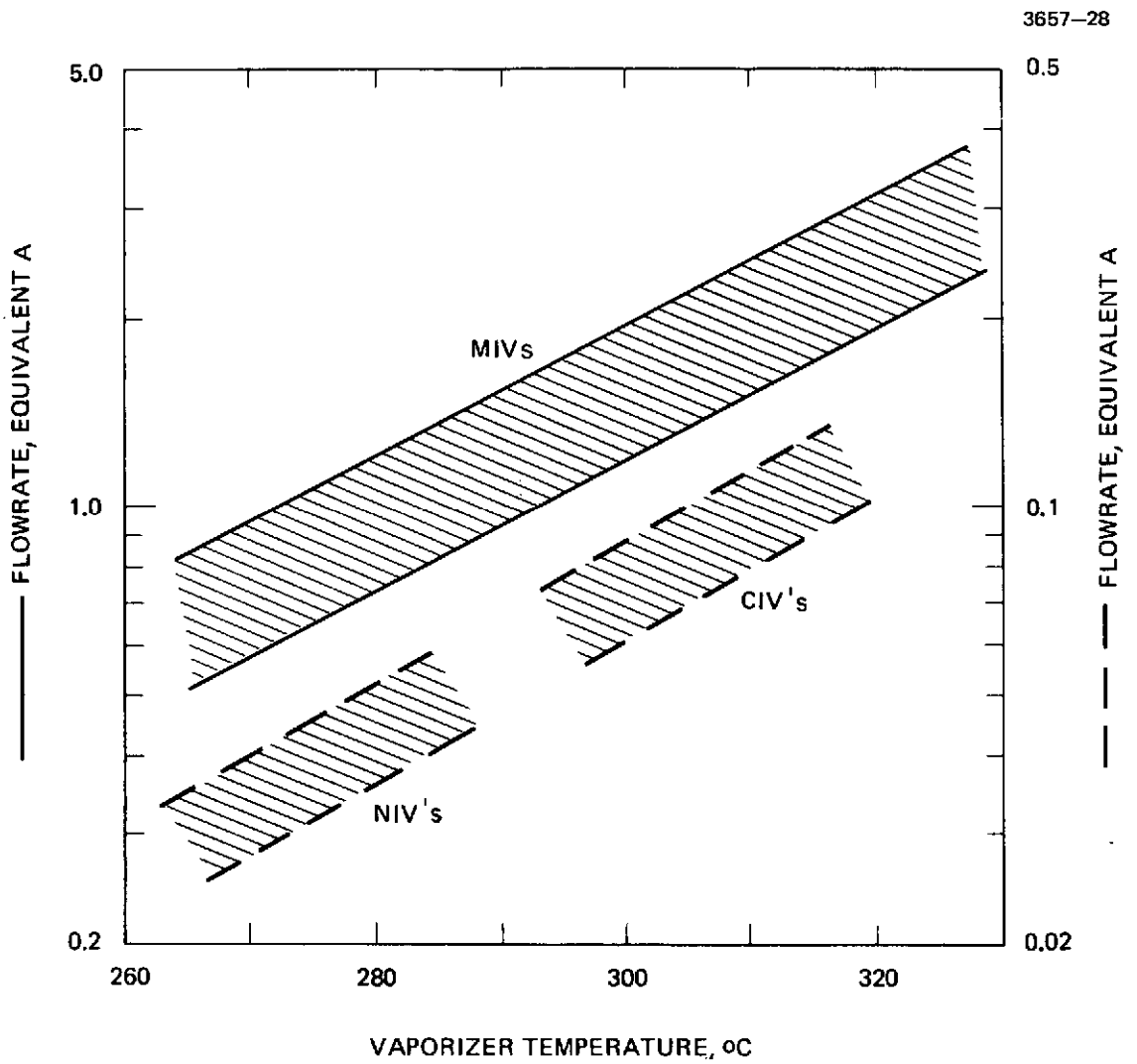

Fig. 69. Vaporizer flowrate calibrations.

G. Materials and Weights

The many requirements placed on the thruster make it necessary to use a variety of materials. A listing of the major parts, materials, and weights is presented in Table 28. The material selection process, which is unique to each part, is discussed more thoroughly in Section II.

H. Magnetic Properties

1. Internal Field

The magnetic field distribution within the 800-series discharge chamber is illustrated in Fig. 70 for both radial and axial components. This distribution is duplicated for each thruster by careful selection of the permanent magnets.

2. External Field

The external magnetic field of the 800-series thruster has not been measured at this time. However, the field of similar thrusters has been measured at NASA LeRC and JPL. These measurements indicate that the external field can be accurately represented as a dipole with a strength of about 18 $A\text{-}M^2$.

I. Environmental Constraints

At this time, a comprehensive set of environmental tests has not been performed on the 800-series design. However, independent tests on components and several 300/400-series thrusters have been conducted by NASA LeRC.[13]

1. Thermal-Low Temperature

Tests conducted at LeRC indicate that a thruster and its associated feed system can be stored at temperatures down to at least $-100^{\circ}C$, with mercury in the feed lines. Startup tests show that no serious problems occur using the normal startup procedure (see Item B).

TABLE 28

30 cm Thruster Weight Breakdown

Item	Quantity	600-Series		700-Series		800-Series[a]	
		Material	Weight, g	Material	Weight, g	Material	Weight, g
Neutralizer Subassembly	1	[b]	300	[b]	255	[b]	346
CIV Subassembly	1	[b]	206	[b]	206	[b]	216
MIV Subassembly	1	[b]	151	[b]	165	[b]	170
Screen Stiffening Ring	1	Moly	330	Moly	184	[b]	–
Accel Stiffening Ring	1	Moly	366	Moly	220	Moly	215
Screen Electrode	1	Moly	173	Moly	175	Moly	146
Accel Electrode	1	Moly	500	Moly	380	Moly	322
Main Optics Support Ring	1	S.S.	360	S.S.	360	Ti	673
Screen Mounting Brackets	12	S.S.	240	S.S.	200	–	–
Accel Mounting Brackets	12	S.S.	113	S.S.	113	S.S.	113
Accel Insulators and Shields	12	Alumina and S.S.	236	Alumina and S.S.	236	Alumina and S.S.	236
Spacers	12	S.S.	48	Ti	8	–	–
Optics Fasteners	misc.	S.S.	197	S.S.	230	S.S.	188
Axial Magnet Retainer	12	S.S.	86	Ti	54	Ti	54
Axial Magnets	12	Alnico V	132	Alnico V	132	Alnico V	132
Radial Magnet Retainer	12	S.S.	10	Ti	22	Ti	22
Radial Magnet	12	Alnico V	170	Alnico V	270	Alnico V	270
Inner Magnet Retainer	1	Mild Steel	42	Mild Steel	42	Mild Steel	42
Outer Magnet Retainer	1	Mild Steel	184	Mild Steel	81	Mild Steel	81
Shield, Pole	1	Tantalum	22	Tantalum	22	–	–
Anode	1	S.S.	196	Ti	104	Ti	108
Outer Shell	1	S.S.	243	Ti	135	Ti	135
Pole	1	Mild Steel	159	Mild Steel	159	Mild Steel	165
Ring, Downstream	1	Mild Steel	235	Mild Steel	122	Mild Steel	122
Ring, Upstream	1	Mild Steel	173	Mild Steel	102	Mild Steel	102
Mask	1	S.S.	558	Ti	122	Ti	120
Rear Shield	1	S.S.	708	Al	252	Al	281
Outer Shield	1	S.S.	270	Al	211	Al	98
Plenum	1	S.S.	160	Ti	74	Ti	74
Insulation and Shields	20	[b]	183	[b]	365	[b]	365.
Backplate	1	S.S.	354	Ti	192	Ti	184
Cover, Rear	1	S.S.	86	Al	13	Al	7
Anode Insulators and Shields	6	[b]	31	[b]	31	[b]	31
Cable Clamp	2	S.S.	22	Al	10	Nylon	58
Bracket-Tee	1	S.S.	18	Ti	10	–	–
Clamp-Tee	1	S.S.	7	Ti	5	–	–
Wire	1	Kapton and and copper	152	Kapton and copper	185	Kapton and copper	265
Insulation	2	—	11		11		–
Frame Structure	1	S.S.	861	Ti	730	Ti	780
Baffle Assembly	1	–	168	–	250	Mild Steel	283
Rear Brace	2	–	–	Al	102	Ti	462
Gimbal Bracket	2	–	–	Ti	356	Ti	356
Fittings, Swagelok	1	S.S.	27	S.S.	27	S.S.	42
Connector, Electrical	2	–	101	–	–	–	–
Miscellaneous	misc.	–	360	–	360	–	497
Total, g			8959		7300		7758
Total, lb			19.73		16.08		17.09

[a]Based on thruster S/N 702-A.
[b]Combinations of Al_2O_3, tantalum, tungsten, stainless steel, inconel, MgO, and nickel.

T1521

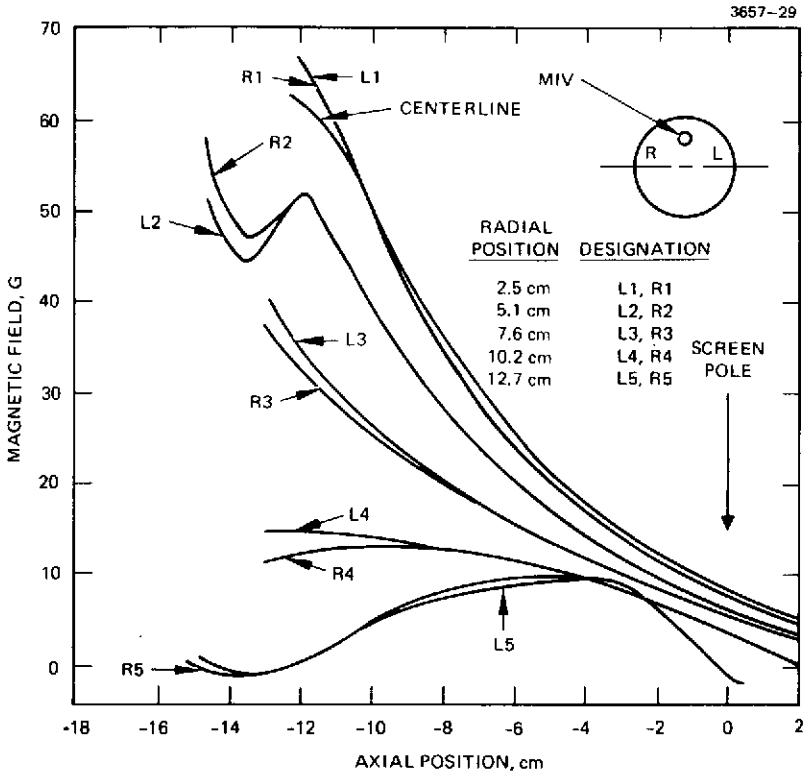

(a) Axial distribution

(b) Radial distribution

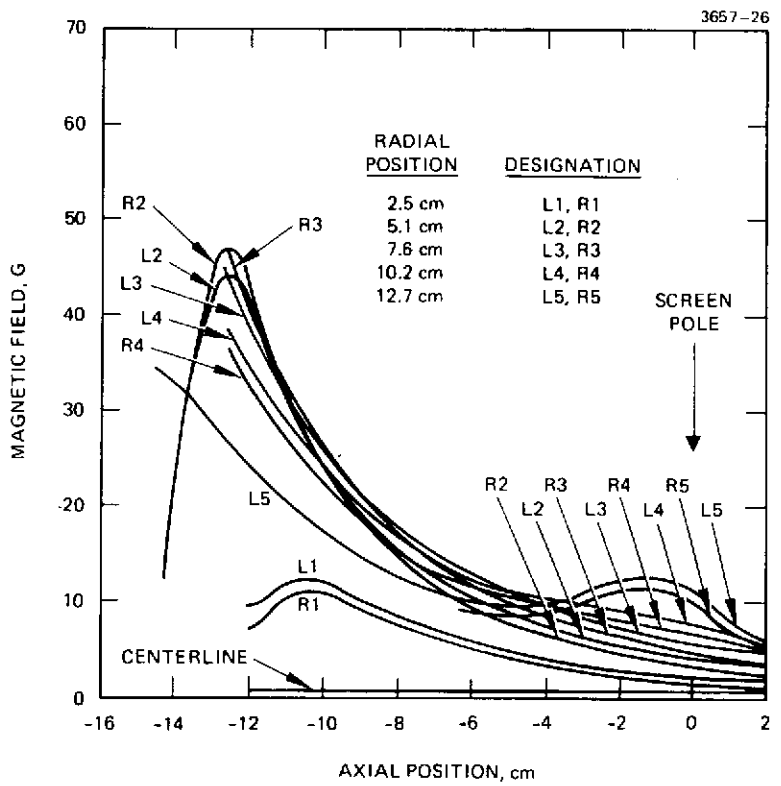

Fig. 70. Magnetic field distributions in the 800-series thruster.

2. Thermal-High Temperature

Tests at NASA LeRC, using a 400-series thruster, indicate that the thruster is relatively insensitive to its thermal environment. Mounting arrangements allowing heat dissipation only in the direction of the ion beam are believed to be acceptable. Further testing with 700/800-series is planned to confirm this conclusion. In addition, LeRC tests with direct solar incidence on the grids up to the equivalent of 2.5 "suns" did not substantially affect thruster operation or performance.

3. Vibration

The 800-series design thruster has been subjected to the vibration test environment shown in Table 29. With minor changes presently being implemented, the thruster is expected to meet the vibration requirements of potential launch vehicles.

J. Electromagnetic Noise

The electromagnetic characteristics of the electron bombardment ion thruster are not well defined at this time. Measurements of radiated noise are essentially impossible with the thrusters operated in metallic vacuum chambers. Conducted noise and transients must consider the contribution and influence of the thruster power processor. Thus, a special test program would be needed to establish the thruster electromagnetic characteristics.

K. Reliability and Wearout Life

In the strict sense, extensive statistical failure rate data are needed to justify predictions of reliability. However, estimates of failure rates can be obtained by comparisons between thruster components and similar components having known failure rates.[14] The results of such a comparative analysis are shown in Table 30. A failure rate of about 16 failures/10^6 hours is predicted for the present 30-cm thruster design. Work to improve high failure rate components could potentially reduce the predicted rate to the range of 10 to 12/10^6 hours.

The present wearout life goal of the 30-cm thruster is 10,000 hours. On-going endurance tests indicate that this goal is reasonable with the 700/800-series design. Proposed improvements, based on 30-cm and 8-cm endurance test experience, will allow the life goal to increase by 50 to 100%.

TABLE 29

Structural Integrity Test Conditions (Thruster S/N 702-A)

Sinusoidal (5 to 2000 Hz) Low level resonance search in x direction[a] (1.0 g) High level resonance search in x direction (11.0 g) Low level resonance search in y direction (1.0 g) High level resonance search in y direction (11.0 g) Low level resonance search in z direction (1.0 g) High level resonance search in z direction (11.0 g) Half Sine Shock 30 g peak in x direction (3 each) 30 g peak in y direction (3 each) 30 g peak in z direction (3 each) Random Vibration 19.8 g rms for 4.5 min. each axis
[a]Axis Orientation: x axis in direction of thrust z axis in direction of neutralizer y axis in orthogonal to neutralizer

T1528

TABLE 30

Estimated Failure Rates for 30-cm Thruster

Subassembly	Failure Rate, Failures/10^9 h
1. Thruster Shell and Structure	5988
2. Optics and Supports	3300
3. Cathode-Isolator-Vaporizer	3178
4. Main Isolator-Vaporizer	1356
5. Neutralizer-Vaporizer	2525

T1529

V. CONCLUSIONS

Over the past 2-1/2 years this program has been the focal point for design improvements resulting from work under concurrent Hughes contracts (NAS 3-15523, -16528 and -16949), and from extensive efforts at NASA LeRC. These improvements involved substantial efficiency gains (about 10 percentage points), definition of beam divergence and double ion corrections, application of dished grids to provide a completely stable ion optical system, more complete definition of operating characteristics, demonstration of long life, and evaluation of thruster structural integrity. In addition, several features which could eventually become requirements for integration with a space vehicle were developed. Such features include mounting from two points (for gimbaling), a single line propellant interface, terminals for all wiring to define the cabling interface, and relatively complete R&QA procedures for thruster fabrication.

As in any lengthy program involving development, one might expect the goals to be adjusted occasionally to meet new requirements and to provide a continuing challenge as progress is made. In terms of performance, the original goals for this program were based on the assumption that ion beam divergence and double ion content were small factors. With the benefit of about eight months work, the goals on performance were mutually redefined to include divergence and double ions. In addition, the total efficiency goal was increased from 71% to 73%. With the efforts of the Hughes and NASA LeRC programs, the revised performance goals were nearly achieved with a total efficiency of about 71.6% at full power. This efficiency level required combined improvements in power and propellant efficiencies of about 10 percentage points to compensate for double ions and beam divergence.

Although many of the improvements mentioned were achieved by joint efforts, the specific contributions of this program should be delineated. Those of significant value to the overall effort include the transfer of dished grid technology from NASA LeRC to Hughes,

parametric evaluation of dished grid designs, cathode operating mechanisms and design studies, parametric discharge chamber studies, thruster automatic control studies, improved component designs (CIV, MIV, NIV, and ion optical system), improved overall mechanical design, structural integrity evaluation, and the development of high quality fabrication techniques. Although the parametric studies were not all inclusive and in several cases did not include tests of the final design (e.g., grid dimensions), this work successfully identified many thruster and component characteristics. This characterization provided direction for subsequent or parallel efforts which resulted in the final designs.

The design and fabrication effort under this program has melded the various requirements, constraints, and original hardware into an essentially flight worthy thruster. Performance, endurance, and structural integrity tests have been performed to demonstrate the ability of this design to meet the primary needs of potential space vehicle programs. Future design and test efforts will undoubtedly find areas for additional improvement, but such work will be starting from the strong foundation provided by the 800-series thruster design.

REFERENCES

1. H. J. King, et al., "Low Voltage 30 cm Ion Thruster," NASA CR 102912, February 1972.

2. C. R. Collett, "Endurance Testing of a 30-cm Kaufman Thruster," AIAA Paper 73-1085, October, 1973.

3. R. L. Poeschel, et al., "2.5 Advanced Technology Ion Thruster," Final Report, NASA CR 134687, September, 1974.

4. V. K. Rawlin, et al., "Design, Fabrication, and Operation of Dished Accelerator Grids on a 30-cm Ion Thruster," AIAA Paper 72-486, April 1972.

5. V. K. Rawlin, "Studies of Dished Accelerator Grids for 30-cm Ion Thrusters," AIAA Paper, 73-1086, October 1973.

6. R. L. Danilowicz, et al., "Measurement of Beam Divergence of 30-cm Diameter Dished Grids, AIAA Paper 73-1051, October, 1973.

7. D. Zuccaro, "Mercury Vapor Hollow Cathode Component Studies," AIAA Paper 73-1141, October 1973.

8. M. J. Mirtich, "Investigation of Hollow Cathode Performance for 30-cm Thrusters," AIAA Paper 73-1138, October 1973.

9. "Hollow Cathodes with BaO-Impregnated Porous Tungsten Inserts and Tips," AIAA Paper 73-1142, October 1973.

10. M. A. Mantenieks, "Investigation of Mercury Isolators," AIAA Paper 73-1088, October 1973.

11. B. G. Herron, J. D. Worden, and J. M. Simpkins, "A 30-cm Thruster Power Processor Test Console," AIAA Paper 73-1104, October, 1973.

12. R. P. Vahrenkamp, "Measurement of Double Ions in the Beam of a 30-cm Mercury Bombardment Thruster," AIAA Paper 73-1057, October, 1973.

13. D. Byers, et al., Private Communications, NASA LeRC, September, 1974.

14. J. H. Molitor, "Ion Propulsion Flight Experience, Life Tests, and Reliability Estimates," AIAA/SAE Propulsion Conference, Sahara Hotel, Las Vegas, Nev. November 4-7, 1973.

APPENDIX A
CATHODE ANALYTICAL AND EXPERIMENTAL STUDIES

The studies discussed in this section were performed to establish the operating limits of components available early in the program and to evaluate new designs. The results of the parametric investigations are organized into the following subject areas:

1. Role of alkaline earth oxides in cathode operation
2. Mechanism for and rate of loss of oxides
3. Cathode heater tests
4. Barium impregnated cathode tests

The initial effort in this work was to establish the role of alkaline earth oxide materials in the operation of mercury vapor hollow cathodes. While the emissive materials were believed to be essential to starting the discharge, it was not certain that they were essential to the operation of the cathode. Starting and operating characteristics of cathodes containing emissive mix and of cathodes free of any emissive materials were determined. These tests demonstrated that emissive mix was essential in order to obtain a cathode which operates in a manner that is compatible with the ion thruster requirements.

Once the need for emissive mix was established, it was necessary to determine the factors which could cause the loss of the alkaline earth oxides during the long term operation of the ion thruster. An analysis indicated that evaporation and chemical reaction are the most probable loss mechanisms. A life test was performed to determine the rate of loss due to these factors. The results of this test indicated that the cathode insert, which is presently used in ion thruster cathodes, lost about 10% of the emissive materials when operated at 1190°K for 1104 hours. Under these conditions, about 2/3 of the loss was due to evaporation and 1/3 was due to chemical reaction.

Another possible life-limiting feature of the ion thruster cathode is the durability of the cathode heater. Long term steady state and

accelerated degradation tests were performed on brazed sheath heaters, and on plasma arc and flame-sprayed heaters of the SERT II type. The tests showed that the upper temperature limit for long term operation of the brazed sheath heater is about 1300°K, and about 1600°K for the plasma arc sprayed heater. A comparison of steady state and cyclic heating of flame sprayed heaters showed the temperature change to be a more important factor in limiting the heater life.

1. Cathode Parametric Studies

Three basic types of cathodes were used in this program.[7] The essential features are listed in Table 31. Except where it is specifically noted in the discussion, the studies were performed using the 1/4-in. cathode.

The tip temperature was generally determined both by means of an optical pyrometer and a thermocouple. The tungsten-5% rhenium/tungsten-26% rhenium pair was used in most cases; the platinum/platinum-rhodium thermocouple was used in the remainder of cases. After the window and emissivity corrections were made on the optical pyrometer readings, the values from both techniques were found to agree to within ±25°K in nearly every case.

The mercury vapor flow was measured by means of a glass pipette feed system. Sufficient long-term data was obtained to calibrate the porous tungsten vaporizer flow characteristics. After this, short term flow rates were obtained from a graph of flow rate as a function of vaporizer temperature.

The operating characteristics of the cathodes were obtained by measuring the steady-state anode and keeper electrode current and voltage. The current-voltage characteristics of the starting of the cathode discharge were obtained by displaying the current and voltages simultaneously on a dual trace oscilloscope. An SCR controlled circuit was used to apply the keeper potential and to trigger the scope trace. The data was recorded by means of an oscilloscope camera.

TABLE 31

Summary of Cathode Features Used in Parametric Tests

Property	1/4 in.	1/8 in.	Experimental 1/4 in.
Tube material	Tantalum	Tantalum	Molybdenum
Tip Material	Thoriated Tungsten	Thoriated Tungsten	Barium impregnated porous tungsten
Tip Orifice Diameter, cm	0.076	0.025	0.076
Tip Orifice Geometry	Exterior Bevel Interior Bevel	Exterior Bevel	Exterior Bevel
Tip Heaters	Tantalum Wire in Tantalum Sheath a) Pressed on Tube b) Brazed on Tube Tungsten-rhenium Wire in Alumina c) Plasma arc sprayed alumina d) Flame sprayed alumina	Tungsten-Rhenium Wire in Alumina a) Plasma arc sprayed alumina b) Flame sprayed alumina	Molybdenum wire enclosed in sintered alumina
Inserts	R-500 coated tantalum R-500 coated nickel cc 4168 coated tantalum	Plain tantalum foil barium impregnated porous tungsten	Barium impregnated porous tungsten

The first cathode studies were conducted using a movable collector which had both a solid and a gridded surface. These studies showed that a collector-to-keeper distance of 2.5 cm would result in a discharge characteristic that roughly duplicated the ion thruster operating conditions. Subsequent studies were performed using an LN_2 cooled collector located about 2.5 cm from the keeper.

The tests were performed in a vacuum station which was pumped by a mercury diffusion pump. The system had a mechanically refrigerated baffle above the pump and two LN_2 cooled traps in the chamber. The chamber operated in the low 10^{-6} Torr range during the testing of the cathode components.

2. Role of Alkaline Earth Oxides

Tests were conducted to determine the role of alkaline earth oxides on hollow cathode initial start, restart and steady operation. This was accomplished by use of oxide-coated and oxide-free cathodes. Details of these tests are discussed more fully in reference 7.

Several series of tests with oxide coating were conducted to study activation and possible deactivation mechanisms. The operating characteristics of these cathodes were equivalent to the "normal" conditions observed in the operation of the cathodes in ion thrusters. The cathodes exhibited "plume" to "spot" mode transitions. The cathode tip operating temperatures were 1070 to 1370°K (depending on the discharge power).

Studies were then made of a cathode that was free of any alkaline earth oxides in order to determine the starting and operating characteristics that could be expected of a totally deactivated cathode. A 1/8-in. cathode with a flame sprayed heater was used in this study because it could operate at a higher temperature than the 1/4-in. cathode with a brazed sheath heater. Both the flat plate and the enclosed keeper geometrics were used. The tests were performed both with a tantalum foil insert that was free of alkaline earth oxides and without any insert.

The purpose was to determine if the bare insert played a role in the cathode operation.

The nonoxide cathodes exhibited high starting temperatures at high flow mercury flow rates and high keeper potentials. The cathode with an open keeper required a minimum mercury vapor flow of 37.5 mg/minute (300 mA) and a keeper potential of 5 kV. At a minimum mercury vapor flow of about 100 mg/min (800 mA) lower starting voltages were possible at higher temperatures. Further increase in flow did not alter this characteristic. It is interesting to note that the starting point of an oxide cathode which had been exposed to the atmosphere for a long period shifted to the nonoxide characteristic. This is shown in Fig. 71. At a 500 V keeper potential the restarting temperature of the nonoxide cathode was 300°K higher than the initial start temperature of the oxide cathode and 700°K higher than the restart temperature of a fully conditioned oxide cathode.

The surface of the nonoxide coated cathode exhibited severe erosion after these tests were completed. The tip face had small pits which appeared to be the result of melting by electric arcs. The study of the oxide free cathode has shown it to be difficult to start and to operate. The high operating temperatures and high mercury vapor flow rates needed to operate the cathodes, makes the cathode incompatible with the present thruster designs.

3. Oxide Degradation Mechanisms

The purpose of this effort was to determine the factors causing the degradation of oxide coatings. Only BaO reactions are considered since BaO is the most volatile and most prevalent of the three oxides used in emissive mixes.

There are three principal reactions that could cause the loss of BaO in an operating cathode. These are evaporation (eq. 18), thermal decomposition (eq. 19), and chemical reaction with the supporting foil (eq. 20).

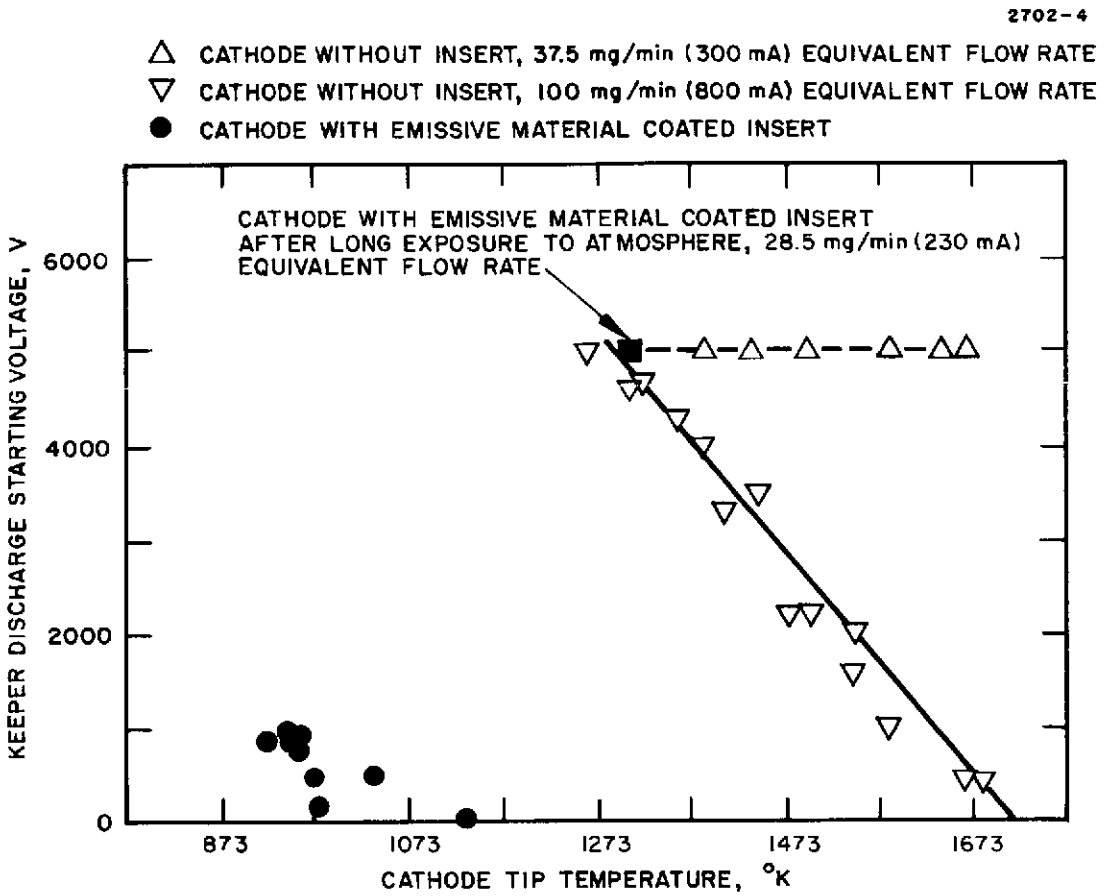

Fig. 71. Starting potential as a function of cathode temperature for oxide and nonoxide cathodes.

$$BaO_{(s)} \rightleftarrows BaO_{(v)} \tag{18}$$

$$BaO_{(s)} \rightleftarrows Ba_{(v)} + 1/2\ O_{2\ (v)} \tag{19}$$

$$BaO_{(s)} + 2/5\ Ta_{(s)} \rightleftarrows 1/5\ Ta_2O_{5\ (s)} + Ba_{(v)} \quad . \tag{20}$$

Although mechanical loss is possible (e.g., due to vibration), it was not considered in this anlaysis. Chemical reactions with atmospheric gases (i.e., poisoning) are not significant to the operating cathode, and thus are not considered in this analysis.

Equilibrium constants for the three reactions can be established by standard thermodynamic techniques. These can be applied directly to the first two reactions but only represent an estimate of the upper limit for the third reaction. The reason is that the latter is a solid state-solid state reaction. Thus, the extent to which this reaction proceeds depends on the contact area between the reactants and the extent of solid state diffusion of the reactants. The constants are presented in Table 32 in terms of the equilibrium vapor pressure of either Ba or BaO vapor resulting from the specific reaction.

An experimental study was performed to determine the rate of loss of BaO due to reactions 1 and 3. It is possible to distinguish between them by using an inert support for the BaO, and thus establish the evaporative loss. As nickel metal does not react with the alkaline earth oxides, it was used to fabricate an insert to support the Triple Carbonate* emissive mix. In order to avoid any reaction of the emissive mix and the tantalum wall of the cathode, the nickel was formed into a cylinder and coated on the interior with the emissive mix. The test consisted of a comparison of six tantalum based inserts and five nickel based inserts.

*J. T. Baker Chemical Co., Phillipsburg, New Jersey (Commodity No. 9805).

TABLE 32

Equilibrium Vapor Pressure of Ba or BaO (Expressed as log P = A - B/T)

Reaction	A[a]	B[a]	P_{eq} at 1100°K	P_{eq} at 1300°K	P_{eq} at 1500°K
$BaO_{(s)} \rightleftharpoons BaO_{(v)}$	8.63	19400	1.0×10^{-9}	5.0×10^{-7}	5.0×10^{-5}
$BaO_{(s)} \rightleftharpoons Ba_{(v)} + 1/2\ O_{2\ (v)}$	9.76	24900	1.3×10^{-13}	4.0×10^{-10}	1.4×10^{-7}
$BaO_{(s)} + 2/5\ Ta_{(s)} \rightleftharpoons 1/5\ Ta_2O_{5\ (s)} + Ba_{(v)}$	8.33	15500	1.7×10^{-6}	2.6×10^{-4}	9.9×10^{-3}

[a] Values for reaction 1 from J. P. Blewett, J. Appl. Phys. 10, 668 (1939).
Values for reactions 2 and 3 from E. S. Rittner, Philips Res. Rpt. 8, 184 (1953).

T1451

The test procedure consisted of briefly heating all the cathodes to about 1270°K to convert the carbonates to oxides; one of each type was used as a control. These were operated at the ambient temperature of the system (about 500°K). The remaining cathodes were set at specific high temperatures and operated continuously for 1104 h. Mercury vapor flow, averaging 10 mg/min (80 mA) per sample, was maintained for the first 470 h of the test.

At the end of the test, the samples were removed for visual inspection. The nickel inserts had a bright metallic surface and no evidence of reaction. All of the tantalum samples were oxidized. The samples operated at 1373 and 1541°K were oxidized to the extent that the tantalum crumbled into small pieces when the inserts were removed from the cathodes.

The samples were dissolved in acid solution and atomic absorption spectroscopy was used to analyze the amount of barium, strontium, and calcium that remained. The results of this analysis are presented in Table 33 and Fig. 72 and 73. The anomalously low value of sample 3 may be due to a loss of sample material. Excluding No. 3, the losses in the tantalum case became significant for samples 13 and 16 which operated at 1373 and 1541°K, respectively. Sample 15 (a nickel based sample which operated at 1473°K) exhibited a much smaller loss. Samples 8, 9, and 10 operated at about 1200°K. The average loss of samples 9 and 10 was about twice that of sample 8.

A comparison of the percent weight loss, as shown in Fig. 74, indicates that the loss due to evaporation is about 2/3 of the total at 1200°K. At temperatures above 1500°K, the loss due to chemical reaction becomes dominant. On the basis of these observations, a 10,000 h lifetime could be attained by operating the nickel based insert at temperatures below about 1300°K, and the tantalum based insert at less than 1200°K.

4. Cathode Heater Endurance Tests

At the time this program was initiated the standard cathode heater used in the 30-cm thruster was a sheath heater brazed

TABLE 33

Results of Atomic Absorption Analysis of the 1104 Hour Thermal Degradation Test on Tantalum and Nickel Based Inserts

Sample Number	Operating Temperature, °K	Ba, mg	Ca, mg	Sr, mg	Ratio of Weight (Sample/Control)			Calculated Total Weight as Carbonates, mg	Ratio of Carbonate Sample/Control
					Ba	Ca	Sr		
Tantalum Based Insert									
6	513	95.5	19.7	44.3				261	
3	1117	70.5	14.1	30.6	0.738	0.716	0.691	188	0.720
9	1180	90.4	18.9	41.8	0.947	0.959	0.944	249	0.954
10	1195	80.5	17.1	36.6	0.843	0.868	0.826	220	0.842
13	1373	77.3	14.9	30.3	0.809	0.756	0.684	199	0.762
16	1541	26.3	8.5	7.4	0.275	0.431	0.167	72	0.276
Nickel Based Inserts									
5	523	58.7	10.0	22.8				148	
2	1115	53.3	9.2	24.0	0.908	0.920	1.052	140	0.946
8	1208	54.8	9.2	22.1	0.934	0.920	0.969	139	0.940
12	1315	49.8	8.5	20.2	0.848	0.850	0.886	127	0.858
15	1473	48.0	8.5	20.5	0.818	0.850	0.899	125	0.844
		(estimated accuracy of atomic absorption analysis 5 to 10%)							

T1452

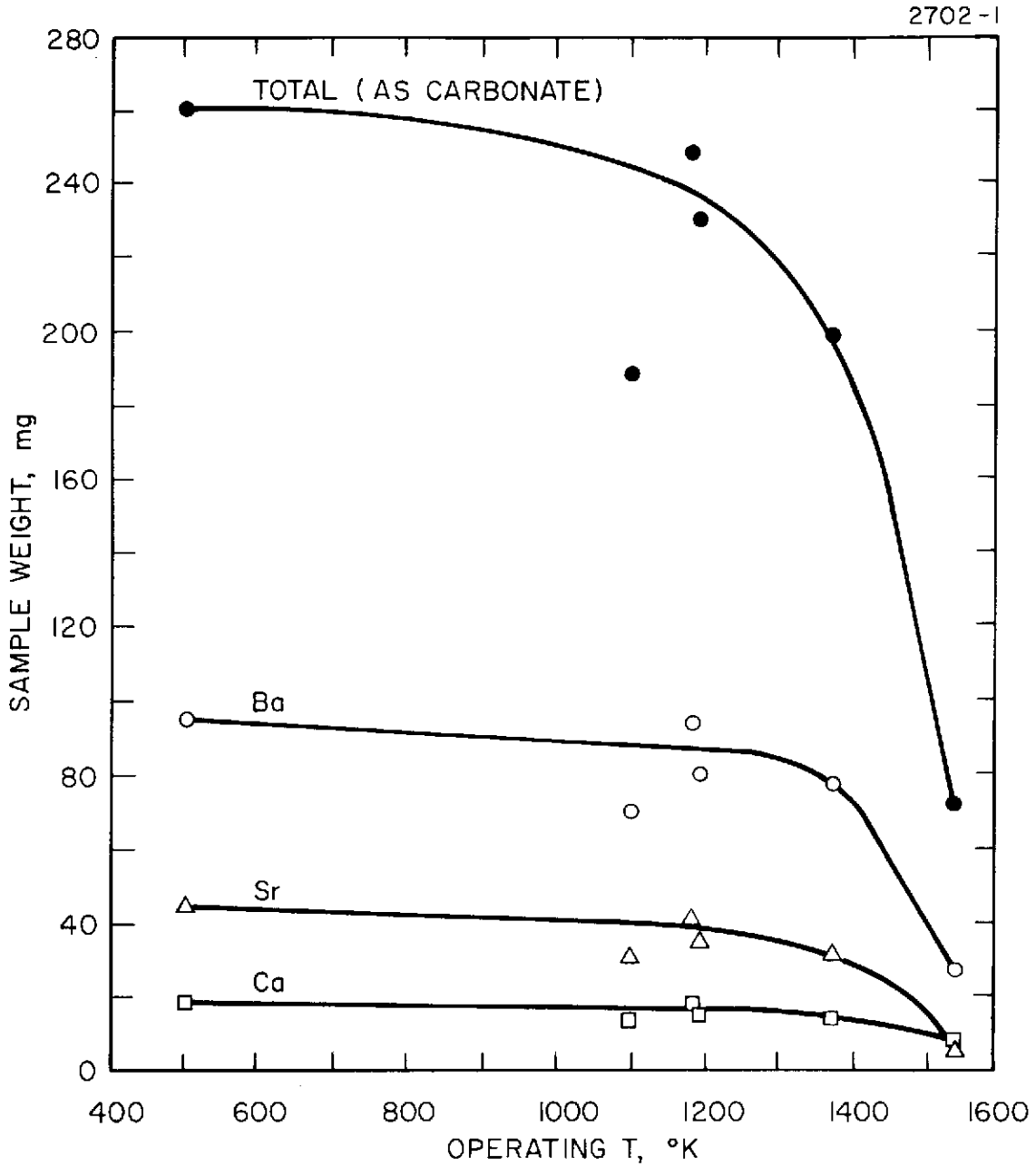

Fig. 72. Weight of emissive mix components after heating of tantalum based inserts for 1104 hours.

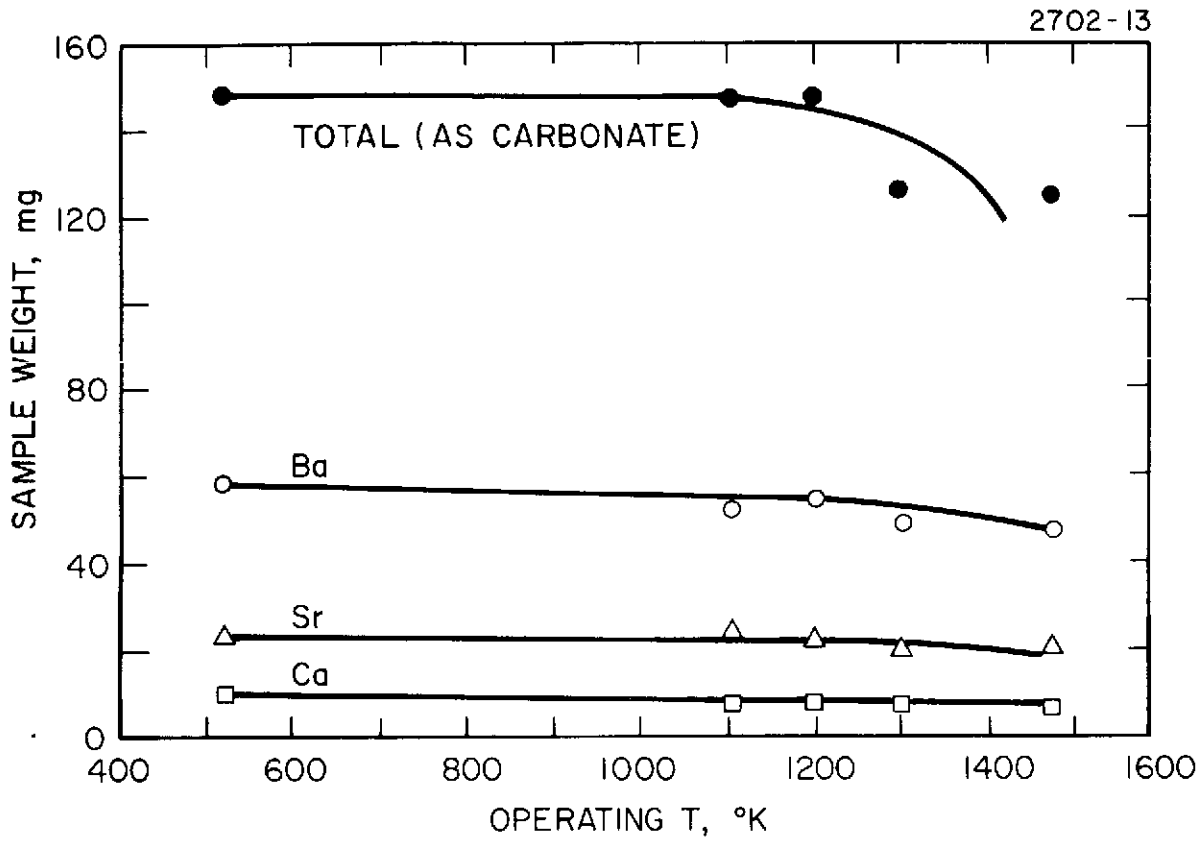

Fig. 73. Weight of emissive mix components after heating of nickel based inserts for 1104 hours.

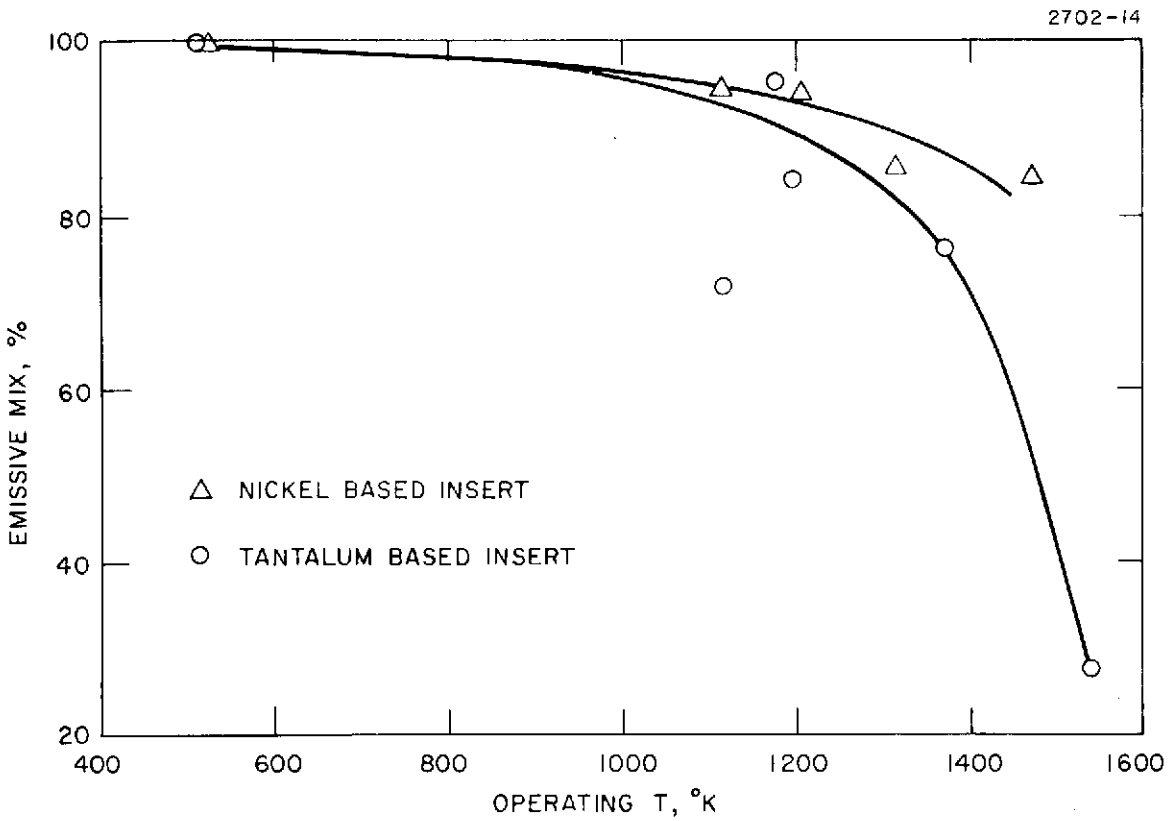

Fig. 74. Percent of emissive mix remaining after 1104 hour test.

to the cathode body. These consisted of a 0.025-cm diameter tantalum center conductor, magnesia insulation, and a 0.062-cm diameter tantalum sheath that was formed by a swaging operation. A new heater design was evolved from the existing 1/8-in. cathode heaters which was in turn a modification of the SERT II heater. The heater consists of a 7 turn 0.025-cm diameter tungsten-26% rhenium wire which is encapsulated in alumina. The alumina is applied by either the plasma arc or flame spray process. The first test was a steady state life test of the two heaters.

Four brazed sheath heaters which were used in the life test and five new samples of brazed sheath heaters were subsequently tested to determine the upper limit for the operating temperature. These heaters were tested in the range of 1300 to 1500°K. The heaters exhibited measurable changes in the hot resistance when operated for periods of 20 to 100 h at temperatures in the range of 1300 to 1430°K. Operation in the range of 1400 to 1500°K resulted in rapid degradation and failure of the heaters. On the basis of these tests, the upper temperature limit for long-term operation of the brazed sheath heaters appears to be about 1300°K. As this value is lower than those at which the plasma sprayed heaters were operated successfully in the 1100 h test, it was decided to adapt the plasma sprayed heater as the standard heater.

Of the six life tested plasma sprayed heaters, one was undamaged as a result of the removal of the inserts and was thus available for high temperature testing. It was operated at 1653°K (at a power of 97 W). The hot resistance was constant until after 244 h of operation. At this point there appeared several bright areas in the ceramic coating. These indicated that the heater was no longer in contact with the alumina at these points. Thus heat transfer was only by radiation at these bright areas. The heat transfer to the cathode tip gradually decreased and the test was terminated at 366 h. At this point, the tip temperature had decreased to 1443°K. Similar results were observed in short term tests of five new plasma sprayed heaters.

Based on these results, and on the results of tests of 1/8-in. cathodes used in the 5-cm thrusters, the plasma sprayed heater was adopted for use on the 1/4-in. cathodes. In the new design, the alumina outer coating thickness was set at 0.025 cm. No failures were observed at normal operating peak power levels of 60 W which is applied only during cathode startup. However, tests carried out to establish heater capability at power levels about 75 W resulted in premature failure of the heaters.

5. Effects of Alumina Thickness and Thermal Cycling

A set of four sprayed heaters were tested to determine the effects of alumina coating thickness on the heater operation and the effects of cyclic heating on heater life. The heaters listed in Tables 34 and 35 first were operated continuously for 312 hours. There was no evidence of any changes in the resistance of the heaters and no visual changes in the appearance of the heaters.

Four heaters were then placed in a cyclic test. Heaters 5 and 6 were operated with a 60 Hz power supply and heaters 7 and 8 were operated using a 10^4 Hz supply. The heat cycle profile to heaters 6 and 7 was a square one; i.e., the full power was applied at the start of the 8-min cycle and cut off at the end of the cycle. A ramped heat cycle was used for No. 5 and 8. In this case the applied power was linearly increased over the first two minutes and then linearly reduced at the end of the 8-min period.

Heater 7, which had a thin coating, developed a bright appearance shortly after the start of the test (about 10 cycles). This indicated possible separation of the heater and the ceramic cover. Heater 5, which had a thin coating, began to exhibit bright areas after about 100 cycles. Of the thick coated heaters, No. 8 developed a bright area at approximately the 634th cycle, while No. 6 did not exhibit the same until about the 832nd cycle. Despite these changes, all the cathodes were operating steadily after 1500 cycles. There were no exposed areas due to loss of ceramic as was the case in the previous test. The

TABLE 34

Comparison of Flame and Plasma Sprayed Heaters in Cyclic Heating Tests

No.	Type	Alumina Coating Thickness, cm	Power Supply Frequency Hz	Tip Operating Temperature, °K	Remarks
1	Plasma	0.028	10^4	1455 ± 30	Bright areas appeared about 632nd cycle-ended test at 692nd cycle due to power supply failure-observed bare heater wire due to loss of alumina.
2	Flame	0.023	10^4	1422 ± 35	Bright areas appeared about 276th cycle-ended test at 833rd cycle-heater still functional — some bare spots present.
3	Plasma	0.033	60	1472 ± 10	Burned out between 199th and 448th cycle.
4	Flame	0.028	60	1487 ± 10	Bright areas appeared about 748th cycle — heater still functional at end of test at 1097th cycle.
Used 60 Hz supply after 276th cycle.					

T1453

TABLE 35

Comparison of Plasma Sprayed Heaters in a Cyclic Heating Test

No.	Alumina Coating Thickness, cm	Power Supply Frequency, Hz	Cycle Profile	Tip Operating Temperature, °K	Remarks
5	0.033	60	Ramped	1445 ± 10	Bright areas appeared at about 100th cycle.
6	0.051	60	Square	1450 ± 10	Bright areas appeared at about 832nd cycle.
7	0.036	10^4	Square	1440 ± 10	Uniform bright area after 10 cycles.
8	0.056	10^4	Ramped	1440 ± 10	Uniform bright area developed between 448 and 634th cycle.

T1454

conclusion drawn from this is that the power supply frequency and the heat cycle profile are not significant factors. The thickness of the ceramic coating is the most critical factor in determining heater life. Operation in a continuous mode appears to be much less severe than cyclic operation of the heaters.

6. Barium Impregnated Tungsten Insert

Cathodes using a barium impregnated porous tungsten tip were designed, fabricated and tested. In this concept, the emissive material (which is normally contained in an insert) is used to fabricate the cathode tip. Thus the emissive material is located at the point of origin of the discharge. A cross-sectional view is given in Fig. 75. The porous tungsten tip is brazed to a molybdenum tube. A molybdenum shield cap is brazed on at the same time. A helical molybdenum wire heater is attached to the cathode. The heater is supported by sintered alumina.

The initial discharge was obtained at a temperature of 1200°K and a mercury vapor flow of 13.6 mg/minute. The cathode initial discharge was into a low voltage or spot mode at a 5 A anode current. Restarts after brief off periods could be made to tip temperatures as low as 943°K. The temperatures were determined by means of a platinum-platinum-10% rhodium thermocouple. Restarts after overnight off periods required tip temperatures of about 1090°K.

The impregnated cathodes were not operated in long-term life tests. Although the operating temperatures were sufficiently low and there was no evidence of change in the cathode operating characteristics during the short-term tests, long-term life tests will be needed to establish this cathode for use in ion thrusters.

7. Cathode Parametric Test Conclusions

Operation of the oxide cathodes and oxide-free cathodes demonstrated that the presence of emissive materials is essential in order to operate the mercury vapor hollow cathode in a mode that is compatible with the ion thruster requirements. Long term operation of

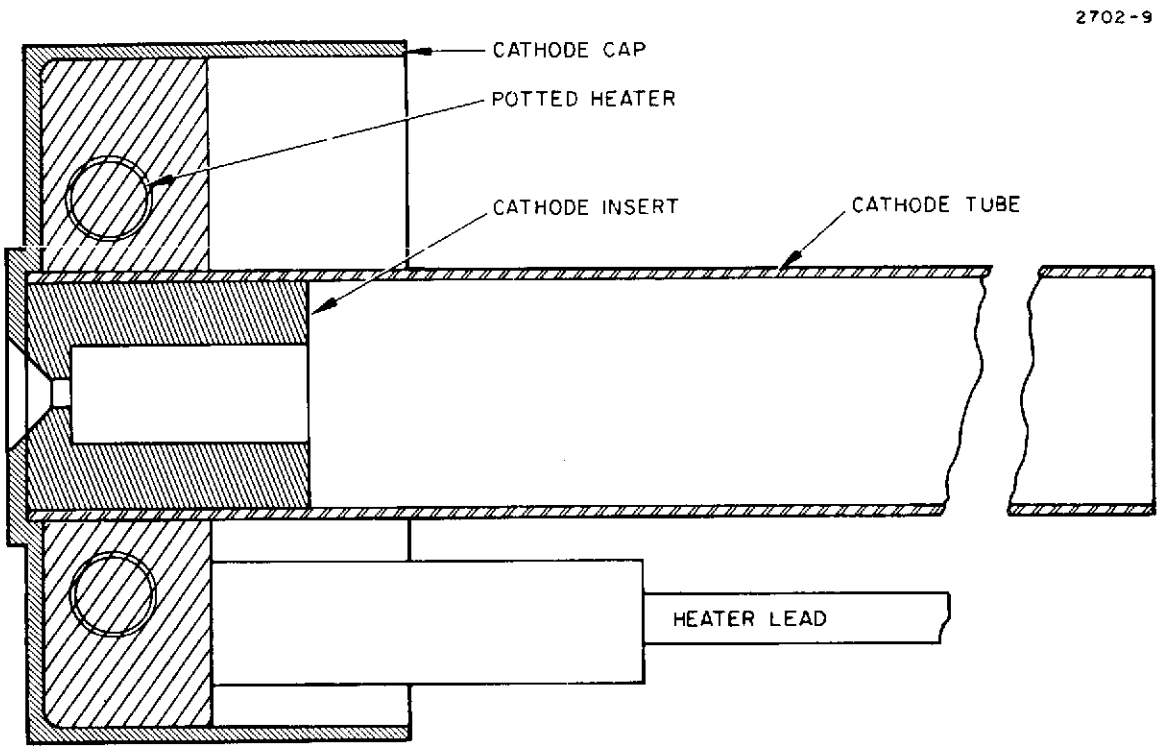

Fig. 75. Cross sectional view of experimental cathode having a barium impregnated tip.

the cathode requires that the tantalum based insert be located so that the operating temperature is below 1200°K in order to limit evaporative and reactive losses to the desired levels.

Tests have shown that the nickel based insert* and the barium impregnated porous tungsten insert can be used in the thruster cathodes. Life tests of the barium impregnated porous tungsten inserts have to be performed to determine the optimum operating conditions. Limited testing has shown that the cathode with a barium impregnated tip has excellent operating characteristics. Life tests of this cathode are needed to determine both the thermal and sputter decay rates.

Testing of plasma and flame sprayed heaters indicated that the flame sprayed heaters appear to have a slight advantage at high temperature. Accelerated degradation tests showed that thermal cycling of the heaters was more damaging than steady operation.

*Thruster tests indicate that local hot spots apparently occur causing nickel inserts to melt. For this reason nickel inserts have been rejected.

APPENDIX B
POWER PROCESSOR TEST CONSOLE DESCRIPTION

The Power Processor Three Bay Test Console used for much of the thruster testing under this program is shown in Fig. 76. This console was also used for the sequencer development discussed later. The major elements of the test console include: (1) power processing, (2) a control system, (3) a sequencer, and (4) instrumentation. These elements are the subject of this appendix.

1. Power Processing Unit (PPU)

The 30-cm ion thruster requires 12 sources of regulated voltage and current to achieve and maintain an operational run state. The power processing circuitry contained in the test console for powering thrusters during development and evaluation testing was implemented with flight-type circuit designs and contains 11 supplies.* Each supply is remotely programmable on either voltage or current over its full output power range with a 0 to 5 Vdc input signal. In addition each provides 0 to 5 Vdc telemetry signals at system common which are proportional to the supply output voltage and current.

The high frequency transistorized power processing system operates from a nominal 250 Vdc power bus and functionally follows the modularized concept used in earlier flight prototype ion thruster power conditioners developed by Hughes. Table 36 lists the major design features of the supplies in the power processing unit.

2. Control System

The thruster control system may best be described by listing the tasks it is required to perform:

- Open loop manual control of each supply

---

* Although the present 30-cm thruster requires a magnetic baffle supply, the test consoles did not include this supply.

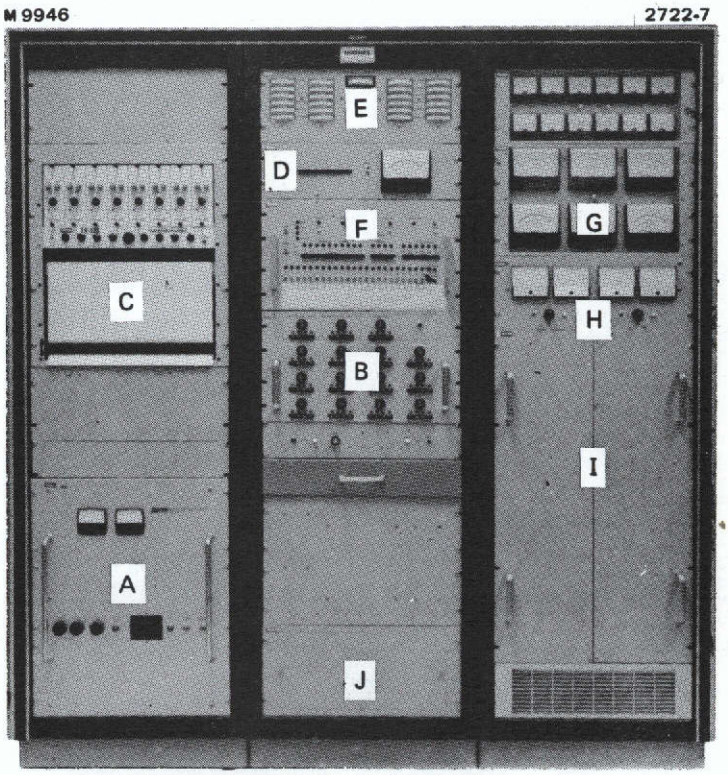

A. BUS POWER SUPPLY (+250 NOMINAL)
B. CONTROLLER
C. 8-CHANNEL STRIP CHART RECORDER
D. TRUE RMS DATA ACQUISITION AND METERING
E. TELEMETRY V&I METER PANEL
F. SEQUENCER
G. DIRECT READING OUTPUT V&I METER PANEL
H. AUXILARY ELECTRO-MAGNET POWER SUPPLIES
I. POWER PROCESSOR UNIT
J. PATCH PANEL AND SIGNAL CONDITIONING UNIT (COVER IN PLACE)

Fig. 76.
30-cm thruster three bay power processor test console.

TABLE 36

Power Supply Specifications

Supply	Maximum Rating Continuous Operation	Regulation Mode and Accuracy	Mechanization Technique
Screen	1500 Vdc @ 3 A	V, ± 1%	8-staggered phased pulsewidth modulated 10 kHz inverters with series connected dc outputs to achieve full power
Accelerator	-2000 Vdc @ 0.2A	V, ± 2%	In line switching regulator to establish input voltage to 10 kHz square wave output inverter
Discharge	50 Vdc @ 20 A	I, ± 2% plus V limiting	3-pulsewidth modulated 10 kHz inverters with series connected AC outputs feeding final output rectification and filtering
Main Vaporizer Cathode Vaproizer Cathode Heater Isolator Heater Neutralizer Vaporizer Neutralizer Heater	20 Vac @ 7 A	I, ± 3%	Magnetic amplifier pulsewidth modulated power control on primary of output transformer. All supply modules driven by single 5 kHz inverter
Cathode Keeper Neutralizer Keeper	60 Vdc @ 1 A 60 Vdc @ 2.5 A	I, ± 2%	

T1458

- Closed loop control of selected supplies based upon voltage and current telemetry derived from the PPU
- Automatic high voltage overload detection and recycle circuitry, as well as additional automatic corrective response capabilities
- Automatic thruster startup and shutdown capability
- Sufficient control capability to allow parametric studies to be carried out.

A simplified block diagram of the thruster control system is presented in Fig. 77. The interface between the control system and its load, (i.e., the PPU/thruster combination) is represented by the vertical dashed line at the right. With minor exceptions, all data traversing this interface do so in the form of 9 to 5 V analog signals. This highly standardized interface allows great flexibility in the choice of controller circuit configurations. It should be noted at this point that some control functions do reside on the load side of the interface. More properly termed regulator functions, these minor control loops reside within each supply to assure accurate and stable response to the analog reference signals arriving via the interface.

As may be seen by inspection of the block diagram, the test console control system is composed of two major components: (1) the controller, which generates the actual reference signals and provides a means for implementing open or closed loop control of the various PPU supplies as well as providing the manual control potentiometers, and a capability to automatically respond to thruster high voltage overloads, and (2) the sequencer, which provides an automatic startup and shutdown capability while at the same time expending the system's automatic response capability. In addition the figure shows the incorporation of a digital computer, which along with its interface, provides an optional configuration for computer control of the system and for data logging and reduction.

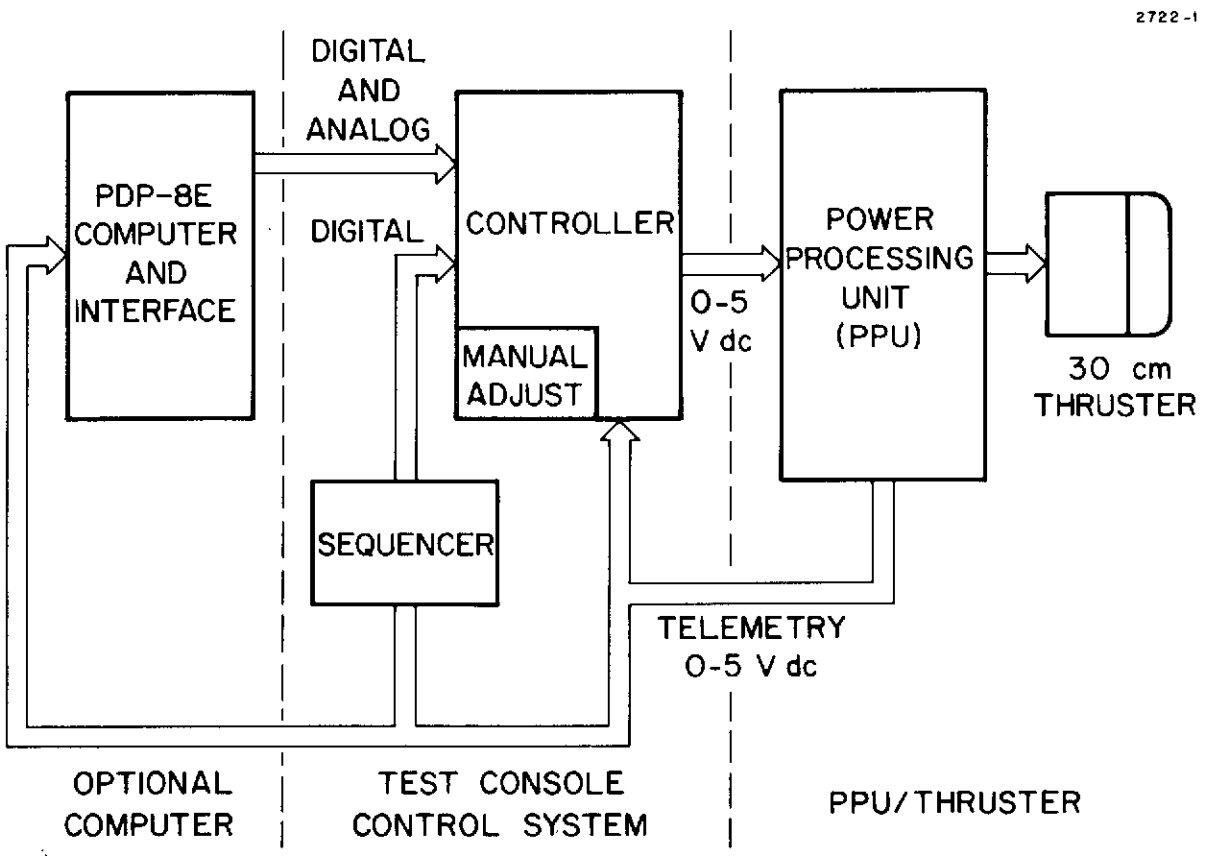

Fig. 77. Thruster control system block diagram.

3. Controller

The controller is the heart of the thruster control system. It is in this unit that the PPU input forcing functions are generated in response to the manual commands of an operator, or under the control of the sequencer or digital computer. The controller is designed to stand alone and to be fully operational in the absence of any direction from either the sequencer or the computer. In this mode the controller performs the following functions:

- Open loop, manual control of the PPU on an individual supply basis
- Closed loop control of the neutralizer, discharge voltage and beam current via the neutralizer vaporizer, cathode vaporizer and main vaporizer supplies respectively
- Automatic high voltage overload detection of the screen and accelerator supplies as well as automatic cutback and recycling of these and other supplies in the event of such an overload, and
- Standardized sequencer and computer interface capability

A simplified block diagram of the controller is presented in Figs. 78 and 79. Special attention is directed to the buffer amplifier schematic since it is in this area that the flexibility and ease of interface which characterize the controller design are most apparent. Each buffer amplifier is provided with a fixed gain integrated operational amplifier which generates the actual output, proceeded by an eight-channel analog multiplexer. Of the eight inputs thus made available to each amplifier, three are connected to 10-turn trim potentiometers for scaling automatic startup, shutdown and overload recycling setpoint levels, one is connected to the front panel manual control associated with the amplifier, one is provided for use with a loop amplifier if the buffer amplifier participates in a closed loop, one is available for controlling on analog reference signals from the

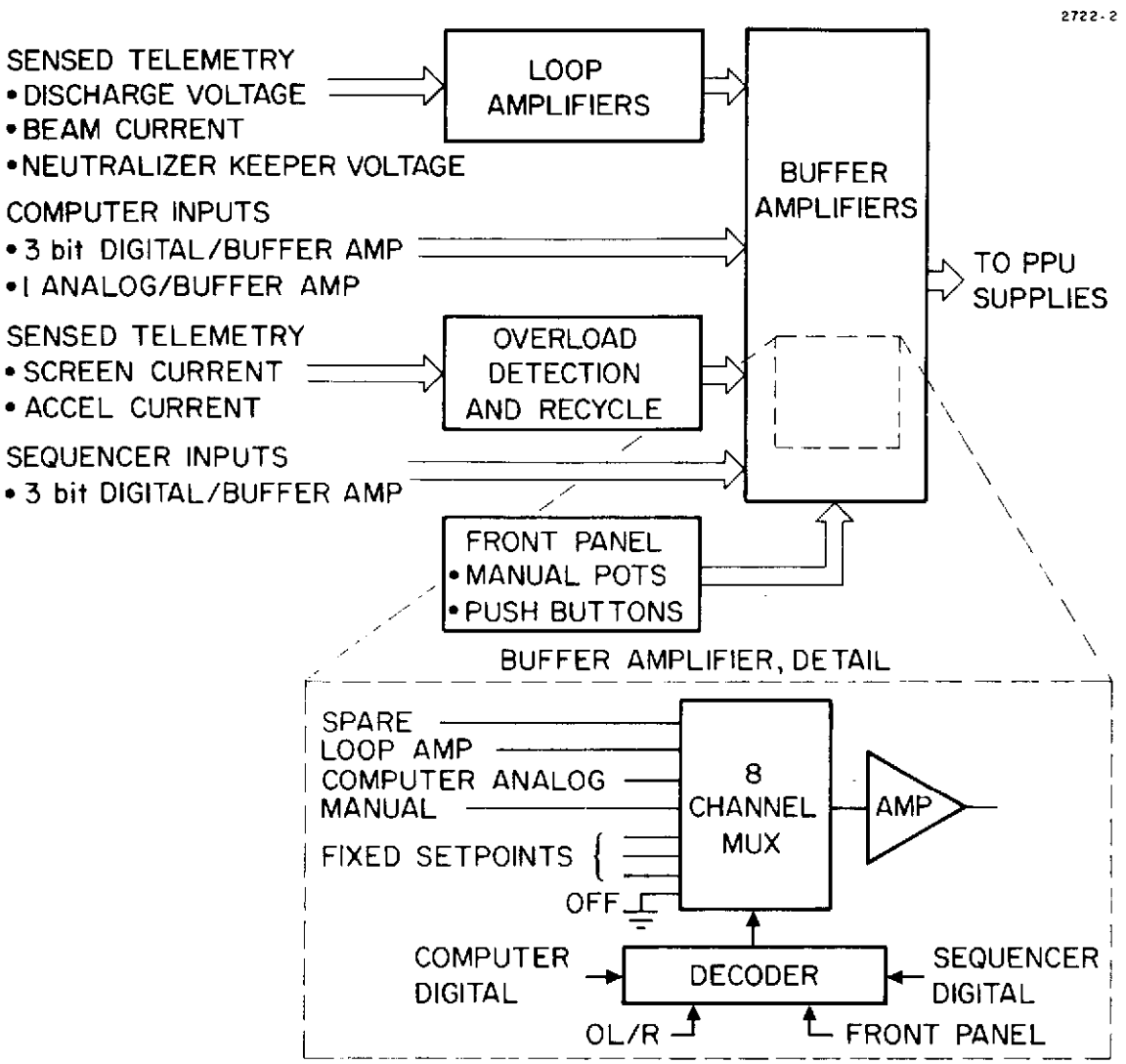

Fig. 78. Control system controller block diagram.

computer, one is tied to system common to act as the off signal reference, and the last is a spare for future expansion. Selection of the input to be routed to each supply in the PPU is accomplished by means of a three-bit code supplied to the MUX from a decoder.

Overload detection and recycling is implemented as a hard wire substantive which overrides the normally selected channel address codes to various MUX amplifiers in response to certain sensed HV overload conditioners to provide a sequential recycle operation involving a number of supplies. A time history of the recycle event is shown in Fig. 80.

In the absense of a signal from the overload circuitry the decoder output is controlled by a set of front panel push buttons (shown in Fig. 79) in the following manner.

OFF: Select the input tied to system common

MAN: Select the front panel manual control

SEQ: Select the input determined by the three bit code presented by the sequencer.

CPU: Select the input determined by the three bit code presented by the computer.

Thus, the interface with the computer or sequencer is accomplished by means of three digital bits which specify the input to the buffer amplifier and allow for a variety of control modes to be implemented at each PPU supply. The set of three bits for each of the eleven controller buffer amplifiers represents a 33-bit digital "state word" which is the major means of interface between either the sequencer or the computer and the controller.

4. Sequencer

Although the controller described in the previous section provides the necessary capability to operate the thruster during steady-state conditions, it lacks the ability to automatically direct the startup and shutdown of the ion engine. The startup procedure selected for

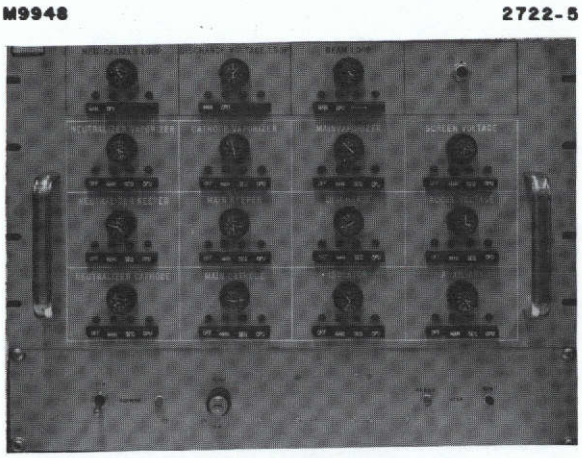

Fig. 79.
Controller front panel
layout.

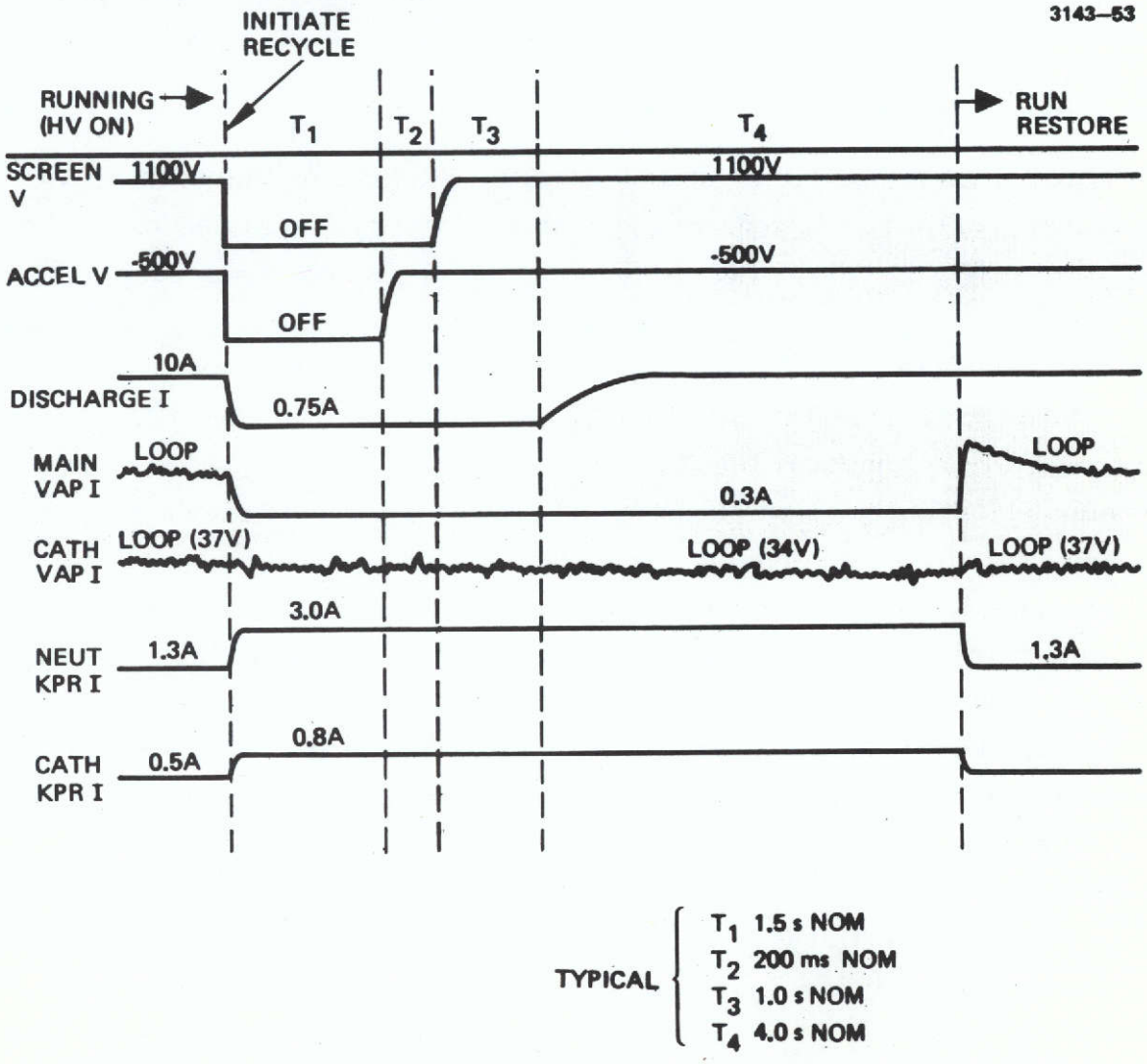

Fig. 80. Thruster/PPU high voltage recycle sequence.

implementing the sequencer is a five segment command sequence which brings the thruster in stages from a cold start to a fully operational state. The shutdown selected is accomplished in only two steps and is intended to maintain uniform temperature distribution throughout the engine structure during cooling.

Although each sequence (startup or shutdown) is initiated only by means of an external command, the decision to advance from one stage to the next within a given sequence is based upon time and telemetry information. For example, a preheat segment of the startup procedure is terminated after the passage of a predetermined period of time; a segment intended to cause ignition of the neutralizer keeper would end once neutralizer keeper current of a given magnitude was sensed.

An automatic sequencer was designed and fabricated in order to provide the control system with these startup and shutdown capabilities as well as to expand the system's ability to automatically and systematically respond to various anomalous conditions occasionally encountered during thruster operation. This unit, which operates by manipulating the controller state word is depicted in block diagram form in Fig. 81 and its front panel layout is shown in Fig. 82.

The sequencer operates by choosing from among a selection of nine 24-bit digital commands contained in a read-only memory (ROM) and expanding the selected word into a 33-bit word suitable for presentation as the controller state word. The ROM also contains a tenth word position, or address, which allows an operator to enter a command word of his choosing by means of switches on the front panel. The ROM thus contains the startup and shutdown procedures as sets of digital command words. The assignment of these words as presently wired into the discrete component ROM is given in Table 37.

A sequential flow chart describing the detailed sequencer operation as presently configured is shown in Fig. 83. The drawing shows all conditions for state word transitions based on time, telemetry and

C-3

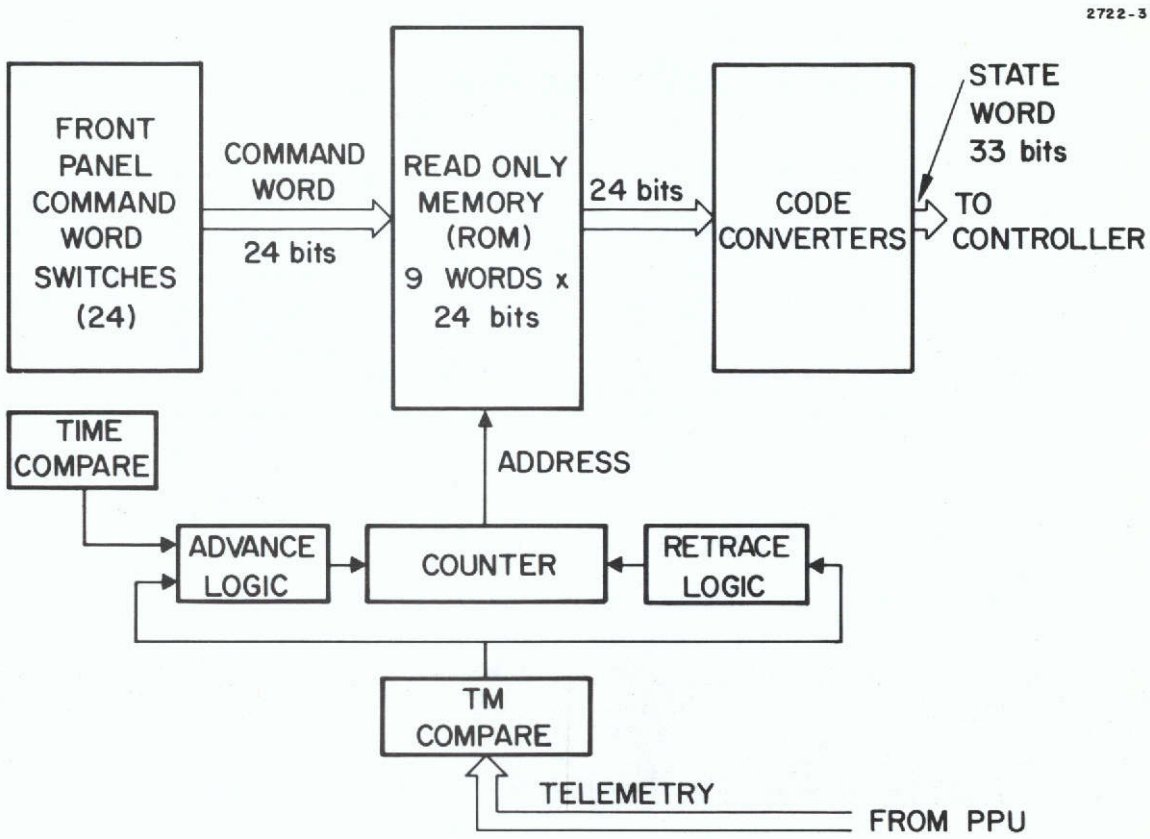

Fig. 81. Test console sequencer block diagram.

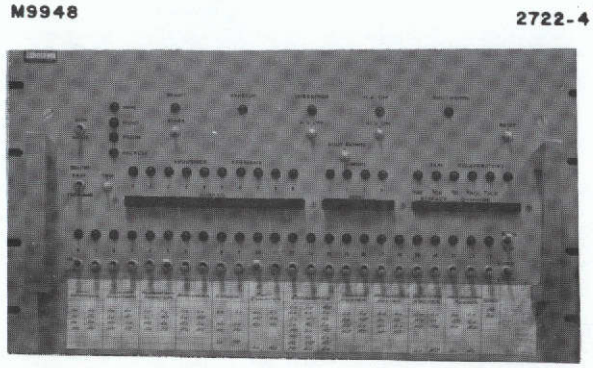

Fig. 82.
Sequencer front panel.

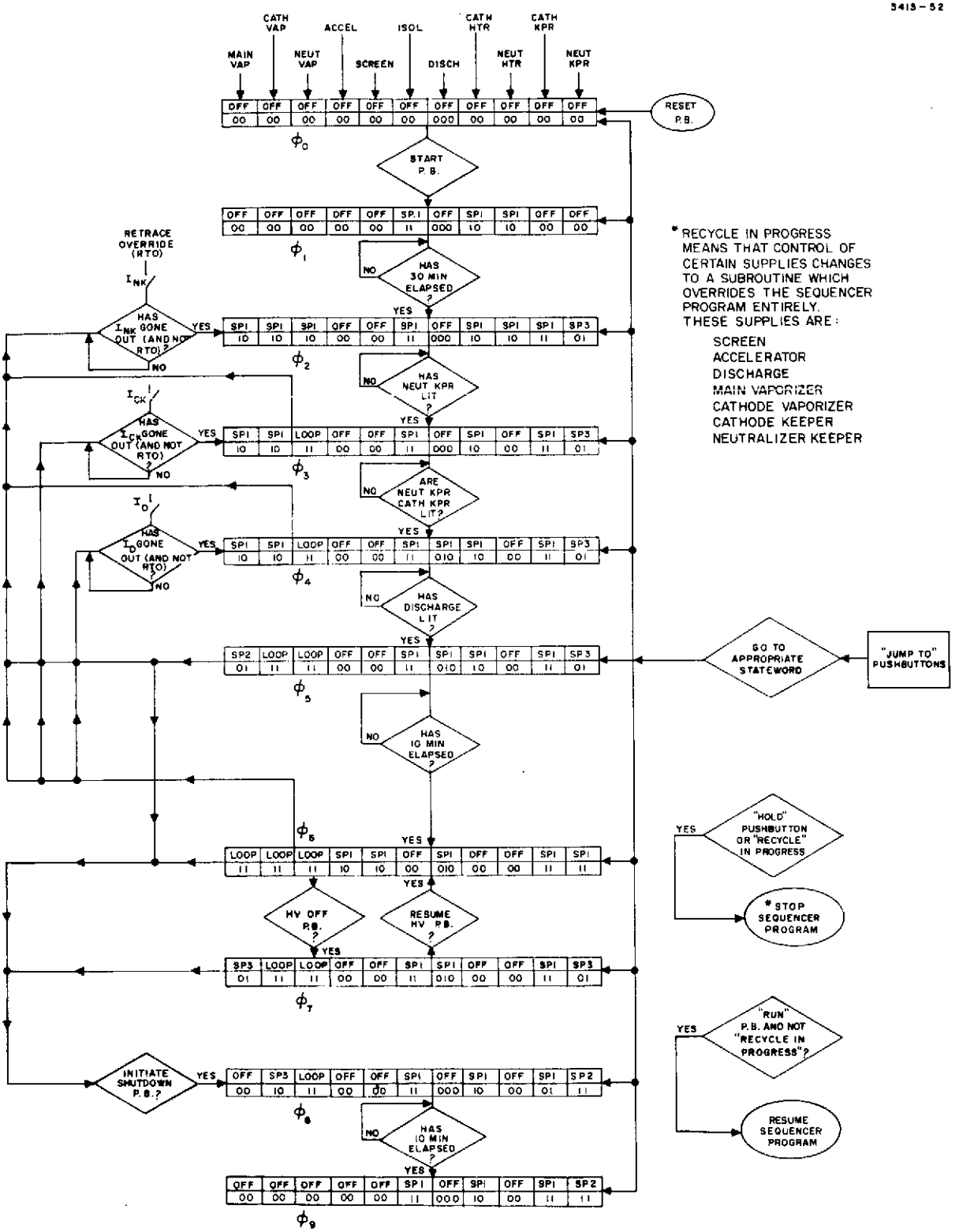

Fig. 83. Sequencer statework flow logic for three bay test console.

TABLE 37

ROM Word Assignments 30-Cm Thruster Sequencer

Address	Segment	Comments
0	Off	All supplies commanded off
1	Preheat	Activate vaporizers and heaters
2	Neutralizer Keeper	Ignite neutralizer keeper
3	Cathode Keeper	Ignite main cathode keeper
4	Discharge 1	Ignite discharge
5	Discharge 2	Hold until thermal equilibrium is established
6	Command Word	Transfer command word from front panel switches to sequencer outputs. This is the steady-state operating segment.
7	High Voltage Off	This special command allows the thruster to be maintained in a hold mode with the high voltages off.
8	Shutdown 1	First command of shutdown procedure.
9	Shutdown 2	Final command of shutdown procedure. Return to 0 at completion.

T1491

operator commands, along with the supply setpoints contained in the various statewords. Table 38 shows the actual current and voltage levels that have been assigned to the supply setpoints for typical 30-cm thruster operation. Fig. 84 shows a typical time history of a 30-cm startup sequence which results from the particular stateword-setpoint assignments and the sequencer startup program that has been implemented and has yielded good results in automatic laboratory thruster startup.

The sequencer is initially set at address 0 and in this state issues an "off" command to all buffer amplifiers which have the "SEQ" button activated (see controller front panel, Fig.82) and are thus under the control of the sequencer. The operator initiates the startup sequence by depressing a "start" button. This causes addresses 1 through 6 to be selected sequentially as the proper time and telemetry conditions are satisfied. This selection is performed by a status counter under the control of the advance logic.

Address 6, the command word, establishes the steady state operating condition of the thruster. Once selected, this address is maintained until the operator takes the proper action to initiate the shutdown procedure (address 8) or simply shut off the high voltages (address 7). Also, while in segment 6, the operator has direct control over each of the controller buffer amplifiers via the 24-command word switches.

As noted earlier in this section, progression through the startup sequence depends in part upon the presence of valid telemetry indications from the two keepers and the discharge supplies. This design principle has been extended so as to allow the sequencer to repeat a portion of the startup when previously established telemetry levels fall below a preassigned reference level. For example, if after the neutralizer keeper has been ignited it should for some reason be extinguished, the sequencer will return to address 2, wait until the keeper is relit, and proceed from that point. This retrace capability is provided for each telemetry channel and may be defeated by means

TABLE 38

Setpoint Chart

	Off	SP1	SP2	SP3
Main Vaporizer	0A	1.0A	0.8A	0.3A
Cathode Vaporizer	0A	1.5A	-	-
Neutralizer Vaporizer	0A	1.5A	-	-
Accelerator	0V	-500V		
Screen	0V	1100V	-	-
Main Isolator	0A	1.9A	-	-
Cathode Isolator	← outboard variable supply →			
Discharge	0A	10A	0.75A	-
Cathode Heater	0A	4.4A	-	-
Neutralizer Heater	0A	5.0A	-	-
Cathode Keeper	0A	0.5A	0.8A	-
Neutralizer Keeper	0A	1.3A	-	3.0A
Magnetic Baffle	← outboard variable supply →			

T1352

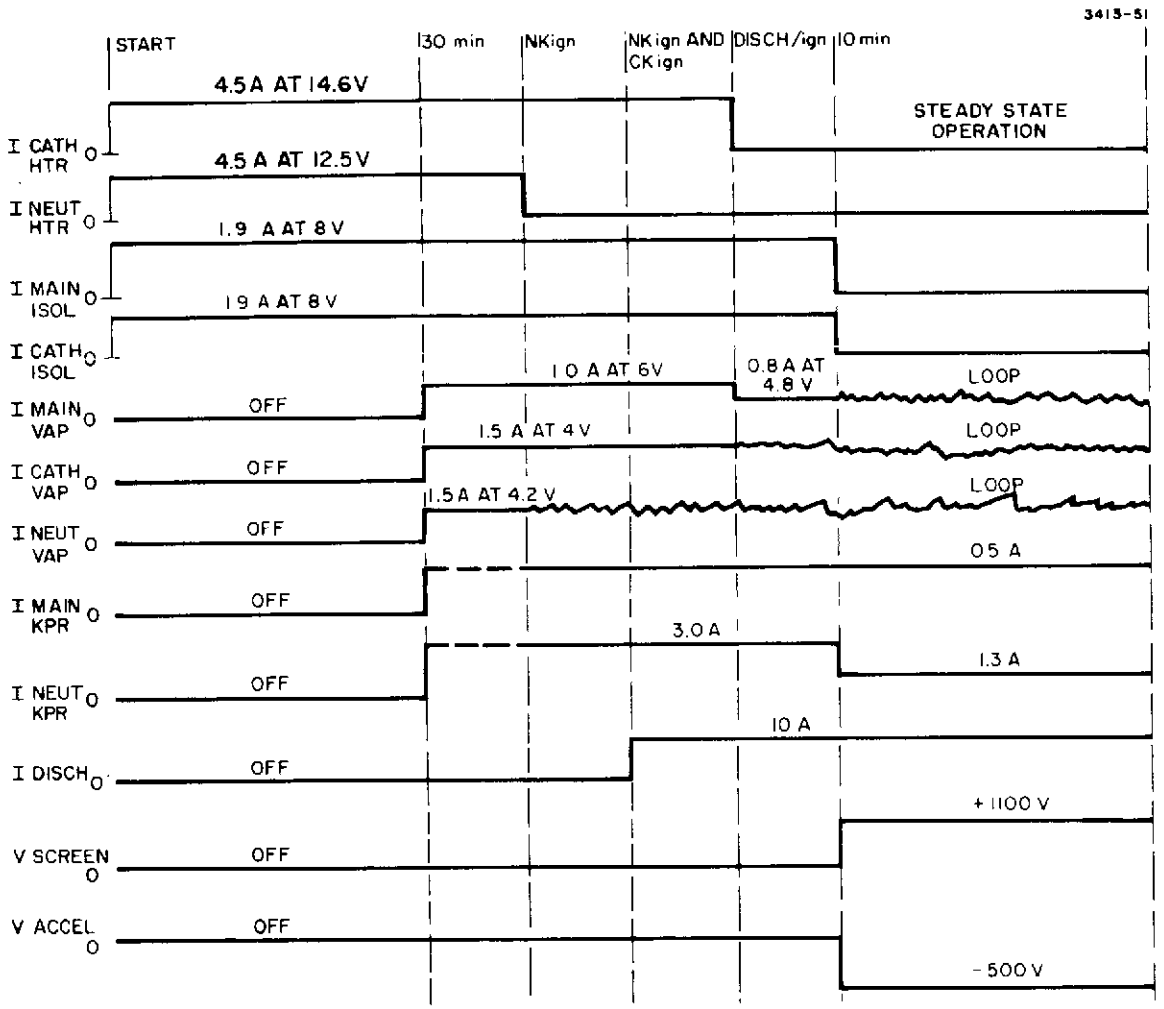

Fig. 84. Typical thruster startup sequence.

of individual override buttons on the front panel. The automatic response capability or recovery to the commanded run state is accomplished by the retrace logic.

Figure 85 is a functional logic diagram showing all of the essential elements in the sequencer together with the external inputs from and outputs to the remainder of the PPU, and the front panel sequencer controls with enough detail that all of its operations can be understood. The 1 out of 10 ROM address is determined by the 4-bit decade counter on the right side of the drawing which is driven by the "Advance Logic" sequence advance or count up 1) and by the "Force Logic" (parallel load or jump to sequence). The operation of the advance and force logic is described by Boolean functions of the present stateword and of all the input variables which include (1) outputs of the telemetry comparators for I_D, I_{CK}, and I_{NK}, (2) outputs from an internal timer, (3) outputs from front panel controls, and (4) output from the "Recycle in Progress" command generated in the controller.

The sequential operation can be better understood by also referring to Figs. 82 and 83. The internal timer has four gated outputs with individual reset lines which can be rewired at a patch area to select four independent strobe signals at any integral number of elapsed minutes from 1 to 99. The timer is reset either from the front panel or when the "seq. advance" occurs. Finally, the "recycle in progress" places the entire sequence in a stall condition while overload recovery in the PPU is taking place.

5. Instrumentation

The instrumentation included as an integral part of the test console is varied and reasonably extensive. Instrumentation for monitoring the various dc output voltages and current of the power processor just prior to routing the power to the thruster is located in the right hand bay directly above the power processing unit. The voltages and currents of the discharge, accelerator and screen supplies are monitored with calibrated 5 in. ±1% mirrored scale meters. Other

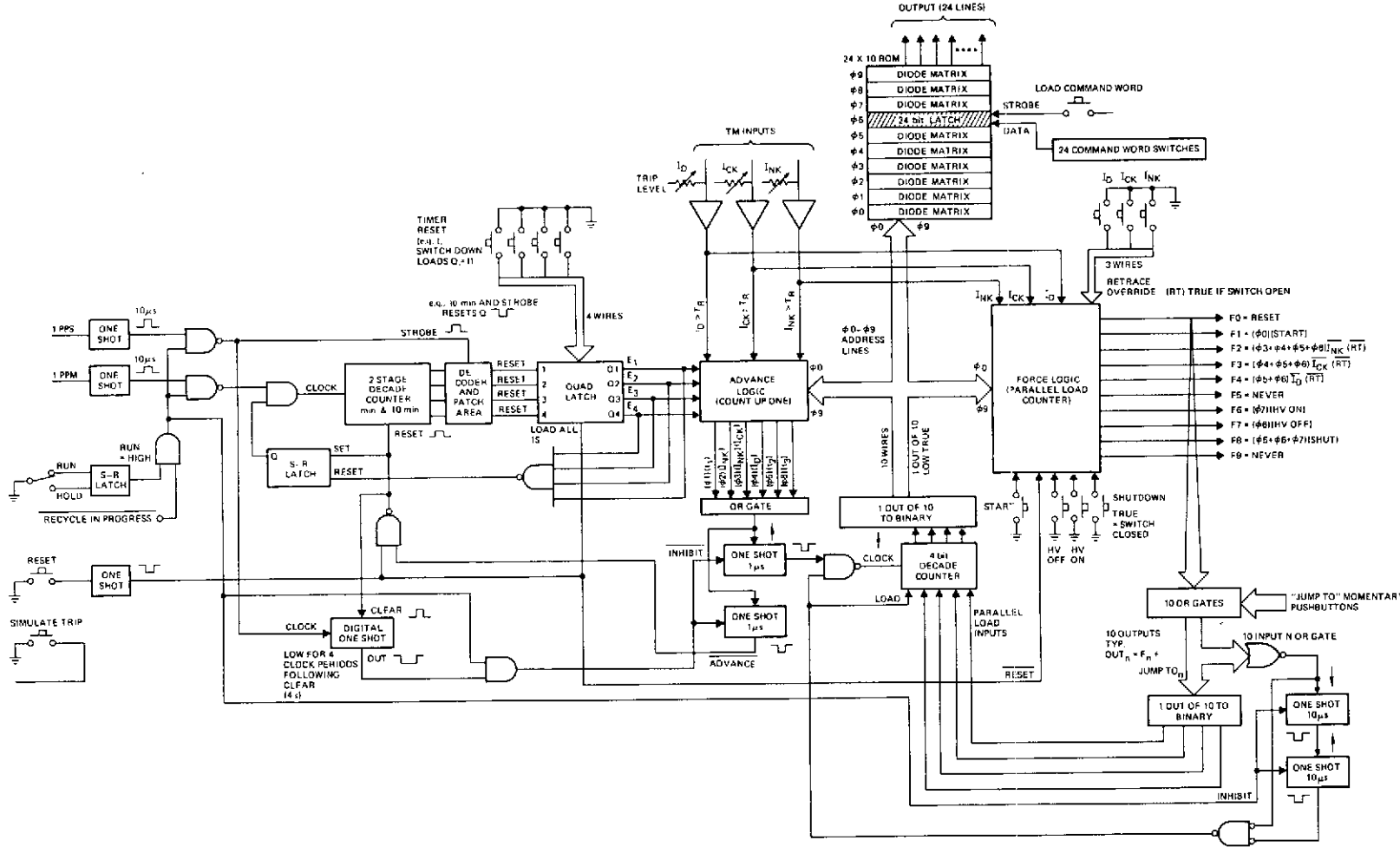

Fig. 85. Functional logic diagram for three bay test console.

dc parameters; cathode and neutralizer keeper voltages and currents, neutralizer coupling voltage, neutralizer emission current, and the current between the power processor common and facility ground are measured with 2 in. ±3% meters. All of the above metering is assembled into the form of a meter panel in which the meters are submounted because of the high voltages behind plexiglass for operator safety.

A 16-channel RMS data acquisition system is employed for monitoring the 5 kHz pulse width modulated square wave outputs of the six heater/vaporizer supplies. The data signal inputs to the RMS Data System are derived from isolated voltage and current instrumentation transformers located at the power output leads of the individual supply modules. The heater current or voltage to be monitored is selected by a multipole pushbutton switch on the front panel of the instrument, or by an external binary code 4-bit word. Each channel has an attenuator pad to scale the incoming ac signal for calibrating the RMS conversion. The output of the RMS converter is routed to a 5 in. ±1% mirrored scale meter for manual data collection by an operator. An additional buffered output is provided for remote readout when collecting data under computer control.

The instrumentation thus far described provides the console operator with high accuracy information required for thruster evaluation. In addition to this direct reading instrumentation 25 meters are clustered on a single panel to monitor the 0 to 5 Vdc voltage and current telemetry signal of the individual flight-type power supplies contained in the power processing unit. This metering provides at a glance an indication of the overall system status.

Located at the bottom of the center bay is a patch panel and a signal conditioning unit that provides a centralized location for terminating and conditioning the telemetry signals prior to distribution to other subsystems in the console or to external monitoring by a computer. The signal conditioning consists of a scaling and buffering amplifier with filtering to eliminate power processor generated noise that may be

present on the telemetry lines. A matrix of accessible terminal tie points for the input signals (before conditioning) and the output signals are provided for monitoring with an oscilloscope and to simplify the selection of signal outputs to be routed to the 8-channel strip chart recorder.

APPENDIX C
STRUCTURAL INTEGRITY TEST DESCRIPTION

Structural integrity (vibration) tests of the 30-cm thruster were performed in accordance with NASA LeRC test specifications. (The test conditions implemented will be discussed for each of the three shake tests as appropriate. Prior to each test, the proposed test procedure was approved by the NASA program manager.)

All shake tests were performed by Approved Engineering Test Laboratories (AETL) with Hughes personnel in attendance to assure conformance with test procedures. Details of the test equipment used are provided in the AETL test reports.

Three types of tests were performed during each shake test: sinusoidal (low and high level), half sine shock, and random vibration. The basic test setups for these three tests are shown schematically in Figs. 86 to 88, respectively. The acceleration spectrum for each of these tests will be discussed for each of the thrusters tested.

1. Vibration Test of Thruster S/N 601

Thruster S/N 601 was vibration tested in January 1973 under sine and half sine shock conditions. Random vibration tests could not be conducted due to the response characteristics of the thruster test fixture.

An initial calibration of the vibration system (without the thruster) was performed. Eight accelerometers were calibrated using an oscillograph. The servo acceleration levels were determined by means of an automatic peak signal selector, which selected the highest signal of the four control accelerometer signals at a given time. This signal controlled the vibration input. The thruster was then installed in the fixture and mounted on a vibration exciter as shown in Fig. 89. The system was subjected to a low level sinusoidal sweep in each of the three major orthogonal axes over the frequency range of 5 to 2000 Hz at an applied double amplitude of 0.127 cm up to a limiting value of 1.0 g peak. The thruster was then subjected to a high level search

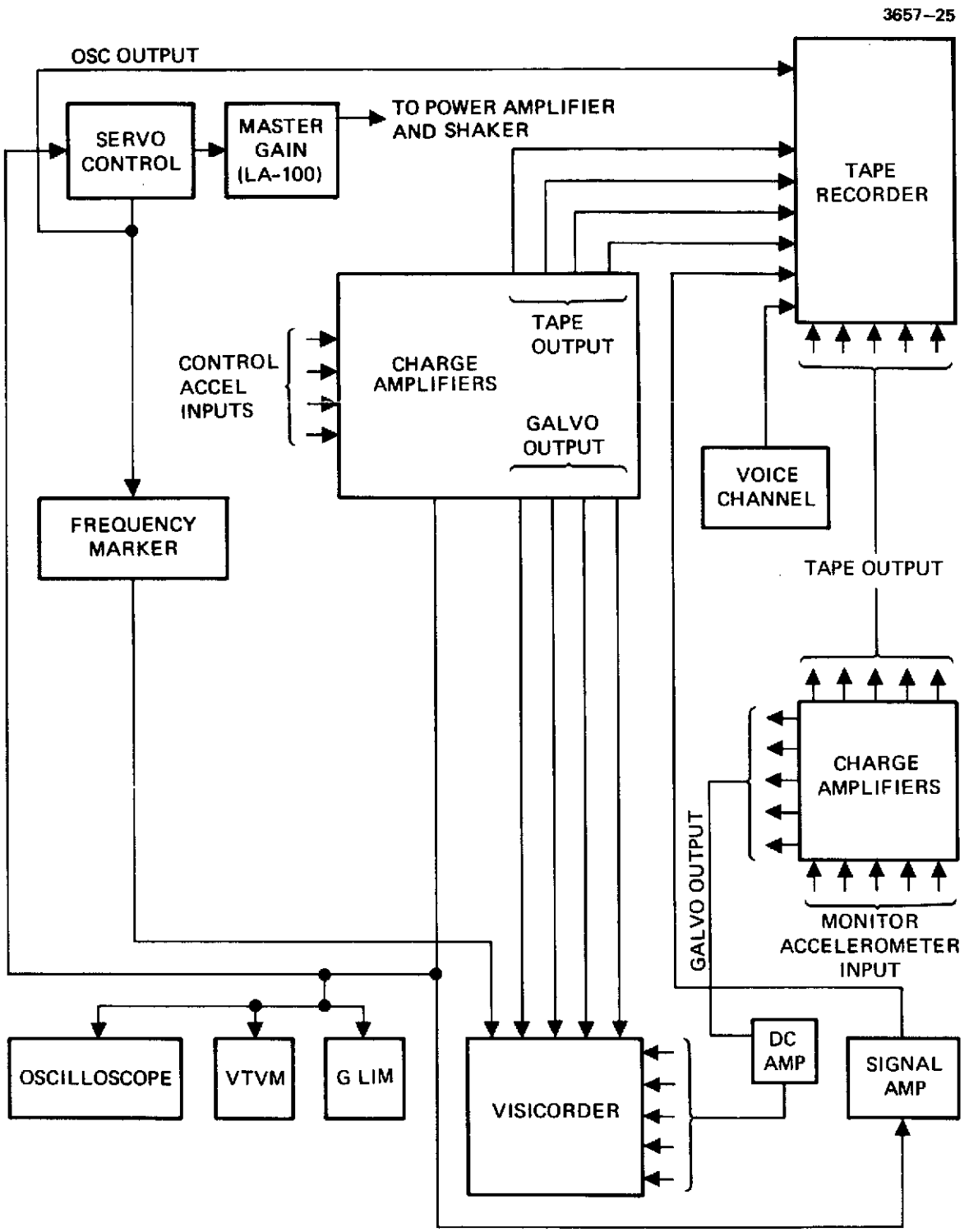

Fig. 86. Block diagram of a signal selected sine vibration system.

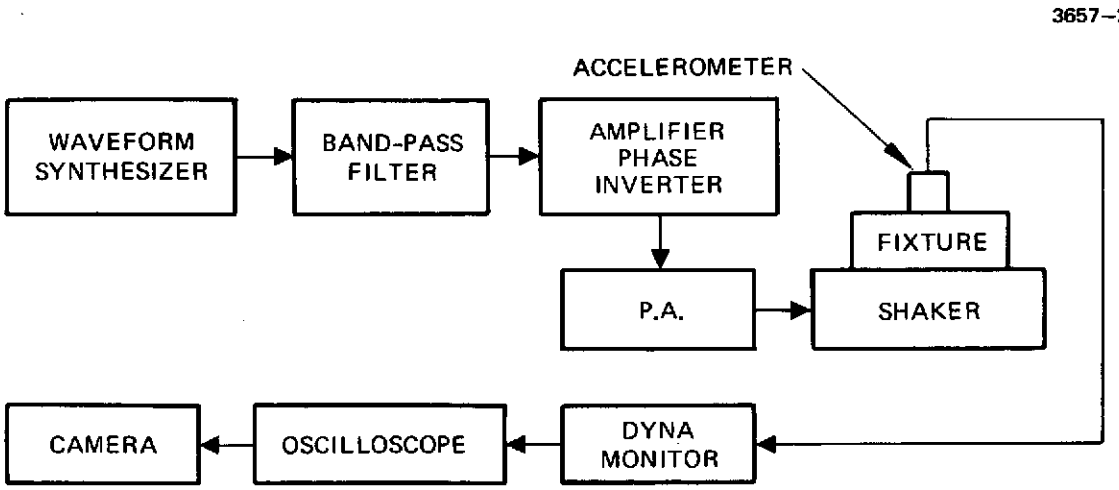

Fig. 87. Block diagram of half-sine shock test setup.

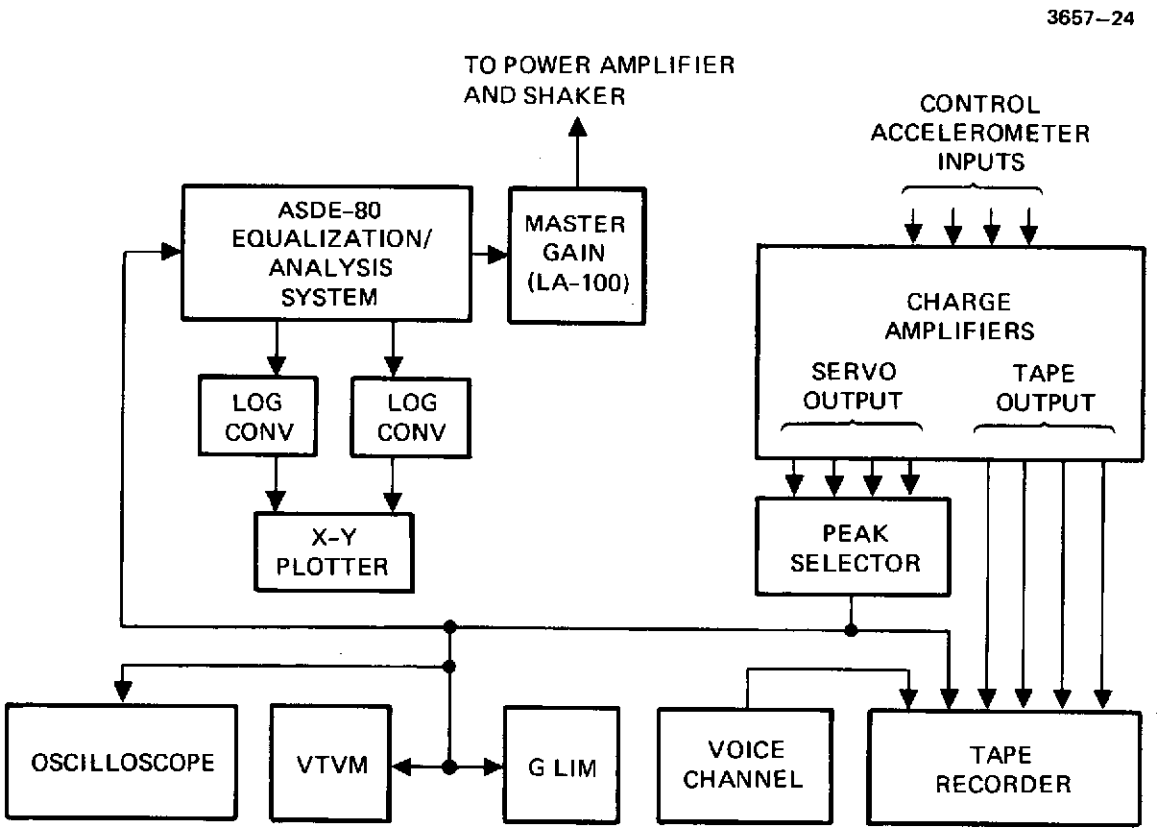

Fig. 88. Block diagram of broadband random vibration system.

3657-50

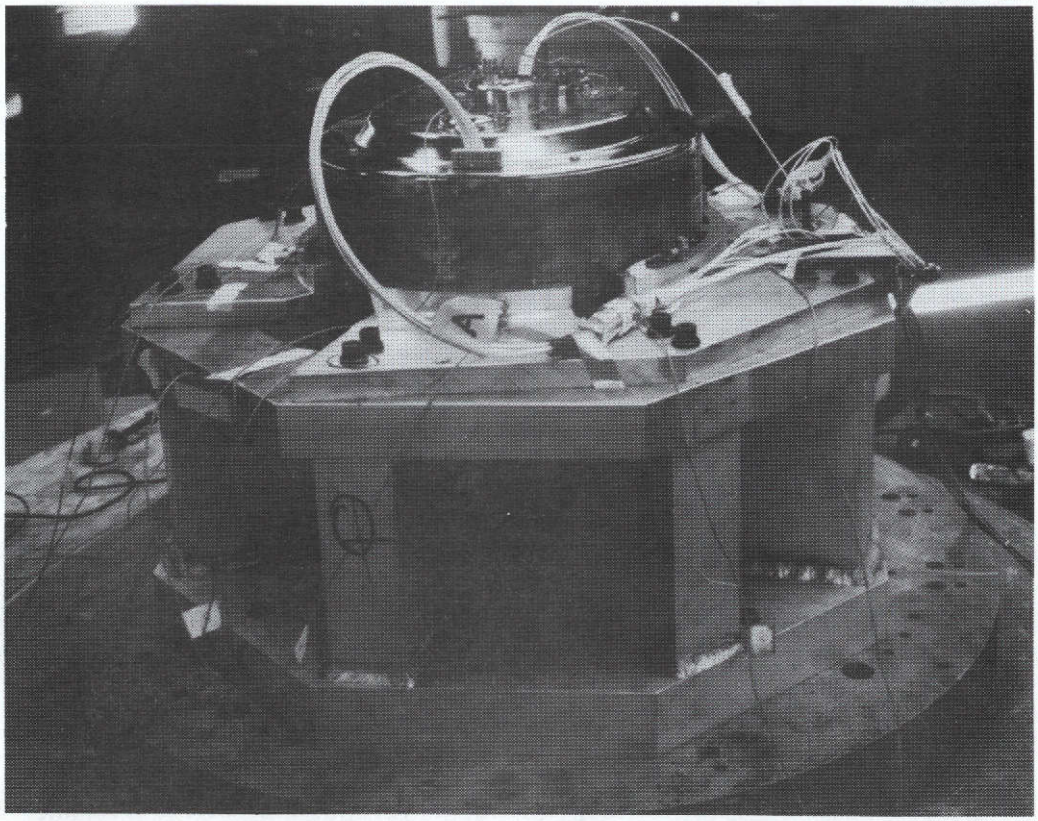

Fig. 89. Vibration test setup for thruster S/N 601.

over the frequency range of 5 to 2000 Hz at an applied double amplitude of 1.27 cm up to a limiting value of 9.0 g peak. During the sinusoidal sweeps, the outputs of all control response accelerometers were recorded on a visicorder.

The locations of accelerometers on the thruster are shown in Fig. 90. Resonance conditions, determined from real time visicorder charts, are shown in Table 39. Lowest resonance frequencies (70 Hz) were associated with the neutralizer. Visual examination at the completion of the 1.0 and 9.0 g sinusoidal sweeps revealed no apparent physical damage, deterioration, or other adverse effects. The thruster was not disassembled for inspection.

An effort was then made to equalize the thruster test fixture for random vibration over the frequency range of 20 to 2000 Hz at the following intensities:

Frequency, Hz	Intensity
20 - 400	0.11 g^2/Hz
400 - 2000	0.22 g^2/Hz
Overall Acceleration:	19.8 g

However, thruster test fixture harmonics in the 1200 to 1500 Hz range forced the random vibration test sequence to be deleted.

The next test performed was a 30 g half sine shock series for each axis. The thruster was subjected to three synthesized shock pulses in each direction of the three major orthogonal axes. Each shock pulse had an amplitude of 30 ±3 g, a duration of 8.0 ms, and approximated a half sinusoid. Accelerometer locations are shown in Fig. 91, and responses are summarized in Table 40. No failures were observed at this point in the testing.

A series of elevated level sine tests was then initiated for the X-axis only. The thruster was subjected to sinusoidal vibration over the frequency range of 5 to 2000 Hz sequentially, at levels of 11.5, 14.0, 16.0 and 18.0 g's. Accelerometer locations and responses are shown in Fig. 92 and Table 41, respectively. Following the 18.0 g run, it was found that two adjacent thruster support insulator brackets had

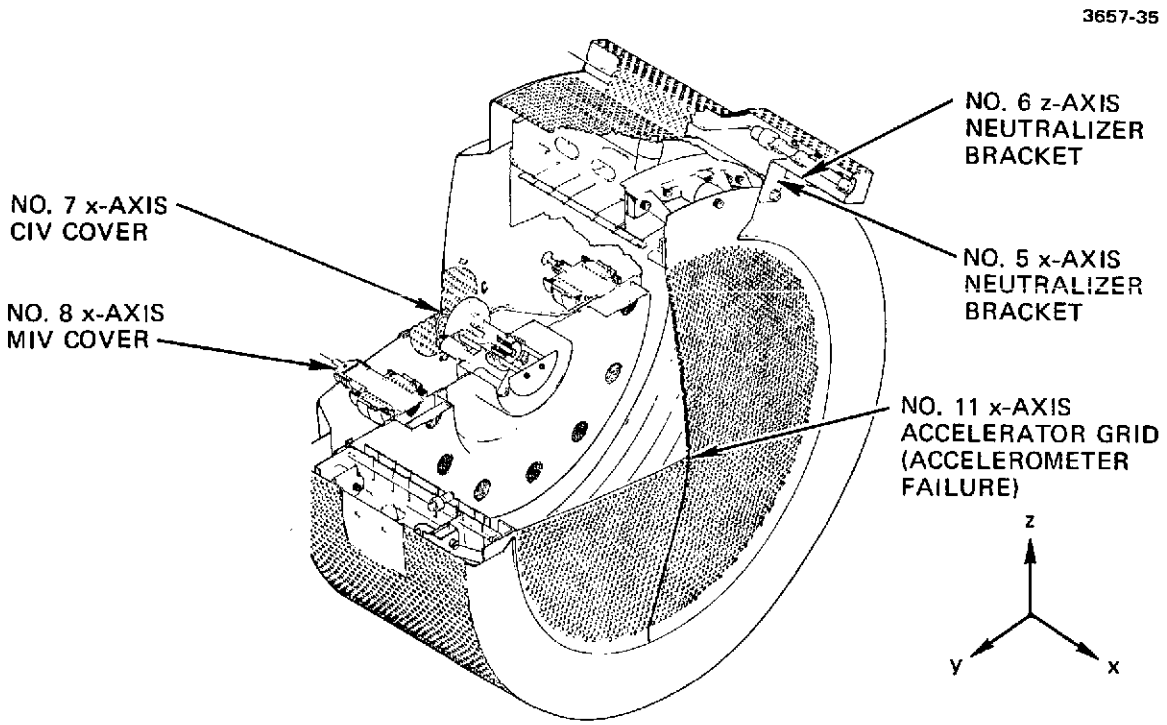

(a)

Fig. 90. Accelerometer locations for sine vibration test of thruster S/N 601.

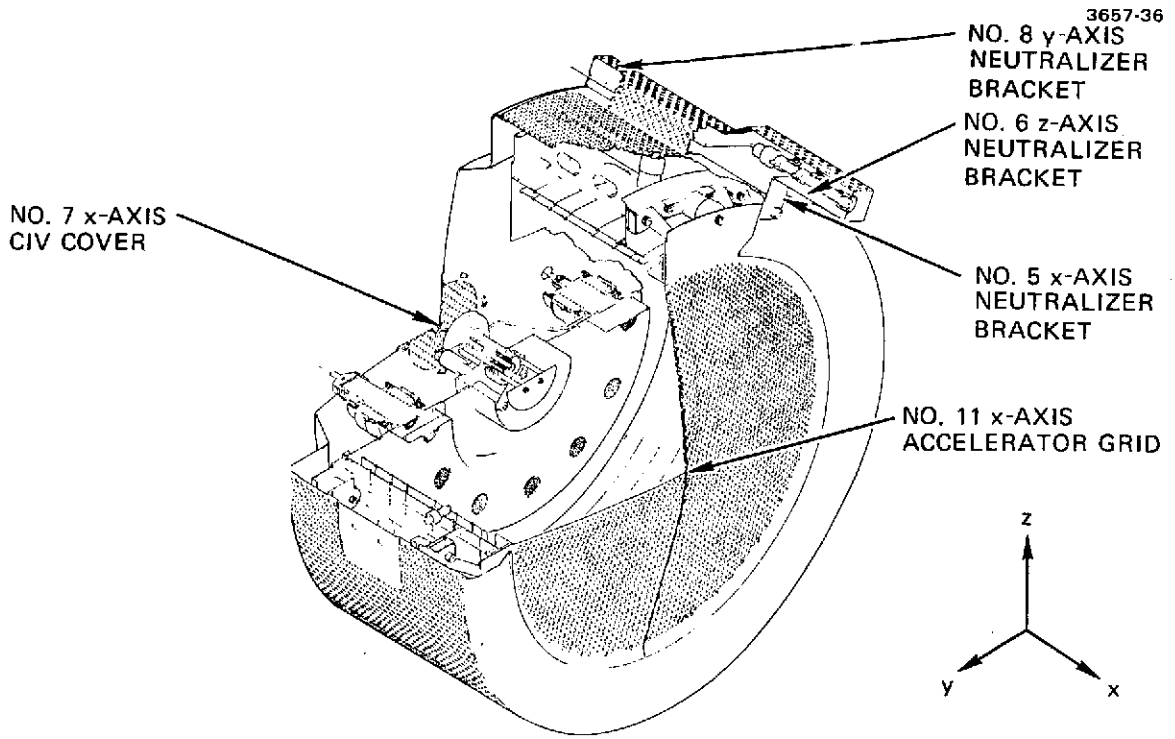

(b)

Fig. 90. Continued.

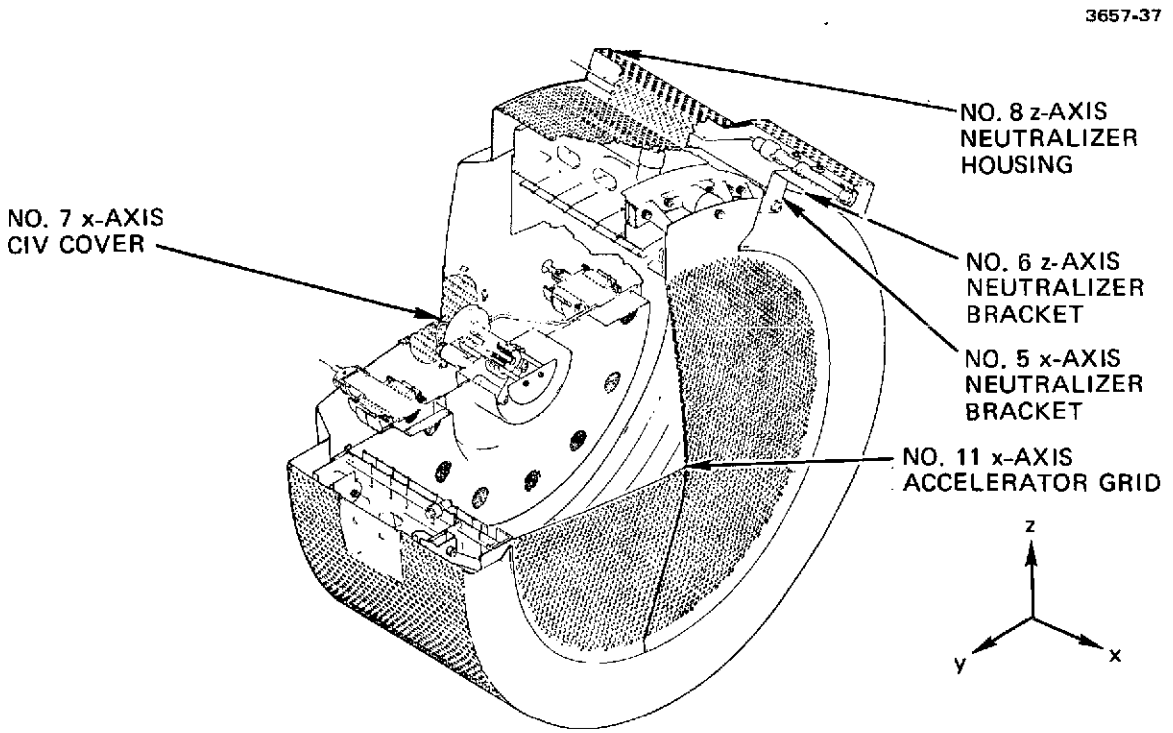

(c)

Fig. 90. Continued.

TABLE 39

Thruster S/N 601

Accelerometer Location	No.	Response Direction	9 g Sine Resonance Conditions					
			X-Axis		Y-Axis		Z-Axis	
			Freq, Hz	Amplitude, g	Freq, Hz	Amplitude, g	Freq, Hz	Amplitude, g
Neutralizer			105	22	70	30	175	50
					125	30	550	60
Neutralizer	5	X			325	40	750	60
					500	47	1200	65
					1200	75	1300	55
Neutralizer	6	Z	105	16	70	33	175	55
					125	30	340	60
Neutralizer	6	Z			340	40	525	65
					700	50	1000	55
					1200	35	1200	50
			19	30	125	32	120	28
			105	110	190	25	360	30
CIV Cover	7	X	170	76	950	18		
			320	28				
			1530	30				
			19	28	70	20	180	28
MIV Cover (X)			105	110	400	20	570	40
Neutralizer	8	X	170	70	600	30	620	30
Bracket (Y&Z)			230	30	800	22	800	30
			1530	40	1000	20	1000	30
			1330	20	85	13	175	12
Fixture			1530	40	400	16	500	22
Cross-Talk	9	Z	1560	32	1000	14	600	20
			1800	14	1250	14	1000	18
					1500	16	1400	18
			1550	27	400	14	500	13
Fixture							900	13
Cross-Talk	10	Y	1800	16			1100	13
					60	45	110	55
			Accelerometer		77	50	140	70
Accelerator	11	X	Failed		125	60	170	50
					160	95	460	50
					470	20		

T1493

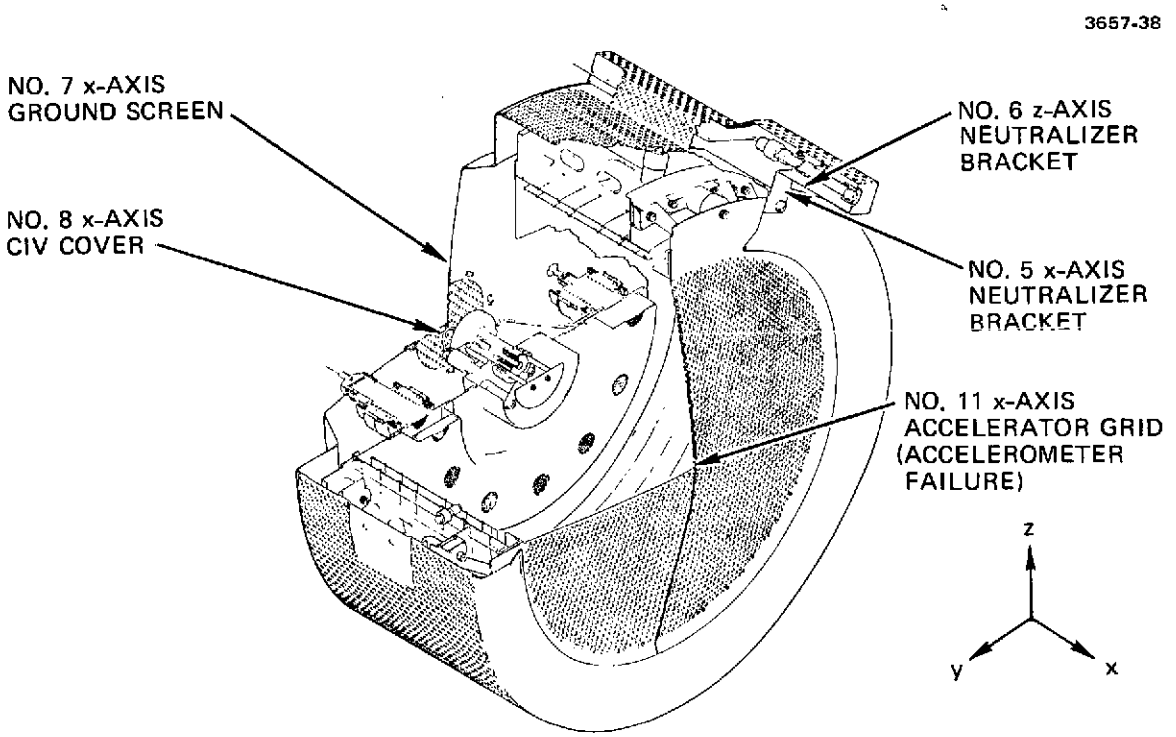

(a)

Fig. 91. Accelerometer locations for shock test of thruster S/N 601.

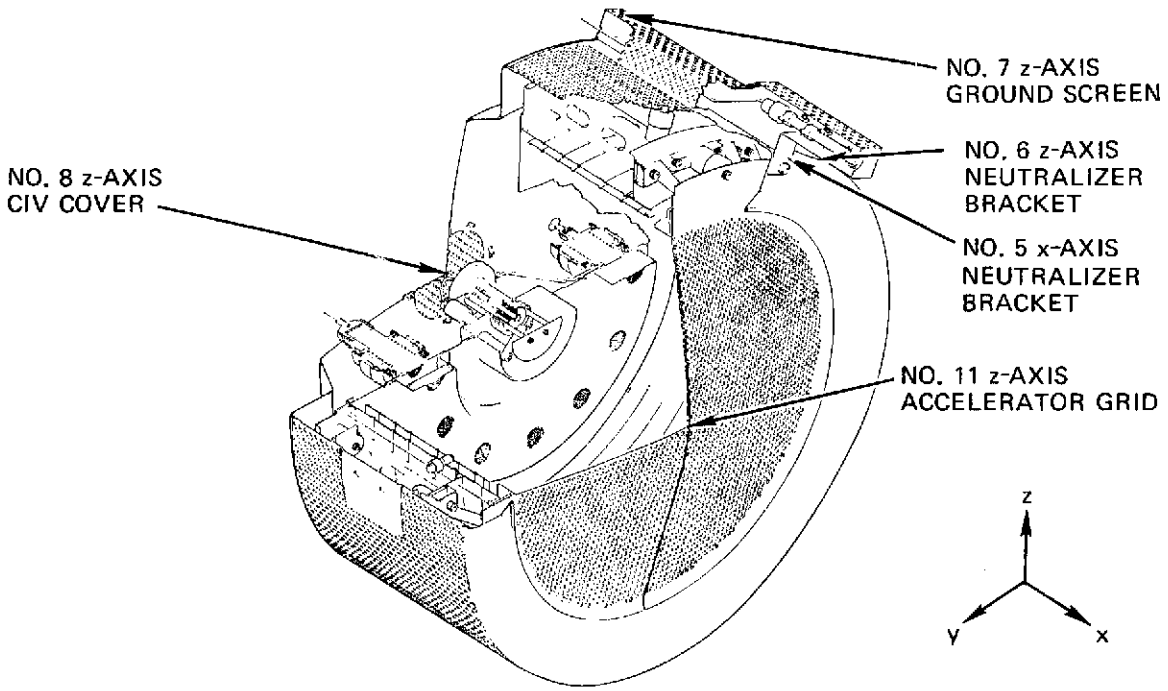

(b)

Fig. 91. Continued.

TABLE 40

Response Data for Shock Test of Thruster S/N 601

Response Data for Shock Test of Thruster S/N 601

Accelerometer Location	Accel-erom-eter No.	Direc-tion	Shock Pulse Direction					
			+X	-X	+Z	-Z	+Y	-Y
Neutralizer	5	X	20	25	10	10	11	10
Neutralizer	6	Z	4	5	30	30	15	10
Ground Screen	7	X	78	80	-	-	-	-
		Z	-		30	30	12	12
CIV Cover	8	X	78	75	-	-	-	-
		Z	-	-	30	30	12	25
Fixture X Talk	9	Z	10	10	-	-	-	-
		X	-	-	15	15	5	5
Fixture X Talk	10	Y	2	1	8	5	-	-
		Z	-	-	-	-	6	8
Accelerator	11	X	30	45	-	-	-	-
		Z	-	-	42	46	22	10

T1530

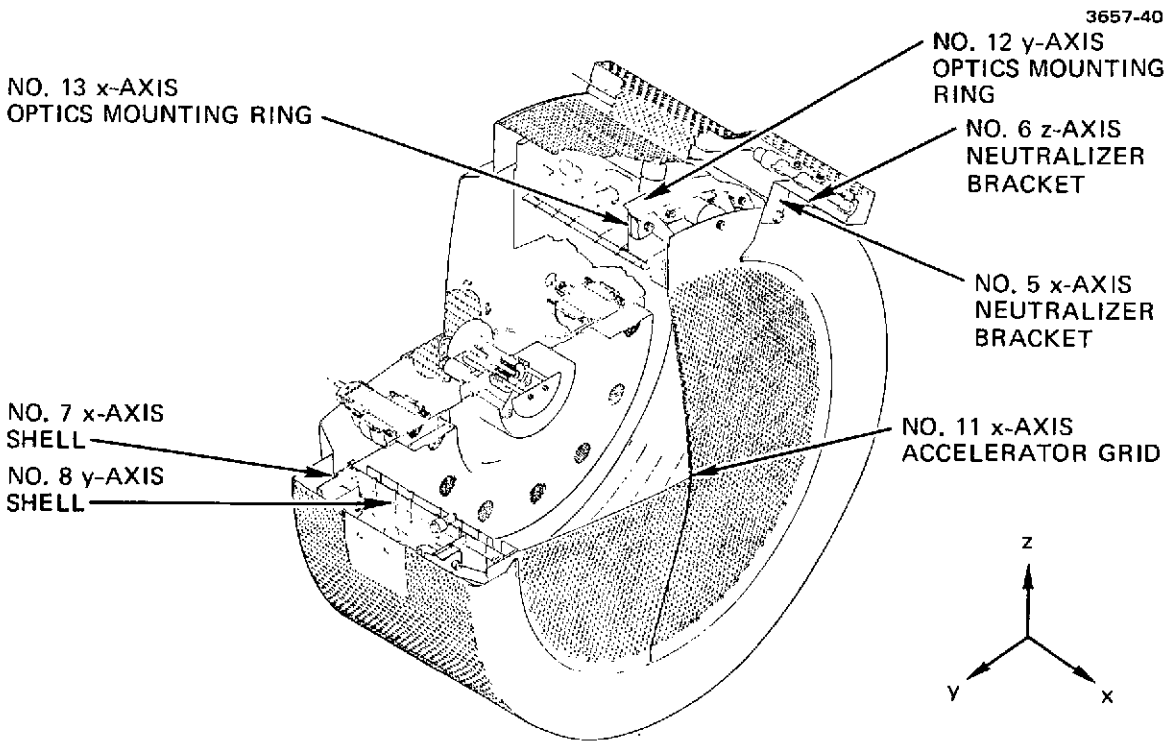

Fig. 92. Accelerometer locations for elevated sine vibration test of thruster S/N 401.

TABLE 41

Resonance Response to Elevated Sine Vibration for Thruster S/N 601

TABLE 41. RESONANCE RESPONSE TO ELEVATED SINE VIBRATION FOR THRUSTER

Accelerometer		Response Direction	Resonance Conditions					
			Acceleration = 14 g		Acceleration = 16 g		Acceleration = 18 g	
Location	No.		Frequency, Hz	Amplitude, g	Frequency, Hz	Amplitude, g	Frequency, Hz	Amplitude, g
Neutralizer	5	X	55 105 320 1250	120 30 120 120	55 320 1100	70 180 230	55 320	160 200
Neutralizer	6	Z	55 170 320 1250	90 80 85 75	55 175 320 1320	100 80 100 80	55 320	120 120
Shell	7	X	55 105	60 80	55 75 1320	90 50 20	55	140
Shell	8	Y	55 90 105 1100	50 50 30 20	55 75 1320	70 45 30	55	120
Optics Mounting Ring	12	Y	55 90	190 150	55 75	>200 80	55	>200
Optics Mounting Ring	13	X	55 105 1300	110 90 30	55	160	55	220
Accelerator	11	X	55 105 320 460 1450	160 80 50 50 105	55	400	55	>400

T1531

fractured. Failure of these brackets caused subsequent shear failure of the remaining four peripheral support insulators since the test was not terminated until the frequency sweep from 5 to 2000 Hz was completed. One of the fractured brackets is shown in Fig. 93, along with a spare bracket assembly for comparison.

In addition to the bracket failure, the five gussets which add support to the ground screen rear shield failed at the thinnest web. Excessive deflection of an "oil canning" mode occurred during all testing.

It is interesting to note that when the support insulators and brakets failed, nearly all the load was transmitted through the CIV and MIV alumina isolator sections with no damage occurring to either. These units were considered to be critical with respect to structural integrity and it was reassuring to note these units survived severe dynamic loading.

Subsequently, a new "600-Series" thruster design was developed. However, before this modified design could be implemented, the need for a two point gimbal interface was identified. Design work was then redirected to produce a 700-Series thruster.

B. Vibration Test of Thruster S/N 702

The development program and resultant design features of the 700-Series thrusters were discussed in Section II. Thruster S/N 701 was dedicated to endurance testing and S/N 702 was built to undergo vibration testing. The test program for S/N 702 was conducted in January 1974.

In light of the low frequency harmonics of the 600-Series vibration test fixture, a new fixture was built by AETL for the test of thruster S/N 702. This fixture with the thruster installed is shown in Fig. 94. The thruster is attached to the fixture only at the gimbal interface.

To verify the suitability of the new test fixture, a transmissibility test was performed using the random vibration frequency intensity spectrum described previously. Results of this test, reported

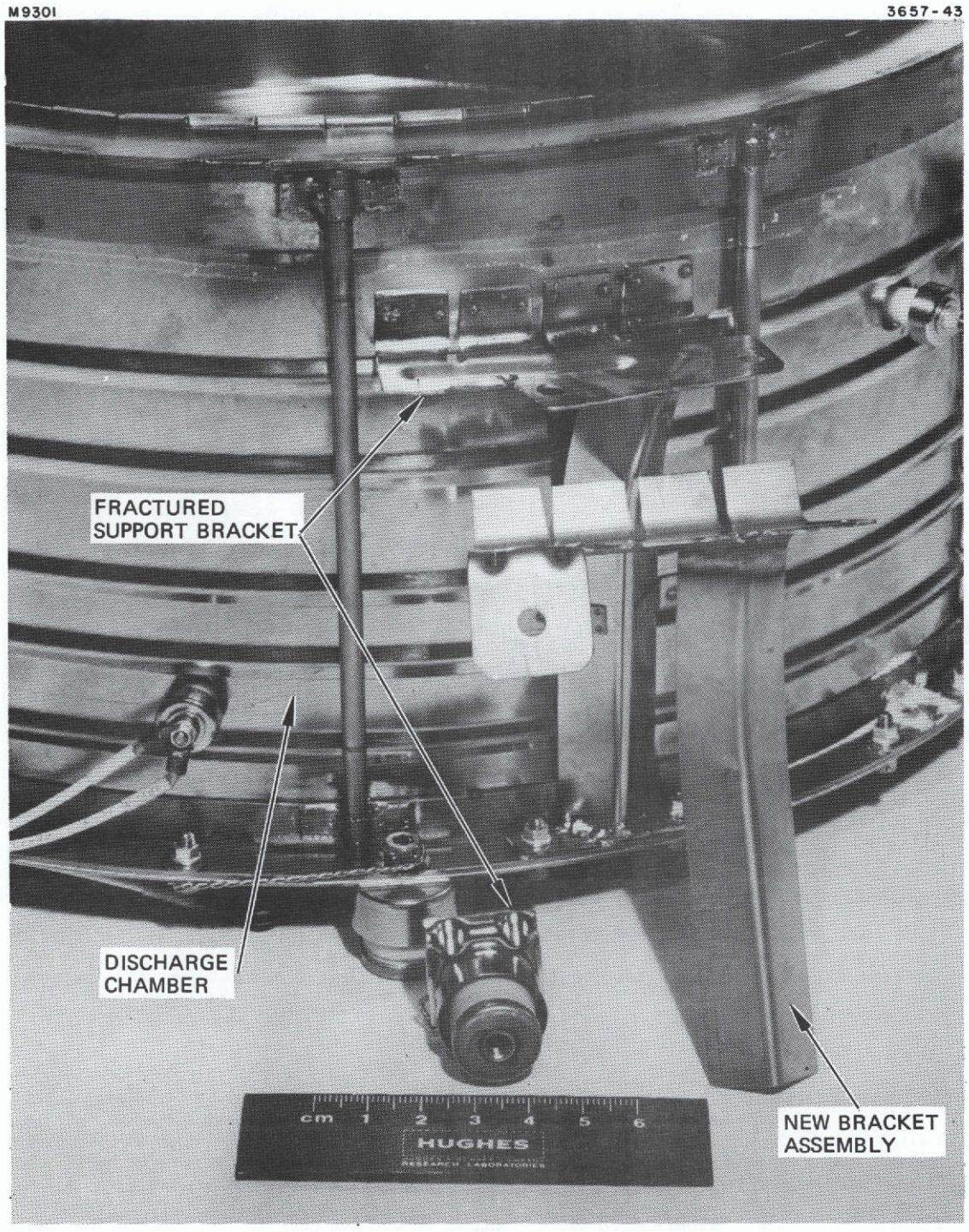

Fig. 93. Photograph of fractured insulator support bracket.

3657-51

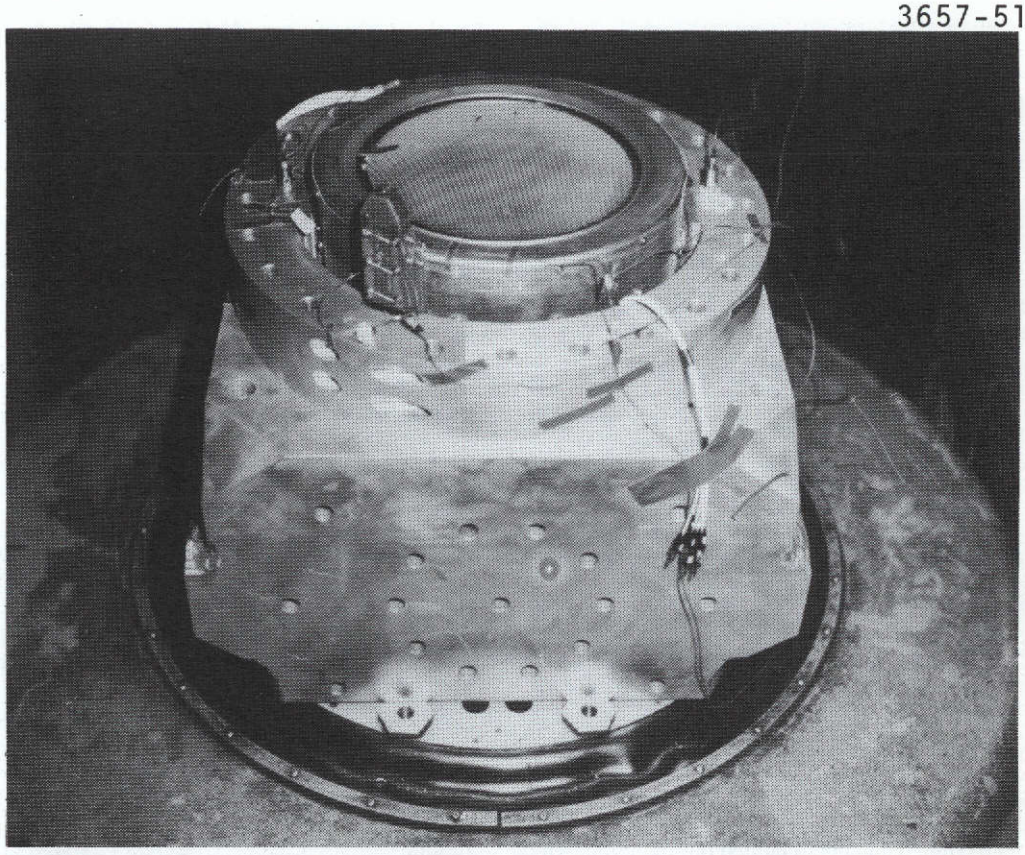

Fig. 94. Vibration test setup for thruster S/N 702.

in AETL Report No. 5430-5227, showed that the fixture would not influence the thruster response.

The thruster was then mounted in the vibration fixture and accelerometers were placed as illustrated in Fig. 95(a). Sinusoidal vibration in the X-axis over the frequency range of 5 to 2000 Hz at a sweep rate of two octaves per minute was applied at a double amplitude of 0.127 cm up to a limiting value of 1.0 g peak. During this portion of testing, the outputs of the accelerometers were recorded on magnetic tape.

The thruster, mounted in the X-axis orientation, was then subjected to sinusoidal sweep over the frequency range of 5 to 2000 Hz at a sweep rate of two octaves per minute at an applied double amplitude of 1.27 cm up to a limiting value of 9.0 g peak.

Following the X-axis sweep, the test fixture was mounted in the Y-axis position, accelerometers were attached, as shown in Fig. 95(b) and a fixture evaluation was performed. With the thruster installed, the 1.0 and 9.0 g sweeps were repeated over a frequency range of 5 to 2000 Hz. At this point in the test, the neutralizer housing was found to be cracked in four places. It was found that the neutralizer bracket did not have sufficient strength to prevent movement of the neutralizer assembly. This movement caused "flexing" of the housing which resulted in cracking the housing. The neutralizer bracket was reinforced and the housing replaced and reinforced to continue testing. A permanent design modification was later made in the bracket to strengthen the overall assembly and minor changes were made in the housing to eliminate the perforated area in the load paths.

After the neutralizer housing was repaired, testing was continued with the 1.0 and 9.0 g sine vibration in the Z-axis. As a result of the Z-axis sine test, the MIV feedline was fractured at the vaporizer and at the manifold fitting. Resonance conditions for the X-, Y- and Z-axis 9.0 g sine test are shown in Table 42.

With no additional damage noted, the random vibration portion of the test was initiated in the Z-axis. At this point the neutralizer housing cracked again and the neutralizer keeper shield separated

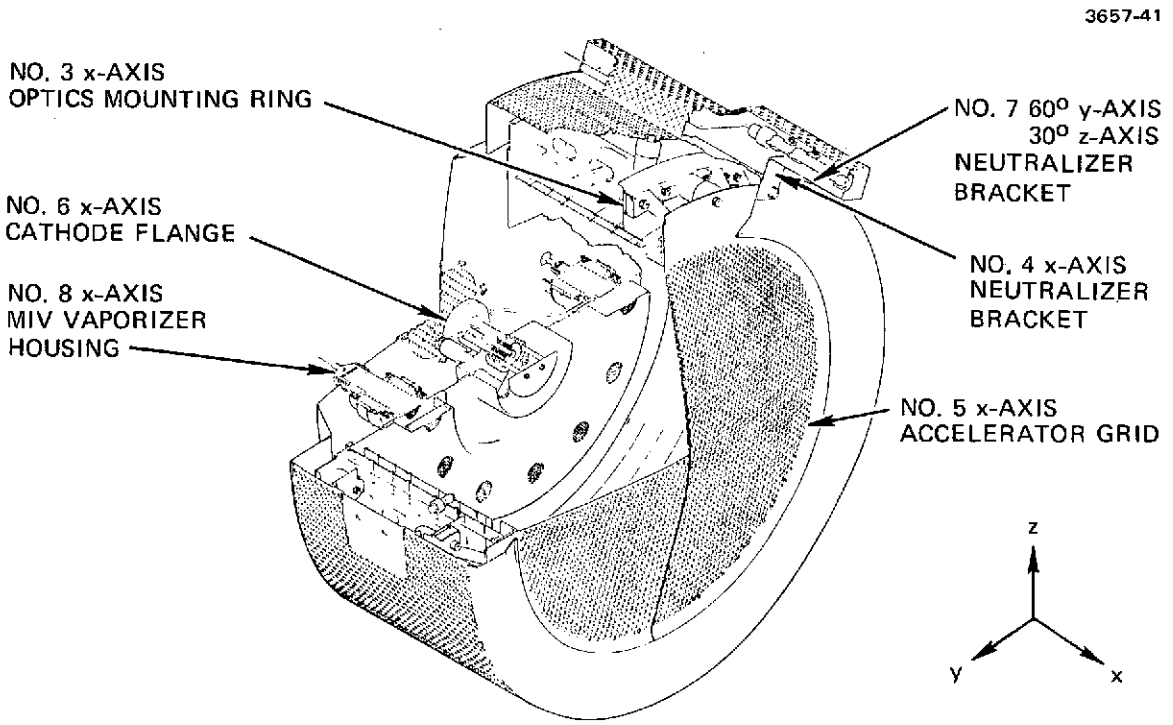

(a)

Fig. 95. Accelerometer locations for sine vibration test of thruster S/N 702.

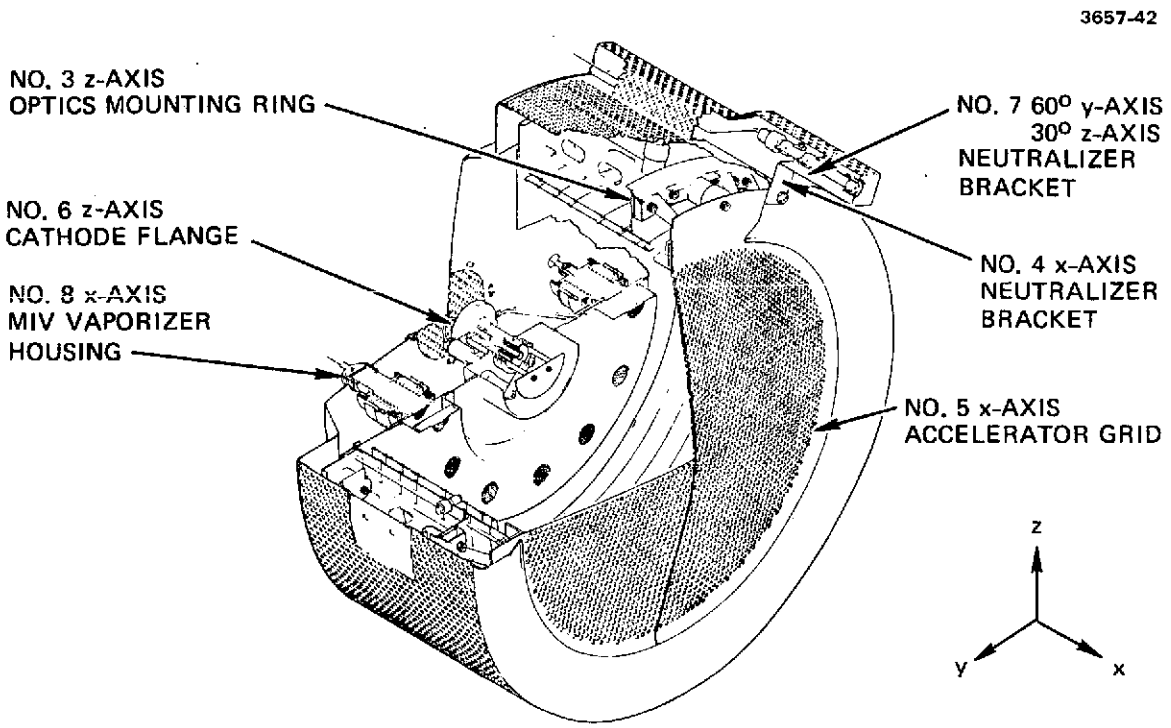

(b)

Fig. 95. Continued.

TABLE 42

Resonance to Sine Vibration for Thruster S/N 702

Accelerometer		Response Direction	9 g sine Resonance Conditions					
			X-Axis		Y-Axis		Z-Axis	
Location	No.		Frequency, Hz	Amplitude, g	Frequency, Hz	Amplitude, g	Frequency, Hz	Amplitude g
Optics Mounting Ring	3	X or Z	145 245 390 430 500	25 64 34 30 35	180 220 280 330	4 2 2 2	110 205 240 310 360	22 55 42 24 17
Neutralizer	4	X	150 245 370 900 1800	22 64 35 30 35	Accelerometer Fell Off		115 210 240 260 330	25 55 28 28 32
Accelerator	5	X	145 240 330 460 620	44 130 84 100 23	185 240 330 320	33 13 36 10	115 210 260 325 360	36 160 50 75 45
Cathode Flange	6	X or Z	150 230	120 60	170 260	18 3	110 215 250 280 300	43 145 100 80 70
Neutralizer	7	Y, Z	170 230 360 1700	40 40 34 22	190 310 410	18 10 3	110 185 215 250 270	40 75 64 45 47
MIV	8	X	140 230 410	100 42 12	165 190 260	11 14 23	110 155 215 240 260	8 8 87 82 80

T1532

from the attachment tab. The neutralizer was safety wired to allow testing to be continued. Random vibration testing was continued in both the X- and Y-axis.

Following the X-axis test the CIV tantalum feedline were found to be fractured near the junction of the two lines. The feedlines were taped and shock testing was initiated. The half sine shock test was performed in the manner described for thruster S/N 601. No additional damage was observed.

Accelerometers were recalibrated for the double amplitude sine test and the thruster was mounted to allow vibration along the X-axis. The thruster was then subjected to a sinusoidal sweep over the frequency range of 5 to 2000 Hz at an applied double amplitude of 2.5 cm up to a limiting value of 18 g peak at a sweep rate of two octaves per minute. Due to equipment limitations, the 2.5 cm double amplitude value could not be obtained and testing was performed at an applied double amplitude of 1.9 cm in the range of 5 to 19 Hz. The resonance results of the 18 g sine test are shown in Table 43.

The 18 g sine test resulted in many additional failures as described below:

- Two rear braces fractured near both attachment points during 18 g sine test as shown in Fig. 96. This fracture permitted the entire back-plate to "oil can" and resulted in damage to a number of other parts.
- The rear extension of the neutralizer cover was broken near the attachment points to the rear shield.
- The rear shield was fractured at the four mounting points at the rear of the thruster assembly.
- Two of the twenty-four attachment points of the outer shield/rear shield were fractured due to excessive deflection at this interface.
- The neutralizer feed tube was fractured at the point where it was clamped to the rear shield.

TABLE 43

Resonance Response to Elevated Sine Vibration for Thruster S/N 702

Accelerometer		Response Direction	18 g Sine Resonance Conditions					
			X-Axis		Y-Axis		Z-Axis	
Location	No.		Frequency, Hz	Amplitude, g	Frequency, Hz	Amplitude, g	Frequency, Hz	Amplitude, g
Optics Mounting Ring	3	X	60 185 235 430 1500	52 85 44 30 18	Not Tested		Not Tested	
Neutralizer	4	X	60 185 250 420 900	40 59 34 28 30	Not Tested		Not Tested	
Accelerator	5	X	60 185 250 360 500	83 120 60 90 90	Not Tested		Not Tested	
Cathode Flange	6	X	60 175 240 350 650	105 95 10 9 7	Not Tested		Not Tested	
Neutralizer	7	Y and Z	60 150 230 360 600	40 120 28 23 15	Not Tested		Not Tested	
MIV	8	X	59 130 175 540	71 27 35 6	Not Tested		Not Tested	

T1534

3657-52

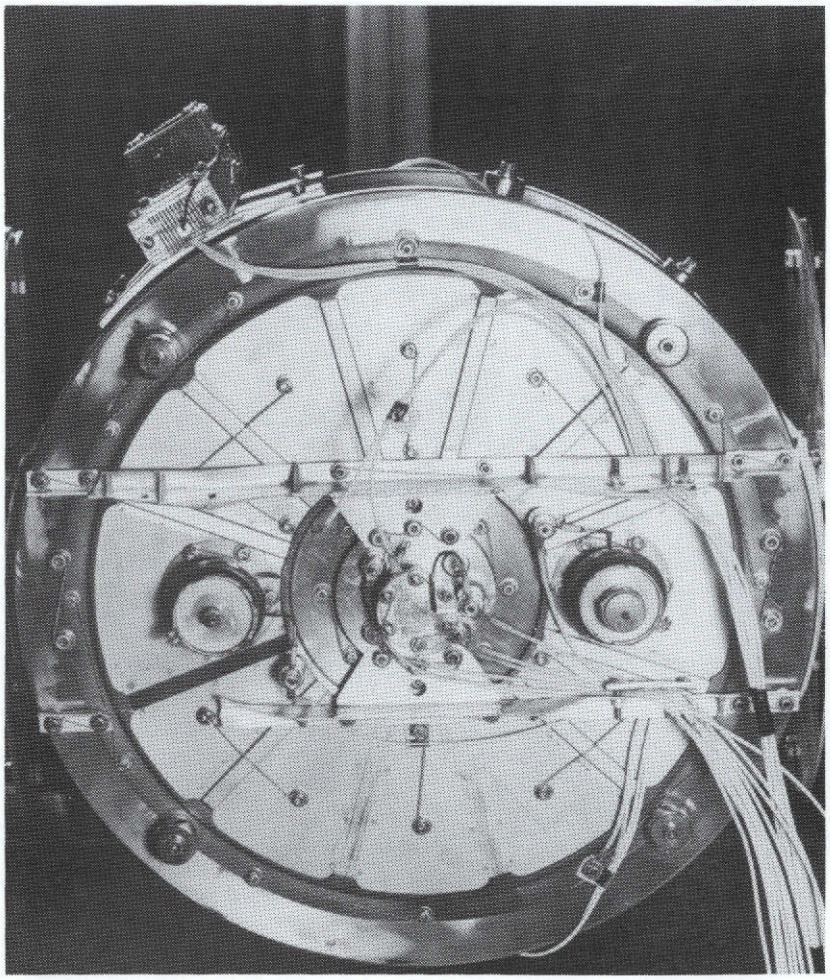

Fig. 96. Photograph of failed rear braces.

- The main isolator heater was fractured at the mounting insulator.
- Six of the twelve radial magnet retainers were broken loose from the backplate allowing two magnets to separate.
- The 0.24 cm diameter feed line connecting the cathode and isolator sections of the CIV assembly was fractured and separated.
- Two tabs on the outer magnet retainer were buckled.
- The CIV and MIV vaporizer heater leads were fractured.
- CIV cathode heater terminal cracked.
- MIV and CIV isolator heater terminals fractured.
- Both rear braces were fractured in several places.
- The propellant distribution plenum was cracked at the corners and several screens were torn off the distribution posts.

After due consideration of the specific damage itemized above and upon subsequent examination of the thruster assembly, it was evident that most of the failures incurred at the 18.0 g level would be eliminated if additional support was given the thruster backplate. In view of the inability of the low strength, aluminum beams to support the loads at the higher test levels, it was suggested that a more complex titanium support structure be used in subsequent thruster assemblies. Such an improved design was subsequently implemented and minor modifications in some of the other failed items were also recommended. These modifications are as follows:

- Modifications to rear shield mounting point.
- Increasing the number of spotwelds attaching the radial magnet retainers to the thruster backplate.
- Incorporation of insulated mounting terminals for CIV and MIV vaporizer heater leads and wiring support.

- Use of larger corner radii (0.254 cm) in fabrication of the propellant distributor plenum spinning.

These modifications, and several others recommended by the NASA LeRC Program Manager, were implemented in the repair of thruster S/N 702. The modified thruster, S/N 702-A, was described in Section II as being basically identical to the 800-series design.

C. Vibration Test of Thruster S/N 702-A

A shake test program similar to that used for the original version of thruster S/N 702 was performed on Thruster S/N 702-A in September, 1974. The shake test was preceded and followed by about 15 hours of performance tests to evaluate possible changes in operating characteristics resulting from the shake tests. The typical test setup for this work is shown in Fig. 97. In terms of fixture and accelerometer calibrations, testing was similar to previously described sequences.

The thruster was first subjected to 5-2000 Hz sinusoidal vibration at 1.0 and 11.0 g levels. No damage was experienced in either the X- or Y-axis tests. However, following the Z-axis sine test, the ground screen was found to have failed in two areas. Both of these areas were slightly buckled before the test due to a slight mismatch between the etched ground screen holes and the mounting screws. This "loose" fit allowed the ground screen to flex and subsequently fatigue the etched webs. One of the failed area is shown in Fig. 98. No changes were found in electrical resistance values. Accelerometer locations and resonance conditions are presented in Fig. 99 and Table 44, respectively.

Following the 11.0 g sine test the thruster was returned to Hughes for detailed inspection. The inspection included removal of the ground screen, the neutralizer cover, the rear cover, the ion optical system assembly, and observation of all portions of the thruster. Torques on all nonsafety wired screws and feedline nuts were compared with pretest values as shown in Table 45. Original torques were

TABLE 44

Resonance Response to Sine Vibration for Thruster S/N 702-A

Accelerometer		Response Direction	11.0 g Resonance Conditions					
			X-Axis		Y-Axis		Z-Axis	
Location	No.		Frequency, Hz	Amplitude, g	Frequency, Hz	Amplitude, g	Frequency, Hz	Amplitude, g
Optics Mounting Ring	5	X Y	132 185 270 380	68 48 20 36	115 170	76 18	75 120 900 1400	32 29 21 21
Neutralizer Bracket	6	X	130 190 245 1250	200 116 84 52	110 180 1250	135 115 60	65 120 160 910	105 120 145 60
Accelerator Grid	7	X	135 200 270	115 110 60	120 200 260	60 90 72	64 120 200 270	35 65 95 33
Cathode Flange	8	X Y	135 200 230	92 38 37	120 175 680	63 28 14	120 175 680	30 26 13
Neutralizer Bracket	9	60^{o}Y 30^{o}Z	180	~140[a]	110 170	~80[a] ~110[a]	110 170	~ 70[a] ~115[a]
MJV Vaporizer Housing	10	X	128 170 230	145 50 53	115 170 240	44 29 36	120 175 200 240	55 18 15 16

[a]Recalibration at conclusion of testing indicated output at approximately 10% of actual level. Values listed are 10x shown on X-Y plots.

T1533

3657-53

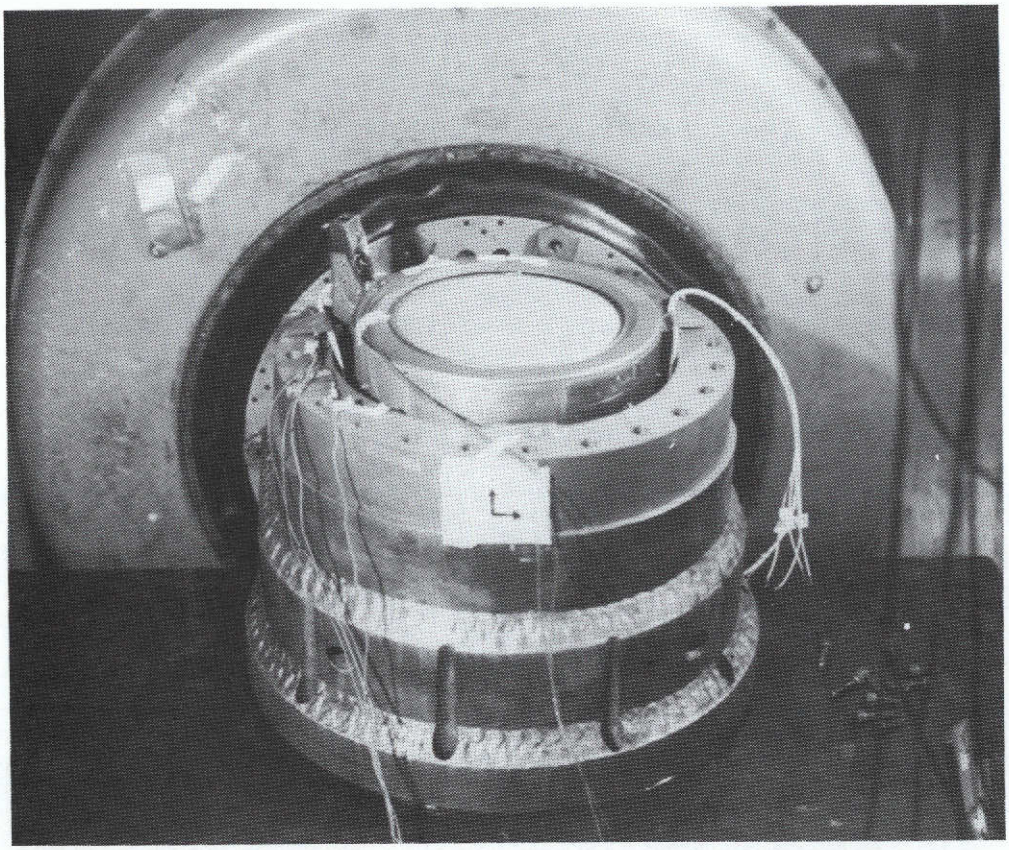

Fig. 97. Vibration test setup for thruster S/N 702-A.

M3657-47

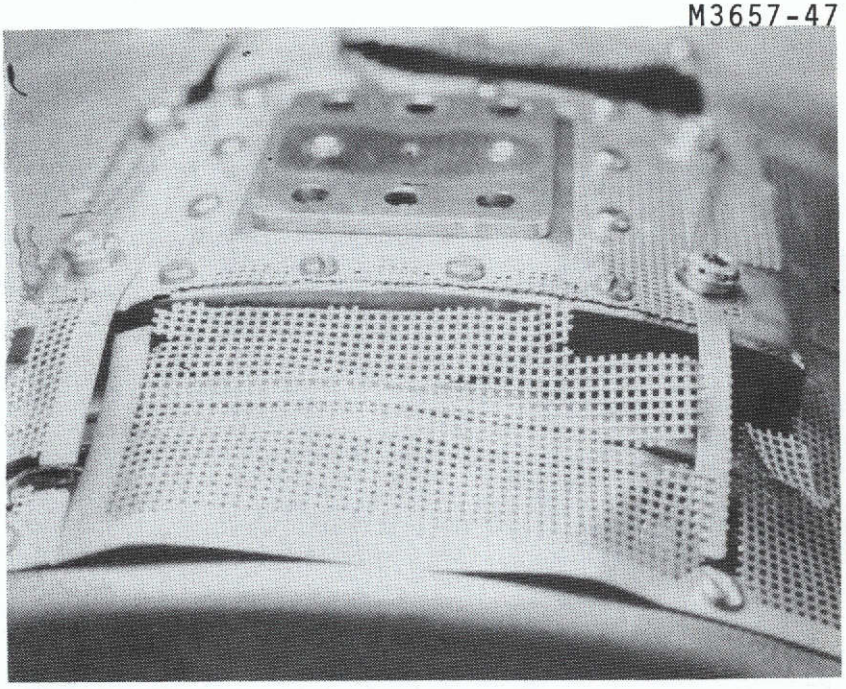

Fig. 98. Photograph of failed ground screen on thruster S/N 702-A.

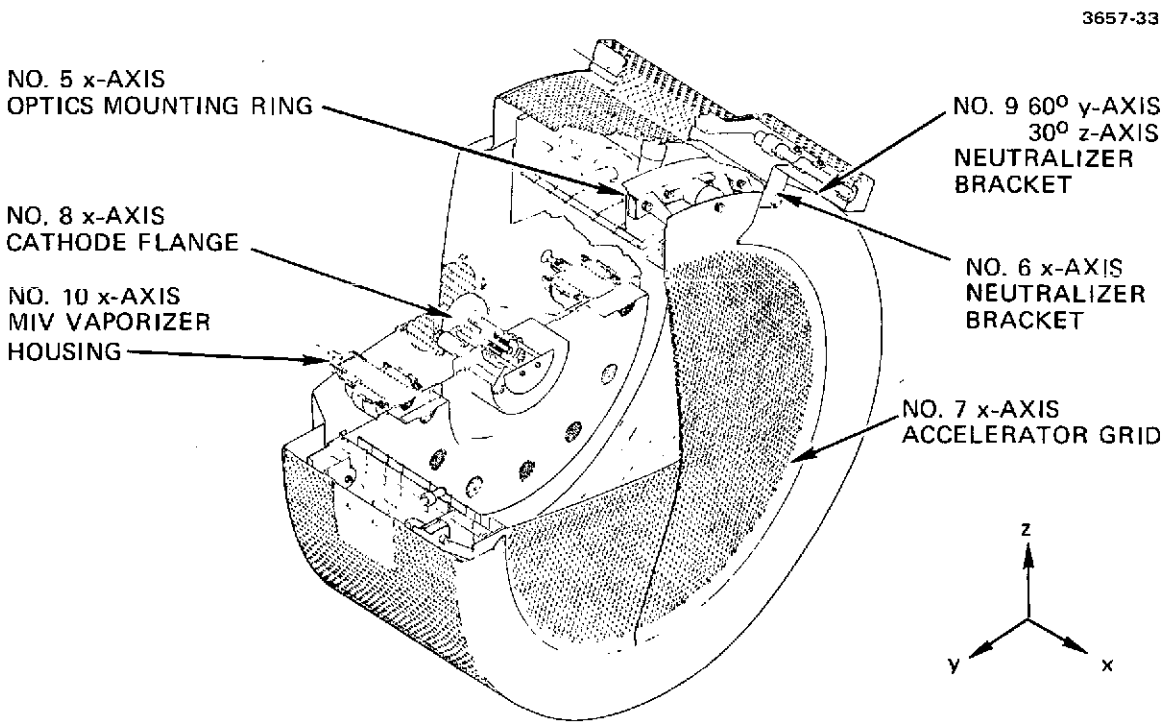

(a)

Fig. 99. Accelerometer locations for sine and random vibration test of thruster S/N 702-A.

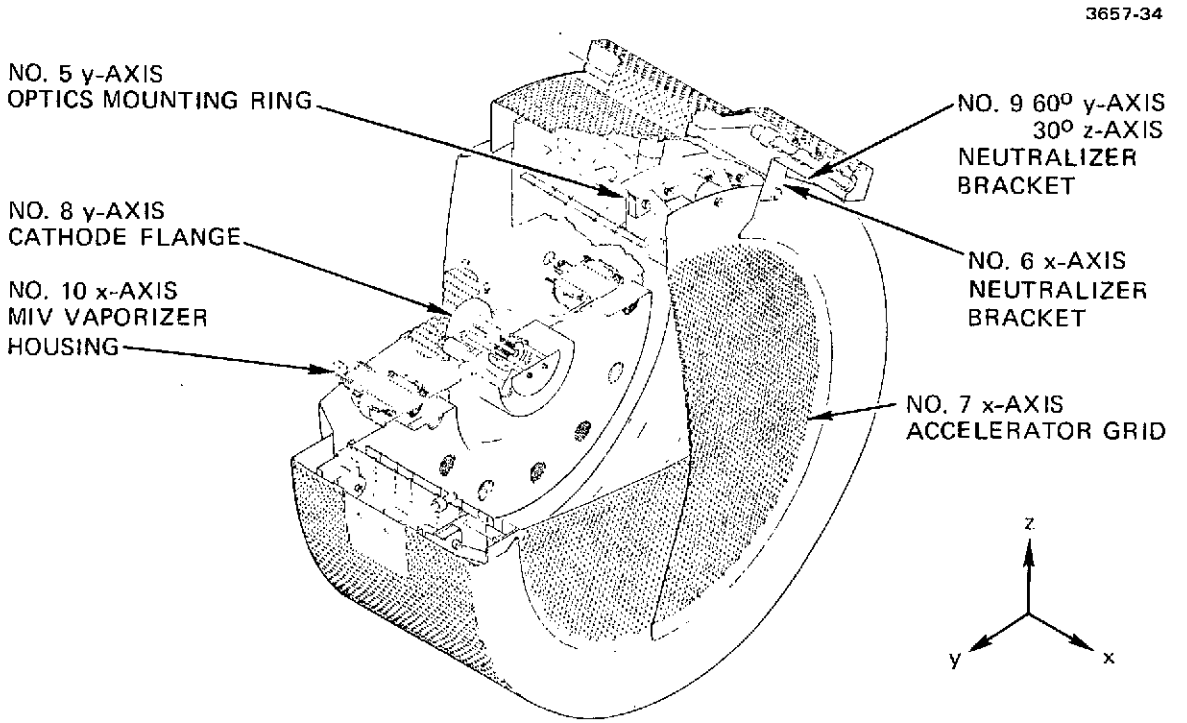

(b)

Fig. 99. Continued.

TABLE 45

Torques on Thruster 702-A Screws and Nuts

Screw/Nut	Torque (± 0.5 in. lb)		
	Pretest[a]	Post Sine Test Inspection[b]	Final Inspection[b]
6-32 Screws	6.0 All Screws	Range: 3.0 to 8.0 Average: 4.8 Retorqued to 12.0	Range: 5.0 to 8.0 Average: 6.6
10-32 Screws	32.0 All Screws	Range: 22.0 to 24.0 Average: 23.0 Retorqued to 32.0	Range: 22.0 to 24.0 Average: 23.0
Swagelok Feedline Nuts	20.0 All Nuts	Range: 15.0 to 28.0 Average: 19.5	Range: 10.0 to 30.0 Average: 18.0

T1535

reestablished before the second shake test series. Representatives from NASA LeRC and from JPL attended this inspection. No additional damage was found during the inspection. The thruster was reassembled with a new ground screen of the same design and returned to AETL.

After appropriate calibrations, the 19.8 g random vibration test was performed for the X-axis. The ground screen cracked, as in the sine test, shortly after the start of random vibration. The electrical resistance check indicated a near open circuit (6.5 MΩ) on the main vaporizer heater. This condition was noted and testing continued.

The Y-axis random vibration test produced no additional damage but the main vaporizer resistance had increase (infinity on meter). Following the Z-axis random vibration, the propellant line braze joint fractured at the propellant interface flange, and the main vaporizer heater resistance dropped to 30Ω. Accelerometer locations are shown in Fig. 99.

The feedline was taped down to allow the shock test to be performed. Three 8 ms, 30 g shock pulses in each direction for X, Y, and Z axes were applied sequentially, with appropriate fixture positioning.

Following the first series of pulses for the +Y and -Y axes, a shell to ground screen short was noted. (It is believed that this was due to a piece of loose ground screen.) The main vaporizer resistance returned to a value of infinity.

The +Z and -Z shock pulses caused the shell-to-ground screen short to disappear. The main vaporizer resistance was measured to be 50 MΩ. The +X and -X shock pulses were applied with no apparent additional failures. However, in removing the thruster from the test fixture (thruster mounting ring), one gimbal pad was found to be loose from the thruster. The thruster was then returned to Hughes for further analysis.

Upon detailed examination, the six gimbal pad insulators were found to have failed on the gimbal end of the insulators. This gimbal pad failure is shown in Fig. 100. Note that these insulators were not replaced during the repair of thruster S/N 702. They had survived the shake test described previously, including sinusoidal vibration at 18 g.

In reviewing the vibration test experience, the following conclusions were reached:

- The ground screen should be strengthened by use of thicker sheet and wider webs. Additional care is required to produce a tight fit between the ground screen and front and rear shields.
- The main vaporizer heater conductor was found to have failed at the terminal joint. In reviewing this failure, it was found that the terminal had been severely bent during MIV installation on the thruster. The reason for the bending was to fit the terminal to an out-of-position support insulator. Since no other similar heater or terminal failures occurred during the vibration tests, it is concluded that the main vaporizer failure was due to mishandling and does not represent a design or fabrication defect.
- A comparison of sine test results for thruster 702 and 702-A shows a substantial amplification increase and a corresponding frequency decrease for the 702-A tests. This change is most obvious for the Y-axis. As noted previously, the gimbal pad insulators on thruster S/N 702-A had not been replaced following the severe testing of the original thruster S/N 702. It is concluded that several of the insulators had been damaged during the 18-q tests on 702. Additional work is planned to reevaluate the gimbal pad insulator design.

- The propellant feedline failure near the failed gimbal pad is attributed to fatigue due to motion of gimbal pad. Additional support for the feedline at the gimbal pad should be considered.

- Neutralizer assembly modifications resulting from earlier tests proved to be successful. No failures were experienced and cathode-to-keeper alignment was unchanged by the vibration testing.

- Modifications incorporated to support the thruster backplate were successful. No failures of components or assemblies mounted on the backplate, except for the main vaporizer, were found.

Following the shake test, the gimbal pad insulators in the failed mount were replaced, the main vaporizer heater was repaired, the broken feedline was rebrazed and the original S/N 702 ground screen was installed. Successful performance tests were then completed as discussed in Section III-A. Thus, this series of design modifications and vibration tests has produced a thruster with basically rugged structural properties, which with minor additional changes is expected to meet presently defined environmental requirements.

3657-48

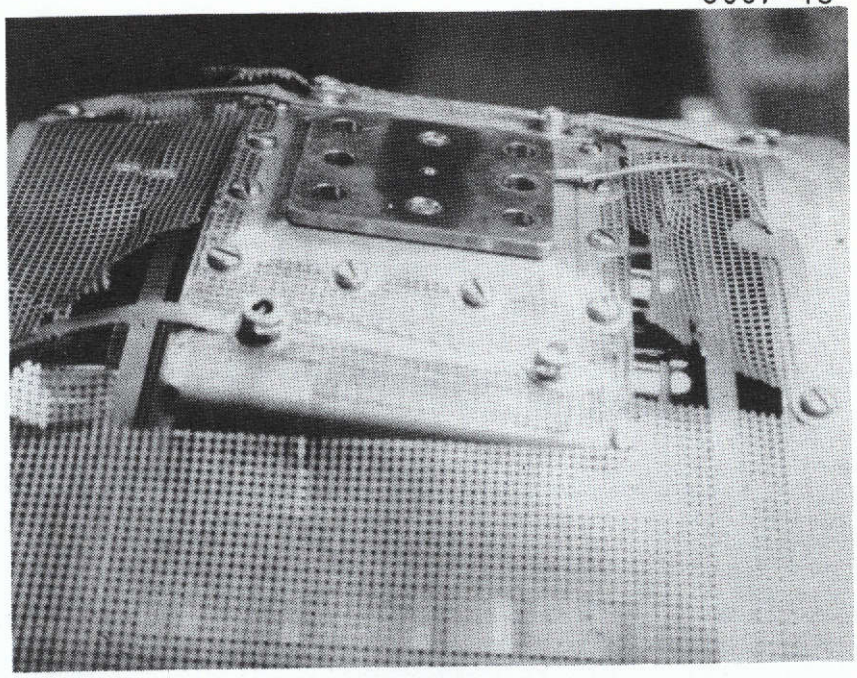

(a)

3657-49

(b)

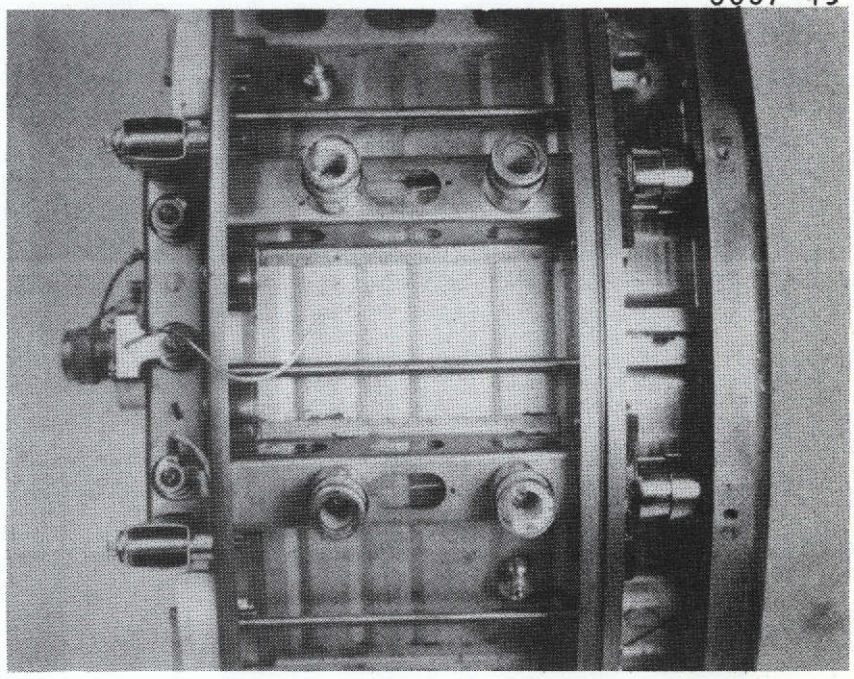

Fig. 100. Photographs of failed gimbal pad and insulators.